UNIVERSITÁ DEGLI STUDI DI PADOVA

**DIPARTIMENTO DI TECNICA E GESTIONE
DEI SISTEMI INDUSTRIALI
SCUOLA DI DOTTORATO IN INGEGNERIA MECCATRONICA E
INNOVAZIONE MECCANICA DEL PRODOTTO
CICLO XXVI**

STRESS ANALYSIS OF PERIODIC NOTCHES BY USING THE STRAIN ENERGY DENSITY APPROACH

Direttore della Scuola: Ch.mo Prof. Alessandro Persona
Supervisore: Ch.mo Prof. Filippo Berto

Dottorando: Reza Afshar Hosseinabadi

2013-2014

Acknowledgements

Completion of this doctoral dissertation was possible with support of several kind people around me, to only some of whom it is possible to give particular mention here.

First and foremost I want to thank my supervisor Prof. Berto for his continuous support and many constructive discussions and suggestions. It has been an honor to be his first Ph.D. student. The good advice, support and friendship with him have been invaluable, in both academic and personal level, for which I am very grateful.

I wish to express my sincere gratitude to Prof. Lazzarin for his invaluable guidance, scholarly inputs and consistent encouragement that I recieved throughout the whole doctoral period. His insightful comments and constructive criticisms at different stages of my research were thought provoking and helped me to focus my ideas.

I gratefully acknowledge the funding resources that made my Ph.D. work possible, and helped to remove financial concerns from my decision to embark on this journey. I would like to acknowledge the academic, technical and financial support of the University of Padova, particularly *Fondazione Cassa di Risparmio di Padova e Rovigo,* for providing scholarships to pursue doctoral studies. My sincere thanks also goes to Prof. Trevisani for providing the financial support in the first year of my study.

I am indebted to the Officine Meccaniche Zanetti for the financial support, whenever I have asked for. I appreciate all their contributions of funding to make my Ph.D. experience productive and stimulating.

I would also like to thank Dr. Filippi for giving me the opportunity to work at OMERA S.r.l.

Last but not least, I'd like to thank my family and my wife, Darya, and dedicate this thesis to them for their absolute and unquestioned love, patience and support.

Table of contents

1. Summary

English
This research focuses on the stress analysis of periodic notches by using the strain energy density approach. Bolts, screws and rotary-shouldered connections, as examples of periodic notched components, play an important role in the performance of the machinery. The contents are related to two-dimensional (2D), as well as three-dimensional (3D) modeling of periodic notches both in the case of round and sharp notches. The analyses are based on the numerical modeling of periodic notches with linear elastic assumption of the material. The simple analytical expressions for the notch stress intensity factors (NSIFs) of periodic sharp notches, as well as theoretical stress concentration factors (SCFs) of periodic blunt notches are obtained. Using the strain energy density (SED) approach, the coarse mesh in the finite element models is used and compared with the results obtained from the fine meshing. In fact, using SED approach, the averaged strain energy in a control volume allows using the coarse meshes in order to determine the NSIFs and SCFs of notched components precisely.
In the case of 3D analysis, the thickness effects with particular attention on coupling modes, which due to Poisson effect are automatically generated, are studied. These modes can have a significant effect on the structural integrity of mechanical components.
In addition, two collaborative industry projects with: Officine Meccaniche Zanetti s.r.l. and Omera s.r.l. are successfully implemented.

Italian
Questa ricerca si concentra su "Analisi delle sollecitazioni di intagliati periodici utilizzando l'approccio di densità di energia di deformazione", si è occupato di problematiche relative alla modellazione bidimensionale e tridimensionale di intagli periodici raccordati e a spigolo vivo. Bulloni, viti e connessioni rotanti spalle, come esempi di componenti intagliati periodiche, svolgono un ruolo importante nelle performance delle macchine. L'attività ha coinvolto prevalentemente la modellazione numerica in campo elastico ed ha permesso di ottenere delle semplici espressioni per la stima dei fattori d'intensificazione delle tensioni (NSIFs) e dei fattori teorici di concentrazione delle tensioni (SCFs) in funzione di tutti i parametri geometrici considerati. Le analisi numeriche sono state effettuate in prima battuta con mesh fitte e successivamente con mesh molto rade. Nel secondo caso l'energia di deformazione mediata in un volume di controllo ha permesso di determinare con precisione i fattori tensionali di riferimento e alcune espressioni per l'applicazione diretta a problematiche simili. Nel caso tridimensionale sono stati studiati e analizzati gli effetti legati allo spessore con particolare riferimento ai modi accoppiati che vengono automaticamente generati per effetto Poisson e che possono incidere in modo rilevante sull'integrità strutturale di componenti meccanici.
I risultati raggiunti sono stati applicati a casi aziendali con due collaborazioni tutt'ora in atto con Officine Meccaniche Zanetti e Omera formalizzate in progetti di ricerca in cui il dottorando è stato il principale protagonista.

The following descriptions briefly explain each of eight investigations, which are published in the international journals:

Paper I: Notch stress intensity factors of flat plates with periodic sharp notches by using the Strain Energy Density [1]

Notch Stress intensity factors (NSIFs) of a number of flat plates with periodic sharp V-notches under a remote applied normal stress are calculated. The main objective of this study is to take advantage of the local strain energy density (SED) averaged on a control volume surrounding the tip of the middle notch and estimate the NSIF of each component by using a relatively coarse mesh. A wide range of notch opening angles, relative distance between periodic notches and relative depth of the notch for different number of notches of flat plate are examined. In total, more than three hundred models have been investigated. A new model of depth reduction factor for different ratios of relative depth of the notch is proposed to match the results from SED approach. In the case of shallow notches, the results of this study are compared with those provided by other researchers in the recent literature. In addition, based on best fit of numerical data from SED approach, some polynomials for non-dimensional NSIF in the case of intermediate and deep notches are presented.

Paper II: Simple new expressions for the notch stress intensity factors in an array of narrow V-notches under tension [2]

Taking advantage of some recent closed form expressions for the strain energy density in a control volume embracing the notch tip, some simple expressions are derived for the Notch Stress Intensity Factors of an infinite array of double symmetric lateral notches and edge notches under tension loading. The new expressions are applicable to narrow notches when the ratio between the notch depth and the plate width, a/W, is lower than 0.025, providing very accurate results.

Paper III: Analytical expressions for the notch stress intensity factors of periodic V-notches under tension by using the strain energy density approach [3]

The notch stress intensity factors (NSIFs) of a wide range of finite-width flat plates with periodic edge notches are presented. A broad series of notch configurations, varying from shallow to very deep notches, as well as complete range of notch spacing and wide range of notch opening angles are considered. The significance of sharp notch approximation for the case of blunt notches with a very small notch radius is also demonstrated. Overall, more than 1200 models are carried out. Due to the desirability of analytical expressions for NSIFs evaluation, the numerical results, obtained from the strain energy density (SED) approach, are used to find some simple analytical expressions for the prediction of NSIFs of periodic sharp notches. The use of a coarse mesh in the finite element (FE) models, as well as multiscaling are the promising advantages of such a method underlined in the present study.

Paper IV: Some recent developments on the application of the strain energy density to shallow threaded plates with sharp notches [4]

The main advantages of the strain energy density (SED) approach and some recent applications

of the SED to the fatigue analysis of welded joints are reviewed. In addition, the paper investigates the scale effect in the threaded plates with sharp notches subjected to tension loading. Some closed form expressions for evaluation of the notch stress intensity factors (NSIFs) of periodic sharp notches, obtained by SED approach, are employed. The new expressions are applicable to narrow notches when the ratio between the notch depth and the plate width, t/W, is lower than 0.025, providing very accurate results. The NSIF ratio of two scaled geometries of periodic sharp notches is a function of averaged SED in the control volume embracing the middle notch tip. The new results are very useful for the assessment under fatigue loading.

Paper V: Stress concentration factors of periodic notches determined from the Strain Energy Density [5]

Stress concentration factors (SCFs) of a number of flat plates and round bars with periodic U- and V-notches are evaluated. Tension, bending and torsion loadings are considered in the investigation. The main objective of the investigation is to take advantage of the local strain energy density (SED) averaged on a control volume surrounding the tip of the middle notch and to estimate the SCF of each component by using a relatively coarse mesh. The unique advantage of SED method is the most prominent application of such a technique in the current study. Systematic FE simulations by considering a wide range of notch acuity and relative frequency of periodic U- and V-notch components are performed. More than two hundred and fifty models have been examined. The results of this study are compared with those provided by other researchers in the past and recent literature. Two new expressions of the notch depth reduction factor for the case of normal stresses (tension and bending) and torsion are also proposed to match the results from SED approach.

Three-dimensional stress analysis

Paper VI: On three-dimensional stress analysis of periodic notched plate under tension [6]

By using the finite element method, three-dimensional models of a number of periodic blunt and sharp notches subjected to tension loading are investigated. The aim of this research is to investigate the thickness effect on the location of maximum stress and notch stress intensity factor (NSIF) of corresponding blunt and sharp periodic notches, respectively. With this aim, different number of periodic notches, as well as different notch opening angles is examined. While for two-dimensional plates weakened by periodic notches some results are available in the literature, this paper first faces the problem of three-dimensional cases. A total of about 100 geometrical configurations are investigated.

It is found that the effect of plate thickness of periodic notched components can be characterized by the relative value with respect to the depth of the notch (H/t). For the blunt periodic notches with relatively higher values of H/t ratio, the value of the maximum tensile stress is located near the free surface. On the contrary, for lower values of H/t, it is placed at the middle plane. The same behavior is observed for sharp periodic notches in terms of notch stress intensity factors.

Paper VII: Three-dimensional Stress Analysis of a Plate Weakened by an Inclined Diamond Hole Under Various Loading Conditions [7]

Three-dimensional (3D) elastic stress distributions in the vicinity of the sharp corners of an inclined diamond hole in a plate are investigated. A detailed 3D finite element model under different loading conditions is analyzed to study the intensity of different fracture modes due to the thickness effect. The stress results are compared with those provided by a recent theory which reduces the 3D governing equations of elasticity to a differential equation system, which includes a bi-harmonic equation and a harmonic equation. They provide the solution of the corresponding in-plane and out-of-plane notch problem, respectively, and have to be concurrently satisfied. By comparing the numerical results and the theoretical stress distributions, a good agreement is found.

Paper VIII: Three-dimensional finite element analysis of single-lap joints: effect of adhesive thickness and Poisson's ratio[8]

Three-dimensional (3D) elastic stress distributions in the vicinity of overlap corners of single-lap joints are investigated. A detailed 3D finite element (FE) model is carried out to study the intensity of the in-plane and out-of-plane stress distributions along the plate width direction. The effects of adhesive thickness and Poisson's ratio are also studied. The FE results show the presence of coupled modes at the overlap corners of the joint. In particular, sharp increment of out-of-plane fracture mode, located very near the lateral free surface of the joint, is worth noting.

Supplementary investigations: Collaborations with industry

Collaboration with OMERA s.r.l: Optimization of bolt-nut connection to reduce the stress concentration

The following 3-step approach is used in this study with the aim of reduction of stress concentration in bolt-nut connection:
Step 1: To analyze the original model, both for the case of linear (to find the K_{tn}), as well as using nonlinear material model and finding the peak stress in term of von-Mises stress at the first engaged thread on the bolt. Selecting the von-Mises criteria is based on the suitability of the criteria for elastoplastic materials, which is the case in this study.
Step 2: To use the optimization module in ANSYS, in order to reduce the stress concentration by modifying the bolt-nut geometry. First, the initial optimized design is modeled. The two parameters as shank diameter of the bolt (d_shank) and the length of the notch by adding a step (W_e) are selected for the optimization purpose. Linear material is assumed, as the aim was to reduce the peak stress and subsequently the stress concentration factor.
Step 3: To analyze the geometrical optimized model from step 2 by applying the elastoplastic material properties. The results then are compared with original model.

The von-Mises stress at the first engaged thread of the bolt of original and optimized model is compared. The enhancement (more than 60%) of the stress state through the optimization procedure is observed.

Collaboration with OMZ s.r.l: Stress analysis (structural and thermal analysis) of different lamination roll designs by using finite element method: comparison case study

The aim of this project is to compare three different designs of rolls (mainly longitudinal deformation, as well as contact pressure due to interference fit for the case of proposed model) under working conditions by using the finite element modeling (FEM).
In term of longitudinal deformation, it is observed that the smaller dispalcement occure for the proposed model, which gives an advantage of conseding it in this study for the lamination application.
The comparison of the temperature distributions for the two considered models shows that the temperature distribution at the near surface of the roll for both models seems the same. However, the relative advantage of proposed model, by having the lower temperature (about 25% less), at a distance y=20 mm from the surface of the roll and beyond was evident.

References

1. P. Lazzarin, R. Afshar, and F. Berto, "Notch stress intensity factors of flat plates with periodic sharp notches by using the strain energy density". *Theoretical and Applied Fracture Mechanics*, 2012. Vol. 60, pp. 38-50.
2. F. Berto, P. Lazzarin, and R. Afshar, "Simple new expressions for the notch stress intensity factors in an array of narrow V-notches under tension". *International Journal of Fracture*, 2012. Vol. 176, pp. 237-244.
3. R. Afshar, F. Berto, P. Lazzarin, and L. P. Pook, "Analytical expressions for the notch stress intensity factors of periodic V-notches under tension by using the strain energy density approach". *Journal of Strain Analysis for Engineering Design*, 2013. Vol. 48, pp. 291-305.
4. R. Afshar and F. Berto, "Some recent developments on the application of the strain energy density to shallow threaded plates with sharp notches". *SDHM Structural Durability and Health Monitoring*, 2013. Vol. 9, pp. 167-180.
5. R. Afshar and F. Berto, "Stress concentration factors of periodic notches determined from the strain energy density". *Theoretical and Applied Fracture Mechanics*, 2011. Vol. 56, pp. 127-139.
6. R. Afshar and F. Berto, "On three-dimensional stress analysis of periodic notched plates under tension". *Science China Physics, Mechanics & Astronomy*, 2013.
7. R. Afshar, F. Berto, and P. Lazzarin. *Three-dimensional stress analysis of a plate weakened by an inclined diamond hole under various loading conditions*. 2013. U. K.: International Association of Engineers.
8. R. Afshar, F. Berto, and P. Lazzarin, "Three-dimensional finite element analysis of single-lap joints: effect of adhesive thickness and Poisson's ratio". *Key Engineering Materials* 2014. Vol. 577-578, pp. 393-396.

2. Introduction

Periodic notched components: stress analysis

The bolt-nut connections, toothed cutting blades, thread bars and splined shafts play a vital role in various industry applications. They are being used in many facilities across different sectors including construction, aerospace, wood industry, electronic devices, etc. Some examples of the periodic notched components are shown in Fig. 1.

Fig. 1: Examples of periodic notched components.

The analysis of the stress distribution in the vicinity of crack and notch tip and the development of different failure criteria for brittle and quasi-brittle materials are topics of active and recent research [1-3].

In some pioneering works the method of complex potentials functions has been used to obtain the stress field and the stress intensity factors in a variety of crack problems [4-7]. Following these works, a vast number of publications have appeared in the literature, considering solutions of crack problems, with emphasis on the stress intensity factors as a comprehensive presentation of these solutions reported in Refs [8-10]. An infinite periodic array of equally spaced cracks under different applied constraints and loadings have been also investigated [10].

The effects of blunt stress raisers are usually quantified in terms of a Stress Concentration Factor (SCF), which is the factor by which the stress at the considered discontinuity is raised over the nominal stress [11]. There are different methods suitable for obtaining SCFs: they are analytical (according to the elasticity theory), numerical (by using the Finite Element (FE) or the Boundary Element Method (BEM)), or experimental (such as photoelasticity or strain gages). An ingenious formula for the SCF [12] has been used for many years for a wide range of notch shapes and loading conditions; it is convenient for engineering applications, due to its simplicity and capability to give approximated values for any notch shape [13]. However, several researchers have pointed out that the formula proposed in Ref. [12] can result in underestimation or overestimation of the SCF in the case of single notches [13-17], and multi-notches [18, 19], respectively. The evaluation of SCFs is not only an academic curiosity but it is very important for the design of many components and real structures. Great efforts have been devoted to provide useful solutions in different engineering fields [20, 21]. The case of multi-notches is a practical case that is worth of investigation as underlined in Refs [18, 19].

By applying a general approach to SCF calculations for components weakened by periodic sharp notches, it was suggested in [12] to replace the periodic notch by a single notch having the same geometry but a smaller depth. Recently that approach has been revised and successfully extended to notches of different acuity by employing some accurate analyses by means of the BEM [18].

Edge cracking and geometrical scaling

The edge cracking which can be developed at the bore of a large caliber gun tube and progressed via heat checking, environmental and fatigue processes, is a K-driven process [22]. The deepest size of the crack is approximately 0.5 mm in a wall of 50 mm total thickness (Fig. 2).
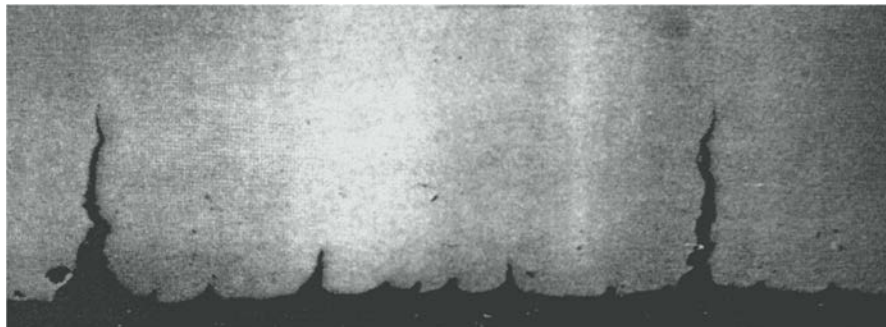

Fig. 2: Micrograph of edge cracking in a gun tube [22].

The creation and subsequent shedding of periodic edge cracks is a natural phenomenon, which occurs in the heat-checked gun tubes, rapidly cooled pressure vessels and rock, dried-out mud flats, paint and concrete and in ceramic coatings and permafrost. Dealing with this topic, a complete state of the art together with a simple developed model assessing the shedding behavior is carried out by Parker [22]. As discussed in that work, the surface topography of the cracking of ice-wedge polygons in Arctic permafrost, of mud flats in Death Valley and of craze-cracks (heat-checking) at the bore of a gun tube are all strikingly similar, yet they span five orders of magnitude in scale, with the maximum plate dimensions for ice and mud being 22 m and 0.25 m, respectively, and with the minimum plate size for gun tube craze cracking being 0.2 mm (Fig.3).
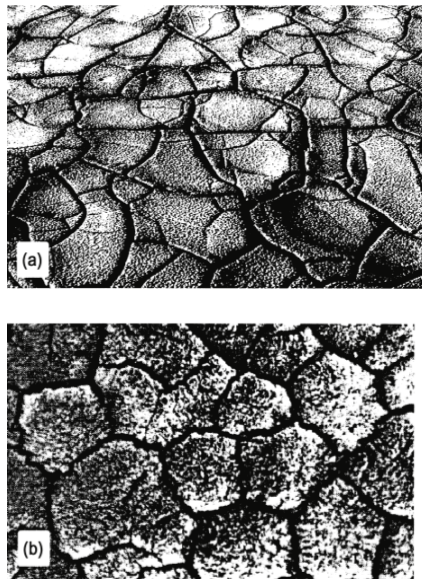

Fig. 3: (a) dried-out mud flats in Death Valley, typical plate size 250 mm; (b) craze cracks (heat-checking) on bore of a gun tube, typical plate size 0.6 mm [23].

Strain energy density (SED) approach for cracks and notches

The necessity of a simple criterion for engineering applications led to development of a point-wise SED approach valid for cracks [24-27] and notches [28]. Factor S was defined as the product of the SED by a critical distance from the point of singularity [26]. Failure was thought of as controlled by a critical value S_c, whereas the direction of crack propagation was determined by imposing a minimum condition on S. The theory was extended to employ the total SED near the notch tip [28], and the point of reference was chosen to be the location on the surface of the notch, where the maximum tangential stress occurs.

As opposed to the direct evaluation of the NSIFs, which needs very refined meshes, the mean value of the elastic SED on the control volume can be determined with high accuracy by using coarse meshes [29-31]. Very refined meshes are necessary to directly determine the NSIFs from the local stress distributions. Refined meshes are not necessary when the aim of the FE analysis is to determine the mean value of the local SED on a control volume surrounding the points of stress singularity. The SED in fact can be derived directly from nodal displacements, so that also coarse meshes are able to give sufficiently accurate values for it. Some recent contributions document the slight variability of the SED as determined from very refined meshes and coarse meshes, considering some typical welded joint geometries and provide a theoretical justification to the weak dependence exhibited by the mean value of the local SED, when evaluated over a control volume centered at the weld root or the weld toe. On the contrary, singular stress distributions are strongly mesh dependent. The NSIFs can be estimated from the local SED value of pointed V-notches in plates subjected to mode I, Mode II or a mixed mode loading. Taking advantage of some closed-form relationships linking the local stress distributions ahead of the notch to the maximum elastic stresses at the notch tip the coarse mesh SED-based procedure is used to estimate the relevant theoretical stress concentration factor K_t for blunt notches. In particular, a circular hole and a U-shaped notch, the former in mode I loading, the latter also in mixed, I + II, mode was studied in [29, 32]. By using the SED concept combined with a coarse mesh in the FE analysis for fatigue strength assessment of welded joints was carried out [30]. A procedure for rapid calculations of the NSIFs based on the SED from coarse meshing is drawn in Ref. [31]. The extension to three-dimensional cases is also possible and very convenient, in particular when edge effects are present or when a narrow spacing between collinear notches is considered. In small bodies a multiscaling and segmentation scheme permits to scale the SED at pico, nano and micro levels [33-35].

Other important advantages can be achieved by using the SED approach. The most important advantages of SED method are as follows:
- It permits the consideration of the scale effect, which is fully included in the NSIF Approach
- It allows the consideration of the contribution of different Modes.
- It permits consideration of the cycle nominal load ratio.
- It overcomes the complex problem tied to the different NSIF units of measure in the case of

different notch opening angles (i.e. crack initiation at the toe ($2\alpha=135°$) or root ($2\alpha=0°$) in a welded joint)

• It overcomes the complex problem of multiple crack initiation and their interaction on different planes.

• It directly takes into account the T-stress and this aspect becomes fundamental when thin structures are analysed.

• It directly includes three-dimensional effects and out-of-plane singularities not assessed by Williams' theory.

• Using the coarse meshing in the finite element model is possible and gives a relatively accurate and fast result.

Three-dimensional effects: local interaction between the loading modes

Due to convenience and relative simplicity, solutions of plane theory of elasticity are popular and serve as a basis for many engineering design procedures, standards and failure assessment codes. In terms of numerical costs, two-dimensional models, based on plane stress or plane strain assumptions, are much more computationally efficient, easier to build and verify in comparison with the corresponding three-dimensional counterparts. However, to approach the through-the-thickness effect of real components requires alternative methods such as three-dimensional theory of elasticity or finite element (FE) method.

The coupling effect was investigated for through-the-thickness cracks in finite thickness plates using analytical and numerical methods [36-38]. In particular, the three-dimensional stress field at sharp notches with arbitrary notch opening angles based on the first order plate theory [39] is studied [40, 41]. The coupled mode in shear loading was called 'the out-of-plane mode, or Mode O', to distinguish it from the conventional Mode 3. It was also demonstrated that the out-of-plane mode is provoked by the three-dimensional effects, linked to Poisson's ratio of the material and described by the same characteristic equation as the conventional Mode III.

The local interaction between the loading modes for the case of pointed and sharply radiused notches in plates with finite thickness was re-analysed [42]. It was demonstrated that the governing equations of three-dimensional elasticity could be reduced to a bi-harmonic equation and a harmonic equation. The former provides the solution of the corresponding plane notch problem, while the latter gives the anti-plane elasticity problem. Having the two equations

simultaneously satisfied in a 3D problem, justifies the theoretical and mutual interaction between different modes.

Main objectives of the research

The main objectives of the research can be summarized as follows:

- To stress analysis of periodic sharp and blunt notches by evaluating the notch stress intensity factors (NSIFs) and stress concentration factors (SCFs), respectively.
- To use the numerical results, obtained from the SED approach, to find some simple analytical expressions for the prediction of NSIFs of periodic sharp notches.
- Three-dimensional FE analysis of some mechanical components with the objective of investigating an out-of-plane shear stress distribution in the highly stressed region.

Sspecific research objectives addressed in the papers

Paper I

The main objective of this study is to take advantage of the local strain energy density (SED) averaged on a control volume surrounding the tip of the middle notch of periodic sharp notches and estimate the NSIF of each component by using a relatively coarse mesh.

Paper II

Taking advantage of some recent closed form expressions for the strain energy density in a control volume embracing the notch tip, some simple expressions are derived for the Notch Stress Intensity Factors of an infinite array of double symmetric lateral notches and edge notches under tension loading.

Paper III

To demonstrate the significance of sharp notch approximation for the case of blunt notches with a very small notch radius. Due to the desirability of analytical expressions for NSIFs evaluation, the numerical results, obtained from the strain energy density (SED) approach, are used to find some simple analytical expressions for the prediction of NSIFs of periodic sharp notches.

Paper IV

The main advantages of the strain energy density (SED) approach and some recent applications of the SED to the fatigue analysis of welded joints are reviewed. In addition, the paper

investigates the scale effect in the threaded plates with sharp notches subjected to tension loading.

Paper V

The main objective of the investigation is to take advantage of the local strain energy density (SED) averaged on a control volume surrounding the tip of the middle notch and to estimate the SCF of each component by using a relatively coarse mesh. The unique advantage of SED method is the most prominent application of such a technique in the current study.

Paper VI

The aim of this research is to investigate the thickness effect on the location of maximum stress and notch stress intensity factor (NSIF) of corresponding blunt and sharp periodic notches, respectively. With this aim, different numbers of periodic notches, as well as different notch opening angles are examined.

Paper VII

A detailed 3D finite element model under different loading conditions is analyzed to study the intensity of different fracture modes due to the thickness effect. The stress results are compared with those provided by a recent theory, which reduces the 3D governing equations of elasticity to a differential equation system, which includes a bi-harmonic equation and a harmonic equation.

Paper VIII

A detailed 3D finite element (FE) model is carried out to study the intensity of the in-plane and out-of-plane stress distributions along the plate width direction. The effects of adhesive thickness and Poisson's ratio are also studied.

References

1. M. R. Ayatollahi and M. Nejati, "Experimental evaluation of stress field around the sharp notches using photoelasticity*". Materials & Design*, 2011. Vol. 32, pp. 561-569.
2. M. R. Ayatollahi and A. R. Torabi, "Brittle fracture in rounded V-shaped notches*". Materials and Design*, 2010. Vol. 31, pp. 607.
3. A. Carpinteri, R. Brighenti, and S. Vantadori, "Notched double-curvature shells with cracks under pulsating internal pressure*". International Journal of Pressure Vessels and Piping*, 2009. Vol. 86, pp. 443-453.
4. P. C. Paris and G. C. Sih, "Stress analysis of cracks, in Fracture Toughness Testing and its applications*". American society for testing and materials, Philadelphia*, 1965. pp. 30-81.
5. G. C. Sih, "Strength of stress singularities at crack tips for flexural and torsional problems*". Journal of Applied Mechanics, Trans. ASME*, 1963. Vol. 30, pp. 419-425
6. G. C. Sih, "Stress distribution near internal crack tips for longitudinal shear problems*". Journal of Applied Mechanics, Trans. ASME*, 1965. Vol. 32, pp. 51-58
7. G. C. Sih, "Heat conduction in the infinite medium with lines of discontinuity *". Journal of Applied Mechanics, Trans. ASME*, 1965. Vol. 32, pp. 293-298
8. M. K. Kassir and G. C. Sih, *Three dimensional crack problems* Mechanics of Fracture. 1975, The Netherlands Noordhoff Int. Publ.
9. G. C. Sih, *Methods of analysis and solutions of crack problems*. Mechanics of Fracture. 1973, The Netherlands: Noordhoff Int. Publ
10. G. C. Sih, *Handbook of stress intensity factors*. 1973, Benthlehem, Pennsylvania: Institute of Fracture and Solid Mechanics, Leigh University.
11. W. D. Pilkey and D. F. Pilkey, *Peterson's stress concentration factors*. Third ed. 2008, New Jersey: John wiley and sons.
12. H. Neuber, *Theory of Notch Stresses*. 1958: Springer Verlag.
13. N. A. Noda and Y. Takase, "Stress Concentration Factor Formulas Useful for All Notch Shapes in a Flat Test Specimen Under Tension and Bending*". Journal of Testing and Evaluation (JTE)* 2002. Vol. 30, pp. 1-13.
14. A. Kato, "Two dimensional stress analysis on a personal computer*". Mem. Coll. Engng, Chubu University*, 1990. Vol. 26, pp. 1-9.
15. A. Kato, "Design equation for stress concentration factors of notched strips and grooved shafts*". The Journal of Strain Analysis for Engineering Design*, 1992. Vol. 27, pp. 21-28.
16. A. Kato and T. Mizuno, "Stress concentration factors of grooved shafts in torsion*". J. Strain Analysis*, 1985. Vol. 20, pp. 173-177.
17. N. A. Noda, M. Sera, and Y. Takase, "Stress concentration factors for round and flat test specimens with notches*". International Journal of Fatigue*, 1995. Vol. 17, pp. 163-178.
18. E. Dragoni and D. Castagnetti, "Concentration of normal stresses in flat plates and round bars with periodic notches*". Journal of Strain Analysis for Engineering Design*, 2010. Vol. 45, pp. 495-503.
19. E. Dragoni and D. Castagnetti, "Concentration of shear stresses in shallow periodic notches*". Journal of Strain Analysis for Engineering Design*, 2011. Vol. 46, pp. 397-404.
20. D. Croccolo and N. Vincenzi, " Stress concentration factors in compression–fit couplings *". Proc. IMechE Vol. 224 Part C: J. Mechanical Engineering Science*, 2010. Vol. 224, pp. 1143-1152.

21.   G. Scire`Mammano and E. Dragoni, "Stress concentrations around a pressurized hole close to a uniformly loaded boundary". *Journal of Strain Analysis for Engineering Design*, 2009. Vol. 44, pp. 569-582.

22.   A. P. Parker, "Stability of arrays of multiple edge cracks". *Engineering Fracture Mechanics*, 1999. Vol. 62, pp. 577-591.

23.   J. P. Gough and J. Morrison, "Craze Cracking in 105mm Artillery and Tank Gun Barrels". *Canadian Defence Research Establishment Pacific Technical Memorandum*, 1984. pp. 84-9.

24.   G. C. Sih, "Energy-density concept in fracture mechanics". *Engineering Fracture Mechanics*, 1973. Vol. 5, pp. 1037-1040.

25.   G. C. Sih, "Some basic problems in fracture mechanics and new concepts". *Engineering Fracture Mechanics*, 1973. Vol. 5, pp. 365-377.

26.   G. C. Sih, " Strain-energy-density factor applied to mixed-mode crack problems ". *International Journal of Fracture* 1974. Vol. 10, pp. 305-321.

27.   G. C. Sih, *Surface and volume energy density applied as failure criterion*. Mechanics of Fracture Initiation and Propagation. 1991, Dordrecht: Kluwer Academic Publisher.

28.   G. C. Sih and J. W. Ho, "Sharp notch fracture strength characterized by critical energy density". *Theoretical and Applied Fracture Mechanics*, 1991. Vol. 16, pp. 179-214.

29.   F. Berto and P. Lazzarin, "A review of the volume-based strain energy density approach applied to V-notches and welded structures". *Theoretical and Applied Fracture Mechanics*, 2009. Vol. 52, pp. 183-194.

30.   P. Lazzarin, F. Berto, F. J. Gomez, and M. Zappalorto, "Some advantages derived from the use of the strain energy density over a control volume in fatigue strength assessments of welded joints". *International Journal of Fatigue*, 2008. Vol. 30, pp. 1345-1357.

31.   P. Lazzarin, F. Berto, and M. Zappalorto, "Rapid calculations of notch stress intensity factors based on averaged strain energy density from coarse meshes: Theoretical bases and applications". *International Journal of Fatigue*, 2010. Vol. 32, pp. 1559-1567.

32.   P. Livieri and P. Lazzarin, "Fatigue strength of steel and aluminium welded joints based on generalised stress intensity factors and local strain energy values". *International Journal of Fracture*, 2005. Vol. 133, pp. 247-276.

33.   G. C. Sih, *Multiscaling in molecular and continuum mechanics: interaction of time and size from macro to nano*. 2007: Springer.

34.   G. C. Sih and X. S. Tang, "Scaling of volume energy density function reflecting damage by singularities at macro-, meso- And microscopic level". *Theoretical and Applied Fracture Mechanics*, 2005. Vol. 43, pp. 211-231.

35.   X. S. Tang and G. C. Sih, "Weak and strong singularities reflecting multiscale damage: Micro-boundary conditions for free-free, fixed-fixed and free-fixed constraints". *Theoretical and Applied Fracture Mechanics*, 2005. Vol. 43, pp. 5-62.

36.   M. Heyder, K. Kolk, and G. Kuhn, "Numerical and experimental investigations of the influence of corner singularities on 3D fatigue crack propagation". *Engineering Fracture Mechanics*, 2005. Vol. 72, pp. 2095-2105.

37.   Z. H. Jin and R. C. Batra, "A crack at the interface between a Kane-Mindlin plate and a rigid substrate". *Eng. Fract. Mech. *, 1997. Vol. 57, pp. 343-354.

38.   T. Nakamura and D. M. Parks, "Antisymmetrical 3-D stress field near the crack front of a thin elastic plate". *International Journal of Solids and Structures*, 1989. Vol. 25, pp. 1411-1426.

39.   T. R. Kane and R. D. Mindlin, "High-frequency extensional vibrations of plates*". Journal of Applied Mechanics, Trans. ASME*, 1956. pp. 277-283.
40.   A. Kotousov, "On stress singularities at angular corners of plates of arbitrary thickness under tension*". International Journal of Fracture*, 2005. Vol. 132, pp. L29-L36.
41.   A. Kotousov, "Fracture in plates of finite thickness*". International Journal of Solids and Structures*, 2007. Vol. 44, pp. 8259-8273.
42.   P. Lazzarin and M. Zappalorto, "A three-dimensional stress field solution for pointed and sharply radiused V-notches in plates of finite thickness*". Fatigue and Fracture of Engineering Materials and Structures*, 2012. Vol. 35, pp. 1105-1119.

3. Methodology: strain energy density (SED) approach

In this section the analytical frame of strain energy density (SED) approach, for the both sharp and blunt notches under Mode I loading, is explained [1].

Analytical frame

With reference to the coordinate system shown in Figure 1, Mode I stress distribution ahead of a V-notch tip is given by the following expressions [2].
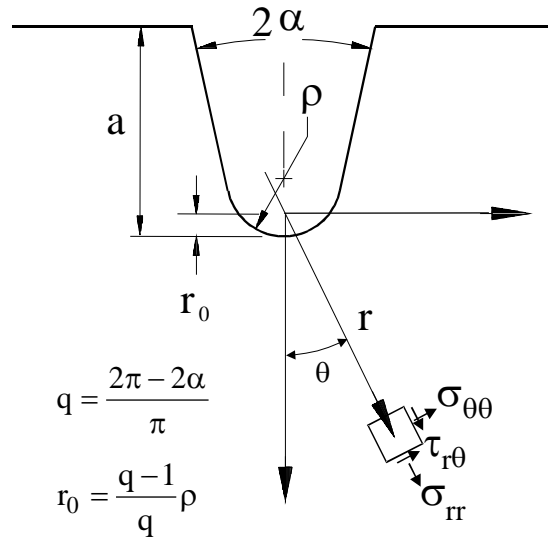

$$2\alpha$$

$$q = \frac{2\pi - 2\alpha}{\pi}$$

$$r_0 = \frac{q-1}{q}\rho$$

Figure 1: Polar coordinate system and stress components [1].

$$\sigma_{ij} = a_1 \; r^{\lambda_1 - 1} \left[f_{ij}(\theta, \alpha) + \left(\frac{r}{r_0} \right)^{\mu_1 - \lambda_1} g_{ij}(\theta, \alpha) \right] \tag{1}$$

where the parameter a_1 can be expressed by the notch stress intensity factor K_I^V in the case of a sharp, zero notch radius, V-notch or by the elastic maximum notch stress σ_{max} in the case of blunt V-notches.

In Eq.(1) r_0 gives the distance evaluated on the notch bisector line between the V-notch tip and origin of the local coordinate system; r_0 depends both on the notch root radius ρ and the opening

angle 2α (Fig.1), according to the expression $r_0 = \rho[(\pi-2\alpha)/(2\pi-2\alpha)]$. The distance r_0 is maximum when $2\alpha=0$, $r_0=\rho/2$, (Glinka, 1985), then r_0 progressively decreases (0.333ρ for $2\alpha=\pi/2$, 0.200ρ for $2\alpha=3\pi/4$, 0 for $2\alpha=\pi$).

The angular functions f_{ij} and g_{ij} are given by [2]:

$$
\begin{Bmatrix} f_{\theta\theta} \\ f_{rr} \\ f_{r\theta} \end{Bmatrix} = \frac{1}{1+\lambda_1+\chi_{b_1}(1-\lambda_1)} \left[\begin{Bmatrix} (1+\lambda_1)\cos(1-\lambda_1)\theta \\ (3-\lambda_1)\cos(1-\lambda_1)\theta \\ (1-\lambda_1)\sin(1-\lambda_1)\theta \end{Bmatrix} + \chi_{b_1}(1-\lambda_1) \begin{Bmatrix} \cos(1+\lambda_1)\theta \\ -\cos(1+\lambda_1)\theta \\ \sin(1+\lambda_1)\theta \end{Bmatrix} \right]
\tag{2}
$$

$$
\begin{Bmatrix} g_{\theta\theta} \\ g_{rr} \\ g_{r\theta} \end{Bmatrix} = \frac{q}{4(q-1)[1+\lambda_1+\chi_{b_1}(1-\lambda_1)]} \left(\chi_{d_1} \begin{Bmatrix} (1+\mu_1)\cos(1-\mu_1)\theta \\ (3-\mu_1)\cos(1-\mu_1)\theta \\ (1-\mu_1)\sin(1-\mu_1)\theta \end{Bmatrix} + \chi_{c_1} \begin{Bmatrix} \cos(1+\mu_1)\theta \\ -\cos(1+\mu_1)\theta \\ \sin(1+\mu_1)\theta \end{Bmatrix} \right)
\tag{3}
$$

The eigenfunctions f_{ij} depend only on Williams' eigenvalue, λ_1, which controls the sharp solution for zero notch radius [3]. The eigenfunctions g_{ij} mainly depend on eigenvalue μ_1, but are not independent from λ_1. Since $\mu_1 < \lambda_1$, the contribution of μ-based terms in Eq.(1) rapidly decreases with the increase of the distance from the notch tip. All parameters in Eqs.(2-3) have closed form expressions [2]. However, for the sake of brevity, only their values for some typical angle are reported herein (see Table 1).

In a generic plane case, the elastic strain energy density $W^{(e)}(r,\theta)$ will depend on Mode I, Mode II and mixed mode terms. However, only Mode I loading will be considered here. Under the plane strain condition, the eigenfunctions f_{ij} and g_{ij} will satisfy the following expressions:

$$
f_{zz}(\theta) = \nu(f_{\theta\theta}(\theta) + f_{rr}(\theta)) \qquad g_{zz}(\theta) = \nu(g_{\theta\theta}(\theta) + g_{rr}(\theta))
\tag{4}
$$

1.1 SHARP V-NOTCHES UNDER MODE I LOADING

The parameter a_1 of Eq.(1) can be linked to the Mode I notch stress intensity factor by means of the simple expression:

$$a_1 = \frac{K_I^V}{\sqrt{2\pi}} \tag{5}$$

where [4]:

$$K_I^V = \sqrt{2\pi} \lim_{r \to 0} \left[\sigma_\theta(r,0)\right] r^{1-\lambda_1} \tag{6}$$

In the presence of a notch root radius equal to zero, the distance r_0 is null, and all μ-related terms in Eq.(1) disappear. Then the elastic strain energy density under Mode I condition becomes

$$W_1^{(e)}(r,\theta) = \frac{1}{2E} r^{2(\lambda_1-1)} \cdot \frac{\left(K_1^V\right)^2}{2\pi} \left[f_{\theta\theta}^2 + f_{rr}^2 + f_{zz}^2 - 2\nu\left(f_{\theta\theta}f_{rr} + f_{\theta\theta}f_{zz} + f_{rr}f_{zz}\right) + 2(1+\nu)f_{r\theta}^2\right] \tag{7}$$

The total strain energy over the area of radius R_c is then (Figure 2):
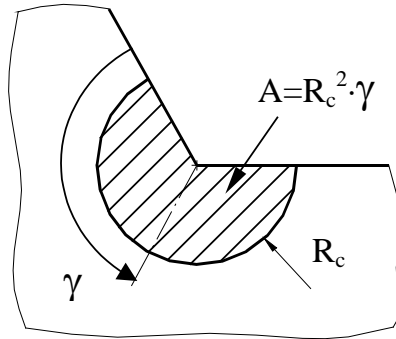
Figure 2: Control volume (area) for sharp V-notch [1].

$$E_1^{(e)} = \int_A W_1^{(e)} \, dA = \int_0^{R_C} \int_{-\gamma}^{+\gamma} W_1^{(e)}(r,\theta) \cdot r \, dr \, d\theta = \frac{1}{E} \frac{I_1(\gamma)}{4\lambda_1} \cdot \left(K_1^V\right)^2 \cdot R_C^{2\lambda_1} \tag{8}$$

where the integral I_1 is

$$I_1(\gamma) = \frac{1}{2\pi} \int\limits_{-\gamma}^{+\gamma} \left[f_{\theta\theta}^2 + f_{rr}^2 + f_{zz}^2 - 2\nu\left(f_{\theta\theta}f_{rr} + f_{\theta\theta}f_{zz} + f_{rr}f_{zz} \right) + 2(1+\nu)f_{r\theta}^2 \right] d\theta \tag{9}$$

In a plane case, the control volume becomes the semicircular sector shown in Figure 2. Its area is

$$A = \int\limits_{0}^{R_C} \int\limits_{-\gamma}^{+\gamma} r \, dr \, d\theta = R_C^2 \gamma \tag{10}$$

Then, by using Eq.(10), the mean value of the elastic strain energy referred to the area is

$$\overline{W}_1^{(e)} = \frac{E_1^{(e)}}{A} = \frac{I_1}{4 E \lambda_1 \gamma} \left(\frac{K_I^V}{R_C^{1-\lambda_1}} \right)^2 \tag{11}$$

where λ_1 is Williams' eigenvalue and $\gamma = \pi - \alpha$.

Under tensile stresses failure occurs when $\overline{W} = W_c$, where the critical value W_c obviously varies from material to material. If the material behaviour is ideally brittle, then W_c can be evaluated by using simply the conventional ultimate tensile strength σ_t, so that:

$$W_c = \sigma_t^2 / 2E \tag{12}$$

Often plain specimens exhibit a non-linear behavior whilst the behavior of notched specimens remains linear. Under these circumstances the stress σ_t should be substituted by "the maximum normal stress existing at the edge at the moment preceding the cracking" [5], who recommends also to use tensile specimens with semicircular notches [6].

Eq. (11) makes it possible to determine the critical value of the radius if one knows the experimental values W_c and K_{Ic}^V that provoke the failure under tensile stresses. If the critical value of the NSIF is determined by means of specimens with $2\alpha \neq 0$, the critical radius can be estimated by means of the expression in [7]:

$$R_c = \left[\frac{I_1 \left(K_{Ic}^V \right)^2}{4\lambda_1 \gamma E W_c} \right]^{\frac{1}{2(1-\lambda_1)}} \tag{13}$$

The integral I_1 of Eqs (13) is given in Table 2, as a function of the notch angle, for three values of Poisson's ratio ν.

When $2\alpha=0$, K_{1c}^v equals the fracture toughness K_{IC}. The material critical radius can be derived by Eq.(13) or by using the more elegant expression recently obtained in [8]:

$$R_c = \frac{(1+v)(5-8v)}{4\pi}\left(\frac{K_{IC}}{\sigma_t}\right)^2 \tag{14}$$

An expression analogous to Eq.(13) has already been used to analyze fatigue strength data from cruciform welded joints made of steel [7, 9, 10], having modeled the welded toe region as a sharp V-notch with $2\alpha=135$ degrees. In those cases K_{IC} had been substituted by the critical value of the generalized stress intensity factor range and W_c had been determined on the basis of the fatigue strength range of butt ground welded joints. Both parameters referred to 5 million cycles and a nominal load ratio equal to zero. R_c was found out to be about equal to 0.3 mm for welded joints made of structural steels and about 0.1 mm for welded joints made of some aluminum alloys.

Blunt V-notches under mode I loading

In the presence of rounded V-notches it is possible to link the parameter a_1 of Eq.(3) to the maximum principal stress present at the notch tip:

$$a_1 = \frac{\sigma_{max}}{r_0^{\lambda_1-1}\left\{1+\frac{(1+\mu_1)\chi_{d_1}+\chi_{c_1}}{1+\lambda_1+\chi_{b_1}(1-\lambda_1)}\left(\frac{q}{4(q-1)}\right)\right\}} = \frac{\sigma_{max}\, r_0^{1-\lambda_1}}{1+\tilde{\omega}_1} \tag{15}$$

where $\tilde{\omega}_1$ is reported in one of the columns of Table 1. By using the elastic maximum notch stress, Eq.(3) becomes

$$\sigma_{\theta\theta}(r,\theta) = \frac{\sigma_{max}}{1+\tilde{\omega}_1}\left(\frac{r_0}{r}\right)^{1-\lambda_1}\left[f_{\theta\theta} + \left(\frac{r}{r_0}\right)^{\mu_1-\lambda_1}g_{\theta\theta}\right]$$

$$\sigma_{rr}(r,\theta) = \frac{\sigma_{max}}{1+\tilde{\omega}_1}\left(\frac{r_0}{r}\right)^{1-\lambda_1}\left[f_{rr} + \left(\frac{r}{r_0}\right)^{\mu_1-\lambda_1}g_{rr}\right] \qquad (16)$$

$$\sigma_{r\theta}(r,\theta) = \frac{\sigma_{max}}{1+\tilde{\omega}_1}\left(\frac{r_0}{r}\right)^{1-\lambda_1}\left[f_{r\theta} + \left(\frac{r}{r_0}\right)^{\mu_1-\lambda_1}g_{r\theta}\right]$$

The elastic strain energy density is then given by the following expression:

$$W_1^{(e)}(r,\theta) = \frac{1}{2E}\left(\frac{\sigma_{max}}{1+\tilde{\omega}}\right)^2\left\{\left(\frac{r}{r_0}\right)^{2(\lambda_1-1)}\tilde{F}_\lambda + \left(\frac{r}{r_0}\right)^{2(\mu_1-1)}\tilde{G}_\mu + 2\left(\frac{r}{r_0}\right)^{\lambda_1+\mu_1-2}\tilde{M}_{\lambda\mu}\right\} \qquad (17)$$

where, following Beltrami's total strain energy criterion, the following relationships are valid:

$$\tilde{F}_\lambda = f_{\theta\theta}^2 + f_{rr}^2 + f_{zz}^2 - 2\nu\left(f_{\theta\theta}f_{rr} + f_{\theta\theta}f_{zz} + f_{rr}f_{zz}\right) + 2(1+\nu)f_{r\theta}^2$$

$$\tilde{G}_\mu = g_{\theta\theta}^2 + g_{rr}^2 + g_{zz}^2 - 2\nu\left(g_{\theta\theta}g_{rr} + g_{\theta\theta}g_{zz} + g_{rr}g_{zz}\right) + 2(1+\nu)g_{r\theta}^2 \qquad (18)$$

$$\tilde{M}_{\lambda\mu} = f_{\theta\theta}g_{\theta\theta} + f_{rr}g_{rr} + f_{zz}g_{zz} - \nu\left(f_{\theta\theta}g_{rr} + g_{\theta\theta}f_{rr} + f_{\theta\theta}g_{zz} + g_{\theta\theta}f_{zz} + f_{rr}g_{zz} + g_{rr}f_{zz}\right) + 2(1+\nu)f_{r\theta}g_{r\theta}$$

Considering the area Ω shown in Figure 3 (reminiscent of some very interesting micrographs recently reported by Gearing and Anand (2004) who dealt with notch-sensitive fracture of polycarbonate), the strain energy can be expressed as
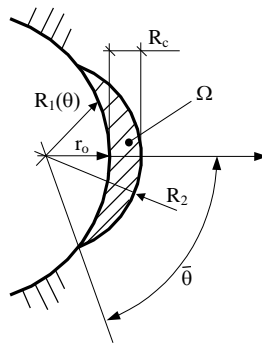

Figure 3. Control area Ω for blunt V-notch; material-dependent distance R_c, which is independent of opening angle; radius R_2 intersects the curvilinear notch root edge or the rectilinear part of the V-notch edge [1].

$$E_1^{(e)} = \int_\Omega W_1^{(e)} d\Omega = \int_{-\bar\theta}^{+\bar\theta} d\theta \int_{R_1(\theta)}^{R_2} W_1^{(e)}(r,\theta)\, r\, dr \tag{19}$$

In a more explicit form

$$E_1^{(e)} = \frac{1}{2E}\left[\frac{\sqrt{2\pi}\,\sigma_{max}}{1+\tilde\omega_1}\right]^2 r_0^{2(1-\lambda_1)}\left(I_\lambda + I_\mu + I_{\lambda\mu}\right) \tag{20}$$

where

$$I_\lambda = \int_{-\bar\theta}^{+\bar\theta} \frac{\left(R_2^{2\lambda_1} - R_1(\theta)^{2\lambda_1}\right)}{2\lambda_1}\tilde F_\lambda\; d\theta$$

$$I_\mu = (r_0)^{2(\lambda_1-\mu_1)}\int_{-\bar\theta}^{+\bar\theta} \frac{\left(R_2^{2\mu_1} - R_1(\theta)^{2\mu_1}\right)}{2\mu_1}\tilde G_\mu\; d\theta \tag{21}$$

$$I_{\lambda\mu} = 2(r_0)^{\lambda_1-\mu_1}\int_{-\bar\theta}^{+\bar\theta} \frac{\left(R_2^{\lambda_1+\mu_1} - R_1(\theta)^{\lambda_1+\mu_1}\right)}{\lambda_1+\mu_1}\tilde M_{\lambda\mu}\; d\theta$$

The third of Eqs (21) is valid only when the notch angle 2α is different from zero. Otherwise, in the presence of a U-shaped notch ($2\alpha=0$), one should use the expression

$$I_{\lambda\mu} = 2(r_0)\cdot\int_{-\bar\theta}^{+\bar\theta} \ln\left[\frac{R_2}{R_1(\theta)}\right]\tilde M_{\lambda\mu}\; d\theta \tag{22}$$

This integral is always null for $2\alpha = 0$. In general, it is possible to write:

$$I_1 = \frac{1}{2\pi}\left(I_\lambda + I_\mu + I_{\lambda\mu}\right) \tag{23}$$

where the introduction of 2π makes I_1 consistent with the expression of the sharp notch case, Eq.(9).

In a synthetic form, the energy in the structural volume can be expressed as

$$E_1^{(e)} = \frac{1}{2E} \left[\frac{\sigma_{max} \sqrt{2\pi}}{r_0^{\lambda_1 - 1} (1 + \tilde{\omega}_1)} \right]^2 \cdot I_1 \tag{24}$$

where I_1 depends on 2α, ρ and R_c.

In the case of a U-shaped notch ($2\alpha=0$), Eq.(24) becomes:

$$E_1^{(e)} = \frac{1}{2E} \left(\frac{\sigma_{max} \sqrt{\pi\rho}}{2} \right)^2 \cdot I_1 \tag{25}$$

The mean value of the strain energy density is then given by:

$$\overline{W}_1^{(e)} = \frac{1}{E} \left(\frac{I_1}{2\Omega} \right) \sigma^2_{max} \ r_0^{2(1-\lambda_1)} \left[\frac{\sqrt{2\pi}}{1+\tilde{\omega}_1} \right]^2 \tag{26}$$

The area Ω is defined as follows:

$$\Omega = \int_{R_1(\theta)}^{R_2} \int_{-\overline{\theta}}^{+\overline{\theta}} r \, dr \, d\theta \tag{27}$$

The ratio ($I_1/2\Omega$) implicitly depends on the material parameter R_c. Since the integration domain varies from case to case (according to the expressions reported in the next section of the paper), the solution of Eq.(26) needs a simple numerical routine.

In general, the integral I_1 and the area Ω depend on 2α, ρ, and R_c. However, I_1 is proportional to $\rho^{2\lambda}$ according to Eq.(21), whereas Ω is proportional to ρ^2. Then a suitable expression for $I_1/2\Omega$ is

$$\frac{I_1}{2\Omega}(2\alpha, \rho, R_C) = \frac{1}{\rho^{2(1-\lambda)}} \cdot H(2\alpha, \frac{R_C}{\rho}) \tag{28}$$

where the function H depends on the notch angle and the critical radius to notch tip radius ratio. Eq. (26) becomes

$$\overline{W}_1^{(e)} = \frac{E_1^{(e)}}{\Omega} = F(2\alpha) \ H(2\alpha, \frac{R_C}{\rho}) \ \frac{\sigma^2_{max}}{E} \tag{29}$$

where

$$F(2\alpha) = \left(\frac{q-1}{q}\right)^{2(1-\lambda_1)}\left[\frac{\sqrt{2\pi}}{1+\tilde{\omega}_1}\right]^2 \tag{30}$$

Parameters F and H are displayed in Table 1 and Table 3, respectively. All coefficients of Table 3 were determined by using for the area Ω the expressions reported in the next section.

Table 1: Parameters for stress distributions, Eqs (1, 15), and local strain energy, Eq.(29) [1].

2α [rad]	q	λ_1	μ_1	χ_{b1}	χ_{c1}	χ_{d1}	$\tilde{\omega}_1$	$F(2\alpha)$
0	2.0000	0.5	-0.5	1	4	0	1	0.7850
$\pi/6$	1.8333	0.5014	-0.4561	1.0707	3.7907	0.0632	1.034	0.6917
$\pi/4$	1.7500	0.5050	-0.4319	1.1656	3.5721	0.0828	1.014	0.6692
$\pi/3$	1.6667	0.5122	-0.4057	1.3123	3.2832	0.0960	0.970	0.6620
$\pi/2$	1.5000	0.5448	-0.3449	1.8414	2.5057	0.1046	0.810	0.7049
$2\pi/3$	1.3334	0.6157	-0.2678	3.0027	1.5150	0.0871	0.570	0.8779
$3\pi/4$	1.2500	0.6736	-0.2198	4.1530	0.9933	0.0673	0.432	1.0717
$5\pi/6$	1.1667	0.7520	-0.1624	6.3617	0.5137	0.0413	0.288	1.4417

Table 2: Integral I_1 for sharp V-notches, as a function of the notch angle and the Poisson coefficient [1].

2α (degrees)	γ/π rad	λ_1	I_1		
			$\nu=0.3$	$\nu=0.35$	$\nu=0.4$
0	1	0.5000	0.8450	0.7425	0.6300
15	23/24	0.5002	0.8431	0.7416	0.6303
30	11/12	0.5014	0.8366	0.7382	0.6301
45	7/8	0.5050	0.8247	0.7311	0.6282
60	5/6	0.5122	0.8066	0.7194	0.6235
75	19/24	0.5247	0.7819	0.7026	0.6152
90	3/4	0.5445	0.7504	0.6801	0.6024
105	17/24	0.5739	0.7124	0.6519	0.5849
120	2/3	0.6157	0.6687	0.6184	0.5624
135	5/8	0.6736	0.6201	0.5796	0.5344
150	7/12	0.7520	0.5678	0.5366	0.5013
160	5/9	0.8187	0.5315	0.5058	0.4767
170	19/36	0.9000	0.4957	0.4755	0.4523

Table 3: Values of the function H for blunted V-shaped notches.
(Coefficients determined numerically with ρ=1mm) [1].

2α (rad)	R_c/ρ	H		
		ν=0.3	ν=0.35	ν=0.4
0	0.01	0.5638	0.5432	0.5194
	0.05	0.5086	0.4884	0.4652
	0.1	0.4518	0.4322	0.4099
	1	0.1314	0.1217	0.1110
π/6	0.01	0.6395	0.6162	0.5894
	0.05	0.5760	0.5537	0.5280
	0.1	0.5107	0.4894	0.4651
	1	0.1428	0.1333	0.1226
π/4	0.01	0.6609	0.6369	0.6093
	0.05	0.5945	0.5717	0.5454
	0.1	0.5264	0.5048	0.4802
	1	0.1447	0.1355	0.1252
π/3	0.01	0.6678	0.6436	0.6157
	0.05	0.5998	0.5769	0.5506
	0.1	0.5302	0.5087	0.4842
	1	0.1435	0.1349	0.1252
π/2	0.01	0.6290	0.6063	0.5801
	0.05	0.5627	0.5415	0.5172
	0.1	0.4955	0.4759	0.4535
	1	0.1328	0.1256	0.1174
2π/3	0.01	0.5017	0.4836	0.4628
	0.05	0.4465	0.4298	0.4106
	0.1	0.3920	0.3767	0.3591
	1	0.1135	0.1079	0.1015
3π/4	0.01	0.4114	0.3966	0.3795
	0.05	0.3652	0.3516	0.3359
	0.1	0.3206	0.3082	0.2938
	1	0.1037	0.0988	0.0932

FEM and strain energy calculations

The following is a brief note on the calculation of the strain energy density by using the finite element method [11].

For a finite element with the following properties [12]:

$\{d\}$:   the vector of nodal displacements

$\{f\}$ the vector of the nodal forces.

By introducing the displacement interpolation matrix $[N]$, which depends on the FE type, it is possible to express the displacement vector $\{u\}$ and the strain vector $\{\varepsilon\}$ for a *generic point* belonging to the FE. Then:

$$\{u\}=[N]\{d\} \tag{31}$$

$$\{\varepsilon\}=\frac{\partial\{u\}}{\partial x_i}=[B]\{d\} \tag{32}$$

Here $[B]$ is the so-called strain-displacement matrix, whose rows are obtained by appropriately differentiating the rows of the displacement interpolation matrix $[N]$. Under linear elastic hypothesis, stresses are linked to strains by means of the well known expression:

$$\{\sigma\}=[E]\{\varepsilon\} \tag{33}$$

Then, the strain energy density in a point P belonging to the FE is:

$$W=\frac{1}{2}\{\varepsilon\}^t\{\sigma\}=\frac{1}{2}\{d\}^t[B]^t[E][B]\{d\} \tag{34}$$

counting on the property

$$([B]\{d\})^t=\{d\}^t[B]^t \tag{35}$$

Finally, the total strain energy stored in the finite element is:

$$E=\int_v W\,dV=\frac{1}{2}\{d\}^t\left(\int_v [B]^t[E][B]\,dV\right)\{d\}=\frac{1}{2}\{d\}^t[K]\{d\} \tag{36}$$

with V being the volume and $[K]$ the stiffness matrix of the FE:

$$[K] = \int_V [B]^t [E][B] dV \tag{37}$$

Equation (36) shows that the elastic strain energy E is directly determined from the nodal displacements, without any calculation involving stresses and strains. Obviously, the same holds true for the mean value of the strain energy density, $\overline{W} = E/V$.

The degree of accuracy in evaluating the elastic strain energy, *E*, depends on the type of FE, i.e. on the order of the polynomial expressions used for the shape functions. A comparison involving sharp V-notches and finite elements with different shape functions has been carried out in Ref. [13].

Different from the strain energy evaluations, the stress evaluations need, as is well known, the derivatives of the displacements. The governing relationship is:

$$\{\sigma\} = [E]\{\varepsilon\} = [E][B]\{d\} \tag{38}$$

The monotonic convergence to an "exact" result requires the element is '*complete*' and '*compatible*' [14]; this means that in the finite element representation of a C^{m-1} variational problem the displacements and their (*m*-1) first derivatives must be continuous across the element boundaries [14]. Obviously, this continuity does not necessarily implicate that the element stresses are continuous too. Stresses obtained at a node belonging to faced finite elements are very different when a coarse mesh is used.

As a natural consequence, the degree of mesh refinement required for the accurate determination of the strain energy is much lower than that required for the stress fields, simply because in the former case no derivation or integration process is really involved.

The most important advantages of SED method are as follows:

- It permits the consideration of the scale effect, which is fully included in the NSIF Approach
- It allows the consideration of the contribution of different Modes.
- It permits consideration of the cycle nominal load ratio.
- It overcomes the complex problem tied to the different NSIF units of measure in the case of different notch opening angles (i.e. crack initiation at the toe (2α=135°) or root (2α=0°) in a welded joint)
- It overcomes the complex problem of multiple crack initiation and their interaction on

different planes.

• It directly takes into account the T-stress and this aspect becomes fundamental when thin structures are analyzed.

• It directly includes three-dimensional effects and out-of-plane singularities not assessed by Williams' theory.

• The degree of mesh refinement required for the accurate determination of the strain energy is much lower than that required for the stress fields.

References

1. P. Lazzarin and F. Berto, "Some expressions for the strain energy in a finite volume surrounding the root of blunt V-notches*". International Journal of Fracture*, 2005. Vol. 135, pp. 161-185.

2. S. Filippi, P. Lazzarin, and R. Tovo, "Developments of some explicit formulas useful to describe elastic stress fields ahead of notches in plates*". International Journal of Solids and Structures*, 2002. Vol. 39, pp. 4543-4565.

3. M. L. Williams, "Stress singularities resulting from various boundary conditions in angular corners of plates in extension*". J. Appl. Mech.*, 1952. Vol. 19, pp. 526-528.

4. R. Gross and A. Mendelson, "Plane elastostatic analysis of V-notched plates*". Int J Fract Mech*, 1972. Vol. 8, pp. 267-276.

5. A. Seweryn, "Brittle fracture criterion for structures with sharp notches*". Engineering Fracture Mechanics*, 1994. Vol. 47, pp. 673-681.

6. A. Seweryn and A. Łukaszewicz, "Verification of brittle fracture criteria for elements with V-shaped notches*". Engineering Fracture Mechanics*, 2002. Vol. 69, pp. 1487-1510.

7. P. Lazzarin and R. Zambardi, "A finite-volume-energy based approach to predict the static and fatigue behavior of components with sharp V-shaped notches*". International Journal of Fracture*, 2001. Vol. 112, pp. 275-298.

8. Z. Yosibash, A. Bussiba, and I. Gilad, "Failure criteria for brittle elastic materials*". International Journal of Fracture*, 2004. Vol. 125, pp. 307-333.

9. P. Lazzarin, T. Lassen, and P. Livieri, "A notch stress intensity approach applied to fatigue life predictions of welded joints with different local toe geometry*". Fatigue and Fracture of Engineering Materials and Structures*, 2003. Vol. 26, pp. 49-58.

10. P. Livieri and P. Lazzarin, "Fatigue strength of steel and aluminium welded joints based on generalised stress intensity factors and local strain energy values*". International Journal of Fracture*, 2005. Vol. 133, pp. 247-276.

11. P. Lazzarin, F. Berto, and M. Zappalorto, "Rapid calculations of notch stress intensity factors based on averaged strain energy density from coarse meshes: Theoretical bases and applications*". International Journal of Fatigue*, 2010. Vol. 32, pp. 1559-1567.

12. R. D. Cook, Finite element modeling for stress analysis. 1995, New York: J. Wiley & Sons.

13. P. Lazzarin, F. Berto, F. J. Gomez, and M. Zappalorto, "Some advantages derived from the use of the strain energy density over a control volume in fatigue strength assessments of welded joints*". International Journal of Fatigue*, 2008. Vol. 30, pp. 1345-1357.

14. K. J. Bathe, *Finite element procedures in engineering analysis*. 1982, New Jersey: Prentice-Hall.

4. Main investigations

List of papers

Paper I

Notch stress intensity factors of flat plates with periodic sharp notches by using the strain energy density.
P. Lazzarin, R. Afshar, and F. Berto
Theoretical and Applied Fracture Mechanics, 2012. Vol. 60, pp. 38-50.

Paper II

Simple new expressions for the notch stress intensity factors in an array of narrow V-notches under tension.
F. Berto, P. Lazzarin, and R. Afshar
International Journal of Fracture, 2012. Vol. 176, pp. 237-244.

Paper III

Analytical expressions for the notch stress intensity factors of periodic V-notches under tension by using the strain energy density approach.
R. Afshar, F. Berto, P. Lazzarin, and L. P. Pook
Journal of Strain Analysis for Engineering Design, 2013. Vol. 48, pp. 291-305.

Paper IV

Some recent developments on the application of the strain energy density to shallow threaded plates with sharp notches.
R. Afshar and F. Berto
SDHM Structural Durability and Health Monitoring, 2013. Vol. 9, pp. 167-180.

Paper V

Stress concentration factors of periodic notches determined from the strain energy density.
R. Afshar and F. Berto
Theoretical and Applied Fracture Mechanics, 2011. Vol. 56, pp. 127-139.

Paper VI

On three-dimensional stress analysis of periodic notched plates under tension.
R. Afshar and F. Berto
Science China Physics, Mechanics & Astronomy, 2013.

Paper VII

Three-dimensional stress analysis of a plate weakened by an inclined diamond hole under various loading conditions.
R. Afshar, F. Berto, and P. Lazzarin
Lecture Notes in Engineering and Computer Science 3 LNECS , 2013, pp. 1953-1958.

Paper VIII

Three-dimensional finite element analysis of single-lap joints: effect of adhesive thickness and Poisson's ratio.
R. Afshar, F. Berto, and P. Lazzarin
Key Engineering Materials 2014. Vol. 577-578, pp. 393-396.

Paper I

Notch stress intensity factors of flat plates with periodic sharp notches by using the Strain Energy Density

Abstract: Notch Stress intensity factors (NSIFs) of a number of flat plates with periodic sharp V-notches under a remote applied normal stress are calculated. The main objective of this study is to take advantage of the local strain energy density (SED) averaged on a control volume surrounding the tip of the middle notch and estimate the NSIF of each component by using a relatively coarse mesh. The unique advantage of the SED method is the most prominent application of such a technique in the current study. A wide range of notch opening angles, relative distance between periodic notches and relative depth of the notch for different number of notches of flat plate are examined. All in all, more than three hundred models have been investigated. A new model of depth reduction factor for different ratios of relative depth of the notch is proposed to match the results from SED approach. In the case of shallow notches, the results of this study are compared with those provided by other researchers in the recent literature. In addition, based on best fit of numerical data from SED approach, some polynomials for non dimensional NSIF in the case of intermediate and deep notches are presented.

Introduction

Muskhelishvili's complex potential approach [1] was used to find stress distributions around circular, elliptical, triangular and rectangular holes in isotropic as well as in anisotropic plates [2]. The same approach was used to give stress fields and stress intensity factors (SIFs) in a variety of crack problems [3-6]. After these pioneering works, a number of publications appeared in the literature focused on cracked components. A comprehensive presentation of those solutions is given in Refs. [7-9] where one can find also the case of an infinite periodic array of equally spaced cracks under various constraint and loading conditions [9].

By proceeding on parallel tracks, a simple formula for the theoretical stress concentration factor (SCF) of periodic notches was proposed by Neuber [10] and widely applied for years to a variety of notch shapes and loading conditions; it is convenient for engineering applications, due to its simplicity and capability to give approximated values for any notch shape [11]. However, several researchers have pointed out that Neuber's formula can result in an underestimation or an overestimation of the SCF in the case of single notches [11-15] and multi-notches [16, 17],

respectively. Dealing with multi-notches under normal stress and torsion, a reformulation of Neuber's formula can be found in Refs [16, 17].

A singular integral equation of plane periodic problem of the theory of elasticity for a half plane with loaded curvilinear edge has been deduced in Ref. [18]. The singular integral has been solved numerically by the method of quadratures for various configurations of the boundary of the half plane. The stress concentration factors are computed for a half plane with sinusoidal edge and for a periodic system of rounded V-shaped notches. On the basis of these results as a limit transition the NSIFs at the tip of sharp V-shaped notches have been derived investigating the influence of the notch opening angle.

In [19] by using the same method, an elastic plane with periodic system of closely located holes has been considered to determine the SCFs and NSIFs at the rounded and sharp tips of the corresponding bilateral notches [19].

An estimation technique based on Green's function method has been used to solve the periodic notch problems of elastic half-plane in Ref. [20]. Using the Somigliana identity or the Betti's reciprocal theorem between the physical field and the field of the fundamental solution, a complex variable boundary integral equation (BIE) for the notch problem in elastic half-plane has been obtained. By using the BIE, multiple notch problems of elastic half-plane have been solved numerically.

The necessity of a simple criterion for engineering applications led to development of a point-wise strain energy density (SED) approach valid for cracks [21-24] and notches [25]. Factor S was defined as the product of the SED by a critical distance from the point of singularity [23]. Failure was thought of as controlled by a critical value S_c, whereas the direction of crack propagation was determined by imposing a minimum condition on S. The theory was extended to employ the total SED near the notch tip [25], and the point of reference was chosen to be the location on the surface of the notch, where the maximum tangential stress occurs. In small bodies a multiscaling and segmentation scheme permits to scale the SED at pico, nano and micro levels [26-28].

Following parallel tracks, the concept of SED averaged over a material-dependent control volume was formalized in Ref. [29] with reference to sharp V-shaped notches under static and fatigue loading conditions. It was demonstrated that the approach based on the concept of an

energy value averaged in a small but finite volume of material is able to accurately predict both the static behavior of severely notched components and the fatigue behavior of welded joints [29]. Further investigations were later carried out in [30-32] with the aim to extend the approach from sharp to blunt notches. To validate the approach, a large body of experimental data was considered as obtained from blunt and sharp V-notched specimens tested under tensile loading conditions [33] and mixed mode loadings [34-39].

By using the SED concept combined with a coarse meshing in FE analysis, a fatigue strength assessment of welded joints was carried out [40]. A procedure for rapid calculations of the notch stress intensity factors (NSIFs) based on the SED from coarse meshing is drawn in Ref. [41]. Refined meshes are not necessary to determine the mean value of the SED density, because this parameter can be determined via the nodal displacements, without involving their derivatives. Dealing with blunt notches, as soon as the SED is known, the theoretical stress concentrations factors (SCFs) can be determined *a posteriori* on the basis of very simple expressions linking the local SED and the SCFs in plane problems. The extension to three-dimensional cases is also possible and very convenient, in particular when edge effects are present or when a narrow spacing between collinear notches is considered.

Recently, by using the SED approach, SCFs of a number of flat plates and round bars with periodic U- and V-notches have been evaluated [42] considering tension, bending and torsion loading conditions. A large bulk of results from systematic FE simulations has been provided, varying notch acuity and relative frequency of periodic U- and blunt V-notches. In addition, two new expressions for the notch depth reduction factor for the case of normal stresses (tension and bending) and torsion have also been proposed based on best fit of the results from the SED-based approach [42].

In this study, the variability of the NSIFs of periodic sharp V-notches is investigated by means of SED used in combination with coarse meshes. A number of flat plates weakened by periodic sharp V-notches subjected to tensile loading are considered with the aim to study the NSIFs in the frame of linear elastic hypotheses.

The main aims of this paper are then as follows:

- to evaluate the local SED on the control volume surrounding the tip of middle notch of periodic-notched components and estimate the relevant NSIF by using FE models with relatively coarse meshes.

- to investigate the effect of the notch opening angle, relative depth of the notch and relative distance between periodic notches on NSIF and compare the results with the equations available in the literature for periodic sharp notches and in particular with the expressions proposed in Ref. [18].
- to present a large bulk of analyses, ranging from small to large opening angle, shallow to deep notches as well as narrow to large spacing of collinear notches.

1. Modeling of periodic notches

The geometries considered in the present investigation as well as the main geometrical parameters are shown in Fig. 1. Different values of the notch-opening angle, 2α, the relative distance between the periodic notches, a/t, and relative depth of the notch, t/d, have been considered in the analyses. The variation of relative depth of the notch is illustrated in Fig. 2. More than 300 different geometries of flat plates have been analyzed by combining the following values of the above-mentioned parameters:

- 2α=30, 45, 60, 90, 120, 135, 160 and 170 degrees;
- a/t=0.0, 0.1, 1.0, 2.0, 5.0, ∞;
- t/d=0.025, 0.05, 0.1, 0.2.

Due to the double symmetry characterizing all plates, only one quarter of the geometry has been modeled. In addition, to investigate the effect of number of notches, N, on the NSIF of the middle notch, two limit cases with N=3 and 30 have been analyzed.
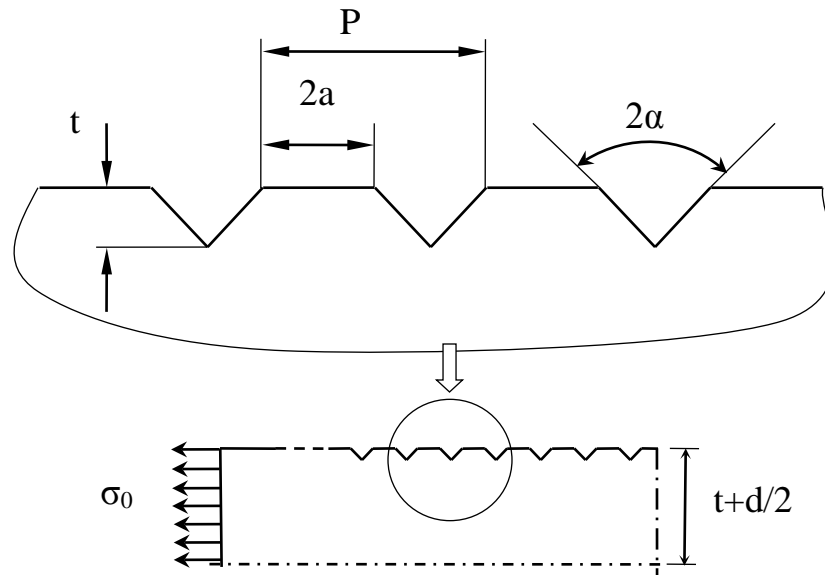
Fig. 1. Schematic of the plates with periodic notch and geometrical parameters.
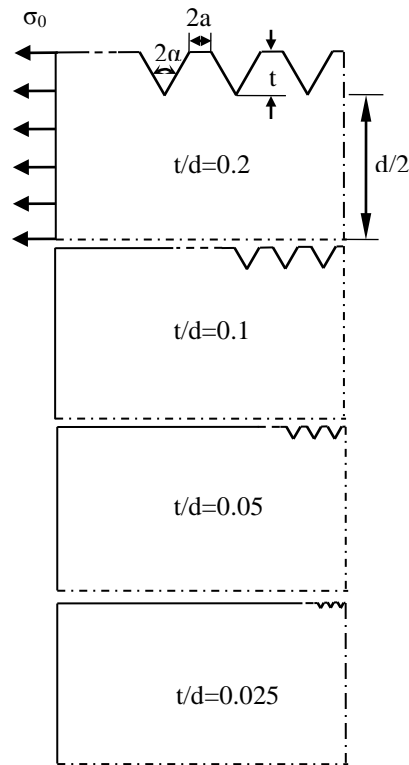
Fig. 2. Different values of relative depth of the notch (t/d) (d=constant=100 mm; t=2.5, 5, 10 and 20 mm; σ_0=100 MPa in all cases)

2. Modeling and SED evaluation

The code ANSYS is used to perform the Finite Element Analyses (FEA). Material is assumed as isotropic and linear elastic with a Young's modulus E=5000 MPa (which is typical of PMMA) and a Poisson's ratio ν=0.3. The 8-nodes iso-parametric element plane 82, with plane strain key-option, is used for the flat plates subjected to tensile loading. To reduce the computational error, a subroutine based on ANSYS parametric design language (APDL) is developed, which allows us to generate different geometries by simply changing the geometrical ratios as defined in the previous section.

The result of applying the tension loading is discussed below.

The elastic deformation energy E_1, averaged on the control area shown in Fig. 3 is:

$$\overline{W} = \frac{E_1}{\Omega} = \frac{e_1}{E} \cdot \left(\frac{K_1}{R_0^{1-\lambda_1}} \right)^2 + \frac{e_2}{E} \cdot \left(\frac{K_2}{R_0^{1-\lambda_2}} \right)^2 \tag{1}$$

where K_1 and K_2 are the mode I and mode II NSIFs according to Ref. [43], E is the Young's modulus, λ_1 and λ_2 are Williams' eigenvalues [44]; finally, e_1 and e_2 are two parameters which depend on the notch opening angle and the Poisson's ratio ν [29].

Under mode I loading, Eq.(1) simplifies and becomes

$$\overline{W} = \frac{e_1}{E} \cdot \left(\frac{K_1}{R_0^{1-\lambda_1}} \right)^2 \tag{2}$$

where e_1 is according to the expression

$$e_1(2\alpha) = \frac{I_1}{4\lambda_1 \gamma} \tag{3}$$

Parameters I_1, λ_1 and γ are listed in Table 1 for three values of the Poisson's ratio, ν.

Table 1. Values of λ_1 and I_1 for sharp V-notches, as a function of the notch angle and the Poisson's ratio [29].

2α (degrees)	γ/π (rad)	λ_1	I_1		
			$v=0.30$	$v=0.35$	$v=0.40$
0	1	0.5000	0.8450	0.7425	0.6300
15	23/24	0.5002	0.8431	0.7416	0.6303
30	11/12	0.5014	0.8366	0.7382	0.6301
45	7/8	0.5050	0.8247	0.7311	0.6282
60	5/6	0.5122	0.8066	0.7194	0.6235
75	19/24	0.5247	0.7819	0.7026	0.6152
90	3/4	0.5445	0.7504	0.6801	0.6024
105	17/24	0.5739	0.7124	0.6519	0.5849
120	2/3	0.6157	0.6687	0.6184	0.5624
135	5/8	0.6736	0.6201	0.5796	0.5344
150	7/12	0.7520	0.5678	0.5366	0.5013
160	5/9	0.8187	0.5315	0.5058	0.4767
170	19/36	0.9000	0.4957	0.4755	0.4523

The optimum value of the radius R_0, which varies from material to material, can be determined by tests from sharp V-notched plates [29] or directly from the fracture toughness of cracked plates. In the following, for sake of simplicity, R_0 is kept constant and equal to 0.1 mm.

In the instance of negligible effect of mode II, the NSIF can be directly correlated to the mean value of the energy $\overline{W}$ by simply inverting Eq. (2):

$$K_1 = \sqrt{\frac{4E\lambda_1\gamma}{I_1} \cdot \overline{W}} \cdot R_0^{(1-\lambda_1)} = \sqrt{\frac{E\overline{W}}{e_1}} \cdot R_0^{(1-\lambda_1)} \tag{4}$$
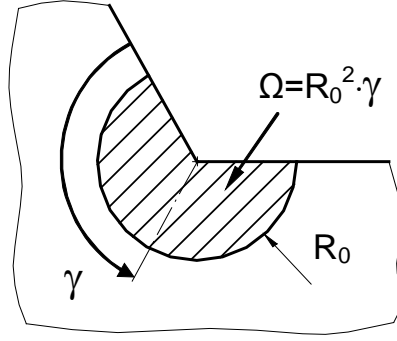
Fig. 3. Control volume (area) surrounding the notch tip [29].

The value $\overline{W}$ is almost independent of the mesh pattern as discussed in Refs [40, 41] and can accurately be determined also by means of coarse meshes. However, a regular mesh pattern is recommended, in particular for small notch opening angles ($2\alpha \leq 45^{\circ}$) and small distances between periodic notches (a/t=0.0, i.e. narrow notches). As soon as the elastic Strain Energy E_1 is numerically determined on the control area Ω in the middle notch (*via* the SENE command of ANSYS code), the mean energy density $\overline{W}$ is obtained by simply dividing the total E_1 by the control area (Fig. 3). R_0 is assumed constant and equal to 0.1 mm in all the FE models.

Mode I NSIFs can be determined directly from the hoop stress component σ_θ ahead of the V-notch tip, along the notch bisector line, as shown in Fig. 4 by using a double logarithmic scale. A convenient expression is [43]:

$$K_1 = \sqrt{2\pi} \lim_{r \to 0} \sigma_\theta(r, \theta = 0) \times r^{1-\lambda_1} \tag{5}$$

where the radial distance r is measured along the notch bisector line.

The direct use of Eq. (5) is possible only with very fine meshes. A best fit of numerical data allows the evaluation of the stress gradients $1-\lambda_1$, which match the theoretical solution [44], within a relative deviation less than 1%, and the intensity of the stress fields.
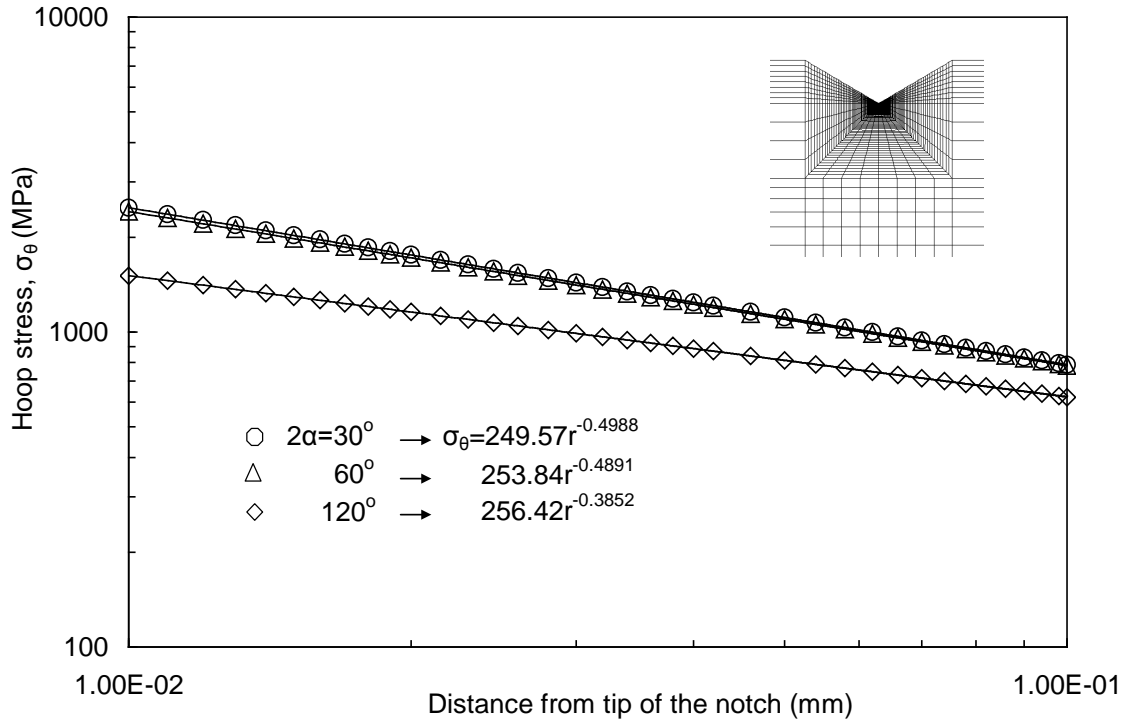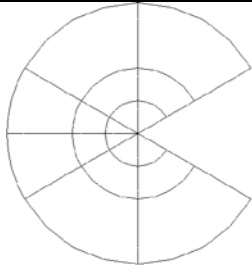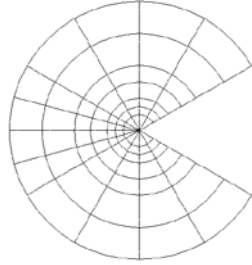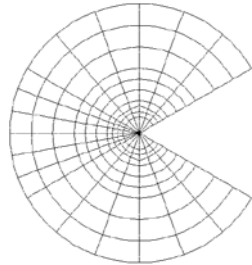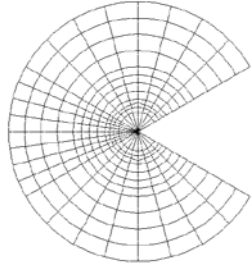
Fig. 4. Plots of hoop stress along the V-notch bisector line as obtained from very fine meshes; single notch for different opening angles 2α, (t=10 mm, d=100 mm, nominal stress=100 MPa)

In order to show the versatility of the SED approach in term of mesh density of the control volume (Ω), the mean values of SED for the case of periodic V-notches $2\alpha=60^{o}$, t/d=0.025 and a/t=1.0 are listed in Table 2 (N=30). The results from the regular and coarse mesh shown in Fig. 5 are compared with those from refined meshes like those previously used to determine the local hoop stress distributions in Fig. 4.

Table 2. Mean values of SED from fine and coarse meshes; periodic notches with 2α=60°.
Geometrical ratios t/d=0.025 and a/t=1.0. Material with E=5000 MPa, ν=0.30. Number of notches N=30

Total Number of FE	Number of FE inside control volume	Control volume $R_0 = 0.1$ mm	W	K_1	ΔW (%)	ΔK_1 (%)
1699	18		0.367775	222.22	6.96	3.42
6588	84		0.348519	216.33	1.36	0.68
14688	180		0.344544	215.09	0.21	0.11
26017	288		0.343826	214.86	–	–
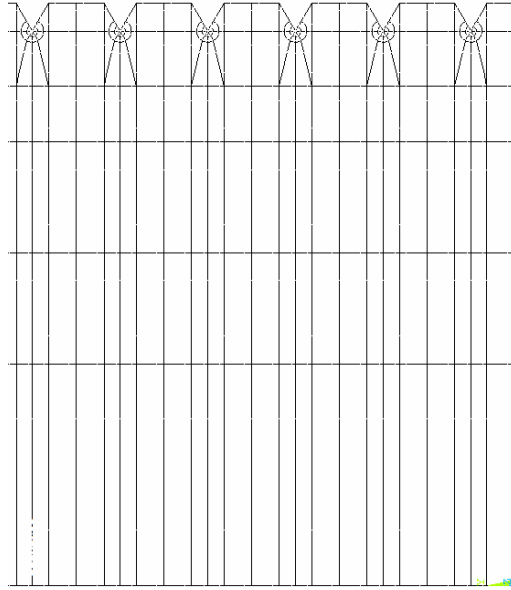
Fig. 5. Coarse mesh pattern, with 18 elements inside the control volume Ω (t/d=0.025; a/t=1.0)

3. Edge effect of periodic notches

Different mesh densities were applied to confirm the versatility of the SED approach, considering both single notches as well as periodic notches of the same length, being here the notch frequency t/P=0.2. Furthermore, in order to analyses the edge effect, the NSIFs of three notches in the symmetric model (Fig. 6) are evaluated and the results are given in Table 3.

A good agreement is found between the K_1 values based on the SED approach (with coarse meshes) and those based on the hoop stress from very refined meshes. The relative deviation is always less than 5%.

(a) Periodic notches   t+d/2   (b) Single notch
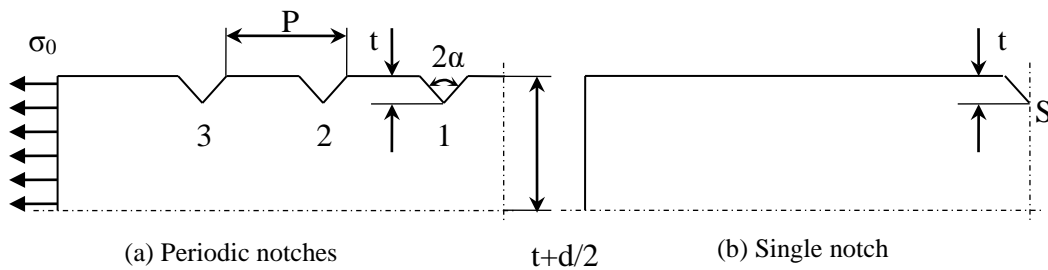
Fig. 6. Schematic of N=3 periodic notches (a) and single notch (b) in a plate of the same length.

Table 3. Values of the NSIF for different notch locations (S: single notch, P1, P2, P3: periodic notch at notch locations 1, 2 and 3) for the case of t/P=0.2.

	K_1 from fine meshes				K_1 from coarse meshes (SED-based calculations)				$\Delta\%$ S	$\Delta\%$ P-1	$\Delta\%$ P-2	$\Delta\%$ P-3
2α	S	P-1	P-2	P-3	S	P-1	P-2	P-3				
30	645.0	570.0	570.0	640.0	626.5	545.2	548.1	615.9	-2.87	-4.36	-3.84	-3.75
60	655.0	563.0	566.0	634.0	641.7	558.8	561.6	630.2	-2.03	-0.74	-0.78	-0.60
90	666.0	584.0	587.0	659.0	658.1	572.3	574.8	644.9	-1.19	-2.00	-2.07	-2.13
120	650.0	558.0	571.0	645.0	654.2	563.9	564.4	635.7	0.65	1.07	-1.16	-1.45
135	615.0	536.0	538.0	610.0	609.7	531.2	533.6	605.3	-0.87	-0.90	-0.81	-0.77

A comparison between periodic sharp notches and single notch is carried out to show the edge effect. A previous study by authors [42] on periodic blunt-notched components indicated that the SED-based calculations in the middle of the array of about 10 notches were accurate enough to estimate the SCFs in the case of periodic blunt-notches. In the present work, in order to better understand the factors related to the edge effect, a number of models are investigated increasing the number of V-notches as a function of the notch opening angle and their relative distance. It is found that the edge effect depends not only on the number of notches but also on the relative distance and the notch opening angle. Varying the opening angle (2α) and the distance a/t, a different number of notches (N) is necessary to eliminate the edge effect. The rule of thumb can be stated as: for the same distance of periodic notches, the smaller is the opening angle, the higher the number of notches is. For instance, Fig. 7 shows that when a/t=0.1 and $2\alpha=30^\circ$, N, the minimum number of notches influenced by the edge effect is 13, whereas we have N=7 for $2\alpha=60^\circ$ and N=5 for $2\alpha=120^\circ$ and 135°.
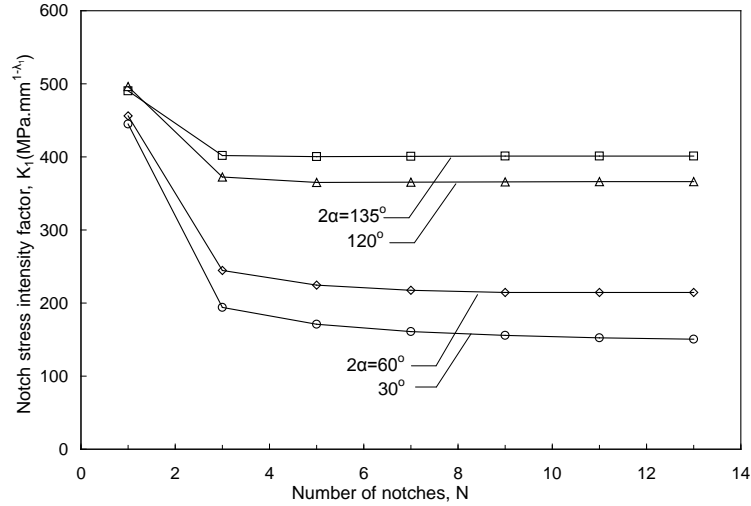
Fig. 7. Convergence of NSIF related to the middle notch as a function of number of notches; models with a/t=0.1 and t/d=0.05.

The first simple equation for evaluation of the SCF in a model with periodic notches by using an equivalent single notch with a reduced depth was proposed in Ref. [10] (see Figure 8). According to Neuber's equation, the factor γ quantifying the reduced depth t* depends only on the frequency of the periodic notch, t/P. The reduced depth, t* turns out to be:

$$t^*=\gamma t \tag{6}$$

With the aim to find the equivalent single notch of periodic sharp-notched component, Neuber's depth reduction factor [10] is also applied, but no direct link based on the frequency of periodic notches is found. This can be explained by the influence of the notch opening angle on the NSIF, different from the periodic blunt notch cases, where the notch opening angle has a negligible effect on the SCF [42]. Furthermore, the Neuber's depth reduction factor was proposed for the case of sharp shallow notches under shear stress [10, 17].

Hence, firstly, in order to avoid any possible edge effect, influenced by the number of notches, N=30 considered hereafter for all the cases. Secondly, periodic notched components with three opening angles 2α=30º, 60º and 120°, are selected in order to find the equivalent single notched components of the same length but reduced depth (Fig. 8).

(a) Periodic notches $t+d/2$ (b) Single notch
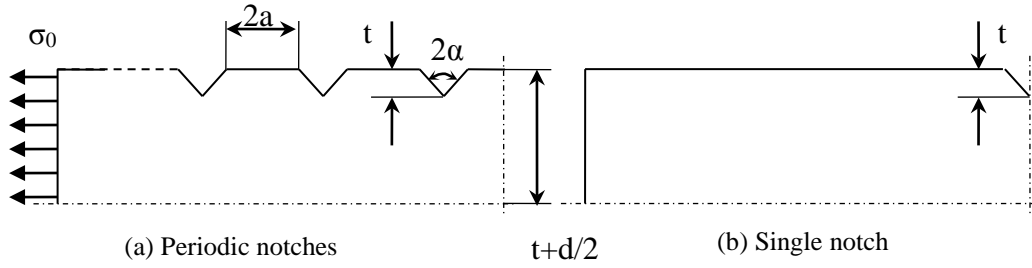
Fig. 8. Schematic of plate with N=30 periodic notches (a) and single notch of reduced depth in a plate with the same length (b).

Based on a best fit of numerical data related to different relative distances between the periodic notches (a/t), a Weibull function for the depth reduction factor is in the form:

$$\gamma = a_0 - b e^{-c(\frac{a}{t})^d} \tag{7}$$

where coefficients a_0, b, c and d depend on the opening angle (2α) and the relative depth of the notch (t/d), (see Table 4). By using these coefficients, the average difference in terms of NSIF between periodic notches and equivalent single notch remains always within the limit of 5%.

Table 4. Coefficients of Eq. (7) for three opening angles ($2\alpha=30^{\circ}$, 60° and 120°) and different t/d.

t/d	$2\alpha=30^{\circ}$				60°			
	a_0	b	c	d	a_0	b	c	d
0.025	9.96E-01	8.98E-01	3.46E-01	1.18E+00	9.95E-01	8.37E-01	3.67E-01	1.14E+00
0.05	9.97E-01	9.14E-01	3.64E-01	1.15E+00	1.01E+00	8.28E-01	3.94E-01	1.36E+00
0.1	1.00E+00	8.95E-01	4.23E-01	1.36E+00	1.00E+00	7.95E-01	5.08E-01	1.33E+00
0.2	9.96E-01	8.58E-01	6.61E-01	1.40E+00	9.96E-01	7.21E-01	7.41E-01	1.43E+00

t/d	$2\alpha=120^{\circ}$			
	a_0	b	c	d
0.025	9.96E-01	6.02E-01	4.51E-01	9.21E-01
0.05	9.97E-01	5.65E-01	4.83E-01	1.06E+00
0.1	9.98E-01	4.95E-01	7.03E-01	1.18E+00
0.2	9.97E-01	3.13E-01	1.20E+00	1.48E+00

4. Results and discussions

In this section, the results of all the geometrical models are presented together with a comparison with the values given in Ref. [18]. The middle notch is systematically considered for mean SED calculations, as already shown in Fig. 3. The number of total notches N has been varied from case to case to obtain the plateau value shown in Figure 7. The SED approach has been applied, taking advantage of a regular coarse mesh in the vicinity of the V-notch tip.

Table 5 summarize the NSIF values for different notch opening angle ($2\alpha=30^o$-170°) in a wide range of relative distances between periodic notches.

Table 5. NSIF values for different notch opening angle ($2\alpha=30^o$-170°) in the wide range of relative distances between periodic notches (a/t=0.0-∞) for the case of t/d=0.1 (d=100 mm, nominal stress 100 MPa; coarse mesh).

a/t	$2\alpha=30^o$	45°	60°	90°	120°	135°	150°	160°	170°
	NSIF K_1 (MPa mm$^{1-\lambda_1}$)								
0.0	193.5	243.9	293.8	399.6	499.8	526.8	514.8	470.8	386.2
0.1	226.2	270.6	316.3	415.9	509.3	532.5	517.1	471.3	386.2
1	409.3	436.7	467.5	531.5	576.9	573.4	533.20	474.6	385.9
2	528.8	545.5	564.7	602.5	617.4	597.6	541.8	475.7	385.8
5	622.5	629.1	638.4	655.6	646.5	613.3	545.3	474.9	385.6
∞	625.5	631.9	640.2	656.2	645.7	612.1	544.3	474.9	385.6

It can be seen from Table 5 that the NSIF increases as a/t increases reaching a maximum value for a/t=5. For a/t=∞ there is a very small decrement (less than 0.5%) but this should be simply due to numerical errors. It is also evident that the variation of the NSIF as a function of a/t strongly depends on the opening angle. The greatest variation is for the minimum opening angle, as expected; for opening angles $2\alpha \geq 150^o$ the NSIF is almost independent on the a/t ratio.

Since the NSIFs depends the absolute dimension of the notch and the plates, it is surely convenient to normalize its value as a function of the notch size. Some preliminary considerations might be useful. It is well known that two notched plates scaled in geometrical

proportion have the same theoretical stress concentration since it simply depends on the geometrical ratios, i.e. notch depth to plate width ratio. Consider now two plates weakened by sharp V-notches, plates and notches in geometric proportion, the corresponding NSIF is different and can be quantified by means of the simple expression [45-47]:

$$K_1 = k_1 \sigma_0 t^{1-\lambda_1} \tag{8}$$

where σ_0 is the reference stress (e.g., the remote tensile stress), $1-\lambda_1$ is the stress singularity in the close vicinity of the notch tip and k_1 is a nondimensional shape factor. In the case of periodic notches the shape factor k_1 does depend on the geometrical ratios t/d and a/t. Table 6 gives the NSIFs and the shape factor k_1 for some plates with a/t=0.1 and t/d=0.025. In addition, the normalized NSIFs of the data presented in Table 6 as a function of depth of the notch (t) is shown in Fig. 9, where the shape factor k_1 clearly appears as the coefficient of the power function.

Table 6. Notch stress intensity factors as a function of depth of the notch (t) with constant relative depth (t/d=0.025) for a plate with periodic notches of 2α=60° and a/t=0.1 (1-λ_1=0.4878).

t (mm)	d (mm)	t/d	K_1 MPa mm$^{0.4878}$	Shape factor k_i
0.250	10	0.025	46.664	0.9176
0.625	25	0.025	72.962	0.9176
2.5	100	0.025	143.476	0.9176
10	400	0.025	282.140	0.9176
25	1000	0.025	441.144	0.9176
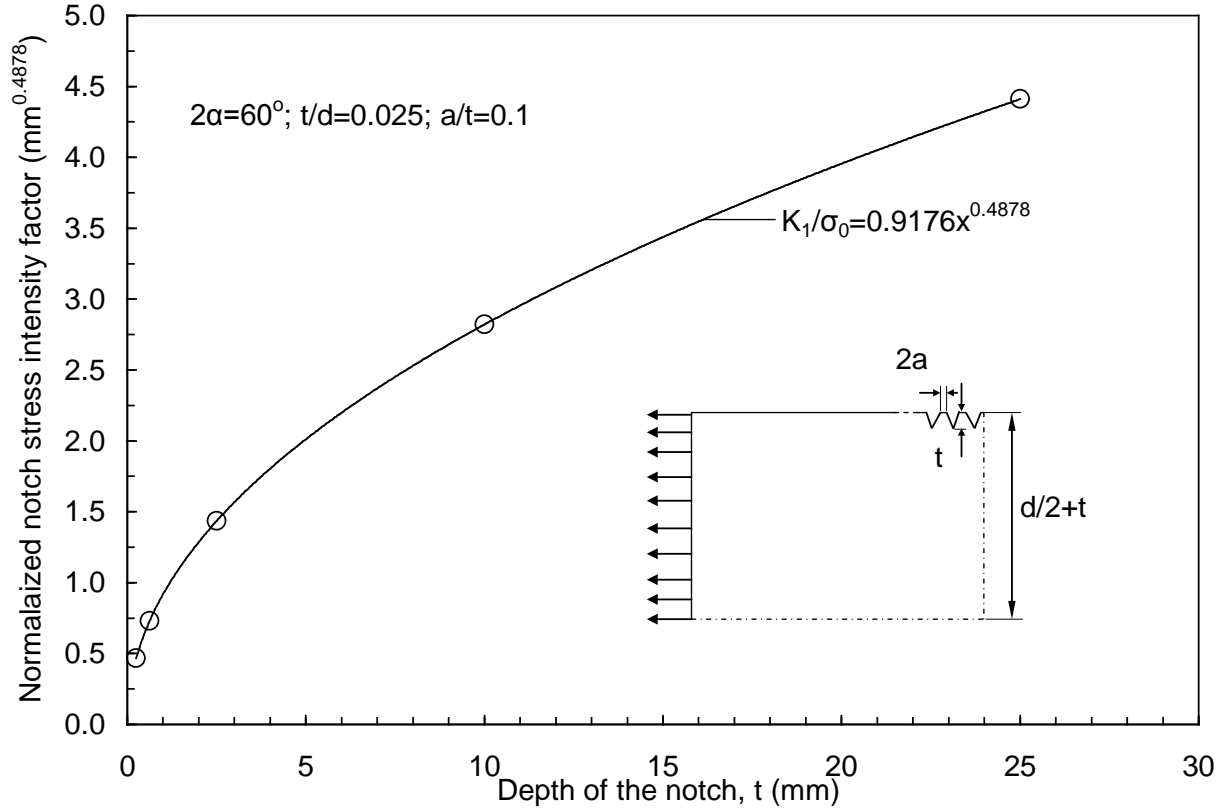
Fig. 9. Normalized notch stress intensity factor as a function of notch depth with constant relative depth (t/d=0.025); plate with periodic notches with $2\alpha=60^{o}$ and a/t=0.1 (scale effect).

In order to perform an explicit comparison with theoretical values reported in Ref. [18], the dimensionless NSIF, F_I^V , in the following is calculated according to the following expression [18]:

$$F_I^V = \frac{K_1}{\sigma_0 t^{1-\lambda_1} \sqrt{\pi}}$$

(9)

where the only variation with respect to Eq. (5) is the term $\sqrt{\pi}$. It should be noted that when the opening angle is $2\alpha=180°$, any stress gradient disappears and Eq.(9) simply gives $\sqrt{2}$. This value will appear on the right hand side of the diagrams for F_I^V reported hereafter.

4.1 Shallow notches: models with t/d=0.025

Fig. 10 shows the variation of the dimensionless NSIF as a function of the notch opening angle varying the relative distance a/t. Here the relative notch depth assumes its minimum values, t/d=0.025, in order to make possible a comparison in engineering terms with the results reported in Ref [18], all related to the case of periodic notches in a semi-infinite plate (a/t→0).
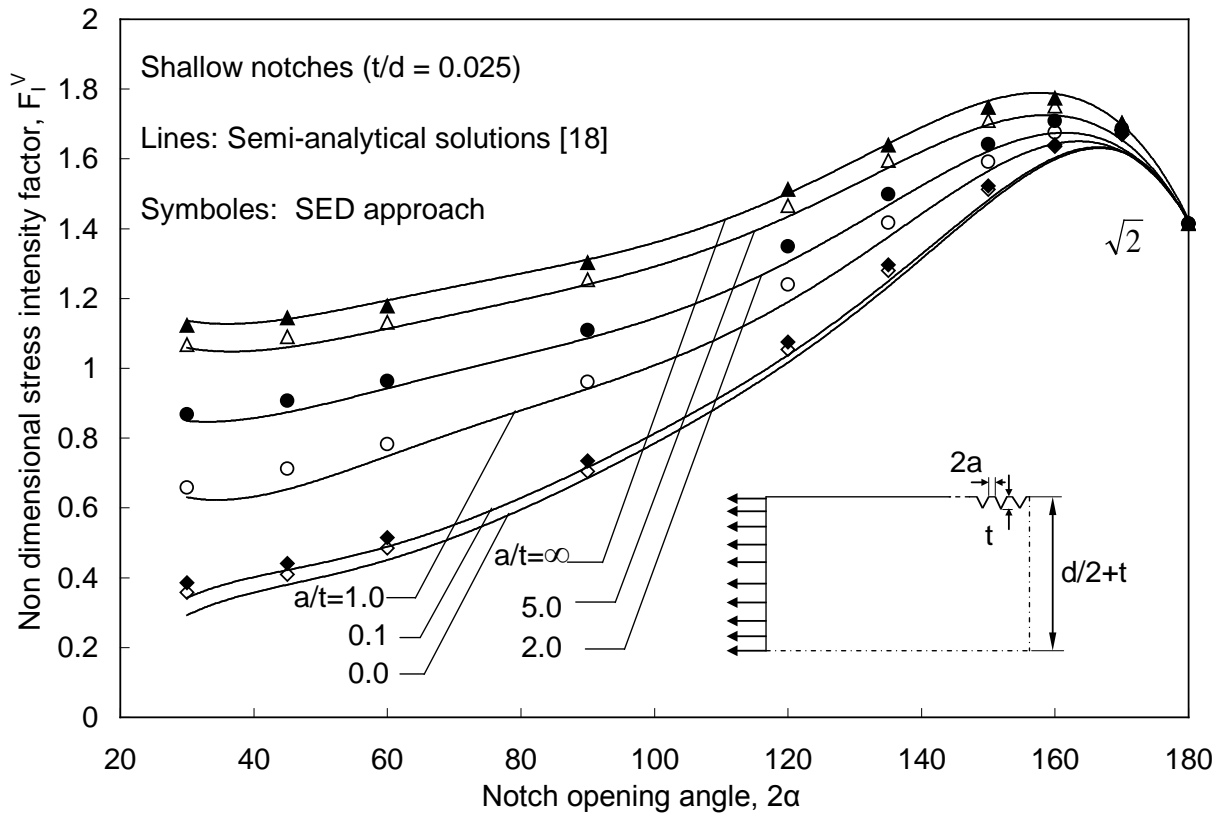
Fig. 10. Variation of dimensionless NSIF with notch opening angle for the modes with t/d=0.025; comparison with data reported in Ref. [18] for periodic notches in infinite plate.

Fig. 10 shows a very good agreement between the present results and those reported in the literature for the infinite plate problem. To make possible a more direct comparison all data are listed also in Table 7. The mean relative deviations for different distances between periodic notches with a/t=0.0, 0.1, 1.0, 2.0, 5.0 and ∞ are: 3.81±6.89, 3.54±3.23, 3.07±0.70, 2.39±0.35,

1.62±0.48 and -0.3±0.29, respectively. It is clear that the relative deviations decrease as the notch opening angle and the a/t ratio increase.

Table 7. Dimensionless NSIF (F_I^V) for various relative distances between periodic notches (a/t=0.0, 0.1, 1.0, 2.0, 5.0 and ∞) and comparison with Ref. [18] for the case of t/d=0.025.

2α (°)	F_I^V											
	[18] a/t=0.0	SED 0.0	[18] 0.1	SED 0.1	[18] 1.0	SED 1.0	[18] 2.0	SED 2.0	[18] 5.0	SED 5.0	[18] ∞	SED ∞
30	0.294	0.359	0.344	0.385	0.630	0.658	0.846	0.869	1.057	1.068	1.133	1.123
45	0.374	0.409	0.416	0.440		0.712	0.885	0.908	1.065	1.090	1.152	1.144
60	0.459	0.485	0.497	0.515	0.752	0.782	0.933	0.964	1.111	1.132	1.186	1.179
90	0.679	0.705	0.710	0.735	0.931	0.960	1.084	1.110	1.234	1.254	1.308	1.303
120	1.02	1.054	1.041	1.076	1.206	1.241	1.318	1.349	1.450	1.465	1.516	1.513
135	1.239	1.280	1.255	1.296	1.376	1.417	1.465	1.499	1.568	1.595	1.642	1.639
150	1.468	1.513	1.477	1.522	1.548	1.591	1.606	1.642	1.689	1.710	1.749	1.747
160	1.59	1.636	1.595	1.640	1.637	1.676	1.669	1.708	1.717	1.751	1.777	1.774
170	1.632	1.670	1.634	1.671	1.645	1.680	1.654	1.688	1.675	1.702	1.727	1.702
180	1.414	1.414	1.414	1.414	1.414	1.414	1.414	1.414	1.414	1.414	1.414	1.414

4.2 Intermediate notches: cases t/d=0.05 and t/d=0.1

Figure 11 shows the variation of dimensionless NSIF for the case of t/d=0.05.
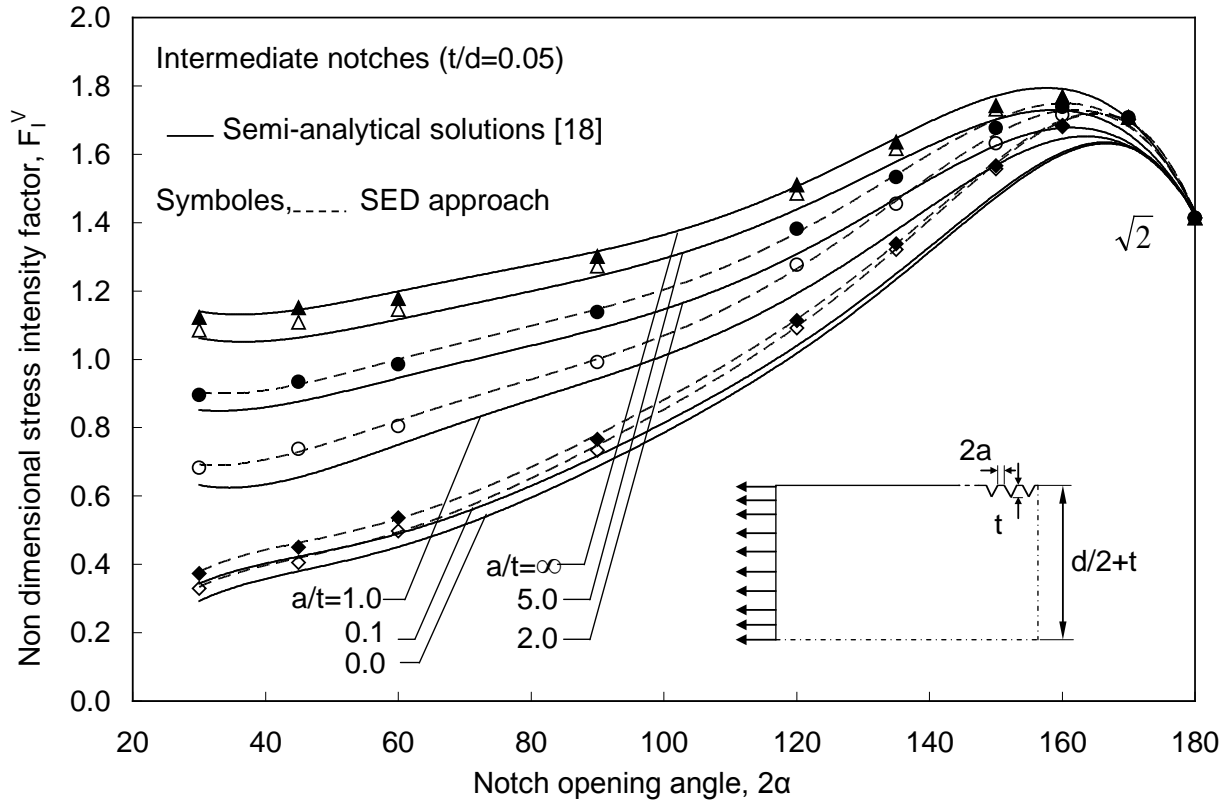
Fig. 11. Variation of dimensionless NSIF with notch opening angle for the models with t/d=0.05; comparison with data reported in Ref. [18] for the infinite plate case.

It is clear that increasing the relative depth t/d from 0.025 to 0.05 the difference between the data of the present work and those reported in Ref. [18] increases. It is no longer possible to consider as infinite the plate with respect to notch depth. The mean difference related to the cases with a/t=0.0, 0.1, 1.0, 2.0, 5.0 and ∞ becomes large and equal to 8.19±1.90, 7.91±0.78, 6.47±1.09, 5.24±0.50, 3.12±0.56 and -0.46±0.28, respectively.

Results for narrow V-notches with a/t=0, the most critical geometry, are reported in Table 8. Here the comparison is between the NSIFs obtained from coarse and fine meshes. The maximum detected error is less than 2%.

Finally Figure 12 shows the variation of dimensionless NSIF for the case of t/d=0.1 mm.
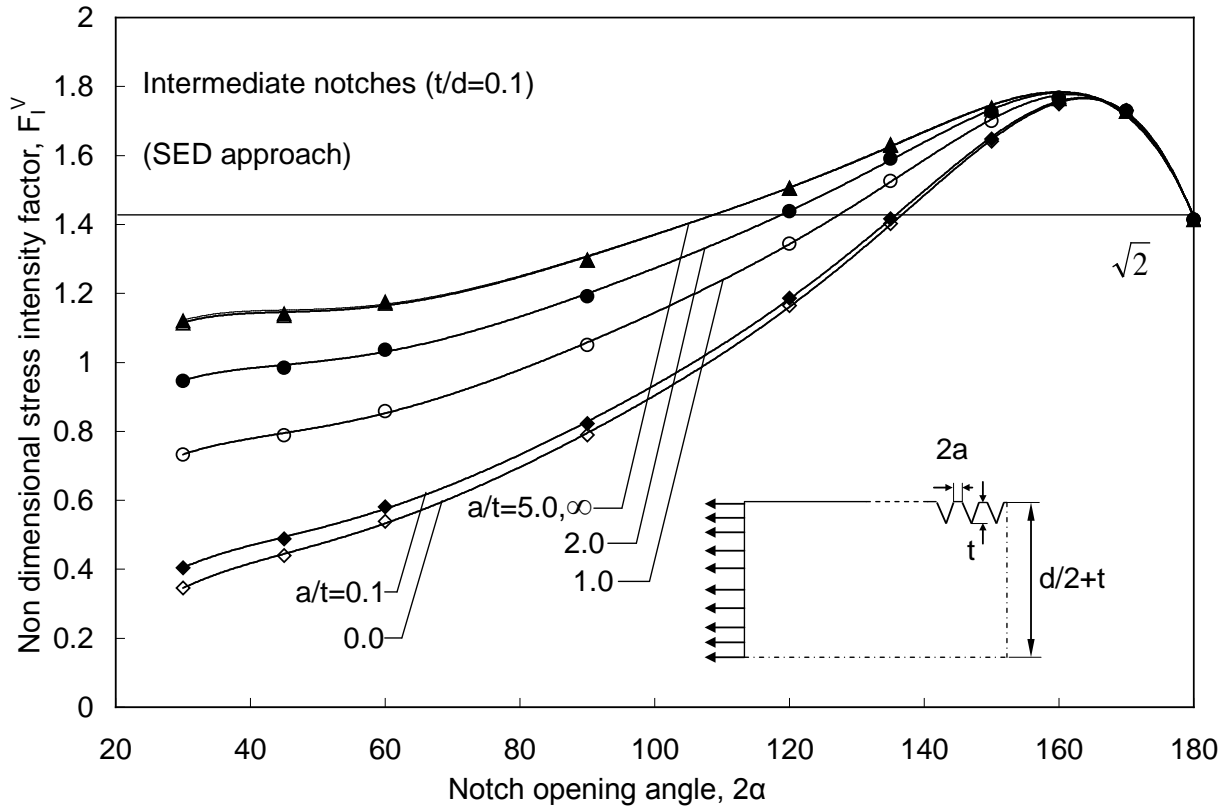
Fig. 12. Variation of dimensionless NSIF with notch opening angle for models with t/d=0.1.

The numerical data of Figures 11 and 12 have been interpolated by using the polynomial form as depicted in appendix.

Table 8. Comparison between fine and coarse mesh-based results; SED approach applied to the models with narrow periodic notches, a/t=0.0, (t/d=0.05).

2α	F_I^V (coarse mesh)	F_I^V (fine mesh)	$\Delta\%$
30	0.329	0.333	-1.06
45	0.405	0.411	-1.56
60	0.498	0.498	-0.17
90	0.734	0.730	0.58
120	1.092	1.090	0.14
135	1.322	1.323	-0.07

4.3 Deep notches: models with t/d=0.2

Fig. 13 the dimensionless NSIF as a function of the notch opening angle for the case of t/d=0.2 in a wide range of relative distances between periodic notches. The corresponding polynomials are given in the Appendix, see Table A.3.
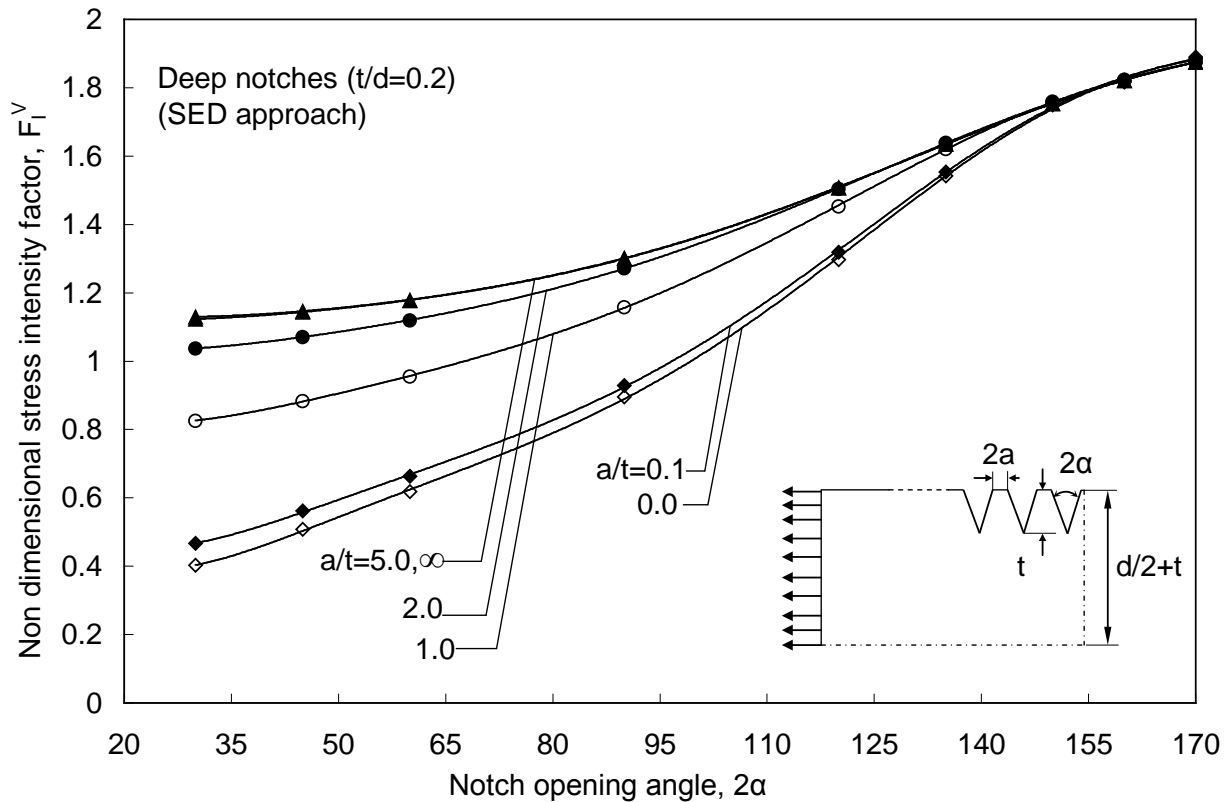
Fig. 13. Variation of dimensionless NSIF with notch opening angle for models with t/d=0.2.

5. Notch reduction factor

On the basis of the present results it is possible to provide three useful diagrams for depth reduction factor, γ for different notch opening angles (2α= 30°, 60° and 120°) and for different ratios of the notch depth over the plate width (t/d) as defined in Eq. (6) (see Figures 14-16). As discussed above a Weibull function for the depth reduction factor is suitable to describe the trend by updating the coefficients according to Table 4. The values of γ are compared with those provided in Refs [10] and [16] which are, up to now, the only available results.
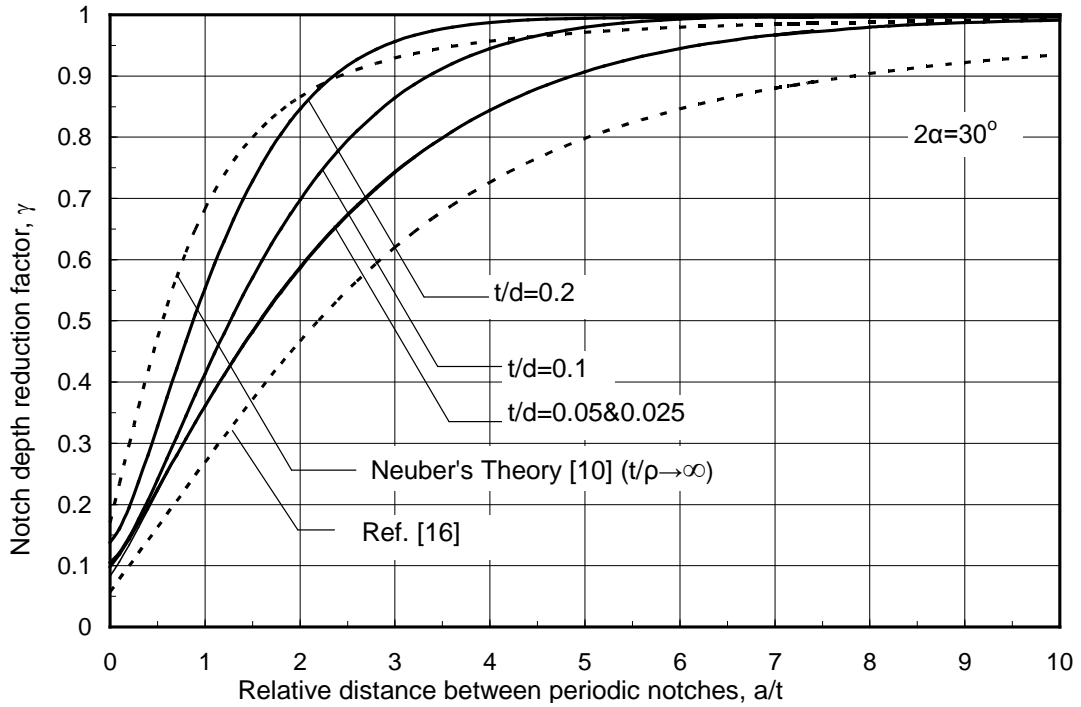
Fig. 14 Plots of notch depth reduction factor, γ, used to convert periodic notches into a single notch; case of 2α=30º.
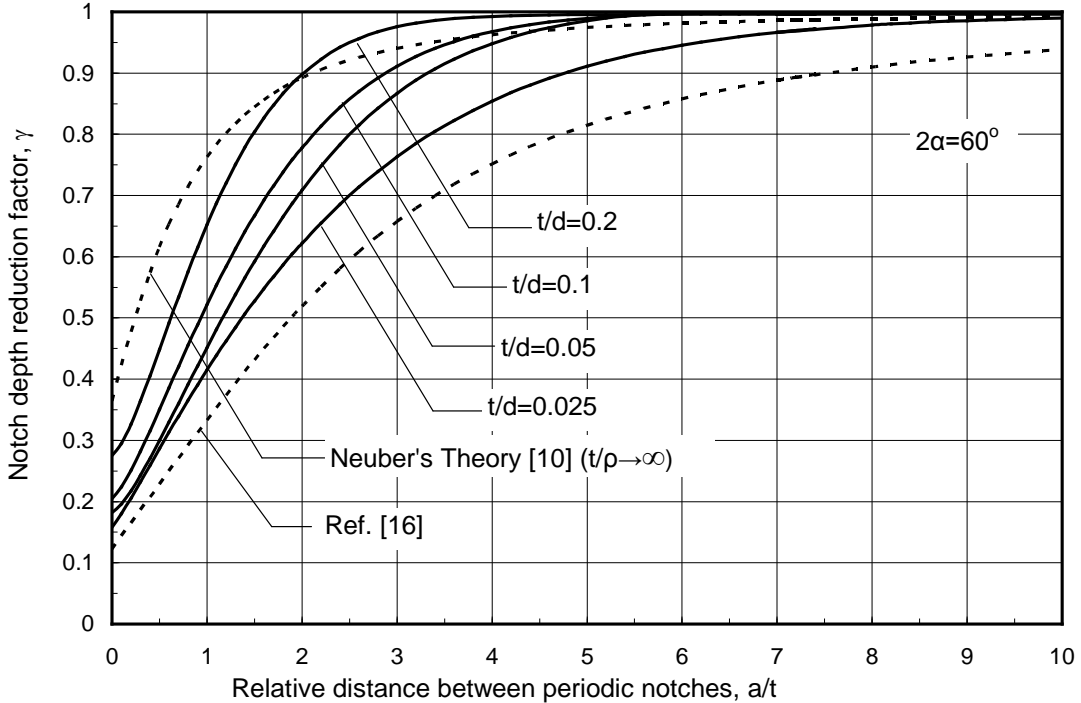
Fig. 15 Plots of the notch depth reduction factor, γ, used to convert periodic notches into a single notch; case of 2α=60º.
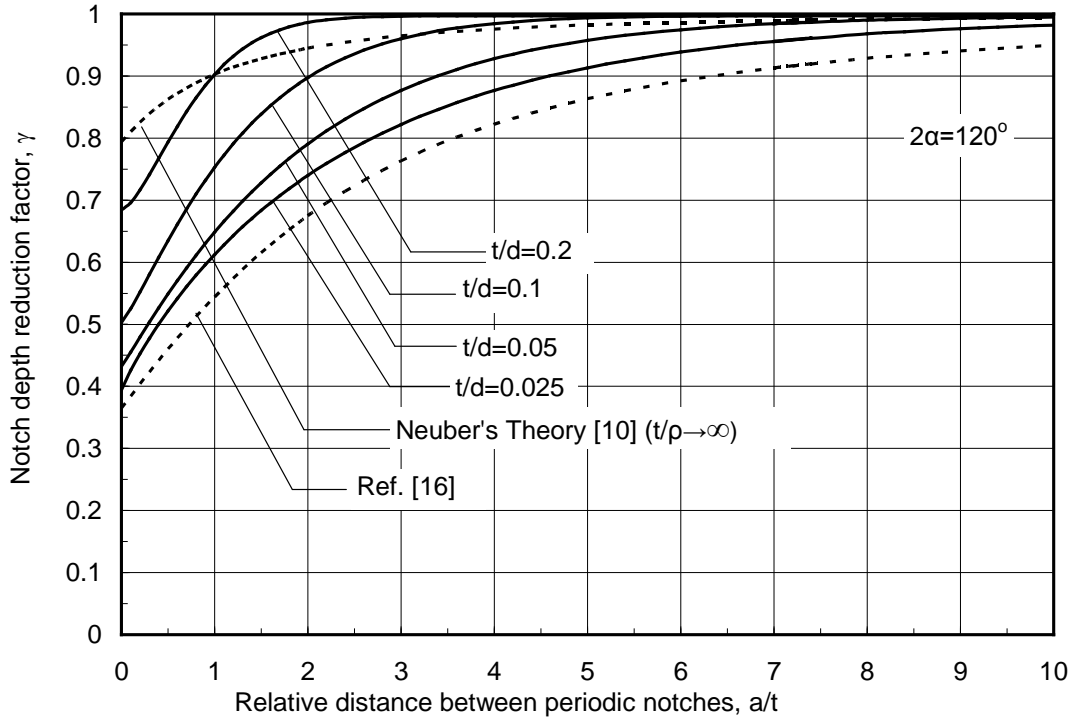
Fig. 16 Plots of the notch depth reduction factor, γ, used to convert periodic notches into a single notch; case of 2α=120°.

In particular the results provided in [10] have been sometimes used outside their range of applicability. In fact it has been applied to notches of varying acuity, without any distinction between sharp and blunt notches. Some very useful guidelines on the use of γ have been provided first in Ref. [16], where it was demonstrated that the original formulation should be limited only to sharp notches whereas a new formulation of the notch reduction factor was proposed for blunt notches. It is interesting to observe that the trend of the reduction factor provided in [16] is quite close to the case t/d = 0.025 and then, as a first approximation, it is applicable also not only to blunt notches but also to shallow sharp notches.

6. Arrays of edge cracks

A system of multiple, equal length edge cracks of depth t and spacing 2a have been considered in a plate of infinite width [48, 49]. The variation of the stress intensity factor normalized by $K_0 = \sigma\sqrt{a}$ is plotted as a function of s=t/(t+a) (see Figure 17). The stress intensity factor is given according to the expression:

$$K_I = F_{I1}(s)\sigma_n\sqrt{\pi t} \tag{10}$$
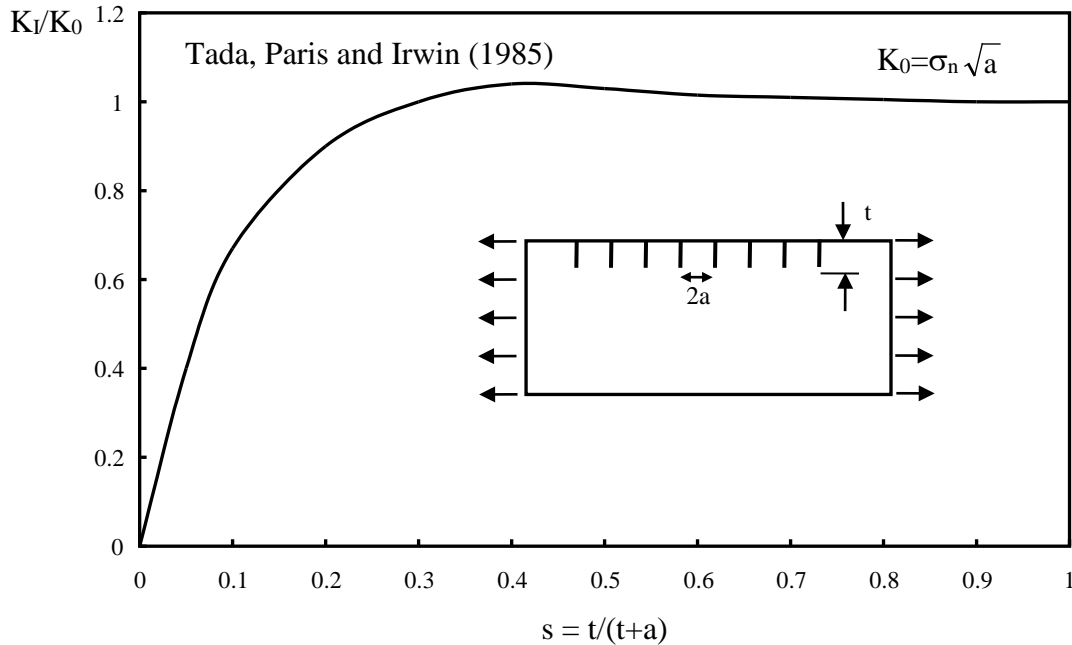
Fig. 17 Tada's diagram for periodic edge cracks

From Figure 17 it is evident that when the cracks become narrow $(s \to 1)$ the ratio between K_I and K_0 tends to 1 and the stress intensity factor depends only on the semi-spacing, a.

Table 9 shows a comparison between the values of F_{I1} from [48] and those obtained by using the SED combined with both a coarse and a fine mesh pattern. Although the diagram by Tada et al. is valid for an infinite plate, the comparison is carried out for different values of t/d, which ranges from 0.0125 to 0.1. As expected, for shallow cracks (i.e. small values of t/d) the agreement between Ref. [48] and the results from SED is very good. A problem occurs for narrow cracks (s=0. 909). In that case the agreement is sound only if a large number of cracks (more than 200) are considered in the FE model. This means that for narrow cracks the stress intensity factor reaches a constant and stable value in the mid crack only for a number of cracks much higher than that necessary to obtain the saturation of K_I for lower values of s. When the t/d ratio increases and the hypothesis of shallow crack is no longer valid, the relative deviation between the results from SED and those provided by Tada's diagram increases.

Table 9. Crack case: comparison between results from SED and
those provided by Tada et al. (1985)

Number of cracks in the FE model	s = t/(t+a)	F_{II} Tada et al.	F_{II} SED			
			t/d = 0.0125	t/d = 0.025	t/d = 0.05	t/d = 0.1
34	0.333	0.810	0.807	0.814	0.839	0.889
34	0.500	0.581	0.578	0.575	0.598	0.642
34	0.909	0.179	0.235	0.233	0.229	0.228
204 (fine mesh)	0.909	0.179	0.178	0.178	0.177	0.177
204 (coarse mesh)			0.177	0.178	0.176	0.175

Finally, Figure 18 plots the stress intensity factor as a function of t/d for different values of a/t, from 0 to infinite. The strong influence of both ratios is evident.
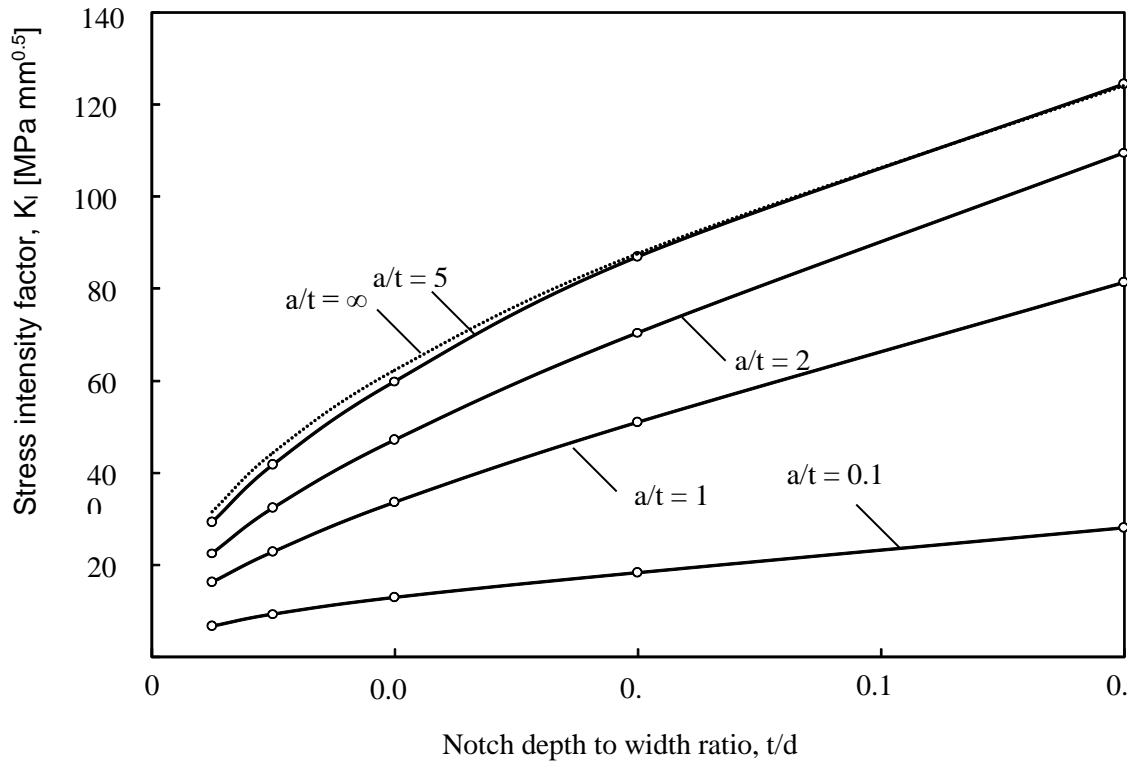
Fig. 18 Plot of the stress intensity factors

60

6. Conclusions

A wide range of notch opening angle, relative distance between periodic notches and relative depth of the notch for different number of notches of flat plate are examined. Local SED approach by considering a control volume surrounding the tip of the middle notch is employed to estimate the NSIF of each component by using a relatively coarse mesh.

By comparing the results with the theoretical solution proposed in the recent literature it has been found a good agreement with the semi-analytical solutions valid for shallow notches. In all the other cases, when the notch depth to plate width ratio does not tend to zero, some new expressions for the notch depth reduction factor are provided based on the SED approach as well as some polynomials for non dimensional NSIF in the case of intermediate and deep notches are presented.

References

[1]   N. I. Muskhelishvili, Some Basic Problems of the Mathematical Theory of Elasticity P.Noordhooff Ltd., The Netherlands, 1962.

[2]   G. N. Savin, Stress Concentration around Holes Pergamon Press, New York, 1961.

[3]   P. C. Paris and G. C. Sih, Stress analysis of cracks, in Fracture Toughness Testing and its applications, ASTM, Philadelphia, 1965, 30-81.

[4]   G. C. Sih, Strength of stress singularities at crack tips for flexural and torsional problems, Journal of Applied Mechanics, Trans. ASME 30 (1963) 419-425.

[5]   G. C. Sih, Stress distribution near internal crack tips for longitudinal shear problems, Journal of Applied Mechanics, Trans. ASME 32 (1965) 51-58.

[6]   G. C. Sih, Heat conduction in the infinite medium with lines of discontinuity Journal of Applied Mechanics, Trans. ASME 32 (1965) 293-298.

[7]   M. K. Kassir and G. C. Sih, Three dimensional crack problems Noordhoff Int. Publ., The Netherlands, 1975.

[8]   G. C. Sih, Methods of analysis and solutions of crack problems Noordhoff Int. Publ, The Netherlands, 1973.

[9]   G. C. Sih, Handbook of stress intensity factors Institute of Fracture and Solid Mechanics, Leigh University, Benthlehem, Pennsylvania, 1973.

[10]   H. Neuber, Theory of Notch Stresses, Springer Verlag, 1958.

[11]   N. A. Noda, Y. Takase, Stress Concentration Factor Formulas Useful for All Notch Shapes in a Flat Test Specimen Under Tension and Bending, Journal of Testing and Evaluation (JTE) 30 (2002) 1-13.

[12]   A. Kato, Two dimensional stress analysis on a personal computer, Mem. Coll. Engng, Chubu University 26 (1990) 1-9.

[13]   A. Kato, Design equation for stress concentration factors of notched strips and grooved shafts, The Journal of Strain Analysis for Engineering Design 27 (1992) 21-28.

[14]   A. Kato, T. Mizuno, Stress concentration factors of grooved shafts in torsion, Journal of Strain Analysis 20 (1985) 173-177.

[15]   N. A. Noda, M. Sera and Y. Takase, Stress concentration factors for round and flat test specimens with notches, International Journal of Fatigue 17 (1995) 163-178.

[16]   E. Dragoni, D. Castagnetti, Concentration of normal stresses in flat plates and round bars with periodic notches, Journal of Strain Analysis for Engineering Design 45 (2010) 495-503.

[17]   E. Dragoni, D. Castagnetti, Concentration of shear stresses in shallow periodic notches, Journal of Strain Analysis for Engineering Design 46 (2011) 397-404.

[18]   M. Savruk, A. Kazberuk, A plane periodic boundary-value problem of elasticity theory for a half-plane with curvilinear edge, Materials Science 44 (2008) 461-470.

[19]   M. Savruk, A. Kazberuk, Stresses in an elastic plane with periodic system of closely located holes, Materials Science 45 (2009) 831-844.

[20]   Y. Z. Chen, Z. X. Wang, Multiple and periodic notch problems of elastic half-plane by using bie based on Green's function method, International Journal of Computational Methods 7 (2010) 539-557.

[21]   G. C. Sih, Energy-density concept in fracture mechanics, Engineering Fracture Mechanics 5 (1973) 1037-1040.

[22]   G. C. Sih, Some basic problems in fracture mechanics and new concepts, Engineering Fracture Mechanics 5 (1973) 365-377.

[23]   G. C. Sih, Strain-energy-density factor applied to mixed-mode crack problems International Journal of Fracture 10 (1974) 305-321.

[24]   G. C. Sih, Surface and volume energy density applied as failure criterion Kluwer Academic Publisher, Dordrecht, 1991.

[25]   G. C. Sih and J. W. Ho, Sharp notch fracture strength characterized by critical energy density, Theoretical and Applied Fracture Mechanics 16 (1991) 179-214.

[26]   G. C. Sih, Multiscaling in molecular and continuum mechanics: interaction of time and size from macro to nano, Springer, Dordrecht, 2007.

[27]   G. C. Sih, X. S. Tang, Scaling of volume energy density function reflecting damage by singularities at macro-, meso- And microscopic level, Theoretical and Applied Fracture Mechanics 43 (2005) 211-231.

[28]   X. S. Tang, G. C. Sih, Weak and strong singularities reflecting multiscale damage: Micro-boundary conditions for free-free, fixed-fixed and free-fixed constraints, Theoretical and Applied Fracture Mechanics 43 (2005) 5-62.

[29]   P. Lazzarin, R. Zambardi, A finite-volume-energy based approach to predict the static and fatigue behavior of components with sharp V-shaped notches, International Journal of Fracture 112 (2001) 275-298.

[30]   F. Berto, P. Lazzarin, A review of the volume-based strain energy density approach applied to V-notches and welded structures, Theoretical and Applied Fracture Mechanics 52 (2009) 183-194.

[31]   P. Lazzarin, F. Berto, Some expressions for the strain energy in a finite volume surrounding the root of blunt V-notches, International Journal of Fracture 135 (2005) 161-185.

[32]   P. Lazzarin, F. Berto, From Neuber's elementary volume to Kitagawa and Atzori's diagrams: an interpretation based on local energy, International Journal of Fracture 135 (2005) L33–L38.

[33]   F. J. Gomez, M. Elices, A fracture criterion for blunted V-notched samples, International Journal of Fracture 127 (2004) 239-264.

[34]   F. Berto, P. Lazzarin, F. Gómez and M. Elices, Fracture assessment of U-notches under mixed mode loading: two procedures based on the 'equivalent local mode I' concept, International Journal of Fracture 148 (2007) 415-433.

[35]   F. Gómez, M. Elices, F. Berto and P. Lazzarin, Local strain energy to assess the static failure of U-notches in plates under mixed mode loading, International Journal of Fracture 145 (2007) 29-45.

[36]   F. Gómez, M. Elices, F. Berto and P. Lazzarin, Fracture of V-notched specimens under mixed mode (I + II) loading in brittle materials, International Journal of Fracture 159 (2009) 121-135.

[37]   F. J. Gómez, M. Elices, F. Berto and P. Lazzarin, A generalised notch stress intensity factor for U-notched components loaded under mixed mode, Engineering Fracture Mechanics 75 (2008) 4819-4833.

[38]   F. J. Gómez, M. Elices, F. Berto and P. Lazzarin, Fracture of U-notched specimens under mixed mode: Experimental results and numerical predictions, Engineering Fracture Mechanics 76 (2009) 236-249.

[39]   F. Berto, D. Croccolo, R. Cuppini, Fatigue strength of a fork-pin equivalent coupling in terms of the local strain energy density, Meterials and Design 29 (2008) 1780-1792.

[40]   P. Lazzarin, F. Berto, F. J. Gomez and M. Zappalorto, Some advantages derived from the use of the strain energy density over a control volume in fatigue strength assessments of welded joints, International Journal of Fatigue 30 (2008) 1345-1357.

[41]   P. Lazzarin, F. Berto and M. Zappalorto, Rapid calculations of notch stress intensity factors based on averaged strain energy density from coarse meshes: Theoretical bases and applications, International Journal of Fatigue 32 (2010) 1559-1567.

[42]   R. Afshar, F. Berto, Stress concentration factors of periodic notches determined from the strain energy density, Theoretical and Applied Fracture Mechanics 56 (2011) 127-139.

[43]   R. Gross and A. Mendelson, Plane elastostatic analysis of V-notched plates, International Journal of Fracture Mechanics 8 (1972) 267-327.

[44]   M. L. Williams, Stress singularities resulting from various boundary conditions in angular corners of plates in extension, Journal of Applied Mechanics 19 (1952) 526-528.

[45]   M. L. Dunn, W. Suwito and S. Cunningham, Fracture initiation at sharp notches: Correlation using critical stress intensities, International Journal of Solids and Structures 34 (1997) 3873-3883.

[46]   M. L. Dunn, W. Suwito and S. Cunningham, Stress intensities at notch singularities, Engineering Fracture Mechanics 57 (1997) 417-430.

[47]   P. Lazzarin and R. Tovo, A notch intensity factor approach to the stress analysis of welds, Fatigue and Fracture of Engineering Materials and Structures 21 (1998) 1089-1103.

[48]   H. Tada, P. C. Paris and G. Irwin, The stress analysis of cracks handbook Paris Productions Incorporated and Del Research Corporate, St Louis, 1985.

[49]   A.P. Parker, Stability of arrays of multiple edge cracks, Engineering Fracture Mechanics 62 (1999) 577-591.

Appendix

The following polynomial form is used to interpolate the numerical data in Figs 11-13.

$$F_I^V = a + bx + cx^2 + dx^3 + ex^4 + fx^5 + gx^6$$

where x stands for the opening angle 2α. The relevant coefficients are reported in the Appendix, see Tables A.1 and A.2

APPENDIX

Table A.1. Polynomial equations of non-dimensional stress intensity factors as a function of notch opening angle (2α=30°-180°) for the models with t/d=0.05 (obtained by numerical interpolating data from the SED approach).

a/t	$F_I^V = a + bx + cx^2 + dx^3 + ex^4 + fx^5 + gx^6$						
	a	*b*	*c*	*d*	*e*	*f*	*g*
0.0	-8.43E-01	9.60E-02	-3.10E-03	5.23E-05	-4.63E-07	2.09E-09	-3.77E-12
0.1	-8.89E-01	1.03E-01	-3.32E-03	5.53E-05	-4.84E-07	2.17E-09	-3.88E-12
1.0	-4.64E-01	9.57E-02	-3.13E-03	5.22E-05	-4.57E-07	2.03E-09	-3.63E-12
2.0	-9.50E-02	8.39E-02	-2.77E-03	4.64E-05	-4.07E-07	1.82E-09	-3.25E-12
5.0	3.46E-01	6.35E-02	-2.12E-03	3.58E-05	-3.16E-07	1.42E-09	-2.58E-12
∞	1.59E-01	8.12E-02	-2.63E-03	4.28E-05	-3.66E-07	1.60E-09	-2.82E-12

Table A.2. Polynomial equations of non-dimensional stress intensity factors as a function of notch opening angle (2α=30°-180°) for the models with t/d=0.1.

a/t	$F_I^V = a + bx + cx^2 + dx^3 + ex^4 + fx^5 + gx^6$						
	a	*b*	*c*	*d*	*e*	*f*	*g*
0.0	-2.42E+00	2.32E-01	-7.35E-03	1.18E-04	-9.96E-07	4.25E-09	-7.26E-12
0.1	-2.32E+00	2.30E-01	-7.34E-03	1.18E-04	-9.97E-07	4.26E-09	-7.26E-12
1.0	-2.16E+00	2.53E-01	-8.20E-03	1.32E-04	-1.12E-06	4.75E-09	-8.05E-12
2.0	-2.08E+00	2.66E-01	-8.72E-03	1.41E-04	-1.19E-06	5.08E-09	-8.60E-12
5.0	-1.94E+00	2.65E-01	-8.73E-03	1.42E-04	-1.20E-06	5.12E-09	-8.68E-12
∞	-1.97E+00	2.66E-01	-8.74E-03	1.42E-04	-1.20E-06	5.12E-09	-8.66E-12

Table A.3. Polynomial equations of non-dimensional stress intensity factors as a function of notch opening angle (2α=30º-170º) for the models with t/d=0.2.

$F_I^V = a + bx + cx^2 + dx^3 + ex^4 + fx^5 + gx^6$						
a/t	a	b	c	d	e	f	g
0.0	-6.97E-01	8.23E-02	-2.59E-03	4.35E-05	-3.88E-07	1.78E-09	-3.27E-12
0.1	-5.93E-01	7.98E-02	-2.54E-03	4.31E-05	-3.85E-07	1.76E-09	-3.25E-12
1.0	-1.81E-01	7.57E-02	-2.47E-03	4.19E-05	-3.72E-07	1.69E-09	-3.07E-12
2.0	4.17E-03	7.95E-02	-2.62E-03	4.37E-05	-3.83E-07	1.71E-09	-3.07E-12
5.0	3.61E-02	9.27E-02	-3.07E-03	5.07E-05	-4.37E-07	1.92E-09	-3.37E-12
∞	-3.47E-03	9.66E-02	-3.20E-03	5.27E-05	-4.54E-07	1.99E-09	-3.49E-12

Paper II

Simple new expressions for the notch stress intensity factors in an array of narrow V-notches under tension

Abstract. Taking advantage of some recent closed form expressions for the strain energy density in a control volume embracing the notch tip, some simple expressions are derived for the Notch Stress Intensity Factors of an infinite array of double symmetric lateral notches and edge notches under tension loading. The new expressions are applicable to narrow notches when the ratio between the notch depth and the plate width, a/W, is lower than 0.025 providing very accurate results.

Keywords: Periodic notches, Notch Stress Intensity Factor (NSIF), Strain Energy Density (SED), notch spacing, narrow notches

1. Introduction. The creation and subsequent shedding of arrays of edge cracks is a natural phenomenon which occurs in heat-checked gun tubes, rapidly cooled pressure vessels and rock, dried-out mud flats, paint and concrete and in ceramic coatings and permafrost. Dealing with this topic a complete state of the art together with a simple model developed to assess the shedding behaviour is carried out by Parker (Parker, 1999). As discussed in that work the surface topography of the cracking of ice-wedge polygons in Arctic permafrost, of mud flats in Death Valley and of craze-cracks (heat-checking) at the bore of a gun tube are all strikingly similar, yet they span five orders of magnitude in scale, with the maximum plate dimensions for ice and mud being, respectively, 22 m and 0.25 m and with the minimum plate size for gun tube craze cracking being 0.2 mm.

A system of multiple, equal length edge cracks of depth a and spacing 2h have been considered by Tada et al. (1985) in a plate of infinite width. The variation of the stress intensity factor normalized by $K_0 = \sigma\sqrt{h}$ is plotted as a function of a/(a+h).

Lachenbruch, in a treatise dated 1962 (Lachenbruch, 1962), has shown that linear elastic fracture mechanics can be applied to edge-cracking in ice and presented fracture toughness values for such cracking.

Bazant and co-workers have produced some papers (see Bazant et al. 1977, among the others) in which are analyzed the sudden cooling of a rock surface and the associated cracking which this

produces. Bazant's analysis was based on LEFM study of the energy of individual cracks and of all cracks. The crack-shedding has been investigated by means of the energy release rate of the entire system of cracks.

Arrays of radial cracks are often observed at the bore of pressurised cylinders. As discussed by Pook (1990), the stress intensity factors of closely spaced regular arrays of edge cracks depends primarily on the crack spacing and, accordingly to Tada et. (1985), are approximately proportional to the square root of crack spacing.

Dealing with theoretical solutions for plates with central collinear cuts it is worth mention some fundamental works by Koiter (1959), Erdogan (1974), Kachanov (1984) and Rubinstein (1987). The formulation by Rubinstein is based on the complex stress potentials and can be extended to any geometry of collinear crack interacting with semi-infinite crack array or to a semi-infinite array of rigid punches on an elastic half-plane.

Although a large number of papers can be found dealing with periodic cracks only few works exist in the literature dealing with periodic notches. The most known reference is Murakami's handbook (2001) which includes the case of central sharp diamond-shaped inclusions with a notch opening angle varying from 0 to 90°. The results reported therein are based on the body force method and are due to the work by Noda et *al.* (1996a) who faced the problem of angular corners using singular integral equations and specifically provided the solution for a row of diamond-shaped inclusions (Noda et *al.* 1996b).

The present work is focused on an infinite row of double symmetric and edge V-notches under tension loading. The main aim of the paper is to present a diagram for different notch opening angles ranging from 30° to 135°. The new diagram has been obtained by evaluating the strain energy density over a control volume of radius R_0 embracing the notch tip (Lazzarin and Zambardi, 2001, Lazzarin and Berto 2005a, 2005b, Berto and Lazzarin, 2009) and taking advantage of the mesh insensitiveness of this parameter which can be precisely and easily evaluated by using a very coarse mesh (Lazzarin et al., 2008 and 2010).

The obtained diagram, which is an extended version of that proposed by Tada et *al.* (1985) for edge cracks, is valid for an infinite plate width but can be applied with errors within 5 percent if the ratio between the notch depth and plate width remains lower than 0.025 (i.e infinite plate width). Some very simple expressions are derived which are suitable both for the direct evaluation of the strain energy density and the notch stress intensity factor as a function of the

notch spacing of narrow notches. The most interesting case of zero distance between two subsequent notches is contemplated by the new equations.

2. Strain energy density in a control volume. Consider a sharp V-notch under Mode I loading and plane strain conditions (Figure 1). The mean value of SED in the semi-circular sector of radius R_0 is (Lazzarin and Zambardi, 2001):

$$\overline{W}_1 = \frac{e_1}{E}\left(\frac{K_1}{R_0^{1-\lambda_1}}\right)^2 \tag{1}$$
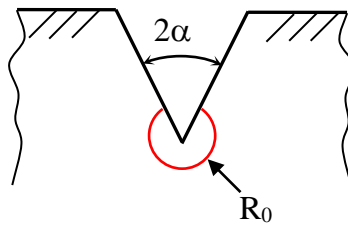
Figure 1. Single notch and control area of radius R_0

In Eq.(1) K_1 is the notch stress intensity factor, λ_1 is Williams'eigenvalue (Williams, 1952) while e_1 depends both on the notch angle 2α and the Poisson's ratio ν (see Table 1, $\nu=0.3$). E is the Young modulus.

The radius R_0 is thought here as a reference value. The ratio between the control radius, R_0, and the notch depth, a, is set equal to 1/100 to consider an area fully embedded in the singular zone. As discussed in a large number of previus papers (see also Gomez et *al*. 2007, Berto et *al*. 2007) R_0 is a material dependent parameter.

The SED method, in fact, was formalised and first applied for the fracture assessment of sharp, zero radius, V-notches and later extended to blunt U- and V-notches under Mode I and mixed mode loading. The control radius of the volume, over which the energy has to be averaged, depends on the ultimate tensile strength, the fracture toughness and Poisson's ratio in the case of static loads, whereas it depends on the un-notched specimen's fatigue limit, the threshold stress intensity factor range and the Poisson's ratio under high cycle fatigue loads. The extension to three-dimensional problems (Harding et *al*. 2010) and to thin structures is immediate (Berto and

Lazzarin, 2010) as well as the direct link with the generalised notch stress intensity factors (Lazzarin et *al*., 2011).

One of the most important advantages of the SED approach is that to provide a mean value which is substantially mesh independent. In fact, contrary to some stress parameters integrated in the local criteria (e.g. maximum principal stress, hydrostatic stress, deviatoric stress), which are mesh-dependent, the SED averaged over a control volume is insensitive to the mesh refinement. As widely documented by Lazzarin et al. (2008, 2010) dealing with sharp V-notches, refined meshes are not necessary, because the mean value of the SED on the control volume can be directly determined *via* the nodal displacements, without involving their derivatives. As soon as the average SED is known, the notch stress intensity factors (NSIFs) quantifying the asymptotic stress distributions can be calculated *a posteriori* on the basis of very simple expressions linking the local SED and the relevant NSIFs. By inverting Eq.(1) K_1 can be easily defined as follows:

$$K_1 = R_0^{1-\lambda_1} \sqrt{\frac{E\overline{W}_1}{e_1}}$$
(2)

Due to the linearity of the problem, the N-SIF value can be computed, similarly to stress intensity factors in linear elastic fracture mechanics as:

$$K_1 = k_1 \sigma_n a^{1-\lambda_1}$$
(3)

where k_1 is a non dimensional parameter that depends on the overall geometry and can be seen as an extension of the shape factor used in the LEFM, σ_n is the reference stress (e.g., the remote tensile stress); $a^{1-\lambda_1}$ quantifies the influence of the specimen size and in particular of the notch depth.

3. Application of the SED to periodic notches. A system of multiple, equal length edge cracks of depth a and spacing 2h has been considered by Tada et *al*. (1985) in a plate of infinite width. The variation of the stress intensity factor normalized by $K_0 = \sigma\sqrt{h}$ is plotted as a function of a/(a+h) (see Figure 2).
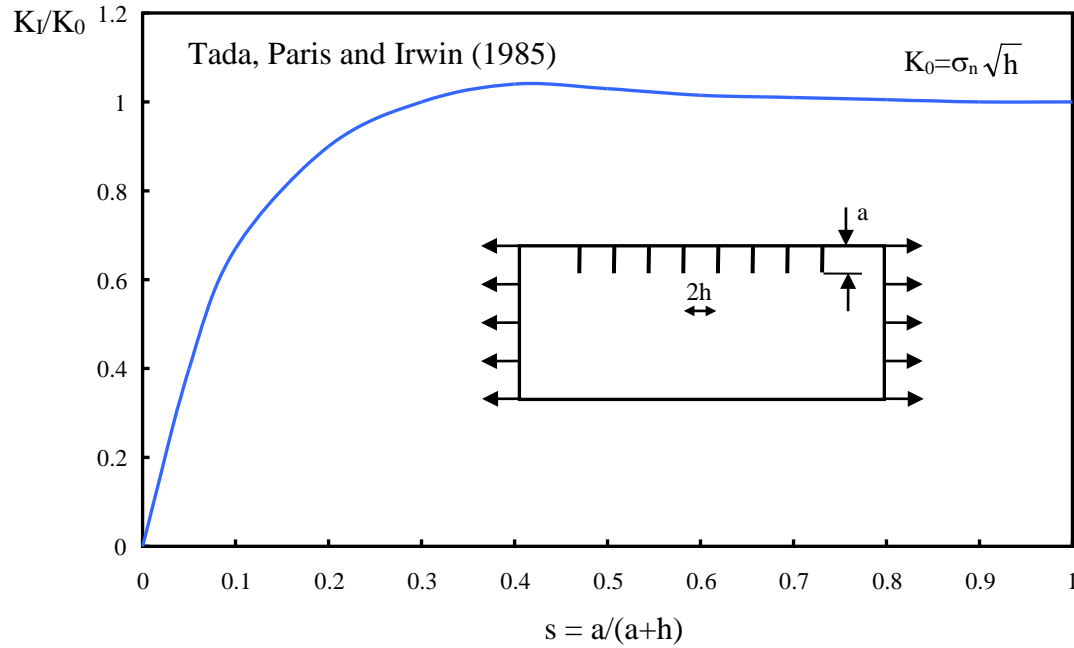
Figure 2. Tada et *al*. diagram for edge cracks

The diagram shows that when the cracks are narrow (i.e. close each other) and s is greater than 0.3, the stress intensity factor K_I can be simply estimated by using the following equation which is valid for an infinite plate width:

$$K_I = K_0 = \sigma_n \sqrt{h} \tag{4}$$

Eq. (4) can be directly applied without requiring numerical simulations and is independent of the notch depth. The only parameter involved is the crack spacing, h, which can be easily measured. Consider now multiple, equal-length double symmetric V-notches and edge notches of depth a under Mode I loading and plane strain conditions (see Figure 3a and b). The notch spacing is 2h while the distance between two subsequent notch edges is called 2c.

An extension of Eq. (4) is proposed here for the first time for narrow notches. The notch stress intensity factor can be expressed as follows:

$$K_I = K_0 = \kappa_0 \sigma_n h^{\lambda_1} \tag{5}$$

In Eq. (5) κ_0 is an adimensional parameter that depends on the notch opening angle.

(a) Double Symmetric Notches   (b) Single Edge Notches (SEN)
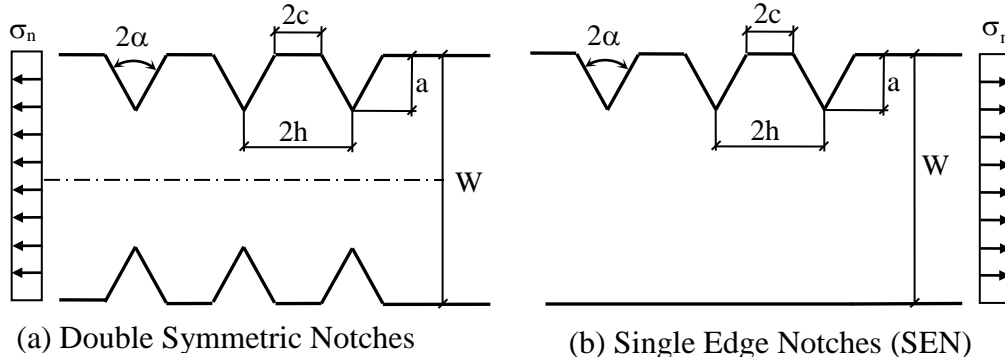
Figure 3. Array of double symmetric notches (a) and edge notches (b)

and λ_1 is Williams'eigenvalue (Williams, 1952) (see Table 1). Equation (5) collapses into Equation (4) when the crack case is considered ($\kappa_0=1$ and $\lambda_1=0.5$).

For an infinite plate width W>>a and narrow notches, being a/(a+c) close to 1 the stain energy averaged over a control volume of radius R_0 can be written as follows:

$$\overline{W}_1 = \frac{\kappa_0^2 e_1}{E}\left(\frac{\sigma_n h^{\lambda_1}}{R_0^{1-\lambda_1}}\right)^2 = \frac{\tilde{e}_1}{E}\left(\frac{\sigma_n h^{\lambda_1}}{R_0^{1-\lambda_1}}\right)^2 \tag{6}$$

By inverting Eq. (6) it is easy to determine parameters κ_0 and $\tilde{e}_1$ that can be expressed according to the following equations:

$$\tilde{e}_1 = \kappa_0^2 e_1 = \frac{E\overline{W}}{\sigma_n^2}\left(\frac{R_0^{1-\lambda_1}}{h^{\lambda_1}}\right)^2 \tag{7}$$

$$\kappa_0 = \sqrt{\frac{E\overline{W}}{e_1\sigma_n^2}}\left(\frac{R_0^{1-\lambda_1}}{h^{\lambda_1}}\right) \tag{8}$$

Table 1. Parameters for determination of SED and NSIF

2α [rad]	λ_1	e_1	$\tilde{e}_1$	κ_0	$\tilde{e}_1$	κ_0
			$mm^{2(1-2\lambda_1)}$	$mm^{1-2\lambda_1}$	$mm^{2(1-2\lambda_1)}$	$mm^{1-2\lambda_1}$
			Double Sym. Notch		Edge Notch	
$\pi/6$	0.5014	0.14492	0.14492	1.000	0.14492	1.000
$\pi/3$	0.5122	0.15038	0.15053	1.000	0.15053	1.000
$\pi/2$	0.5445	0.14623	0.14464	1.000	0.14464	1.000
$2\pi/3$	0.6157	0.12964	0.07608	1.305	0.07608	1.305
$3\pi/4$	0.6736	0.11721	0.03573	1.811	0.03573	1.811

The values of κ_0 and $\tilde{e}_1$ are listed in Table 1 for five different characteristic notch opening angles (2α=30, 60, 90, 120 and 135°) both for symmetric and edge notches.

They have been obtained by evaluating the SED, $\overline{W}_1$, (over a control volume $R_0 = a/100$) for the case of an infinite plate width (a/W<0.01). From Table 1 it is well visible that no differences occur between symmetric and edge notches.

By means of κ_0 and $\tilde{e}_1$ it is possible to straightforwardly evaluate the notch stress intensity factor and the SED over an area of radius R_0 by using Eq. (5) and (6), respectively. It is well visible from the table that κ_0 is equal to 1 until an opening angle lower or equal to 90° while it increases for larger values (120 and 135°).
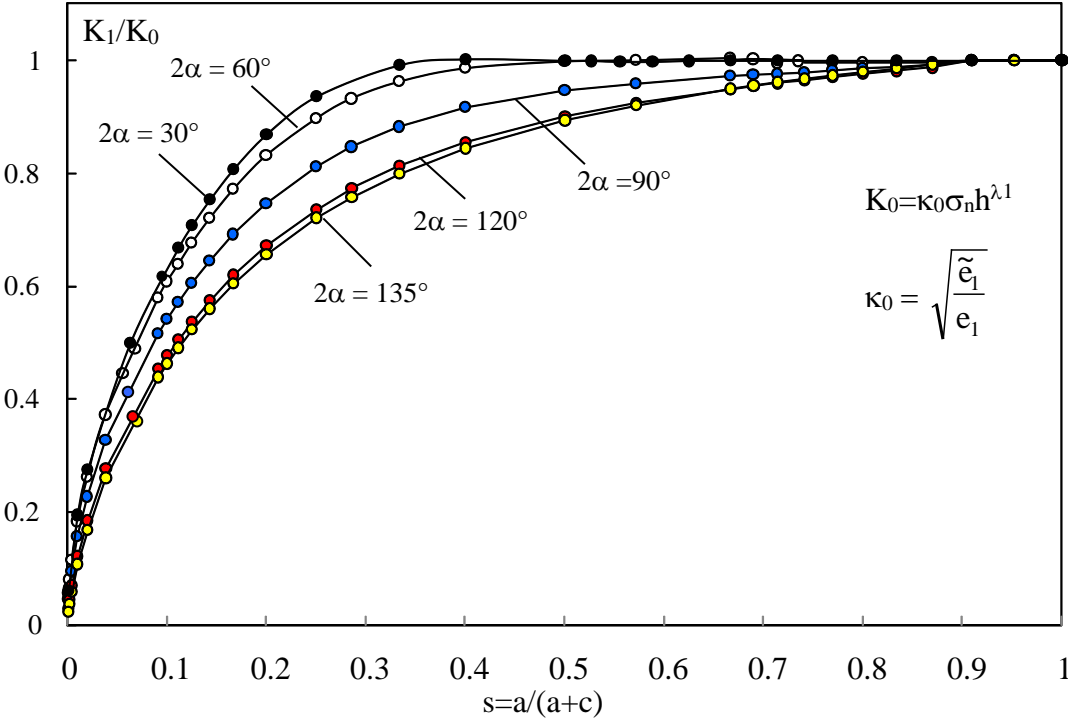
Figure 4. New generalised diagram for edge and double symmetric periodic notches

It is also possible to express the ratio between K_1 and K_0 in a general form by combining Eqs (3) and (5). It yields to the final expression

$$\frac{K_1}{K_0} = \frac{k_1}{\kappa_0}\left(\frac{a^{1-\lambda_1}}{h^{\lambda_1}}\right) \tag{9}$$

By plotting Eq. (8) an extended version of the Tada et *al.* diagram has been obtained for double symmetric notches and edge notches (see Figure 4). The ratio between K_1 and K_0 is plotted as a function of the normalised parameter s =a/(a+c). For s > 0.8, on the right hand side of the diagram, the ratio is very close to 1 independently of the notch opening angle.

When s > 0.8 and a/W <0.025 Equation (5), in combination with the values of κ_0 listed in Table 1, assures an high accuracy for the evaluation of K_1, being the relative deviation within ±5%.

4. Conclusions. Some new expressions for the notch stress intensity factor and the strain energy density applicable to narrow periodic lateral (symmetric and edge) notches are presented. The notch stress intensity factor for a plate having an infinite width is a function only of the notch

spacing raised to William's eigenvalue. The equation gives accurate results when the ratio between the notch depth and the plate width is lower than 0.025 and collapses into Tada et *al*. solution in the crack case. Finally a generalized diagram is proposed valid for typical notches with an opening angle ranging from 30° to 135°. Future developments will consider the case of a finite witdth.

References

Bazant, Z.P., Ohtsubo, H. (1977) Stability conditions for propagation of a system of cracks in a brittle solid, *Mechanics Research Communications* , **4**, 353-66.

Berto, F., Lazzarin, P., Gómez, F.J., Elices, M. (2007) Fracture assessment of U-notches under mixed mode loading: two procedures based on the equivalent local mode I concept. *International Journal of Fracture* **148**, 415–433.

Berto, F., Lazzarin, P. (2009). A review of the volume-based strain energy density approach applied to V-notches and welded structures, *Theoretical and Applied Fracture Mechanics* 52, 183-194.

Berto, F. Lazzarin, P. (2010). On higher order terms in the crack tip stress field, *International Journal of Fracture* 161, 221–226

Erdogan, F. (1962) On the stress distribution in plates with collinear cuts under arbitrary loads, Proceedings of the Fourth US National Congress of Applied Mechanics, 547-554.

Gómez, F.J., Elices, M., Berto, F., Lazzarin, P. (2009) Fracture of V-notched specimens under mixed mode (I+II) loading in brittle materials, *International Journal of Fracture* **159**, 121–135.

Harding, S. Kotousov, A. Lazzarin, P., Berto, F. (2010) Transverse singular effects in V-shaped notches stressed in Mode II, *International Journal of Fracture* **164**, 1-14.

Kachanov, M. (1985) A simple technique of stress analysis in elastic solids with many cracks, *International Journal of Fracture* **28**, R11-R19.

Koiter, W.T. (1959) An infinite row of collinear cracks in an infinite elastic sheet. *Ing. Arch.* **28**, 168-172.

Lachenbruch, A.H. (1962) Mechanics of thermal contraction cracks and ice-wedge polygons in permafrost. Geological Society of America Special Paper, Baltimore, MD:Waverly Press.

Lazzarin, P., Zambardi, R. (2001) A finite-volume-energy based approach to predict the static and fatigue behaviour of components with sharp V-shaped notches, *International Journal of Fracture*, **112**, 275-298.

Lazzarin, P., Berto, F. (2005a) Some expressions for the strain energy in a finite volume surrounding the root of blunt V-notches, *International Journal of Fracture* **135**, 161-185.

Lazzarin, P., Berto, F. (2005b) From Neuber's elementary volume to Kitagawa and Atzori's diagrams: an interpretation based on local energy. *International Journal of Fracture* **135**, L33–L38.

Lazzarin, P., Berto, F., Gómez, F.J., Zappalorto, M. (2008) Some advantages derived from the use of the strain energy density over a control volume in fatigue strength assessments of welded joints, *International Journal of Fatigue* **30**,1345-1357.

Lazzarin, P., Berto, F., Zappalorto, M. (2010) Rapid calculations of notch stress intensity factors based on averaged strain energy density from coarse meshes: Theoretical bases and applications, International Journal of Fatigue 32, 1559-1567.

Lazzarin P, Zappalorto M, Berto F. (2011) Generalised stress intensity factors for rounded notches in plates under in-plane shear loading. . International Journal of Fracture 170, 123-144.

Murakami, Y. (2001) Stress intensity factors handbook, Volume 5, Elsevier Science Ltd, Oxford UK.

Noda, N.A., Oda, K., Inoue, T. (1996a) Analysis of newly-defined stress intensity factors for angular corners using singular integral equations of the body force method, *International Journal of Fracture* **76**, 243-261.

Noda, N.A., Kawashima, Y., Moriyama, S., Oda, K. (1996b) Interaction of newly defined stress intensity factors for angular corners in a row of diamond-shaped inclusions, *International Journal of Fracture* **82**, 267-295.

Parker, A.P. (1999) Stability of arrays of multiple edge cracks, *Engineering Fracture Mechanics* **62**, 577-591.

Pook, L.P. (1990) Stress intensity factor expressions for regular crack arrays in pressurised cylinders, *Fatigue and Fracture of Engineering Materials and Structures* **13**, 135-143.

Rubinstein, A. A. (1987) Semi-infinite array of cracks in a uniform stress field, *Engineering Fracture Mechanics* **26**, 15-21.

Tada, H., Paris P.C, Irwin, G. (1985) *The stress analysis of cracks handbook*, St Louis, Paris Productions Incorporated and Del Research Corporate, 2nd ed.

Williams, M. L. (1952) Stress singularities resulting from various boundary conditions in angular corners of plates in tension, *Journal of Applied Mechanics* **19**, 526-528.

Paper III

Analytical expressions for the notch stress intensity factors of periodic V-notches under tension by using the strain energy density approach

Abstract: This paper presents the notch stress intensity factors (NSIFs) of a wide range of finite-width flat plates with periodic edge notches. A broad series of notch configurations, varying from shallow to very deep notches, complete range of notch spacing and wide range of notch opening angles are considered. The significance of sharp notch approximation for the case of blunt notches with a very small notch radius is also demonstrated. Overall, more than 1200 models are carried out. Due to the desirability of analytical expressions for NSIFs evaluation, the numerical results, obtained from the strain energy density (SED) approach, are used to find some simple analytical expressions for the prediction of NSIFs of periodic sharp notches. The use of a coarse mesh in the finite element (FE) models as well as multiscaling are the promising advantages of such a method underlined in the present study.

Keywords: Notch stress intensity factor (NSIF); Periodic notches; Strain energy density (SED); Finite element method; Analytical expressions.

Nomenclature

a	Notch depth
2c	Notch spacing
E	Young's modulus
e_1	shape function
$\tilde{e}_1$	a dimensional parameter that depends on the notch opening angle
FE	Finite Element
2h	Pitch of the notch
K_0	Notch stress intensity factor
κ_0	a dimensional parameter that depends on the notch opening angle
K_1	Notch stress intensity factor

k_1	Dimensionless parameter
K_a	Notch stress intensity factor expressed in terms of k_a
k_a	Dimensionless parameter based on the notch depth
K_h	Notch stress intensity factor expressed in terms of k_h
k_h	Dimensionless parameter based on the pitch of the notch
NSIF	Notch stress intensity factor
n	Scale factor
R_0	Radius of control volume
s=a/(a+c)	Dimensionless parameter
SED	Strain energy density
W	Width of the plate
2α	Notch opening angle
σ_n	Applied remote stress
λ_1	William's eigenvalue (mode I)
ρ	Notch radius
ν	Poisson's ratio
$\overline{W}_1$	Mean value of strain energy density

1. Introduction

While dealing with stress concentrations arising in periodic notches, some useful guidelines are provided in Refs. [1, 2] for the case of tension and torsion loadings respectively. Boundary element method is used to modify the depth reduction factor, which converts a periodic notch into a single notch to find an equivalent stress concentration factor (SCF). The criterion, proposed first by Neuber [3], links the periodic notch to an equivalent single notch with a smaller

depth [1, 2].

The evaluation of SCFs is not only an academic curiosity but it is very important for the design of many components and real structures. Gross and Mendelson first proposed to extend the definition of the Stress Intensity Factor, commonly used to describe crack stress fields, to open notches [4]. The problem of sharp V-notches in brittle or quasi-brittle materials under static loads, has been analyzed by many researchers [5-12]. In the particular field of fatigue strength assessment, in [13] it has been shown that the N-SIF approach can be conveniently used by reconsidering a large bulk of experimental data from transverse non-load-carrying fillet welds.

The issue of stress concentrations at rounded edges of shaft–hub interference fits is addressed in [14]. By adopting local approaches, great efforts have been devoted to provide useful solutions in different engineering fields. In [15] some practical linear-elastic equations for evaluation of the critical value of the J-integral in plates with U-notches under tension are presented and applied to brittle and quasi-brittle materials. In another work, the fictitious notch rounding concept is applied to V-shaped notches with root holes subjected to mode I loading [16]. By using the strain energy density (SED) approach, SCFs of a number of flat plates and round bars with periodic U- and V-notches are evaluated. Tension, bending and torsion loading conditions have been considered [17].

Dealing with some natural phenomena in terms of creation and subsequent shedding of an array of edge cracks, a complete state of the art together with a simple model is reported in Ref. [18] to assess the shedding behavior of edge cracks in heat-checked gun tubes. In another study [19], occurrence of arrays of radial cracks, which often are observed at the bore of pressurized cylinders, is discussed according to the stress intensity factors (SIFs) of closely spaced regular arrays of edge cracks. The SIFs depend primarily on the crack spacing and in line with Ref. [20]

are approximately proportional to the square root of crack spacing. Although a large number of papers can be found dealing with periodic cracks, only few works exist in the literature dealing with periodic notches. The most known reference is [21], which includes the case of central sharp diamond-shaped inclusions with a notch opening angle varying from 0 to 90°.

In the presence of sharp periodic notches and by means of SED, used in combination with coarse meshes, the variability of the notch stress intensity factors (NSIFs) of periodic sharp notches is studied in Ref.[22]. A new model of depth reduction factor for different ratios of relative depth of the notch is proposed to match the results from the SED approach. In the case of shallow notches, the results are compared with some semi-analytical solutions provided in [23]. In addition, based on best fit of numerical data from SED approach, some polynomials for non-dimensional NSIFs in the case of intermediate and deep notches are presented.

In a previous work by the authors [24], a new diagram was obtained by evaluating the SED over a control volume of radius R_0 embracing the notch tip [25-27] and taking advantage of the mesh insensitiveness of this parameter, which can be precisely and easily evaluated by using a very coarse mesh [28, 29]. The obtained diagram, which is an extended version of that proposed by Tada et *al.* [20] for edge cracks, is valid for an infinite plate width but can be applied with errors within 5 percent if the ratio between the notch depth and plate width remains lower than 0.025 (i.e. infinite plate width). Some very simple expressions were derived which are suitable both for the direct evaluation of the SED and the NSIF as a function of the notch spacing of narrow notches.

The motivation of this study is to complete previous studies on periodic notches by the same Authors [22, 24].

In Ref. [22] the study was mainly focused on the depth reduction factor of the equivalent single notch for sharp periodic V-notches as well as on the introduction of some polynomials for non-dimensional NSIFs in the case of intermediate and deep notches. With the aim to extend the famous Tada-Paris diagram valid for periodic cracks [20] to sharp notches an attempt was made in Ref. [24] to derive some simple analytical expressions for the NSIFs of an infinite array of double symmetric lateral notches and edge notches under tension loading.

In this study, a broad series of notch configurations, varying from shallow to very deep notches, complete range of notch spacing and wide range of notch opening angles are considered to extend the approach adopted in [24] to finite-width flat plates weakened by periodic notches. The main objective of this paper then is to use the numerical results, obtained from the SED approach, to find some simple analytical expressions for the assessment of NSIFs from periodic sharp notches in a complete range of notch spacing as well as a broad range of relative depth of the notch and notch opening angles.

2. Application of the SED to periodic narrow sharp-notched components with infinite width: an extension of Tada Paris diagram

A system of multiple, equal length edge cracks of depth a and spacing 2h has been considered by Tada et *al*. [20] in a plate of infinite width. The variation of the SIF normalized by $K_0 = \sigma\sqrt{h}$ is presented as a function of s=a/(a+h). It is shown that in the case of narrow cracks and being s greater than 0.3, the SIF (K_I) can be simply estimated by using the following equation, which is valid for an infinite plate width:

$$K_I = K_0 = \sigma_n \sqrt{h} \tag{1}$$

Eq. (1) can be directly applied without requiring numerical simulations and is independent of the notch depth. The only parameter involved is the crack spacing, h, which can be easily measured. Consider now multiple, equal-length double symmetric V-notches of depth a under Mode I loading (see Fig. 1).

An extension of Eq. (1) is proposed in [24] only for narrow notches by using the 2D plane element with plane strain assumption in all FE models to matches the Tada Paris diagram valid for the crack case. The NSIF can be expressed as follows:

$$K_1 = K_0 = \kappa_0 \sigma_n h^{\lambda_1} \tag{2}$$

In Eq. (2) κ_0 is a dimensional parameter that depends on the notch opening angle and λ_1 is Williams'eigenvalue [30]. The values of λ_1 as a function of notch opening angle are given in Table A.1 (Appendix). Eq. (2) collapses into Eq. (1) when the crack case is considered ($\kappa_0=1$ and $\lambda_1=0.5$). For an infinite plate width W>>a and narrow notches, being a/(a+c) close to 1 the strain energy averaged over a control volume of radius R_0 can be written as follows:

$$\overline{W}_1 = \frac{\kappa_0^2 e_1}{E}\left(\frac{\sigma_n h^{\lambda_1}}{R_0^{1-\lambda_1}}\right)^2 = \frac{\tilde{e}_1}{E}\left(\frac{\sigma_n h^{\lambda_1}}{R_0^{1-\lambda_1}}\right)^2 \tag{3}$$

By inverting Eq. (3) it is easy to determine parameters κ_0 and $\tilde{e}_1$ that can be expressed according to the following equations:

$$\tilde{e}_1 = \kappa_0^2 e_1 = \frac{E\overline{W}_1}{\sigma_n^2}\left(\frac{R_0^{1-\lambda_1}}{h^{\lambda_1}}\right)^2 \tag{4}$$

$$\kappa_0 = \sqrt{\frac{E\overline{W}_1}{e_1\sigma_n^2}}\left(\frac{R_0^{1-\lambda_1}}{h^{\lambda_1}}\right) \tag{5}$$

The values of κ_0 and $\tilde{e}_1$ are given in Ref. [24] for five different characteristic notch opening angles (2α=30, 60, 90, 120 and 135°) both for symmetric and edge notches. By means of κ_0 and

$\tilde{e}_1$ it is possible to straightforwardly evaluate the NSIF and the SED over an area of radius R_0 by using Eq. (2) and (3), respectively.

Due to the linearity of the problem, the NSIF value can be computed, similarly to SIFs in linear elastic fracture mechanics (LEFM) as:

$$K_1 = k_1 \sigma_n a^{1-\lambda_1} \tag{6}$$

where k_1 is a non dimensional parameter that depends on the overall geometry and can be seen as an extension of the shape factor used in the LEFM, σ_n is the reference stress (e.g., the remote tensile stress); $a^{1-\lambda_1}$ quantifies the influence of the specimen size and in particular of the notch depth.

It is also possible to express the ratio between K_1 and K_0 in a general form by combining Eqs. (2) and (6). It yields to the following final expression:

$$\frac{K_1}{K_0} = \frac{k_1}{\kappa_0} \left(\frac{a^{1-\lambda_1}}{h^{\lambda_1}} \right) \tag{7}$$

Fig. 1 shows the plot of the extended version of the Tada et *al*. diagram for double symmetric notches and edge notches. The ratio between K_1 and K_0 is plotted as a function of the normalized parameter s = a/(a+c). For s > 0.8, on the right hand side of the diagram, the ratio is very close to 1 independently of the notch opening angle.

When s > 0.8 and a/W < 0.025 Eq. (7), in combination with the values of κ_0, assures an high accuracy for the evaluation of K_1, being the relative deviation within ±5%.
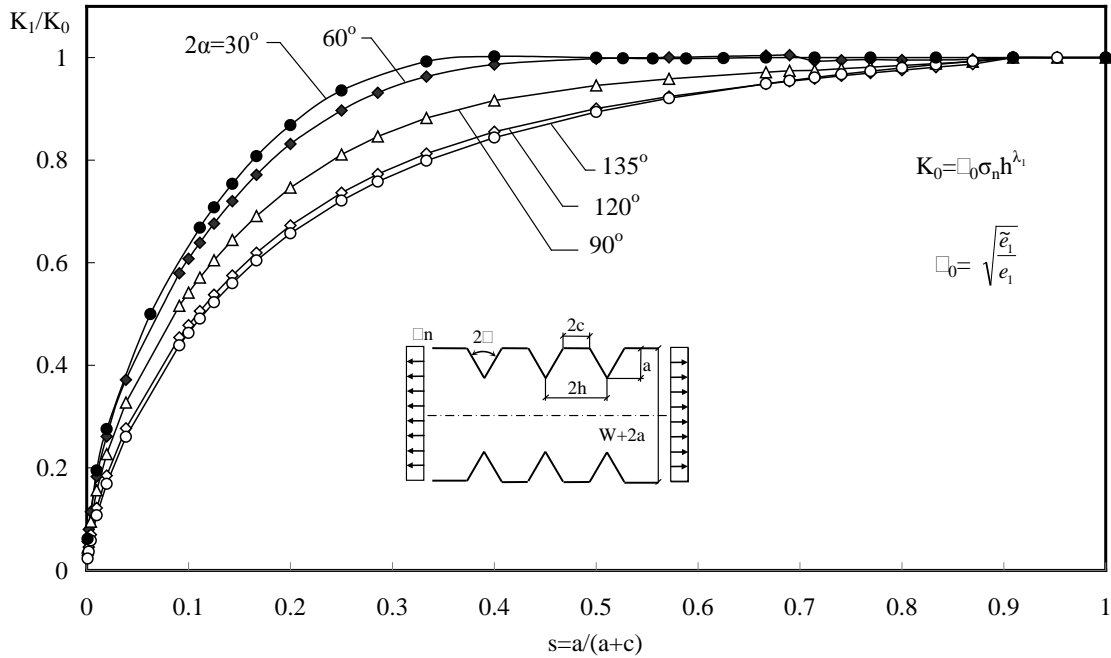
Fig.1. New generalised diagram for edge and double symmetric periodic notches [24].

3. NSIFs evaluation of periodic sharp-notched components with finite width

3.1. Comparison between the sharp notch and the blunt notches with a very small notch radius

In order to show the significance of the sharp notch approximation for the case of blunt notches with a very small notch radius ρ, a comparison for two notch opening angles $2\alpha=60°$ and $120°$ is performed. The relative pitch of the notch is set constant for all the cases and equal to $a/2h=0.25$.

In addition, three relative depths of the notch ($a/W=0.05$, 0.1 and 0.2) for each opening angles are examined to study the possible effect of the notch depth on the normalized average SED (the width of the plate is constant and equal to $W=100$ mm). The average SED for each relative depth of the notch (a/W) and opening angles (2α) are normalized with respect to the corresponding case of sharp notch ($\rho=0.0$). The comparison between sharp notches and the blunt notches with a

very small ρ in term of normalized average SED for the above mentioned notch opening angles
is shown in Figs. 2 and 3, respectively.
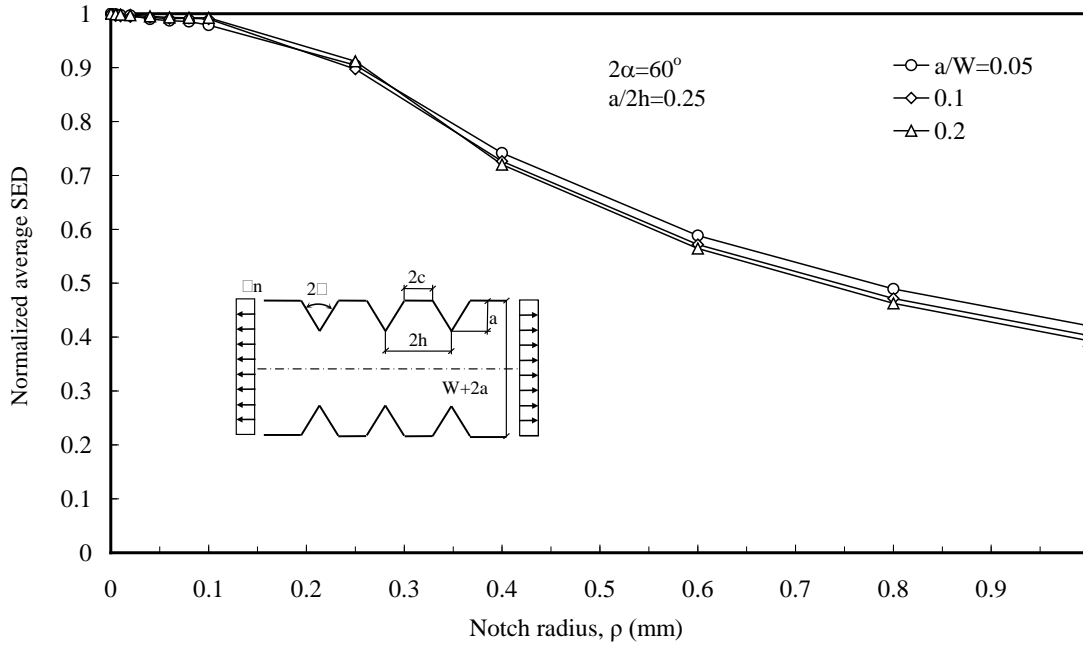
Fig. 2. Comparison between the sharp notch and the blunt notches with a very small ρ in term of
average SED for opening angle $2\alpha=60^{\circ}$ with different relative depth of the notch (a/2h=0.25,
W=100 mm, σ_n=100 MPa).
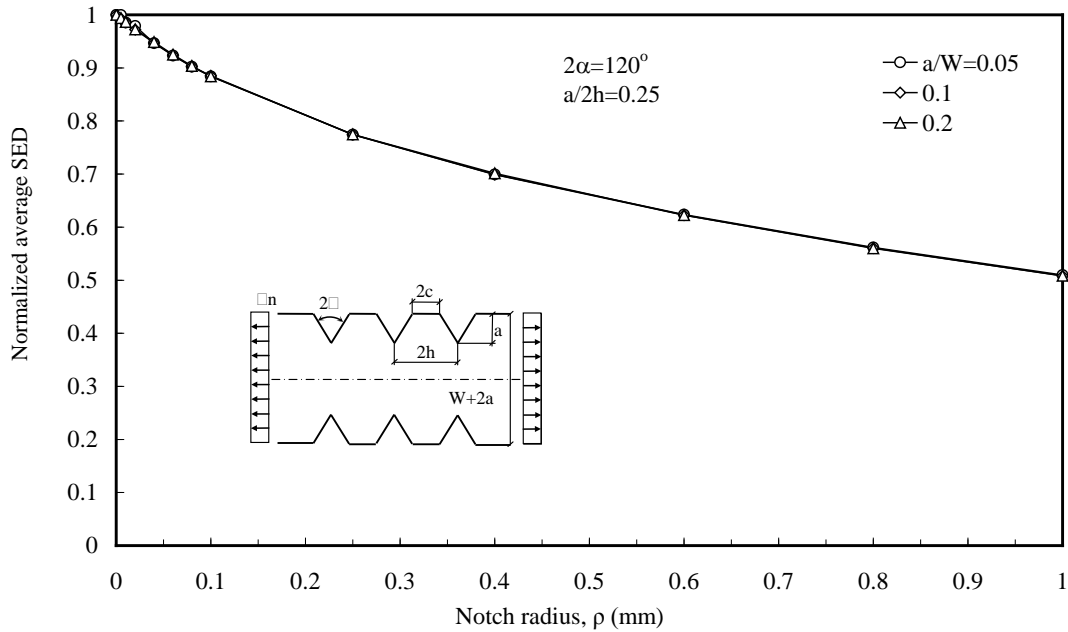
Fig. 3. Sharp and the blunt notch comparison with very small ρ in term of average SED for opening angle $2\alpha=120^{\circ}$ with different relative depth of the notch (a/2h=0.25, W=100 mm, σ_n=100 MPa).

As it can be seen form Figs. 2 and 3, the average SED of the blunt notches is very close to the case of sharp notch (with a maximum difference equal to 11%) until a certain range of ρ ($\approx$0.25 mm for $2\alpha=60^{\circ}$ and about 0.1mm for 120°) and then decreases rapidly. According to Eq. (9) a maximum difference equal to 11% in terms of SED leads to a maximum deviation of 3.3% in terms of NSIF estimation. This means that, for instance in the case of $2\alpha=60^{\circ}$ and the blunt notches with $\rho\leq$0.25 mm, the approximation of sharp notch in term of analytical formulation is more convenient.

In addition, the effect of the depth of the notch on the normalized average SED is negligible for both opening angles at least for the considered geometrical configurations. Fig. 3 clearly shows the exact agreement of the normalized average SED for the three values of relative depths of the notch in the whole range of 0.0$\leq\rho\leq$1.0. Increasing the depth of the notch leads to rise in the

average SED. However, the values of the normalized average SED (with respect to the sharp notch case) are constant for the three values of relative depths of the notch.

3.2. Modeling and the SED evaluation of periodic sharp notches

Modeling by means of coarse meshes and SED evaluation of periodic sharp notches are explained in detail in Ref. [22]. In this section, only a short explanation on the main expressions related to the SED are summarized.

A very wide range of notch configurations in term of relative depth of the notch, shallow (a/W=0.025) to very deep notches (a/W =0.8), relative distance between the notches (c/a) and notch opening angle (2α) have been investigated (Fig. 4). The values of the above-mentioned parameters are as follows:

- a/W=0.025, 0.05, 0.1, 0.2, 0.35, 0.5, 0.6, 0.7, 0.8.

- c/a=0.0-∞;

- 2α=30, 45, 60, 90, 120 and 135 degrees;
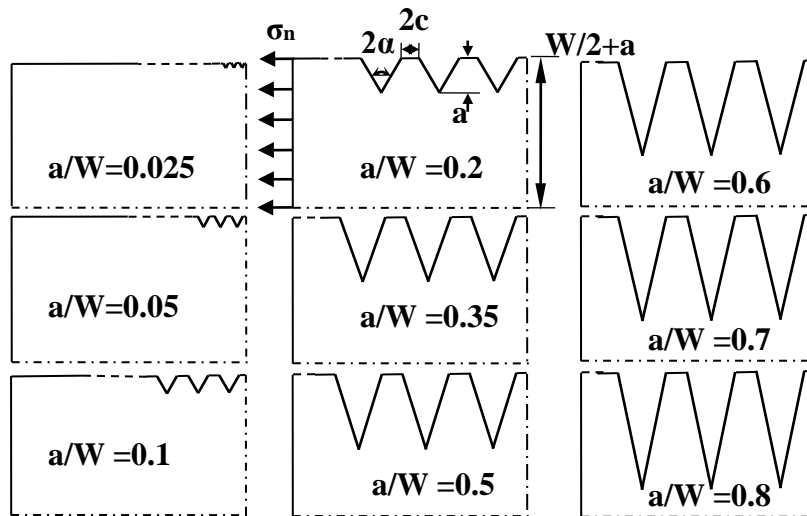
Fig. 4. Different values of relative depth of the notch (a/W) (W=constant=100 mm; a=2.5, 5, 10, 20, 35, 50, 60, 70 and 80 mm; σ_n=100 MPa in all cases)

Considering a sharp V-notch subjected to Mode I loading (Fig. 5), assuming plane strain conditions, the mean value of the SED in the semi-circular sector of radius R_0 can be evaluated accordingly to the following equation [27]:

$$\overline{W}_1 = \frac{e_1}{E}\left(\frac{K_1}{R_0^{1-\lambda_1}}\right)^2 \tag{8}$$

where K_1 is the NSIF, λ_1 is Williams'eigenvalue [30], e_1 is a shape function that depends both on the notch angle 2α and the Poisson's ratio ν and E is the Young's modulus.
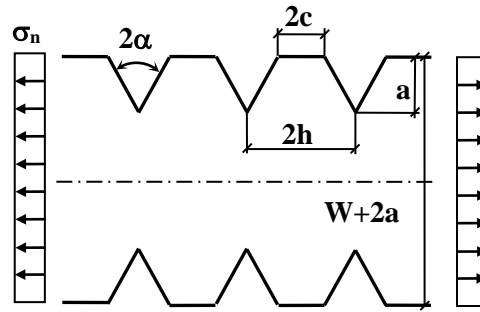
Fig. 5. A schematic of periodic double symmetric notches.

By inverting Eq.(8) K_1 can be easily defined as follows:

$$K_1 = R_0^{1-\lambda_1}\sqrt{\frac{E\overline{W}_1}{e_1}} \tag{9}$$

The variations of K_1 as a function of $s=a/(a+c)$ for different values of relative depth of the notch, ranging from shallow ($a/W=0.025$) to very deep notches ($a/W=0.8$), have been shown in Figs 6-10.
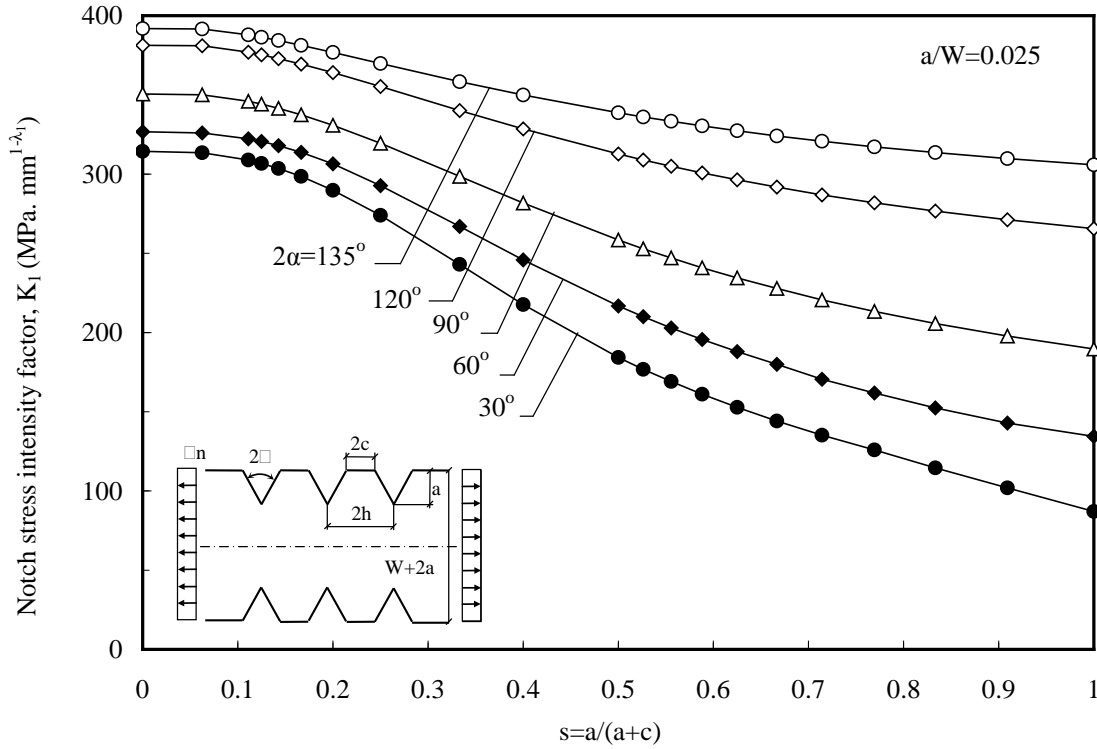
Fig.6. Variation of K_1 as a function of s=a/(a+c) for relative depth of the notch a/W=0.025.

Fig.6 shows that for shallow notches (a/W=0.025) and for the all opening angles in the range of 2α=30-135° NSIF decreases by decreasing the distance between periodic notches (c), but the slope is steeper for smaller opening angles than for larger ones. However, as expected, for a large distance between periodic notches (when s is smaller than 0.07), the slope is constant and equal to the case of a single notch (s=0.0). Moreover, the larger the opening angle, the higher is the NSIF value for all values of s in the range of 0≤s≤1.
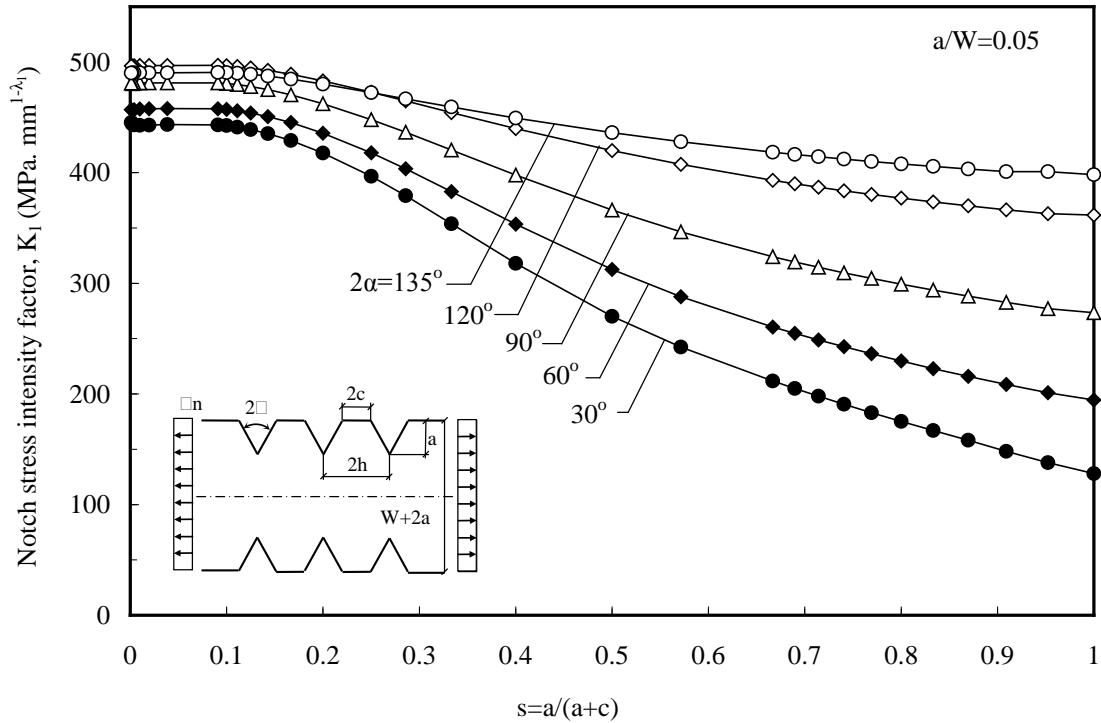
Fig.7. Variation of K_1 as a function of $s=a/(a+c)$ for relative depth of the notch a/W=0.05.

By increasing the relative depth of the notch from a/W=0.025 to 0.05, the same behavior of shallow notches is seen in Fig.7, with two exceptions: first, the limit value of s, where NSIF is constant, has been increased from s≈ 0.07 to 0.1. The second difference is observed for larger opening angles (2α=135°) when the variation of NSIF is decreasing as s rises, with a slight decrease of K_1 value for a larger distance between periodic notches (i.e. s≤0.25).
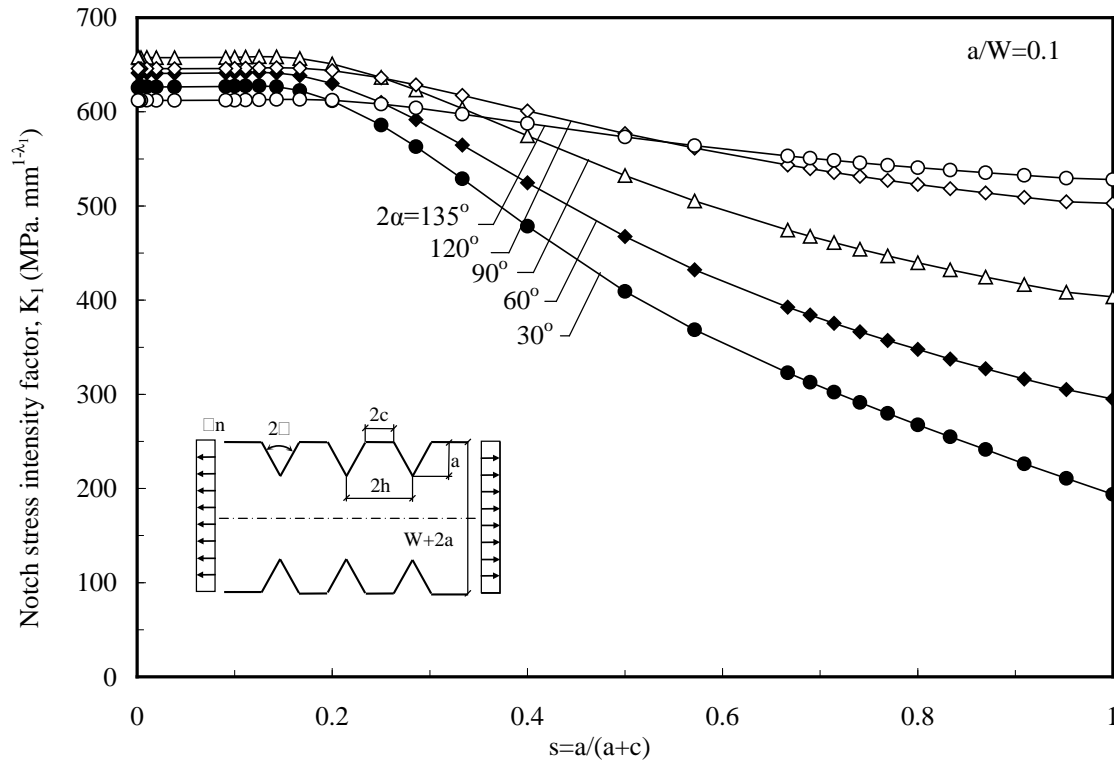
Fig.8. Variation of K_1 as a function of s=a/(a+c) for relative depth of the notch a/W=0.1.

According to Fig.8 by further increasing the depth of the notch, obviously the NSIF values rise and similar to the case of a/W=0.05 the fluctuations of NSIF for the larger opening angles, i.e. 2α=120 and 135° tend to a gradual trend. In particular, for the case 2α=135° this change is more stabilized, but the drop of K_1 is more pronounced and in a wider range of s (s≤0.5).
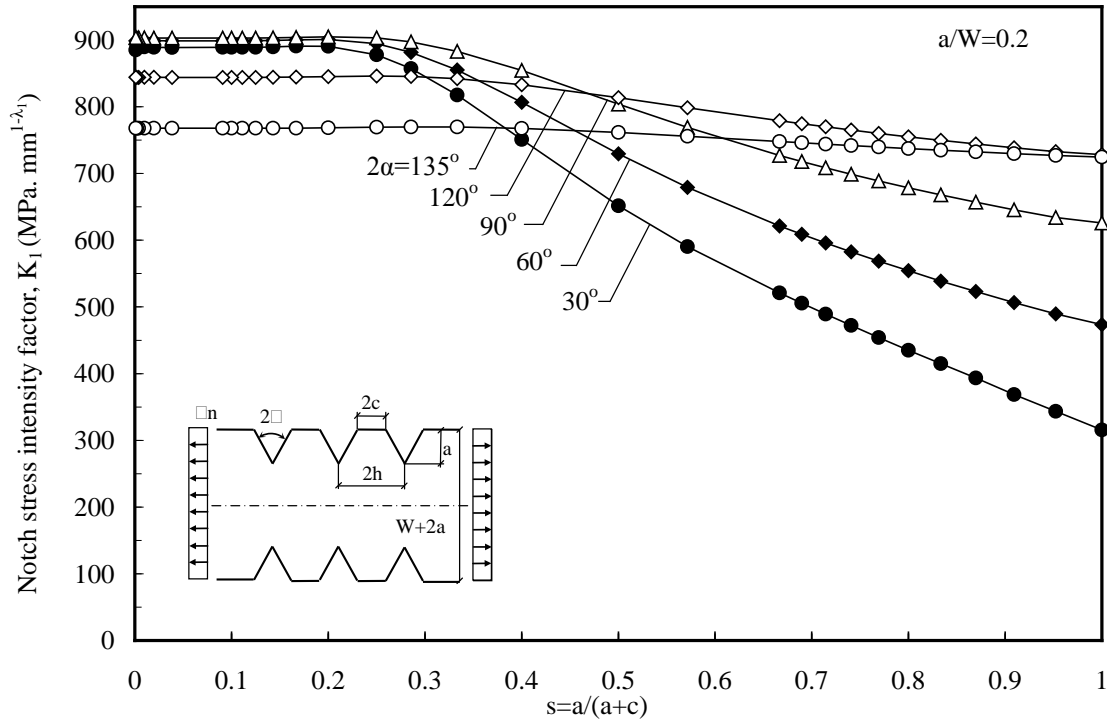
Fig.9. Variation of K_1 as a function of s=a/(a+c) for relative depth of the notch a/W=0.2.

It can be seen from Fig. 9 that as the notch depth increases and becomes deep (a/W=0.2) the similar stabilizing trends for larger opening angles are observed. In particular, the variation of NSIFs for the largest opening angle ($2\alpha=135^\circ$) becomes negligible and the trend is almost constant for the whole range of distances between periodic notches.
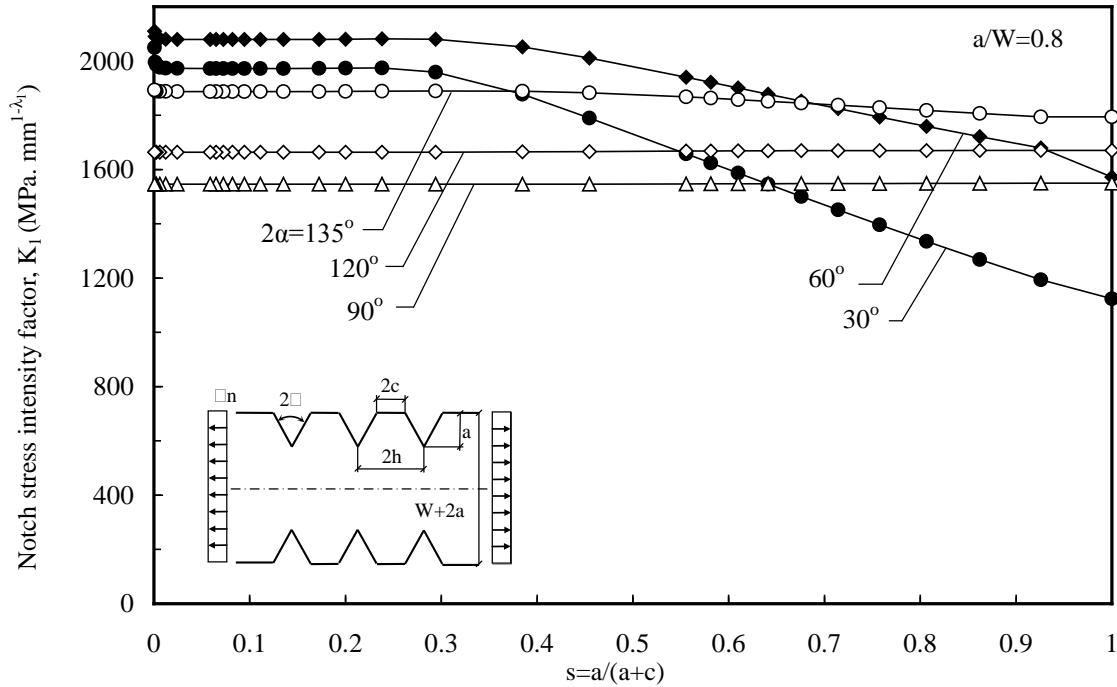
Fig.10. Variation of K_1 as a function of s=a/(a+c) for relative depth of the notch a/W=0.8.

Finally, Fig.10 shows the variation of NSIFs for very deep notches (a/W=0.8). It can be seen that for three opening angles 2α=90-135°, the NSIFs are almost stable in the total range of s. A slight leaning of 2α=60° to a constant NSIF value is also observed.

The validation of the obtained NSIFs for different values of relative depth of the notch is extensively discussed in a previous work by the authors [22] by comparing the results with some semi-analytical solutions for periodic shallow V-notches proposed in [23].

4. Scale effect of periodic notches

Following the guidelines given in [31], scaling the geometrical dimensions by a factor "n", the NSIF value can be obtained by using the following equation:

$$K_{i,b} = K_{i,a} \cdot n^{1-\lambda_i} \tag{10}$$

where the first index "i" is 1 or 2 according to the loading mode and the second index is a or b representing the former or latter geometry.

Applying the similar concept to the periodic notches under mode I loading (Fig. 11) it is possible to give the ratio of the two NSIFs as follows:

$$\frac{K_{1,b}}{K_{1,a}} = \sqrt{\frac{\overline{W_{1,b}}}{\overline{W_{1,a}}}} = \left(\frac{h_b}{h_a}\right)^{1-\lambda_1} = \left(\frac{a_b}{a_a}\right)^{1-\lambda_1} = \left(\frac{W_b}{W_a}\right)^{1-\lambda_1} \tag{11}$$

An arbitrary case of a periodic V-notched component ($2\alpha=60°$, a=10 mm, W=100 mm, $\sigma_n=100$ MPa and number of notches N=60) is chosen to demonstrate the validity of Eq. (11) against the FE results. The relative data are given in Table 1.
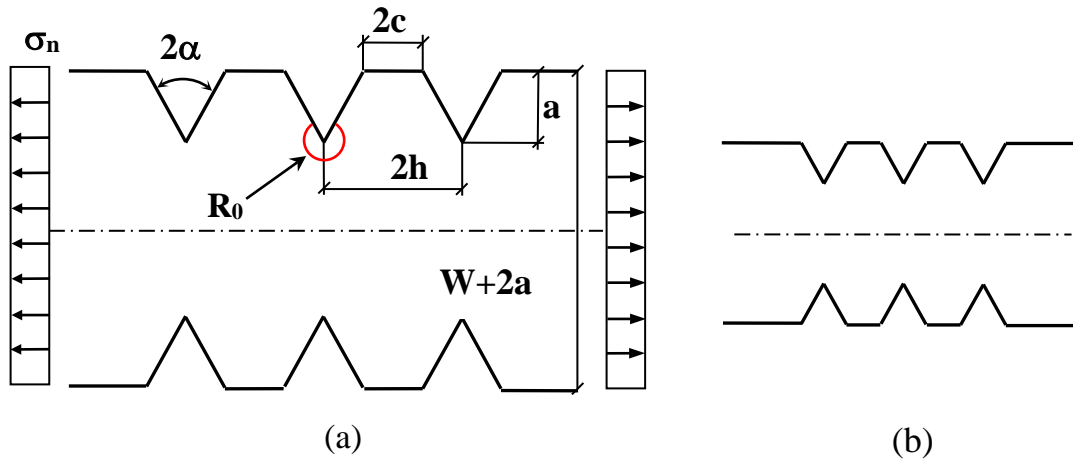
Fig. 11. Scaling of double symmetric periodic notches.

Table 1. NSIFs of a periodic notched component($2\alpha=60^{o}$, a=10 mm ,W=100 mm, σ_n=100 MPa and number of notches N=60) and several scaled configurations.

a (mm)	W (mm)	a/W	$\overline{W}$ (SED)	$\sqrt{\dfrac{\overline{\overline{W}}_{1,b}}{\overline{\overline{W}}_{1,a}}}$	$\left(\dfrac{a_b}{a_a}\right)^{1-\lambda_1}$	K_1 (FEM) MPa mm$^{0.4878}$	K_1 (Eq. (11)) MPa mm$^{0.4878}$	$\Delta\%$
10	100	0.1	24.759			295.014		
2.5	25	0.1	6.431	0.51	0.51	150.357	150.46	-0.07
5	50	0.1	12.578	0.71	0.71	210.274	209.46	-0.38
20	200	0.1	48.867	1.40	1.40	414.467	413.02	-0.35
40	400	0.1	96.872	1.97	1.97	583.552	581.18	-0.4
100	1000	0.1	244.844	3.14	3.07	927.736	905.70	-2.4

From Table 1 the exact agreement of Eq. (11) in terms of NSIF evaluation can be observed (the small inevitable error is due to the numerical calculations).

According to expression (11) there is a need to redefine K_0 to re-establish the non dimensionality of k_0 and to obtain an expression very similar to Eq. (2) being in this case the half of the pitch of the notch, h, the main geometrical parameter evolved:

$$K_h = k_h \sigma_n h^{1-\lambda_1} \tag{12}$$

The values of the non-dimensional parameter k_h, used for the normalization of NSIFs in Figs 12-15, are given in Table 2 for a wide range of periodic notches from narrow to deep case.

Table 2. The non-dimensional parameter k_h,for different opening angles and relative depth of the notch, used for normalization of NSIFs.

a/W	$2\alpha=30°$	60°	90°	120°	135°
0.025	1.0624	1.1236	1.2494	1.5122	1.7011
0.05	1.1073	1.1599	1.3137	1.5773	1.7670
0.1	1.1858	1.2543	1.4137	1.6799	1.8677
0.2	1.3665	1.4358	1.5991	1.8647	2.0444
0.35	1.6424	1.7008	1.8498	2.0982	2.2333

Table 2 provides k_h values also for the case of narrow periodic notches (c=0.0) and for different notch depths and opening angles.

Normalized NSIFs according to Eq. (12) as a function of s=a/(a+c) for different values of relative depth of the notch, ranging from shallow (a/W=0.025) to relatively deep notches (a/W=0.2), have been shown in Figs 12-15.
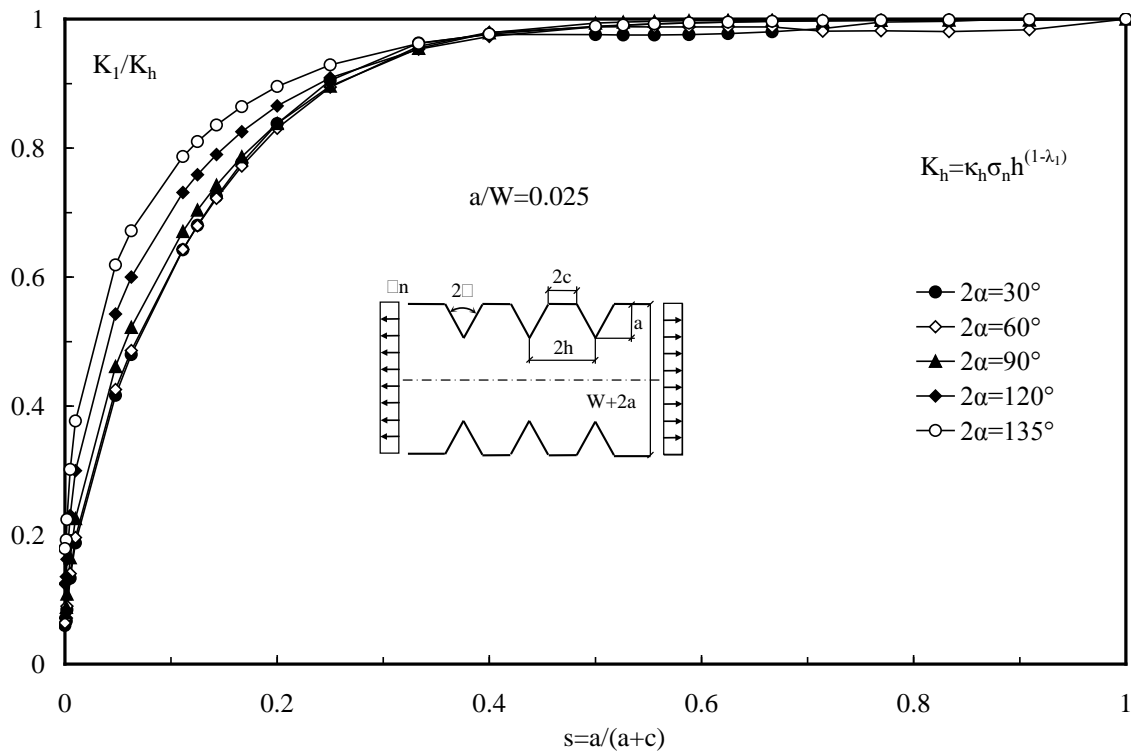
Fig. 12. Normalized NSIFs as a function of s=a/(a+c) for relative depth of the notch a/W=0.025.
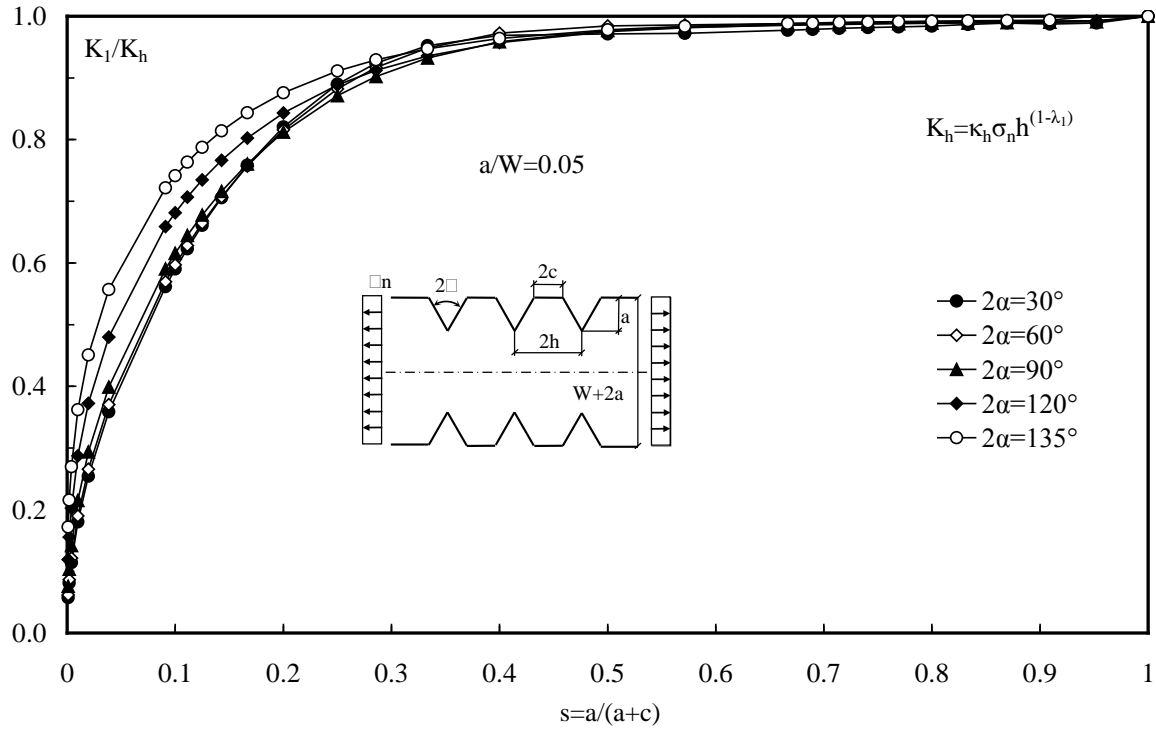
Fig. 13. Normalized NSIFs as a function of s=a/(a+c) for relative depth of the notch a/W=0.05.
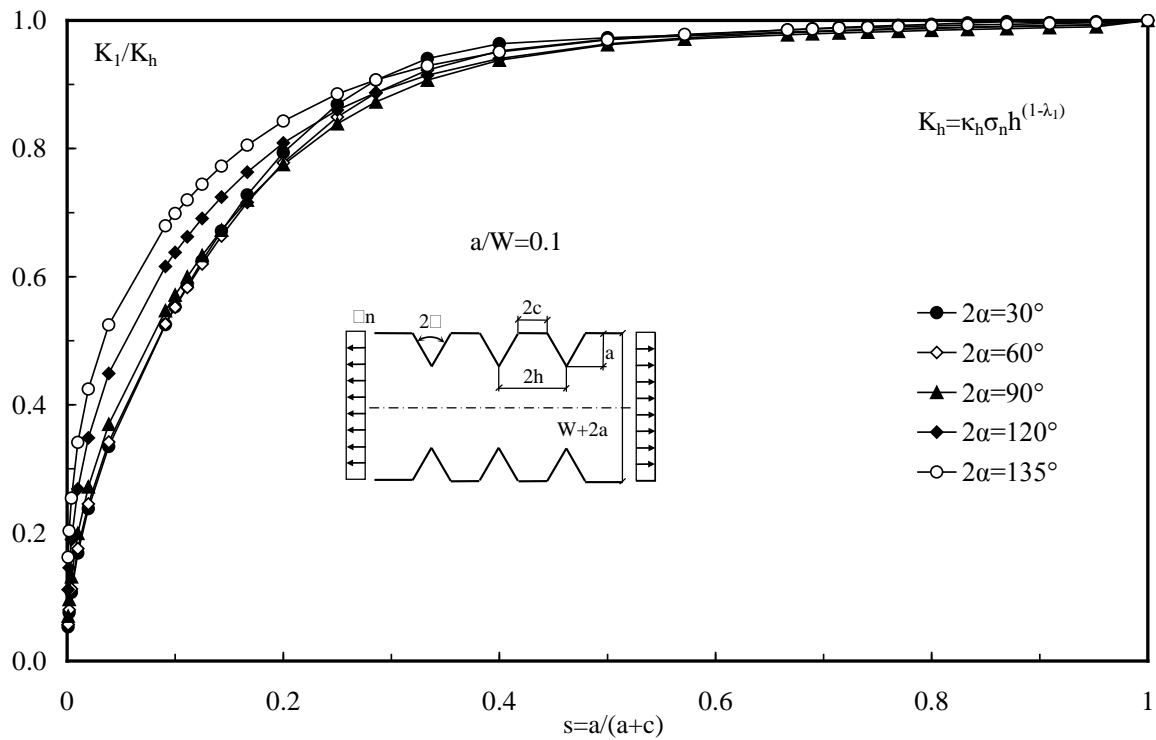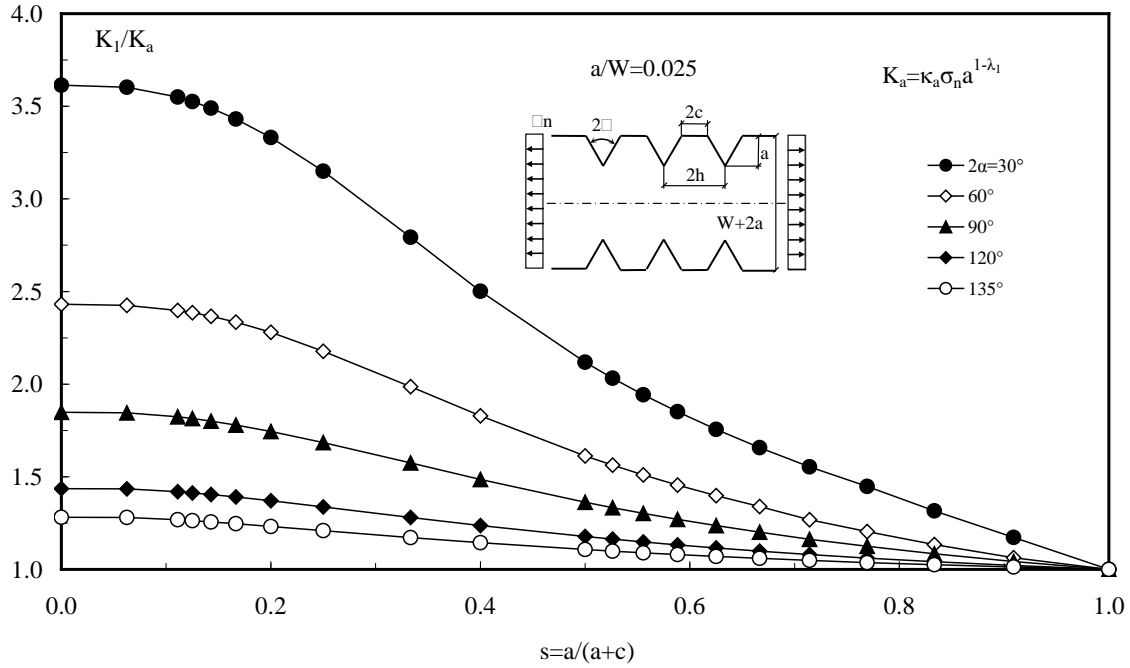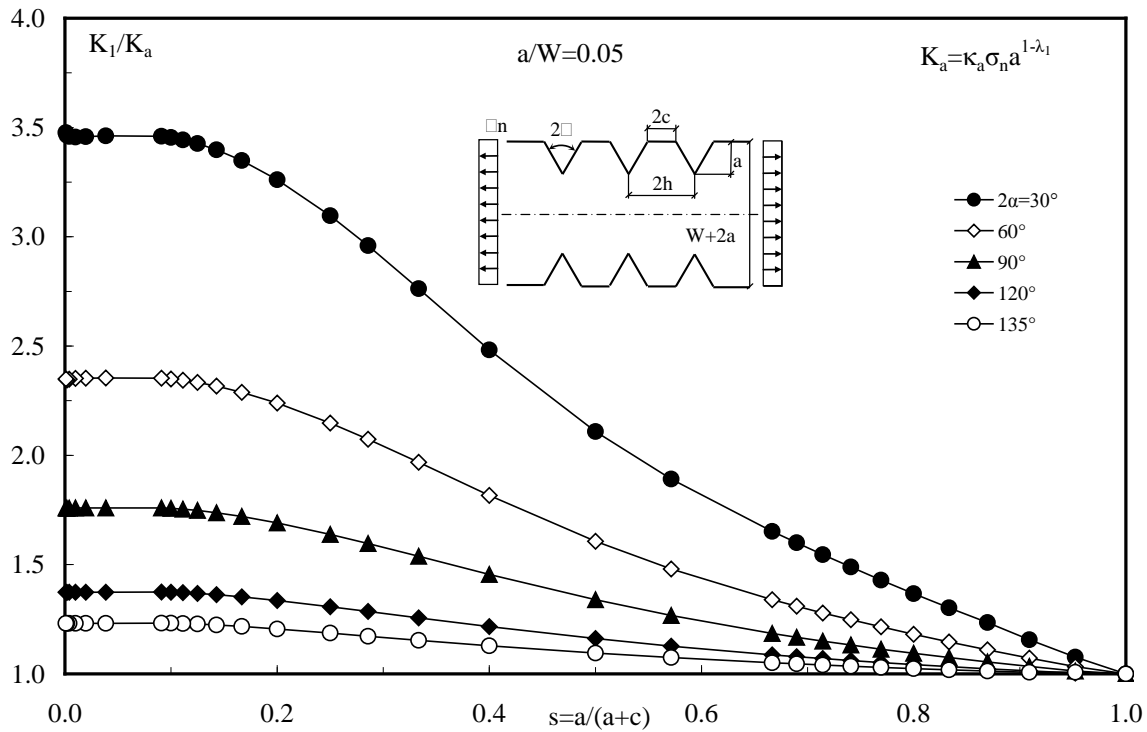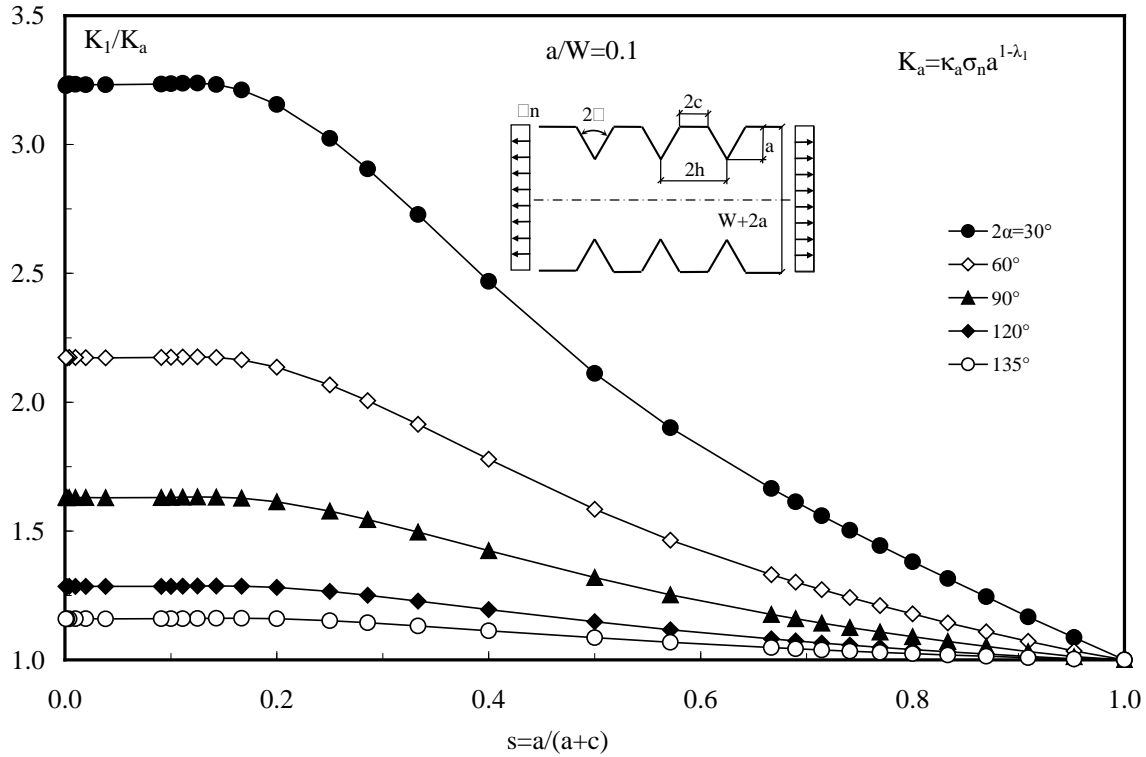

Fig. 14. Normalized NSIFs as a function of s=a/(a+c) for relative depth of the notch a/W=0.1.
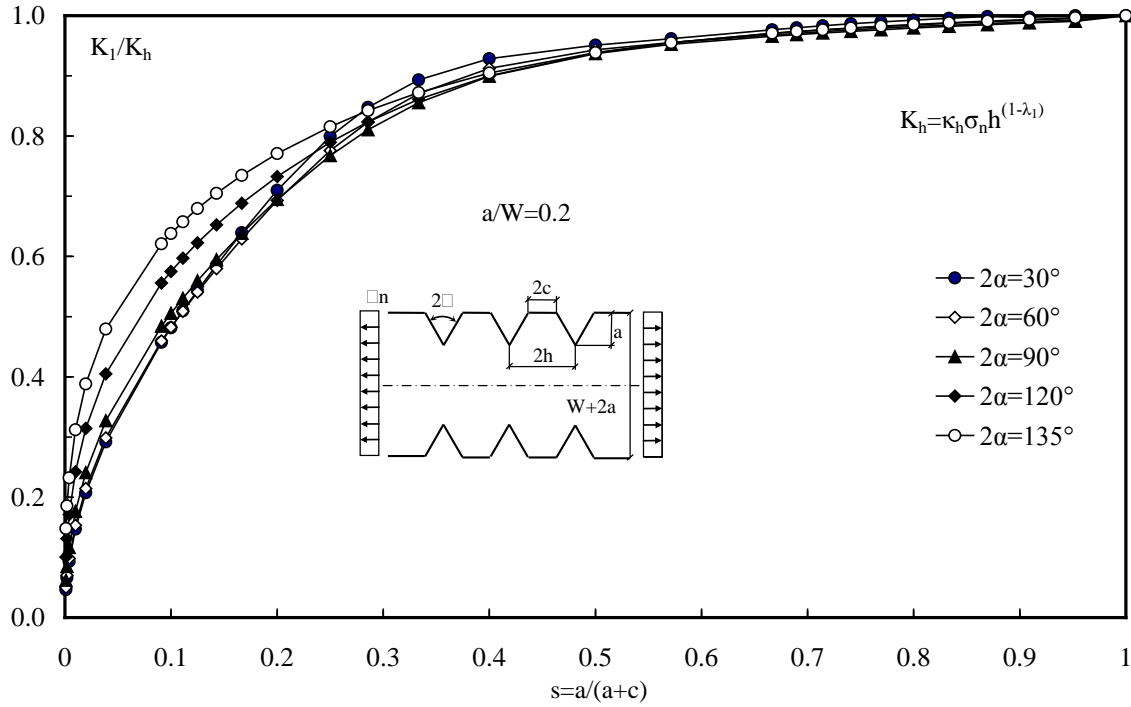
Fig. 15. Normalized NSIFs as a function of s=a/(a+c) for relative depth of the notch a/W=0.2.

From Figs 12-15 it can be seen the trend of the data summarized by means of Eq. (12) in the case of narrow periodic notches of finite-width plates, which is similar to Fig. 1 for infinite-width of the plates. However, in terms of graphical representation, the lines for different opening angles intersect each other and this makes far from easy the practical and direct use of such normalized diagrams.

For the above mentioned practical reason, it is more useful to employ another parameter and to present the plots of the normalized NSIFs in a more apparent manner. In this new representation, the depth of the notch (a) is the main geometrical parameter:

$$K_a = k_a \sigma_n a^{1-\lambda_1} \tag{13}$$

The values of the non-dimensional parameter k_a, used for normalization of NSIFs for a large range of periodic notches from shallow to the exceedingly deep cases are provided in Table 3.

Table 3. The non-dimensional parameter κ_a, for different opening angles and relative depth of the notch, used for normalization of NSIFs.

a/W	$2\alpha=30°$	$60°$	$90°$	$120°$	$135°$
0.025	0.5509	0.8595	1.2494	1.8676	2.2681
0.05	0.5742	0.8873	1.3137	1.9481	2.3547
0.1	0.6149	0.9595	1.4137	2.0748	2.4903
0.2	0.7087	1.0983	1.5991	2.3029	2.7259
0.35	0.8517	1.3010	1.8498	2.5914	2.9366
0.5	0.9910	1.4936	2.0893	2.7552	3.1182
0.6	1.0827	1.6176	2.2151	2.8601	3.2825
0.7	1.1738	1.7397	2.3291	2.9734	3.4811
0.8	1.2644	1.8547	2.4376	3.1004	3.7082

Table 3 lists also the values of κ_a for narrow periodic notches (c=0.0) for different notch depths and opening angles.

In addition, as the main aim of this study is to provide the analytical expressions for NSIF evaluation, the polynomials for k_a estimation for different notch to depth ratios as well as notch opening angles in the whole range of notch spacing ($0 \leq s \leq 1$) are presented in Table A.2 (Appendix). As an example, the case of a/W=0.1 is depicted in Fig. 16 to show the trend of the proposed polynomial. In addition, in order to demonstrate the versatility of the present analytical equations for NSIF estimation of periodic notch plates under tension, a worked example is explained step by step in the Appendix.
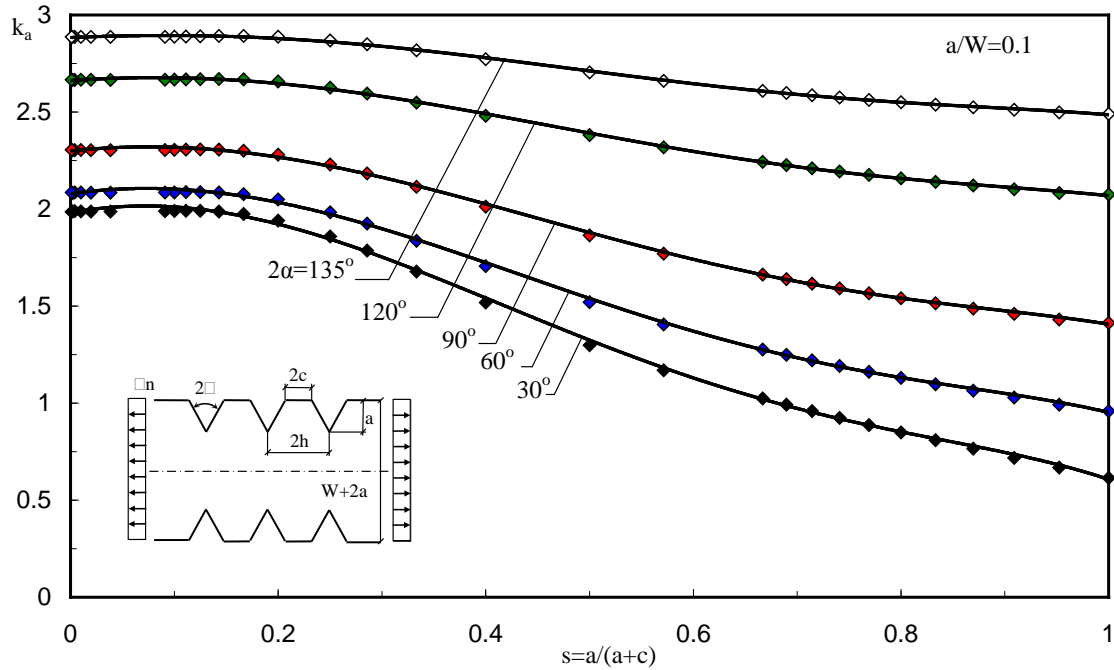
Fig. 16. Polynomial graphs for estimation of non-dimensional parameter k_a in the whole range of notch spacing s for the case of a/W=0.1.

By estimating k_a from the proposed polynomials and once known geometrical parameters of the periodic V-notched components, it is very easy to use Eq. (13) and to obtain the NSIF quickly and without FE modeling.

Normalized NSIFs according to Eq. (13) as a function of s=a/(a+c) for different values of relative depth of the notch, ranging from shallow (a/W=0.025) to very deep notches (a/W=0.8), have been shown in Figs 17-20.

Fig.17. Normalized NSIFs as a function of s=a/(a+c) for relative depth of the notch a/W=0.025.

Fig.18. Normalized NSIFs as a function of s=a/(a+c) for relative depth of the notch a/W=0.05.

Fig.19. Normalized NSIFs as a function of s=a/(a+c) for relative depth of the notch a/W=0.1.

By comparing Figs. 17-19, it can be seen that changing the notch depth from shallow (a/W=0.025) to relatively medium notches (a/W=0.1) leads to a change of the normalized NSIFs both in the case of large and small opening angles. In the case of large opening angles (2α≥120º), the slope of the normalized NSIF becomes more stable in the whole range of s, whereas for small opening angles (2α≤90º), it only extends to the initial, limited values of s (s<0.15) and then it converges sharply to 1.0 at s=1.0.
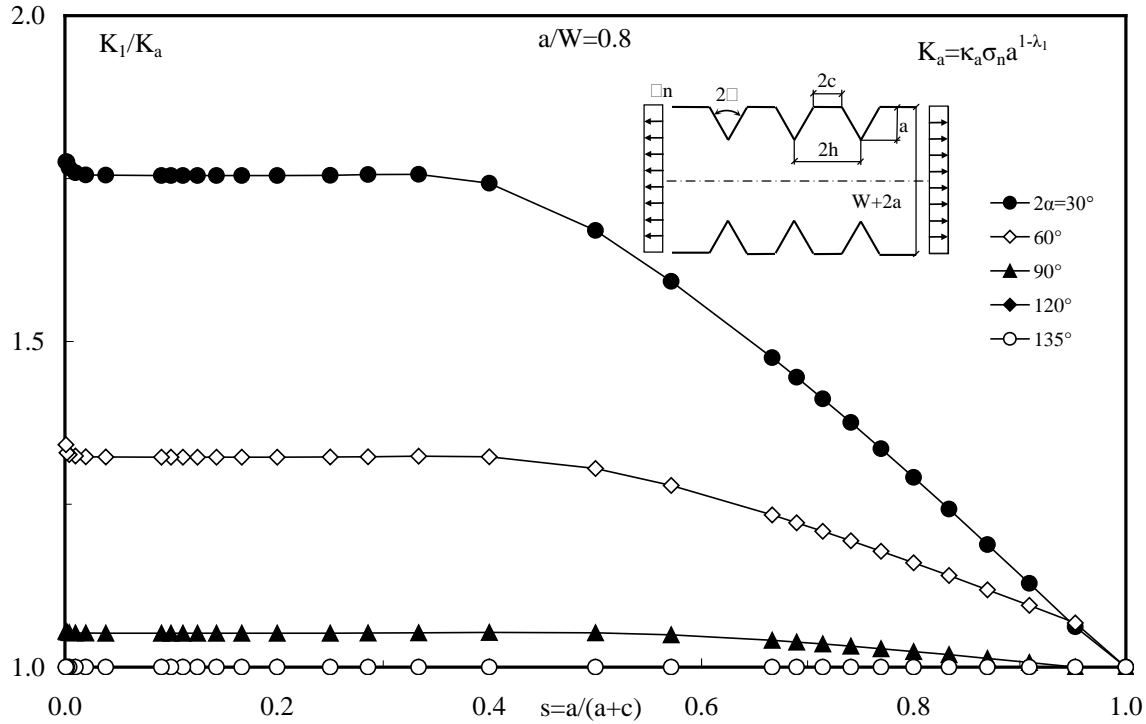
Fig.20. Normalized NSIFs as a function of s=a/(a+c) for relative depth of the notch a/W=0.8.

Finally, as a graphical means of NSIF estimation from the graphs in Figs. 17-20, one can easily determine the NSIFs for different notch depths as well as opening angles by having the known parameter such as the notch spacing (c). It is worth mentioning that for deep notches (when a/W≥0.5) and opening angles 2α≥120 regardless of the distance between periodic notches, it is possible to estimate the NSIF by using only Eq. (13).

Alternatively, as a more practical and quick method, Eq. (13) permits to estimate the NSIFs of periodic V-notched components analytically by only using the non-dimensional coefficients listed in Table A.1 and without FE modeling.

6. Conclusions

A broad range of notch configurations, varying from shallow to very deep notches, complete range of notch spacing and wide range of notch opening angles are considered in this study. The effects of relative depth of the notch, opening angle and notch spacing are examined. The

significance of sharp notch approximation for the case of blunt notches with a very small notch radius is discussed as well.

Local SED approach by considering a control volume surrounding the tip of the middle notch is employed to estimate the NSIF of each component by using a relatively coarse mesh in the FE models. The FE results are used to introduce a simple analytical expression with relevant non-dimensional coefficients in the polynomial forms. The proposed analytical expression permits to estimate the NSIFs of periodic V-notched components very quickly by only using the given non-dimensional coefficients in a wide range of relative depth of the notch, notch opening angles and total range of notch spacing.

Acknowledgment

References

1. Dragoni, E. and Castagnetti, D. Concentration of normal stresses in flat plates and round bars with periodic notches. *Journal of Strain Analysis for Engineering Design*, 2010, 45(7), 495-503.

2. Dragoni, E. and Castagnetti, D. Concentration of shear stresses in shallow periodic notches. *Journal of Strain Analysis for Engineering Design*, 2011, 46, 397-404.

3. Neuber, H. *Theory of Notch Stresses*, 2nd edition Springer, 1958 (Verlag, Germany).

4. Gross, R. and Mendelson, A. Plane elastostatic analysis of V-notched plates. *Int J Fract Mech*, 1972, 8, 267-76.

5. Chen, D-H. Stress intensity factors for V-notched strip under tension or in-plane bending. *International Journal of Fracture*, 1994, 70(1), 81-97.

6. Dunn, M., Suwito, W., Cunningham, S. and May, C. Fracture initiation at sharp notches under mode I, mode II, and mild mixed mode loading. *International Journal of Fracture*, 1997, 84(4), 367-81.
7. Dunn, M.L., Suwito, W. and Cunningham, S. Fracture initiation at sharp notches: Correlation using critical stress intensities. *International Journal of Solids and Structures*, 1997, 34(29), 3873-83.

8. Gómez, F.J. and Elices, M. Fracture of components with V-shaped notches. *Engineering Fracture Mechanics*, 2003, 70(14), 1913-27.

9. Gómez, F.J. and Elices, M. A fracture criterion for sharp V-notched samples. *International Journal of Fracture*, 2003, 123, 163-75.

10. Knésl, Z. A criterion of V-notch stability. *International Journal of Fracture*, 1991, 48(4), 79-83.

11. Nui, L.S., Chehimi, C. and Pluvinage, G. Stress field near a large blunted tip V-notch and application of the concept of the critical notch stress intensity factor (NSIF) to the fracture toughness of very brittle materials. *Engineering Fracture Mechanics*, 1994, 49(3), 325-35.

12. Strandberg, M. Fracture at V-notches with contained plasticity. *Engineering Fracture Mechanics*, 2002, 69(3), 403-15.

13. Lazzarin, P. and Tovo, R. A notch intensity factor approach to the stress analysis of welds. *Fatigue and Fracture of Engineering Materials and Structures*, 1998, 21(9), 1089-103.

14. Croccolo, D., De Agostinis, M. and Vincenzi, N. Normalization of the stress concentrations at the rounded edges of a shaft–hub interference fit: extension to the case of a hollow shaft. *The Journal of Strain Analysis for Engineering Design*, 2012, 47(3), 131-9.

15. Barati, E. and Berto, F. A comparison between rapid expressions for evaluation of the critical J-integral in plates with U-notches under mode I loading. *Journal of Strain Analysis for Engineering Design*, 2011, 46(8), 852-65.

16. Berto, F. and Zappalorto, M. The fictitious notch rounding approach applied to V-notches with root holes subjected to mode I loading. *Journal of Strain Analysis for Engineering Design*, 2012, 47(3), 176-86.

17. Afshar, R. and Berto, F. Stress concentration factors of periodic notches determined from the strain energy density. *Theoretical and Applied Fracture Mechanics*, 2011, 56(3), 127-39.

18. Parker, A. P. Stability of arrays of multiple edge cracks. *Engineering Fracture Mechanics*, 1999, 62(6), 577-91.

19. Pook, L. P. Stress intensity factor expressions for regular crack arrays in pressurized cylinders. *Fatigue and Fracture of Engineering Materials and Structures*, 1990, 13(2), 135-43.

20. Tada, H., Paris, P. C. and Irwin, G. *The stress analysis of cracks handbook* 2nd, edition, 1985 (St Louis: Paris Productions Incorporated and Del Research Corporate).

21. Murakami, Y. *Stress intensity factors handbook*. 2001 (Oxford UK: Elsevier Science Ltd).

22. Lazzarin, P., Afshar, R. and Berto, F. Notch stress intensity factors of flat plates with periodic sharp notches by using the strain energy density. *Theoretical and Applied Fracture Mechanics,* 2012, 60(1), 38-50.

23. Savruk, M. and Kazberuk, A. A plane periodic boundary-value problem of elasticity theory for a half-plane with curvilinear edge. *Materials Science*, 2008, 44(4), 461-70.

24. Berto, F., Lazzarin, P. and Afshar, R. Simple new expressions for the notch stress intensity factors in an array of narrow V-notches under tension. *International Journal of Fracture*, 2012, 176(2), 237-44.

25. Lazzarin, P. and Berto, F. Some expressions for the strain energy in a finite volume surrounding the root of blunt V-notches. *International Journal of Fracture*, 2005, 135(1-4), 161-85.

26. Lazzarin, P. and Zambardi, R. A finite-volume-energy based approach to predict the static and fatigue behavior of components with sharp V-shaped notches. *International Journal of Fracture*, 2001, 112(3), 275-98.

27. Berto, F. and Lazzarin, P. A review of the volume-based Strain Energy Density approach applied to static and fatigue strength assessments of notched and welded structures. *Theoretical and Applied Fracture Mechanics*, 2009, 52(3), 183-194.

28. Lazzarin, P., Berto, F., Gomez, F. J. and Zappalorto, M. Some advantages derived from the use of the strain energy density over a control volume in fatigue strength assessments of welded joints. *International Journal of Fatigue*, 2008, 30(8),1345-57.

29. Lazzarin, P., Berto, F. and Zappalorto, M. Rapid calculations of notch stress intensity factors based on averaged strain energy density from coarse meshes: Theoretical bases and applications. *International Journal of Fatigue*, 2010, 32(10), 1559-67.

30. Williams, M. L. Stress singularities resulting from various boundary conditions in angular corners of plates in extension. *Journal of Applied Mechanics*, 1952, 19, 526-8.
31. Lazzarin, P. and Tovo, R. A unified approach to the evaluation of linear elastic stress fields in the neighborhood of cracks and notches. *International Journal of Fracture*, 1996, 78(1), 3-19.

Appendix

The values of λ_1 as a function of notch opening angle (2α) are given in Table A.1.

Table A.1

The following polynomial equation has been used for interpolation of the numerical data to estimate k_a :

$$k_a = as^5 + bs^4 + cs^3 + ds^2 + es + f$$

in which s stands for normalized notch spacing (s=a/(a+c)). The relevant coefficients are given in Table A.2.

Table A.2

Worked example

Suppose we have a periodic notch plate with following properties:

W=100 mm

a=10 mm

$2\alpha=60^{\circ}$
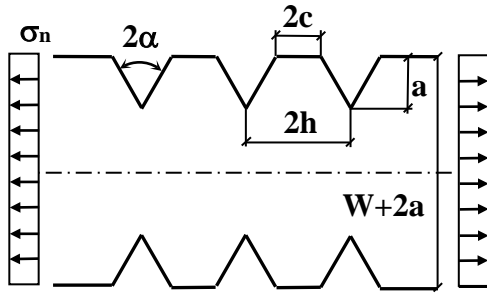
σ_n=100 MPa

2c=5 mm→c=2.5 mm

Solve: According to the geometrical data: a/W=0.1 and s=a/(a+c)=(10/(10+2.5)=0.8. The value of K_1 for this configuration can be found from FE method (Fig. 8) and it is equal to 347 MPa mm$^{(1-\lambda_1)}$, which the value of λ_1 for this opening angle from Table A.1 is equal to 0.5122.

Now by using $K_a = k_a \sigma_n a^{1-\lambda_1}$ (Eq. (13)):

It is enough to find the dimensionless parameter k_a from Table A.2:

$k_a = as^5 + bs^4 + cs^3 + ds^2 + es + f$

a/W=0.1; $2\alpha=60^\circ$;s=0.8   a=−3.738   b= 5.729   c = 1.520   d = −5.392   e = 0.753   f = 2.076

and

which gives $k_{a=}1.127$

Now by replacing k_a in Eq. (13), the value of K_a by means of analytical equation can be obtained as follows:

$K_a=1.127$ x 100 x 10 $^{(1-0.5122)}=346.5$ MPa mm$^{(1-\lambda_1)}$

By comparing this value with the one obtained from FE method (Fig. 8), the sound agreement can be observed (with error less than 0.2 %).

Table A.1. Values of λ_1 for sharp V-notches, as a function of the notch angle.

2α (degrees)	λ_1
0	0.5000
15	0.5002
30	0.5014
45	0.5050
60	0.5122
75	0.5247
90	0.5445
105	0.5739
120	0.6157
135	0.6736
150	0.7520
160	0.8187
170	0.9000

Table A.2. Polynomial equations for non-dimensional coefficient k_a in Eq. (13) for different relative depth of the notch and opening angles.

$k_a = as^5 + bs^4 + cs^3 + ds^2 + es + f$							
a/W	2α	a	b	c	d	e	f
0.025	30°	1.674	-10.206	17.791	-11.607	0.9132	1.982
	60°	2.116	-9.379	14.967	-9.695	0.767	2.082
	90°	2.201	-8.885	13.213	-8.102	0.516	2.306
	120°	3.204	-10.540	13.115	-6.926	0.335	2.681
	135°	3.623	-11.115	12.707	-6.087	0.233	2.908
0.05	30°	1.002	-8.126	15.799	-11.170	1.082	1.979
	60°	1.241	-7.513	13.766	-9.646	0.958	2.076
	90°	1.927	-8.143	12.736	-8.292	0.779	2.304
	120°	3.179	-10.452	13.280	-7.412	0.679	2.670
	135°	3.218	-10.121	12.182	-6.403	0.588	2.894
0.1	30°	-3.647	3.997	4.928	-7.675	1.022	1.976
	60°	-3.738	5.729	1.520	-5.392	0.753	2.076
	90°	-2.950	4.970	0.430	-3.914	0.571	2.297
	120°	-2.228	4.171	-0.630	-2.281	0.374	2.661
	135°	-2.280	4.851	-2.287	-0.891	0.208	2.884
0.2	30°	-12.488	28.646	-19.429	1.802	0.169	1.990
	60°	-11.018	26.661	-19.937	3.380	-0.086	2.084
	90°	-8.278	21.064	-17.061	3.772	-0.216	2.308
	120°	-4.140	11.289	-10.123	2.821	-0.219	2.671
	135°	-1.554	4.649	-4.660	1.540	-0.138	2.889
0.35	30°	-15.348	38.691	-31.935	7.961	-0.561	2.036
	60°	-9.949	26.790	-23.825	6.732	-0.560	2.110
	90°	-4.253	12.726	-12.662	4.082	-0.392	2.349
	120°	1.021	-1.332	-0.088	0.329	-0.052	2.713
0.5	30°	-11.764	32.099	-29.688	9.156	-0.930	2.112
	60°	-5.300	16.233	-16.695	5.687	-0.628	2.195
	90°	0.520	0.840	-2.926	1.441	-0.197	2.409
0.6	30°	-8.135	23.511	-23.140	7.467	-0.770	2.148
	60°	-3.931	12.531	-13.645	4.997	-0.605	2.273
	90°	1.514	-2.096	-0.066	0.516	-0.109	2.453
0.7	30°	-5.168	16.314	-17.497	5.980	-0.645	2.190
	60°	-3.708	11.294	-12.253	4.638	-0.590	2.367
	90°	1.772	-3.181	1.264	0.019	-0.054	2.505
0.8	30°	-3.639	12.615	-14.801	5.530	-0.681	2.239
	60°	-4.547	12.380	-12.479	4.633	-0.586	2.470
	90°	1.699	-3.350	1.764	-0.224	-0.021	2.568

Paper IV

Some recent developments on the application of the strain energy density to shallow threaded plates with sharp notches

Abstract   In this study, the main advantages of the strain energy density (SED) approach and some recent applications of the SED to the fatigue analysis of welded joints are reviewed. In addition, the paper investigates the scale effect in the threaded plates with sharp notches subjected to tension loading. Some closed form expressions for evaluation of the notch stress intensity factors (NSIFs) of periodic sharp notches, obtained by SED approach, are employed. The new expressions are applicable to narrow notches when the ratio between the notch depth and the plate width, t/W, is lower than 0.025 providing very accurate results. The NSIF ratio of two scaled geometries of periodic sharp notches is a function of averaged SED in the control volume embracing the middle notch tip. The new results are very useful for the assessment under fatigue loading.

Keywords: Periodic notches, Notch Stress Intensity Factor (NSIF), Strain Energy Density (SED), Narrow notches.

1   Introduction

Toothed cutting blades, thread bars and splined shafts play a vital role in various industry applications. They are being used in many facilities across different sectors including: construction, aerospace, wood industry, electronic devices, etc. The variability of the notch stress intensity factors (NSIFs) of periodic blunt and sharp V-notches is investigated by means of the strain energy density (SED) approach in combination with coarse meshes in the finite element method (FEM) (Afshar and Berto, 2011, Berto, Lazzarin and Afshar, 2012, Lazzarin, Afshar and Berto, 2012).

The necessity of a simple criterion for engineering applications led to development of a point-wise SED approach valid for cracks (Sih, 1973, Sih, 1973, Sih, 1974, Sih, 1991) and notches (Sih and Ho, 1991). Factor S was defined as the product of the SED by a critical distance from the point of singularity (Sih, 1974). Failure was thought of as controlled by a critical value S_c, whereas the direction of crack propagation was determined by imposing a minimum condition on S. The theory was extended to employ the total SED near the notch tip (Sih and Ho, 1991), and the point of reference was chosen to be the location on the surface of the notch, where the maximum tangential stress occurs.

By using the SED concept combined with a coarse mesh in the FE analysis, a fatigue strength assessment of welded joints was carried out (Lazzarin et al., 2008). A procedure for rapid calculations of the NSIFs based on the SED from coarse meshing is drawn in Ref. (Lazzarin, Berto and Zappalorto, 2010). The extension to three-dimensional cases is also possible and very convenient, in particular when edge effects are present or when a narrow spacing between collinear notches is considered. In small bodies a multiscaling and segmentation scheme permits to scale the SED at pico, nano and micro levels (Sih and Tang, 2005, Tang and Sih, 2005, Sih, 2007).

As alternatives of the SED approach, a review of the dual boundary element method for modeling crack growth in two-dimensional and three-dimensional mixed mode problems is presented and compared with available alternative solutions in Ref. (Cisilino and Aliabadi, 2010). In another work, a model based on cohesive crack concept is developed for finite element analysis of quasi-brittle materials (Cendón et al., 2000, Gálvez et al., 2012).

The creation and subsequent shedding of periodic edge cracks is a natural phenomenon which occurs in heat-checked gun tubes, rapidly cooled pressure vessels and rock, dried-out mud flats, paint and concrete and in ceramic coatings and permafrost. Dealing with this topic a complete state of the art together with a simple developed model assessing the shedding behavior is carried out by Parker (Parker, 1999). As discussed in that work, the surface topography of the cracking of ice-wedge polygons in Arctic permafrost, of mud flats in Death Valley and of craze-cracks (heat-checking) at the bore of a gun tube are all strikingly similar, yet they span five orders of magnitude in scale, with the maximum plate dimensions for ice and mud being, respectively, 22 m and 0.25 m and with the minimum plate size for gun tube craze cracking being 0.2 mm. Recently, some new expression for the NSIFs of periodic sharp notches is developed, which is an extended version of that proposed by Tada et *al.* (Tada, Paris and Irwin, 1985) for edge cracks. It is valid for an infinite plate width, but can be applied with errors within 5 percent if the ratio between the notch depth and plate width remains lower than 0.025. The expressions are suitable both for the direct evaluation of the SED and NSIF as a function of the narrow notch spacing (Berto, Lazzarin and Afshar, 2012).

In this paper, the scale effect of periodic narrow-sharp notches by using the aforementioned closed form expressions in the macro-meso scale range is studied. The theoretical results reported here can be directly applied to the fatigue design.

2   Advantages of the SED for fatigue assessment

As opposed to the direct evaluation of the NSIFs, which needs very refined meshes, the mean value of the elastic SED on the control volume can be determined with high accuracy by using coarse meshes (Lazzarin et al., 2008, Berto and Lazzarin, 2009, Lazzarin, Berto and Zappalorto, 2010).Very refined meshes are necessary to directly determine the NSIFs from the local stress distributions. Refined meshes are not necessary when the aim of the FE analysis is to determine the mean value of the local SED on a control volume surrounding the points of stress singularity. The SED in fact can be derived directly from nodal displacements, so that also coarse meshes are able to give sufficiently accurate values for it. Some recent contributions document the slight variability of the SED as determined from very refined meshes and coarse meshes, considering some typical welded joint geometries and provide a theoretical justification to the weak dependence exhibited by the mean value of the local SED when evaluated over a control volume centered at the weld root or the weld toe. On the contrary singular stress distributions are strongly mesh dependent. The NSIFs can be estimated from the local SED value of pointed V-notches in plates subjected to mode I, Mode II or a mixed mode loading. Taking advantage of some closed-form relationships linking the local stress distributions ahead of the notch to the maximum elastic stresses at the notch tip the coarse mesh SED-based procedure is used to estimate the relevant theoretical stress concentration factor K_t for blunt notches. In particular, a circular hole and a U-shaped notch, the former in mode I loading, the latter also in mixed, I + II, mode was studied (Livieri and Lazzarin, 2005, Berto and Lazzarin, 2009). Other important advantages can be achieved by using the SED approach. The most important advantages of SED method are as follows:

- It permits consideration of the scale effect, which is fully included in the NSIF Approach
- It permits consideration of the contribution of different Modes.
- It permits consideration of the cycle nominal load ratio .
- It overcomes the complex problem tied to the different NSIF units of measure in the case of different notch opening angles (i.e crack initiation at the toe (2α=135°) or root (2α=0°) in a welded joint)
- It overcomes the complex problem of multiple crack initiation and their interaction on different planes.

- It directly takes into account the T-stress and this aspect becomes fundamental when thin structures are analysed.

- It directly includes three-dimensional effects and out-of-plane singularities not assessed by Williams' theory.

2.1   Synthesis of fatigue analysis based on SED in a control volume

The mean value of the SED in a circular sector of radius R_0 located at the fatigue crack initiation sites has been used to summarise fatigue strength data from steel welded joints of complex geometry (Fig. 1).

Local SED ($\Delta\overline{W}$), averaged in a finite size volume surrounding weld toes and roots is a scalar quantity which can be given as a function of mode I-II NSIFs in plane problems and mode I-II-III NSIFs in three dimensional problems. The evaluation of the local SED needs precise information about the control volume size. From a theoretical point of view, the material properties in the vicinity of the weld toes and the weld roots depend on a number of parameters as residual stresses and distortions, heterogeneous metallurgical micro-structures, weld thermal cycles, heat source characteristics, load histories and so on. To device a model capable of predicting R_0 and fatigue life of welded components on the basis of all these parameters is really a task too complex. Thus, the spirit of the approach is to give a simplified method able to summarize the fatigue life of components only on the basis of geometrical information, treating all the other effects only in statistical terms, with reference to a well-defined group of welded materials and, for the time being, to arc welding processes.

In a plane problem all stress and strain components in the highly stressed region are correlated to mode I and mode II NSIFs.

The material parameter R_0 can be estimated by using the fatigue strength $\Delta\sigma_A$ of the butt ground welded joints (in order to quantify the influence of the welding process, in the absence of any stress concentration effect) and the NSIF-based fatigue strength of welded joints having a V-notch angle at the weld toe constant and large enough to ensure the non singularity of mode II stress distributions.

The mean value of the SED, ΔW, as determined on a control volume embracing the weld toe or the weld root was directly used as parameter for fatigue strength assessments of welded joints (see Refs. (Livieri and Lazzarin, 2005, Berto and Lazzarin, 2009)). The relevant ΔW-N

scatterband is shown in Fig. 1, where a large bulk of fatigue test data (about 900 data) from different welded joints with a main plate thickness ranging from 6 to 100 mm are plotted. Details on welded joint geometries, materials and welding technologies are reported in some previous papers.
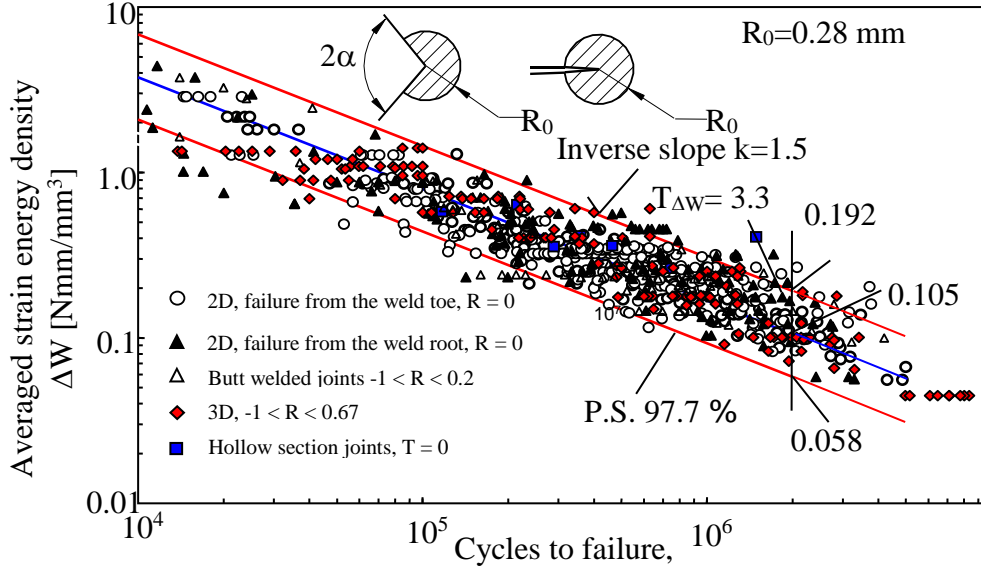
Fig. 1. Fatigue strength of the welded joints as a function of the averaged local SED; R is the nominal load ratio (Berto and Lazzarin, 2009).

3   SED in a control volume applied to sharp notches

Dealing with a sharp V-notch subjected to Mode I loading (see Fig. 3), assuming a plane strain condition, the mean value of the SED in the semi-circular sector of radius R_0 is (Lazzarin and Zambardi, 2001):

$$\overline{W}_1 = \frac{e_1}{E}\left(\frac{K_1}{R_0^{1-\lambda_1}}\right)^2 \tag{1}$$

where K_1 is the NSIF, λ_1 is Williams'eigenvalue (Williams, 1952), e_1 is a shape function that depends both on the notch angle 2α and the Poisson's ratio ν and E is the Young modulus.

By inverting Eq.(1) K_1 can be easily defined as follows:

$$K_1 = R_0^{1-\lambda_1} \sqrt{\frac{E\overline{W}_1}{e_1}} \tag{2}$$

Due to the linearity of the problem, the NSIF value can be computed, similarly to stress intensity factors (SIFs) in linear elastic fracture mechanics (LEFM) as:

$$K_1 = k_1 \sigma_n t^{1-\lambda_1} \tag{3}$$

where k_1 is a non dimensional parameter that depends on the overall geometry and can be seen as an extension of the shape factor used in the LEFM, σ_n is the reference stress (e.g., the remote tensile stress); $t^{1-\lambda_1}$ quantifies the influence of the specimen size and in particular of the notch depth.

Results of narrow V-notches with a/t=0, the most critical geometry, are reported in Table 1. Here the comparison is between the NSIFs obtained from coarse and fine meshes. The maximum detected error is less than 2%.

Table 1. Comparison between fine and coarse mesh-based results; SED approach applied to the models with narrow periodic notches, a/t=0.0, (t/d=0.05).

2α (°)	F_I^V (coarse mesh)	F_I^V (fine mesh)	$\Delta\%$
30	0.329	0.333	-1.06
45	0.405	0.411	-1.56
60	0.498	0.498	-0.17
90	0.734	0.730	0.58
120	1.092	1.090	0.14
135	1.322	1.323	-0.07

3.1 Application of the SED to periodic narrow notches: an extension of Tada Paris diagram

A system of multiple, equal length edge cracks of depth a and spacing 2h has been considered by Tada et *al*. (Tada, Paris and Irwin, 1985) in a plate of infinite width. The variation of the SIF normalized by $K_0 = \sigma \sqrt{h}$ is presented as a function of s=t/(t+h). It is shown that in the case of narrow cracks and having a s value greater than 0.3, the SIF (K_I) can be simply estimated by using the following equation, which is valid for an infinite plate width:

$$K_I = K_0 = \sigma_n \sqrt{h} \tag{4}$$

Eq. (4) can be directly applied without requiring numerical simulations and is independent of the notch depth. The only parameter involved is the crack spacing, h, which can be easily measured. Consider now multiple, equal-length double symmetric V-notches of depth a under Mode I loading and plane strain conditions (see Fig. 3).

An extension of Eq. (4) is proposed in (Berto, Lazzarin and Afshar, 2012) only for narrow notches to matches the Tada Paris diagram valid for the crack case. The NSIF can be expressed as follows:

$$K_1 = K_0 = \kappa_0 \sigma_n h^{\lambda_1} \tag{5}$$

In Eq. (5) κ_0 is a dimensional parameter that depends on the notch opening angle and λ_1 is Williams'eigenvalue (Williams, 1952). Equation (5) collapses into Equation (4) when the crack case is considered ($\kappa_0=1$ and $\lambda_1=0.5$). For an infinite plate width W>>t and narrow notches, being t/(t+a) close to 1 the stain energy averaged over a control volume of radius R_0 can be written as follows:

$$\overline{W_1} = \frac{\kappa_0^2 e_1}{E}\left(\frac{\sigma_n h^{\lambda_1}}{R_0^{1-\lambda_1}}\right)^2 = \frac{\tilde{e}_1}{E}\left(\frac{\sigma_n h^{\lambda_1}}{R_0^{1-\lambda_1}}\right)^2 \tag{6}$$

By inverting Eq. (6) it is easy to determine parameters κ_0 and $\tilde{e}_1$ that can be expressed according to the following equations:

$$\tilde{e}_1 = \kappa_0^2 e_1 = \frac{E\overline{W}_1}{\sigma_n^2} \left(\frac{R_0^{1-\lambda_1}}{h^{\lambda_1}} \right)^2 \tag{7}$$

$$\kappa_0 = \sqrt{\frac{E\overline{W}_1}{e_1 \sigma_n^2}} \left(\frac{R_0^{1-\lambda_1}}{h^{\lambda_1}} \right) \tag{8}$$

The values of κ_0 and $\tilde{e}_1$ are given in Ref. (Berto, Lazzarin and Afshar, 2012) for the five different characteristic notch opening angles (2α=30, 60, 90, 120 and 135°) both for symmetric and edge notches. By means of κ_0 and $\tilde{e}_1$ it is possible to straightforwardly evaluate the NSIF and the SED over an area of radius R_0 by using Eq. (5) and (6), respectively. It is also possible to express the ratio between K_1 and K_0 in a general form by combining Eqs (3) and (5). It yields to the final expression:

$$\frac{K_1}{K_0} = \frac{k_1}{\kappa_0} \left(\frac{t^{1-\lambda_1}}{h^{\lambda_1}} \right) \tag{9}$$

4   Scale effect for not narrow periodic notches

Since the NSIF depends on the absolute dimension of the notch and the plates, it is surely convenient to normalize its value as a function of the notch size. Some preliminary considerations might be useful. It is well known that two notched plates scaled in geometrical proportion have the same theoretical stress concentration since it simply depends on the geometrical ratios, i.e. notch depth to plate width ratio. Consider now two plates weakened by sharp V-notches, plates and notches in geometric proportion, the corresponding NSIF is different and can be quantified by means of the simple expression (Dunn, Suwito and Cunningham, 1997, Dunn, Suwito and Cunningham, 1997, Lazzarin and Tovo, 1998):

$$K_1 = k_1 \sigma_0 t^{1-\lambda_1} \tag{10}$$

where σ_0 is the reference stress (e.g., the remote tensile stress), $1-\lambda_1$ is the stress singularity in the close vicinity of the notch tip and k_1 is a nondimensional shape factor. In the case of periodic notches the shape factor k_1 does depend on the geometrical ratios t/d and a/t. Table 2 gives the NSIFs and the shape factor k_1 for some plates with a/t=0.1 and t/d=0.025. In addition, the normalized NSIFs of the data presented in Table 2 as a function of depth of the notch (t) is shown in Fig. 2, where the shape factor k_i clearly appears as the coefficient of the power function.

Table 2. NSIFs as a function of depth of the notch (t) with constant relative depth (t/d=0.025) for a plate with periodic notches of $2\alpha=60^o$ and a/t=0.1 ($1-\lambda_1$=0.4878) (Lazzarin, Afshar and Berto, 2012).

t (mm)	d (mm)	t/d	K_1 MPa mm$^{0.4878}$	Shape factor k_i
0.250	10	0.025	46.664	0.9176
0.625	25	0.025	72.962	0.9176
2.5	100	0.025	143.476	0.9176
10	400	0.025	282.140	0.9176
25	1000	0.025	441.144	0.9176
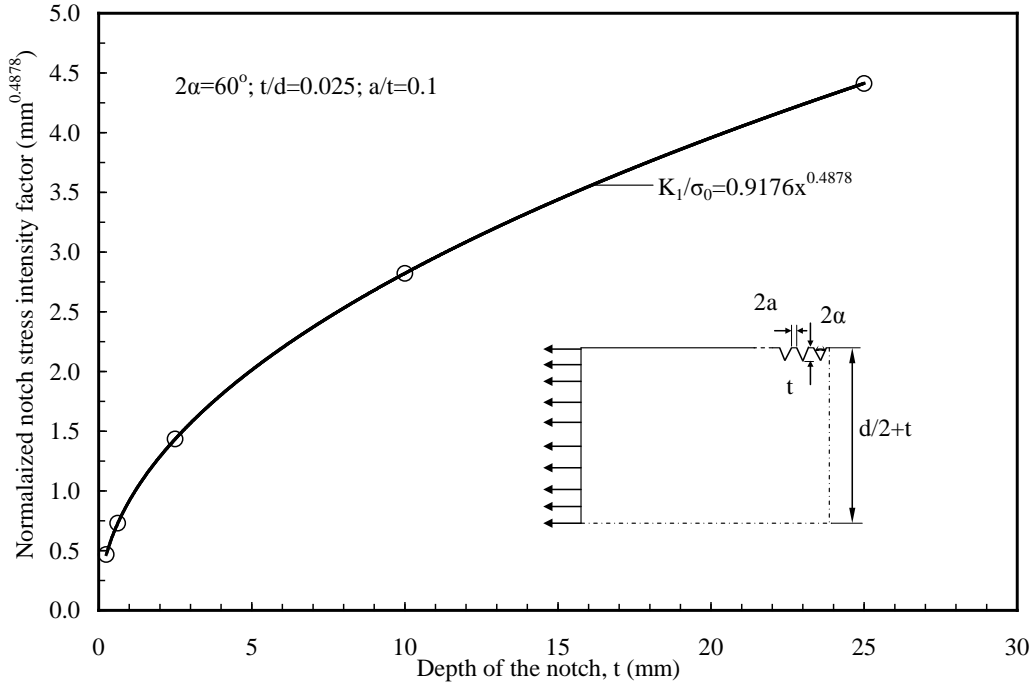
Fig. 2. Normalized NSIFs as a function of notch depth with constant relative depth (t/d=0.025); plate with periodic notches with 2α=60° and a/t=0.1 (scale effect) (Lazzarin, Afshar and Berto, 2012).

Following the guidelines given in (Lazzarin and Tovo, 1996), scaling the geometrical dimensions by a factor of "n", the NSIF value can be obtained by using the following equation:

$$K_{i,b} = K_{i,a} \cdot n^{1-\lambda_i} \tag{11}$$

where the first index "i" is 1 or 2 according to the loading mode and the second index is a or b representing the former or later geometry.

Applying the similar concept to the periodic notches under mode I loading (Fig. 3) it is possible to give the ratio of the two NSIFs as follows:

$$\frac{K_{1,b}}{K_{1,a}} = \sqrt{\frac{\overline{W_{1,b}}}{\overline{W_{1,a}}}} = \left(\frac{h_b}{h_a}\right)^{1-\lambda_1} = \left(\frac{t_b}{t_a}\right)^{1-\lambda_1} = \left(\frac{W_b}{W_a}\right)^{1-\lambda_1} \tag{12}$$

According to Eq. (12) there is the need to redefine K_0 according to the following expression to re-establish non dimensionality of k_0 and to obtain an expression very similar to Eq. (3) being in this case the spacing between the notches, h, the main parameter:

$$K_0 = k_0 \sigma_n h^{1-\lambda_1} \tag{13}$$
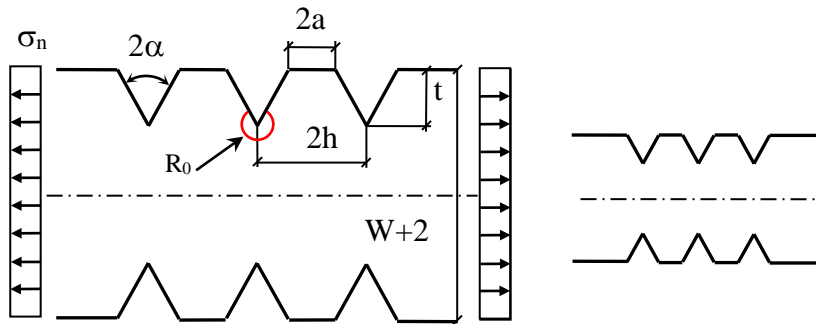
Fig.3. Scaling of threaded plate with double symmetric notches.

The non-dimensional parameter k_0 will be provided for a large range of periodic notches from the narrow to the deep case. Differently from Eq. (5) which provides a κ_0 equal to 1 for the opening angles ranging from 0° to 90°, the new defined k_0 will be substantially different from 1 just when the case $2\alpha=90°$ will be considered.

By plotting Eq. (9) an extended version of the Tada et *al*. (Tada, Paris and Irwin, 1985) diagram is obtained for double symmetric notches and edge notches (Berto, Lazzarin and Afshar, 2012). The trend of the NSIFs for a threaded plate with sharp notches in an infinite plate (t/W=0.01) is shown in Fig. 4 (shallow notches). On the left hand side of the diagram the notches are very far from each other and the results collapse into the case of a single notch. On the other hand, on the right side the diagram matches the case of narrow notches (a=0).
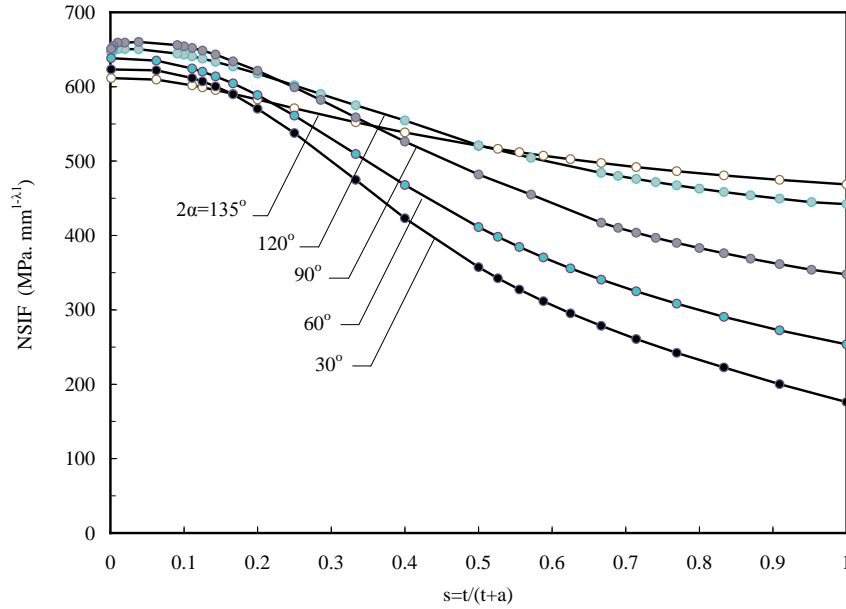
Fig. 4. New generalised diagram for edge and double symmetric periodic notches (Berto, Lazzarin and Afshar, 2012).

Fig. 5 shows the variation of the dimensionless NSIF as a function of the notch opening angle varying the relative distance a/t. Here the relative notch depth assumes its minimum values, t/W=0.025, in order to make possible a comparison in engineering terms with the results reported in Ref. (Savruk and Kazberuk, 2008), all related to the case of periodic notches in a semi-infinite plate (a/t→0).
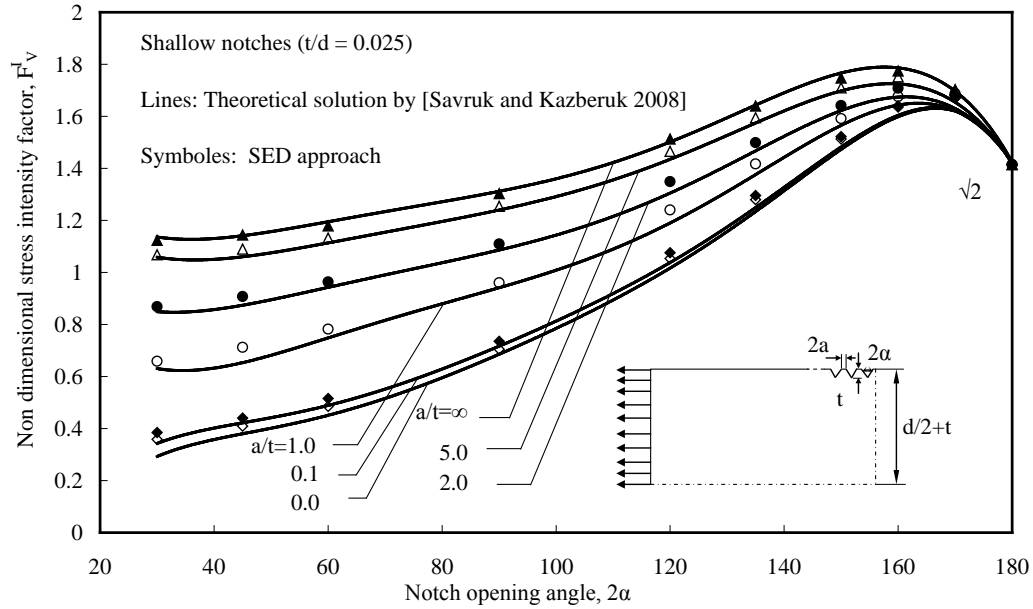
Fig. 5. Variation of dimensionless NSIF with notch opening angle for the modes with t/d=0.025; comparison with data reported in Ref. (Savruk and Kazberuk, 2008) for periodic notches in infinite plate (Lazzarin, Afshar and Berto, 2012).

It can be observed from Fig. 5 that there is a very good agreement between the present results and those reported in the literature for the infinite plate problem. The mean relative deviations for different distances between periodic notches with a/t=0.0, 0.1, 1.0, 2.0, 5.0 and ∞ are: 3.81±6.89, 3.54±3.23, 3.07±0.70, 2.39±0.35, 1.62±0.48 and -0.3±0.29, respectively. It is clear that the relative deviations decrease as the notch opening angle and the a/t ratio increases.

5 Conclusions

By using the SED concept combined with a coarse mesh in the FE analysis, fatigue strength assessment of some welded components is addressed .The NSIF of a narrow threaded plate with an infinite width is only a function of the notch spacing raised to William's eigenvalue. The equation gives accurate results when the ratio between the notch depth and the plate width is lower than 0.025 and collapses into Tada et *al*., solution in the crack case. The problem of the NSIF ratio of two scaled geometries of periodic sharp notches is also addressed.

References

Afshar, R.;F. Berto (2011): Stress concentration factors of periodic notches determined from the strain energy density. *Theoretical and Applied Fracture Mechanics,* vol. 56, pp. 127-139.

Berto, F.;P. Lazzarin (2009): A review of the volume-based strain energy density approach applied to V-notches and welded structures. *Theoretical and Applied Fracture Mechanics,* vol. 52, pp. 183-194.

Berto, F.;P. Lazzarin;R. Afshar (2012): Simple new expressions for the notch stress intensity factors in an array of narrow V-notches under tension. *International Journal of Fracture,* vol. 176, pp. 237-244.

Cendón, D. A.;J. C. Gálvez;M. Elices;J. Planas (2000): Modelling the fracture of concrete under mixed loading. *International Journal of Fracture,* vol. 103, pp. 293-310.

Cisilino, A. P.;M. H. Aliabadi (2010): Crack growth modeling for mixed-mode problems. *Structural Durability and Health Monitoring,* vol. 6, pp. 213-238.

Dunn, M. L.;W. Suwito;S. Cunningham (1997): Fracture initiation at sharp notches: Correlation using critical stress intensities. *International Journal of Solids and Structures,* vol. 34, pp. 3873-3883.

Dunn, M. L.;W. Suwito;S. Cunningham (1997): Stress intensities at notch singularities. *Engineering Fracture Mechanics,* vol. 57, pp. 417-430.

Gálvez, J. C., et al. (2012): An embedded cohesive crack model for finite element analysis of quasi-brittle materials. *Engineering Fracture Mechanics*.

Lazzarin, P.;R. Afshar;F. Berto (2012): Notch stress intensity factors of flat plates with periodic sharp notches by using the strain energy density. *Theoretical and Applied Fracture Mechanics,* vol. 60, pp. 38-50.

Lazzarin, P.;F. Berto;F. J. Gomez;M. Zappalorto (2008): Some advantages derived from the use of the strain energy density over a control volume in fatigue strength assessments of welded joints. *International Journal of Fatigue,* vol. 30, pp. 1345-1357.

Lazzarin, P.;F. Berto;M. Zappalorto (2010): Rapid calculations of notch stress intensity factors based on averaged strain energy density from coarse meshes: Theoretical bases and applications. *International Journal of Fatigue,* vol. 32, pp. 1559-1567.

Lazzarin, P.;R. Tovo (1996): A unified approach to the evaluation of linear elastic stress fields in the neighborhood of cracks and notches. *International Journal of Fracture,* vol. 78, pp. 3-19.

Lazzarin, P.;R. Tovo (1998): A notch intensity factor approach to the stress analysis of welds. *Fatigue and Fracture of Engineering Materials and Structures,* vol. 21, pp. 1089-1103.

Lazzarin, P.;R. Zambardi (2001): A finite-volume-energy based approach to predict the static and fatigue behavior of components with sharp V-shaped notches. *International Journal of Fracture,* vol. 112, pp. 275-298.

Livieri, P.;P. Lazzarin (2005): Fatigue strength of steel and aluminium welded joints based on generalised stress intensity factors and local strain energy values. *International Journal of Fracture,* vol. 133, pp. 247-276.

Parker, A. P. (1999): Stability of arrays of multiple edge cracks. *Engineering Fracture Mechanics,* vol. 62, pp. 577-591.

Savruk, M.;A. Kazberuk (2008): A plane periodic boundary-value problem of elasticity theory for a half-plane with curvilinear edge. *Materials Science,* vol. 44, pp. 461-470.

Sih, G. C. (1973): Energy-density concept in fracture mechanics. *Engineering Fracture Mechanics,* vol. 5, pp. 1037-1040.

Sih, G. C. (1973): Some basic problems in fracture mechanics and new concepts. *Engineering Fracture Mechanics,* vol. 5, pp. 365-377.

Sih, G. C. (1974): Strain-energy-density factor applied to mixed-mode crack problems *International Journal of Fracture* vol. 10, pp. 305-321.

Sih, G. C. (1991): *Surface and volume energy density applied as failure criterion*. Dordrecht, Kluwer Academic Publisher.

Sih, G. C. (2007): *Multiscaling in molecular and continuum mechanics: interaction of time and size from macro to nano*, Springer.

Sih, G. C.;J. W. Ho (1991): Sharp notch fracture strength characterized by critical energy density. *Theoretical and Applied Fracture Mechanics,* vol. 16, pp. 179-214.

Sih, G. C.;X. S. Tang (2005): Scaling of volume energy density function reflecting damage by singularities at macro-, meso- And microscopic level. *Theoretical and Applied Fracture Mechanics,* vol. 43, pp. 211-231.

Tada, H.;P. C. Paris;G. Irwin (1985): *The stress analysis of cracks handbook*. St Louis, Paris Productions Incorporated and Del Research Corporate.

Tang, X. S.;G. C. Sih (2005): Weak and strong singularities reflecting multiscale damage: Micro-boundary conditions for free-free, fixed-fixed and free-fixed constraints. *Theoretical and Applied Fracture Mechanics,* vol. 43, pp. 5-62.

Williams, M. L. (1952): Stress singularities resulting from various boundary conditions in angular corners of plates in extension. *J. Appl. Mech.,* vol. 19, pp. 526-528.

Paper V

Stress concentration factors of periodic notches determined from the Strain Energy Density

Abstract: In this work, stress concentration factors (SCFs) of a number of flat plates and round bars with periodic U- and V-notches are evaluated. Tension, bending and torsion loadings are considered in the investigation. The main objective of the investigation is to take advantage of the local strain energy density (SED) averaged on a control volume surrounding the tip of the middle notch and to estimate the SCF of each component by using a relatively coarse mesh. The unique advantage of SED method is the most prominent application of such a technique in the current study. Systematic FE simulations by considering a wide range of notch acuity and relative frequency of periodic U- and V-notch components are performed. More than two hundred and fifty models have been examined. The results of this study are compared with those provided by other researchers in the past and recent literature. Two new expressions of the notch depth reduction factor for the case of normal stresses (tension and bending) and torsion are also proposed to match the results from SED approach.

Keywords: Stress concentration factor (SCF), periodic notches, finite element, Strain Energy Density (SED), tension, bending, torsion.

1.   Introduction

The analysis of the stress distribution in the vicinity of crack and notch tip and the development of different failure criteria for brittle and quasi-brittle materials are topics of active and recent research [1-3].

In some pioneering works the method of complex potentials functions has been used to obtain the stress field and the stress intensity factors in a variety of crack problems [4-7]. Following these works, a vast number of publications have appeared in the literature concerning solutions of crack problems with emphasis on the stress intensity factors being a comprehensive presentation of these solutions reported in Refs [8-10]. An infinite periodic array of equally spaced cracks under different applied constraints and loadings have been also investigated [10]. The effects of blunt stress raisers are usually quantified in terms of a Stress Concentration Factor (SCF), which is the factor by which the stress at the considered discontinuity is raised over the nominal stress [11]. There are different methods suitable for obtaining SCFs. They are analytical

(according to the elasticity theory), numerical (by using the Finite Element (FE) or the Boundary Element Method (BEM)), or experimental (such as photoelasticity or strain gages). An ingenious formula for the SCF [12] has been used for many years and for a wide range of notch shapes and loading conditions; it is convenient for engineering applications, due to its simplicity and capability to give approximated values for any notch shape [13]. However, several researchers have pointed out that the formula proposed in Ref. [12] can result in underestimation or overestimation of the SCF in the case of single notches [13-17], and multi-notches [18, 19], respectively. The evaluation of SCFs is not only an academic curiosity but it is very important for the design of many components and real structures. Great efforts have been devoted to provide useful solutions in different engineering fields [20, 21]. The case of multi-notches is a practical case that is worth of investigation as underlined in Refs [18, 19].

By applying a general approach to SCF calculations for components weakened by periodic sharp notches, it was suggested in [12] to replace the periodic notch by a single notch having the same geometry but a smaller depth. Recently that approach has been revised and successfully extended to notches of different acuity by employing some accurate analyses by means of the BEM [18, 19].

Dealing with some specific geometries, an estimation technique based on Green's function method has been used to solve the periodic notch problems of elastic half-plane [22]. In another study, both static and dynamic stress analyses of shrink-fit compound tubes containing periodic notches on the outer surface of the inner tube were investigated [23]. Based on their results, critical locations for fatigue failure were recognized as the bore and the notch root. The rotating bending fatigue tests were performed to investigate the fatigue limit of specimens with double-notches [24]. By using a 3-D elastic Finite Element (FE) model, the effect of stress concentrations at the double-notched tips on the fatigue limits was analyzed. A reliability analysis on fatigue testing of multi-notched specimens in order to find the optimum number of specimens required in the fatigue tests was carried out [25].

The necessity of a simple criterion for engineering applications led to development of a point-wise strain energy density (SED) approach valid for cracks [26-29] and notches [30]. Factor S was defined as the product of the SED by a critical distance from the point of singularity [28]. Failure was thought of as controlled by a critical value S_c, whereas the direction of crack propagation was determined by imposing a minimum condition on S. The theory was extended

to employ the total SED near the notch tip [30], and the point of reference was chosen to be the location on the surface of the notch, where the maximum tangential stress occurs. In small bodies, the high ratio between surface and volume leads to considering the local discontinuities present in the material. Hence, the adoption of a multiscaling and segmentation scheme is the only way to capture what happens at pico, nano and micro levels [31-33] where the SED can be also scaled [32].

Following parallel tracks, the concept of SED averaged over a material-dependent control volume was formalized first in Ref. [34] with reference to sharp V-shaped notches under static and fatigue loading conditions. It was demonstrated that the approach based on the concept of an energy value averaged in a small but finite volume of material is able to accurately predict both the static behavior of severely notched components and the fatigue behavior of welded joints [34]. Further investigations were later carried out in Refs [35, 36] with reference to blunt U- and V-notches. Some closed-form expressions were given to link the SED over the control volume and the elastic peak stress on the notch tip. To validate the approach, a large body of experimental data from blunt and sharp V-notched specimens made of PMMA, tested under tensile loading conditions was used [37-43].

By using the SED concept combined with a coarse meshing in FE analysis, a fatigue strength assessments of welded joints carried out [44]. More recently, a procedure for rapid calculations of notch stress intensity factor (NSIF) and SCFs based on the SED from coarse meshing is presented [45].

In the presence of sharp V-notches, the stress distributions are singular and the intensity of the stress fields is given in terms of the notch stress intensity factors (NSIFs) which are largely used in the literature for fatigue strength assessments of welded joints and other notched components. Very refined meshes are necessary to determine directly the NSIFs from the local stress distributions. Refined meshes are not necessary when the aim of the finite element analysis is to determine the mean value of the local strain energy density on a control volume surrounding the points of stress singularity. The SED in fact can be derived directly from nodal displacements multiplied by the stiffness matrix of the finite elements, so that also coarse meshes are able to give sufficiently accurate values for it. The calculation of the elastic strain energy does not involve stresses and strains. On the other hand, differently from SED, the stress evaluation requires the derivatives of the nodal displacements and this is the cause of less accuracy.

Dealing with blunt notches, as soon as the SED is known, the SCFs can be determined a posteriori on the basis of very simple expressions linking the local SED and the SCFs in plane problems. Generally, there is no numerical method that is effective for analyzing all notch shapes with less than 1 % error [13]. It is well known that meshing in FE model is always the most challenging part of a FE analysis, as the result directly depends on the mesh density. Therefore, evaluation of SCFs by using a coarse mesh in FE model is a remarkable advantage of SED method and this is true, in particular, dealing with complex three-dimensional components for which a linear relation between stress and strain is verified but also in those cases where the hypothesis of linearity ceases its validity due to edge effects or narrow spacing between collinear notches.

In this study, the effect of periodic notches on the SCF is investigated by means of SED used in combination with the very coarse meshes. A number of flat plates and round bars weakened by periodic U- and V-notches subjected to tensile, bending and torsion loading are considered with the aim to study the stress concentration regions in the frame of linear elastic hypotheses.

The main aims of this paper are then as follows:

- to evaluate the local SED on the control volume surrounding the tip of middle notch of multi-notched components and to estimate the relevant SCF by using in the FE models with relatively coarse meshes.

- to investigate the effect of the notch pitch and depth on the stress concentration and compare the results with equations available in the literature for periodic notches and in particular with the new modified expressions proposed in Refs [18, 19]. A large bulk of analyses have been carried out ranging from narrow to large spacing of collinear notches.

- to provide two new equations for the notch depth reduction factor for the cases of normal stresses (tension and bending) and torsion and suitable for any shape of notch. These new equations, which are based on FE results of SED with coarse meshes, can be used in combination with the available equations for single notches to determine the SCFs of periodic notches.

2.   Modeling of periodic notches

The geometries considered in the present investigation as well as the main geometrical parameters are shown in Figure 1. Different values of the notch opening angle, 2α, the relative

frequency of the periodic notch, t/P, and finally, the notch acuity, ρ/t, have been varied in the analyses. The relative depth of the notch, t/d, is assumed 0.1 for all the cases.

 A total number of 250 different geometries, including flat plates and round bars, have been analyzed by combining the following values of the above mentioned parameters:

$2\alpha=0^o$ and 60°; t/d=0.1; t/P =0.01, 0.2, 0.4,…2; ρ/t=0.2, 0.4, …2.

Due to the double symmetry of flat plates and axis-symmetry of round bars, only one quarter of the geometry has been modeled. The number of periodic notches is 10 in all the geometries considered here.
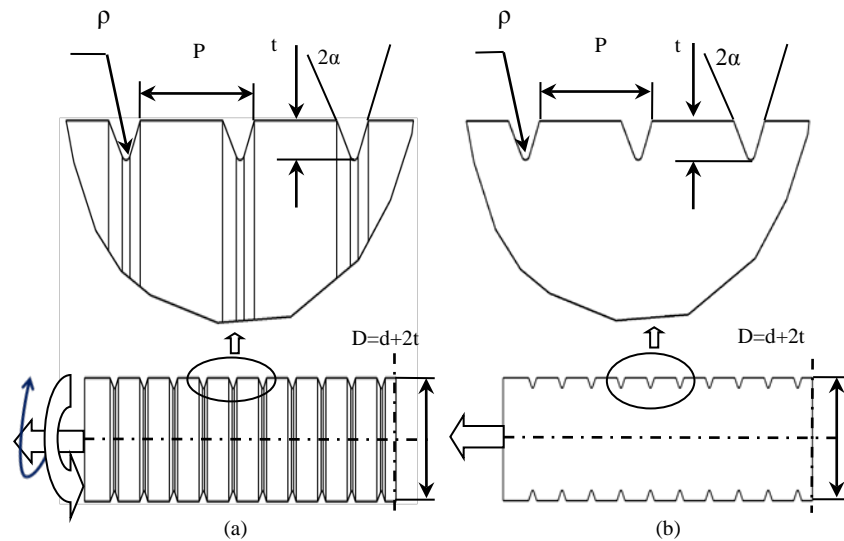
Figure 1. Schematic of the geometries used for the periodic notch analysis; (a): round bar (b): flat plate.

3.   Modeling and SED evaluation

The commercial code ANSYS is used to perform the Finite Element Analyses (FEA). Material is assumed as isotropic and elastic with a Young's modulus E=206000 MPa and a Poisson's ratio ν=0.3. Two types of element are used in FEA: the 8-nodes iso-parametric element plane 82, with plane strain and axis-symmetric key-options, is used for flat plates and round bars subjected to tensile loading. In addition, for the case of round bars under bending and torsion, which are axis-symmetric structures with a non axis-symmetric applied load, the harmonic element plane 83 is used. To reduce any computational error, a subroutine based on ANSYS parametric design language (APDL) is developed and different geometrical cases are generated by simply changing

the four geometrical ratios defined in the previous section. The results from the three loading cases are widely discussed below.

3.1 Tension loading

The strain energy averaged over the control volume shown in Figure 2 can be expressed, as a function of the maximum elastic stress at the notch tip according to Ref. [36]:

$$\overline{W}_1 = F(2\alpha) \times H(2\alpha, \frac{R_c}{\rho}) \times \frac{\sigma_{max}^2}{E} \tag{1}$$
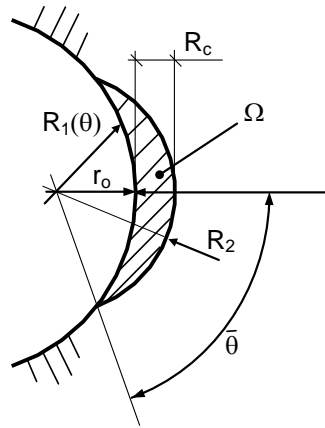
Figure 2. Scheme of the control area Ω for blunt notches [36].

where the parameters F and H (given in Ref. [36]) are considered in the paper.

This equation allows us to evaluate the maximum elastic stress using the mean value of the SED, averaged over a given control volume. The SED value is almost independent of the mesh pattern as discussed in Refs [44, 45] and can accurately be determined with very coarse meshes. As soon as E_1 (the elastic Strain Energy) is numerically determined on the control area Ω in the middle notch (the latter calculated by using the SENE command of ANSYS code), the total $\overline{W}_1$ is obtained by simply dividing the total E_1 by the control area (Figure 2).

R_c is assumed constant and equal to 0.1 mm in all FE models. This value of R_c allows the control volume (Ω) to embrace only the curvilinear edge of the notch, not exceeding to the rectilinear flanks [30]. Under this hypothesis, Eq. (1) is always applicable.

Once the SED on the control volume is evaluated by means of FEA using coarse meshes, the maximum stress at the notch tip can be calculated by simply inverting Eq. (1) as follows:

$$\sigma_{\square\square} = \sqrt{\frac{\overline{W}_1 E}{F(2\alpha) \times H(2\alpha, \frac{R_\square}{\rho})}} \qquad (2)$$

Finally, the SCF can be calculated:

$$K_t = \frac{\sigma_{max}}{\sigma_n} \qquad (3)$$

In Eq. (3) σ_n is the nominal normal stress referred to the net cross sectional area.

3.2 Bending

The same equations used for tension can be used also for the evaluation of the maximum stress at the notch tip in the case of bending. The nominal stress σ_n is again referred to the net cross sectional area. Eq. (3) is applied for calculation of the SCF.

3.3 Torsion

In the case of torsion loading, in analogy to mode I loading, the energy averaged over a control volume can be determined as follows:

$$\overline{W}_3 = H(2\alpha, \frac{R_c}{\rho}) \times \frac{\tau_{max}^2}{2G} \qquad (4)$$

where function H for the cases $2\alpha=0°$ and $60°$ has been determined here from FEA with fine meshes (see Ref. [36]). The shear modulus of elasticity G is assumed constant and equal to 79 GPa.

Once the SED is known from a FE model with a coarse mesh, it is possible to evaluate the maximum stress at the notch tip by inverting Eq. (4):

$$\tau_{max} = \sqrt{\frac{2G\overline{W}_3}{H\left(2\alpha, \frac{Rc}{\rho}\right)}} \qquad (5)$$

Finally, the SCF can be calculated:

$$K_t = \frac{\tau_{max}}{\tau_n} \tag{6}$$

In Eq. (6) τ_n is the nominal shear stress referred to the net cross sectional area.

4. Periodic notches

The first simple equation for the evaluation of the SCF in a model with periodic notches by using an equivalent single notch with a reduced depth was proposed in Ref. [12] (see Figure 3). According to that equation, the factor quantifying the reduced depth, γ, only depends on the frequency of the periodic notch, t/P, and it can be expressed as follows [12]:

$$\gamma = \frac{P}{\pi t} \tanh\left(\frac{\pi t}{P}\right) \tag{7}$$
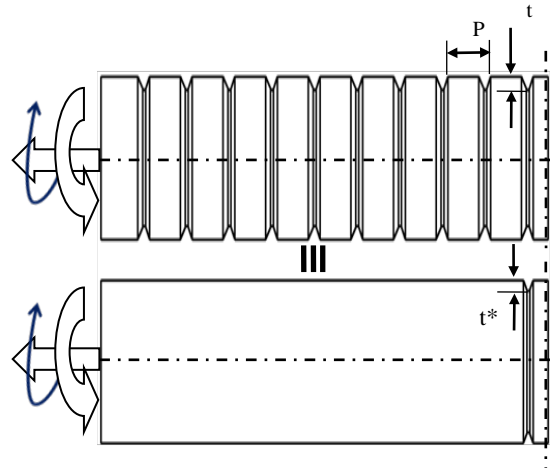
Figure 3. Equality of periodic and single notches.

In a recent study based on the BEM, a correction of Eq. (7) with a factor k=3 to extend the range of applicability to any value of notch acuity is suggested [18]. In fact the formula proposed in [12] is valid only for infinitely sharp notches ($\rho/t \rightarrow 0$) and in presence of shear stresses. On the other hand, a wide range of geometries have been considered in Ref. [18] varying the main geometrical parameters and ranging from shallow to deep notches. The variation of the notch acuity has been considered as well. The recent equation assumes the following general form:

$$\gamma = \frac{P}{k\pi t} \tanh\left(\frac{k\pi t}{P}\right) \tag{8}$$

The reduced depth factor in the case of normal stress is then [18]:

$$\gamma = \frac{P}{3\pi t} \tanh\left(\frac{3\pi t}{P}\right)$$

(9)

In a more recent investigation by the same Authors [19], the case of a bar under torsion and weakened by periodic U-shaped shallow notches has been considered. The BEM in combination with a computationally efficient thermal analogy has been used to evaluate the SCFs and then the notch depth reduction factor.

For an ideally sharp notch, a sound agreement with the analytical frame proposed in [12] has been found. However, considering a wide range of rounded notches, a new reduction factor k=2 has been found as the most suitable for accurate assessments of SCFs [19].

Dealing with single notches, some equations given in [15] and [13, 46] (see Appendix A) provide the values of the SCF as a function of the notch opening angle, the relative depth of the notch, t/d, and the notch acuity ρ/t.

The equations assume the following general form:

$$K_t = f(2\alpha, t/d, \rho/t)$$

(10)

It is worth noting that the equation proposed in [15] is sensitive to a variation of the notch opening angle while the frame proposed in Refs [13, 46] is independent of 2α.

With the aim to evaluate the SCFs, the same procedure adopted in Ref. [18] is used herein. First, for each configuration of periodic notches, γ is calculated based on the relative frequency of the periodic notch, t/P, and by using Eqs. (7, 9), proposed in [18].

Next for each case, the reduced depth, t* has been evaluated as follows:

t*=γt

(11)

Finally, according to equations presented in [15] and [13, 46], the SCFs have been evaluated. Eq. (11) is used with the updated ratios ρ/t* and t*/d taking into account the reduced depth t*.

5.   Validation of the available equations for single notches and accuracy of the SED with coarse meshes

Before proceeding to the modeling of multi-notch configurations, a single notch with two opening angles, 2α=0° and 60°, is considered for different values of the notch acuity. The relative deviation between SED values obtained by FE models using relatively coarse meshes

and other equations available in the literature is presented in Table 1 for the case 2α=60°. An example of the coarse mesh used for SED evaluation is shown in Figure 4. A maximum value of 6-7 elements in the control volume is used to evaluate the SED while the entire model consists of about 70 elements. A very good agreement has been found between the SCFs based on the SED approach (with coarse meshes) and the direct calculation of the SCFs with very refined meshes (about 2000 elements). The comparison with equations provided in Refs [13, 15] shows that the relative error is less than 5% for each considered notch configuration confirming the sound accuracy of the above mentioned equations for single notches.

In addition, different mesh densities were applied to confirm the versatility of the SED approach by considering both single and periodic notches, as depicted in Table 1. For the case of periodic notches, different pitch values were examined, showing the effectiveness of the method in the case of narrow spacing of collinear notches, which leads to geometrical nonlinearity of the model.
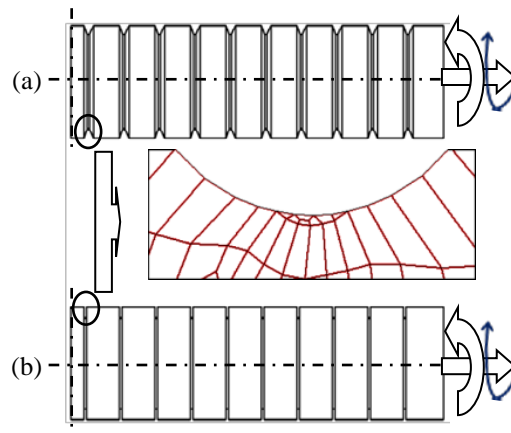
Figure 4. The symmetric model of periodic notches with opening angles

of (a) $2\alpha = 60^o$ and (b) $2\alpha = 0^o$.

Table 1. Relative deviations between SED-based results and data from the literature (single notch with $2\alpha = 60°$). Comparison between coarse and fine mesh for narrow and wide spacing.

ρ/t	K_t (FE)	K_t (SED)	K_t (NO) [13]	K_t (NE) [12]	K_t (KA) [15]	$\Delta\%$ (SED-NO)	$\Delta\%$ (SED-NE)	$\Delta\%$ (SED-KA)
0.20	5.10	5.03	4.85	4.62	4.89	3.69	8.97	2.79
0.40	3.64	3.64	3.61	3.45	3.65	0.82	5.22	-0.27
0.60	3.07	3.07	3.07	2.93	3.10	-0.15	4.69	-0.90
0.80	2.75	2.75	2.89	2.76	2.77	-5.12	-0.51	-0.80
1.00	2.53	2.53	2.53	2.41	2.55	-0.07	4.82	-0.64

No. of Elements (Inside the Ω)	K_t (SED)	$\Delta\%$	K_t (SED)	$\Delta\%$
	Wide spacing (t/P=0.2, ρ/t=0.2)		Narrow spacing (t/P=0.6, ρ/t=0.4)	
8	4.1190	-0.05	2.1193	-0.05
31	4.1209	0.00	2.1203	-0.01
60	4.1211	0.00	2.1204	0.00
109	4.1211	0.00	2.1205	0.00

6.   A new proposal for the notch depth reduction factor based on SED

The optimal value of factor k in Eq. (8) has been evaluated here by minimizing the relative deviation between the results from FE analyses of periodic notches and those from the application of Eq. (8) used in combination with the equations reported in [15] for single notches. The same procedure adopted by means of the BEM [18] is used herein by using the FE method. The optimization process has been carried out by means of the free version of CURVEEXPERT package. The coefficient k was found to be equal to 3.03 for tension and bending and equal to 1.70 for torsion loading. It is worth noting that the same values of k have been obtained also by directly comparing the FE results of SED in periodic notches with those directly obtained by evaluating the SED in equivalent single notches both with fine and coarse meshes.

The results are in good agreement with those reported in Refs [18] and [19], where k=3 has been proposed for tension and k=2 has been suggested for torsion (longitudinal shallow notches) [18, 19]. Dealing with torsion loading, the higher deviation of the coefficient k obtained by FEM with respect to that obtained by BEM [19] can be explained by the lower sensitivity of the SCFs on the equivalent notch depth with respect to the tension loading case, where a small variation of t induces very large variations of K_t.

In addition, by means of the same optimization process used in [18] for the generalized equation in [18] a new expression for γ was proposed and set here, based on SED results. In the new equation, the notch depth reduction factor assumes the following form:

$$\gamma = a - be^{-c\left(\frac{t}{P}\right)^d} \tag{12}$$

Parameters a, b, c and d have been calculated to assure a relative average deviation always within the limit of 5% between the SCFs obtained by using in combination Eq. (12) and the equation for single notches given in [15]. The values have been compared with those directly derived by the SED approach applied with coarse meshes on periodic notches. The same results have also been confirmed by comparing the FE results of SED in periodic notches with those directly obtained by evaluating the SED in equivalent single notches, both with fine and coarse meshes.

The parameters introduced in Eq. (12) for the case of tension, bending and torsion are listed in Table 2.

Table 2. Coefficients for the cases of normal and torsion loading in Eq. (12)

Normal stress (tension and bending)	Torsion
$\gamma = a - be^{-c\left(\frac{t}{P}\right)^d}$	
a =0.9900495	a =0.98534753
b =0.9589001	b =0.97106507
c =0.0568707	c =0.15985867
d =-1.6195059	d =-1.48472198

7. Results and discussion

In this section, the results from FE models and the comparison with theoretical assessed values of the four aforementioned geometrical and loading configurations are summarized.

Two different values of the opening angle have been considered, being $2\alpha=0°$ and $60°$. Figure 4 shows the middle notch used for the SED evaluation and the typical adopted mesh. The SED approach was always applied, with taking advantage of a free and very coarse mesh, being the maximum number of elements inside the volume equal to 7. For the entire plates, weakened by single and periodic notches, a maximum refinement degree corresponding to 70 and 300

elements has been used respectively. Very close results, within a range of ±1%, have been obtained by using only 2 elements inside the control volume.

In order to confirm the versatility of SED approach and to check the results in terms of mesh density, an extensive comparison of fine and coarse meshes has been carried out by considering different pitch ratios. In the refined FE models, which consisted of more than 2000 elements, the SCFs have been evaluated directly by using the maximum stress at the notch tip. The differences in terms of K_t are always lower than 2% (see Table 1).

It is worth noting that, while for analytical solutions all the values of SCF for single notches are available in Tables 3-6, the missing data for SED referred to multiple notches are due to the geometrical limitations given by the pitch values, which do not allow us to model every configuration of periodic notches.

7.1 Symmetric model under tension

In this section, the FE results from symmetric flat plates under tension are presented in Table 3 and compared with the values predicted by the different available equations taken from the literature.

Table 3. Comparison of K_t by SED approach with FE results, the present model and SCFs obtained by using equations in [12] and [18] in a wide range of notch acuity, frequency of periodic notch and two opening angles: the case of symmetric model under tension. Abbreviations: NE: Neuber's Eq. [12], NO: Noda's Eqs [13, 46], KA: Kato's Eqs [15], DR: Dragoni Eqs [18, 19], PM: Present Model.

t/P	ρ/t	K_t (SED-0)	K_t (SED-60)	K_t (NO-NE) [13,12]	K_t (NO-DR) [13,18]	K_t (KA-DR) $(2\alpha = 0^o)$ [15,18]	K_t (KA-DR) $(2\alpha = 60^o)$ [15,18]	K_t (PM)	$\Delta\%$ (KA-DR, SED)	$\Delta\%$ (PM, SED)
0.01	0.20	4.82	4.81	4.81	4.80	4.90	4.90	4.88	1.87	1.46
	0.40	3.68	3.62	3.59	3.59	3.65	3.64	3.64	0.55	0.55
	1.00	2.58	2.63	2.54	2.53	2.54	2.54	2.54	-3.42	-3.42
	2.00		1.99	2.01	2.01	2.00	2.00	2.00	0.50	0.50
0.2	0.20	4.56	4.31	4.65	3.94	3.98	3.98	4.08	-7.66	-5.34
	0.40	3.14	3.12	3.49	3.01	3.03	3.03	3.10	-2.88	-0.64
	1.00	2.18	2.19	2.48	2.21	2.20	2.20	2.24	0.46	2.28
	2.00		1.73	1.98	1.82	1.79	1.79	1.81	3.47	4.62
0.4	0.20	3.27	3.26	4.31	3.21	3.23	3.23	3.14	-0.92	-3.68
	0.80	1.89	1.93	2.53	2.04	2.03	2.03	1.99	5.18	3.11
	1.00	1.75	1.76	2.35	1.92	1.91	1.91	1.88	8.52	6.82
0.6	0.20	2.80	2.81	3.94	2.84	2.83	2.83	2.68	0.71	-4.63
	0.40	2.10	2.14	3.01	2.26	2.25	2.25	2.15	5.14	0.47
	0.80	1.66		2.38	1.87	1.85	1.85	1.78	11.45	7.23

0.8	0.20	2.46	3.64	2.60	2.59	2.59	2.42	5.28	-1.63
	0.40	1.89	2.81	2.10	2.09	2.09	1.98	10.58	4.76
	0.60	1.64	2.46	1.88	1.87	1.87	1.78	14.02	8.54
1.0	0.20	2.26	3.40	2.43	2.42	2.42	2.26	7.08	0.00
	0.40	1.76	2.66	1.98	1.97	1.97	1.87	11.93	6.25
1.2	0.20	2.16	3.21	2.30	2.29	2.29	2.16	6.02	0.00
	0.40	1.69	2.53	1.90	1.89	1.89	1.79	11.83	5.92
1.4	0.2	2.11	3.06	2.20	2.20	2.20	2.08	4.27	-1.42
1.6	0.2	2.12	2.94	2.12	2.12	2.12	2.03	0.00	-4.25
1.8	0.2	2.15	2.84	2.06	2.05	2.05	1.98	-4.65	-7.91
2.0	0.2	2.20	2.75	2.00	2.00	2.00	1.95	-9.09	-11.36

The SCF values for the two considered opening angles have been estimated by using the equation reported in [15] in combination with the reduction factor for periodic notches proposed in [18] (see Eq. (9)). The values have been compared with those obtained by means of SED with coarse meshes. The comparison shows a very close agreement with a relative deviation, Δ, less than 14% for all the considered cases and in many cases less than 5%. These results confirm the sound proposal made in [18] for the notch depth reduction factor.

It is also worth noting that usually the effect of notch opening angle varies depending on the sharpness and depth of notch. In this study, the depth of the notch is considered constant for all of the cases; therefore, the only effective parameter is the notch acuity.

The numerical results from coarse meshes, re-converted in terms of the SCFs, have been compared also with results obtained by implementing the equations for single notches given in [13] in combination with the depth reduction factors according to Eq. (7) [12] and Eq. (9) [18].

By analyzing the results reported in Table 3, it can be observed that there is a good agreement between the SED approach and equations proposed in Refs [13] and [15], either by applying the reduction factor proposed in [12] and [18], in the case of small depth to pitch ratio (t/P=0.01). However, by increasing t/P, overestimation caused by the use of Eq. (7) is evident.

The assessment made by using the new proposed equation for γ (Eq. (12)) together with the equation provided in [15] (or alternatively with SED applied to the equivalent single notch) produces a relative deviation, Δ, within 6% (with the only exception of few cases) with respect to the SCF values, directly obtained by modeling periodic notched components with a coarse mesh (which are equal to those obtained from very refined meshes).

Figures 5 and 6 show the comparison between SED approach and the equations given in [13] for single notches by implementing the depth reduction factors according to Eqs (7) and (9) in the

case of two frequencies of periodic notches (t/P=0.2 and 0.4). The overestimation due to the application of Eq. (7) [12] is evident and this discrepancy increases by increasing t/P (see Figure 5). In addition, it can be seen that by increasing ρ/t, the difference between SCFs evaluated by means of the SED and the values obtained by using the equations given in [13] in combination with Eq. (9) also increases. These discrepancies can be reduced by introducing the new expression for γ (Eq. (12)), which assures a higher accuracy to fit the numerical data obtained by using SED method for a wider range of notch acuities (see Table 3).
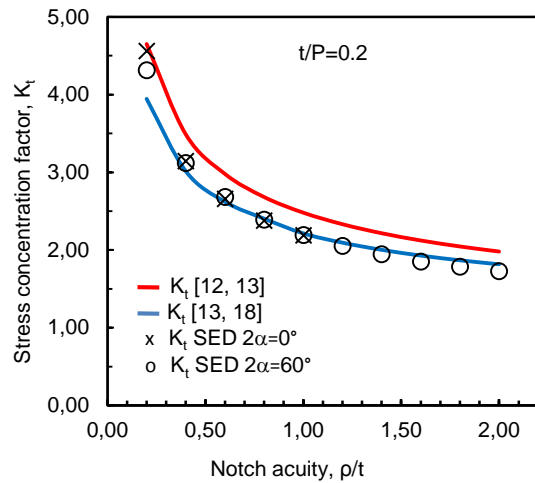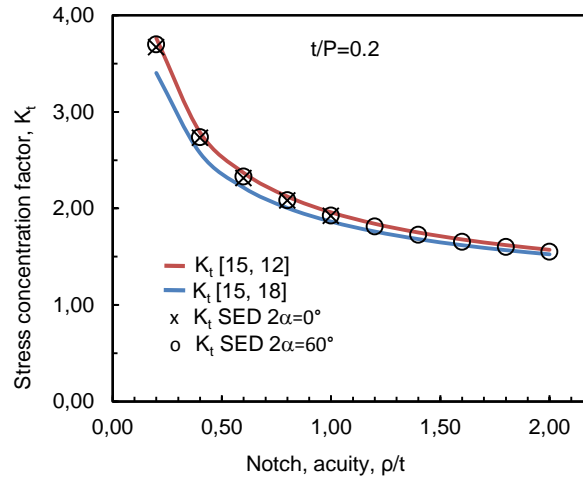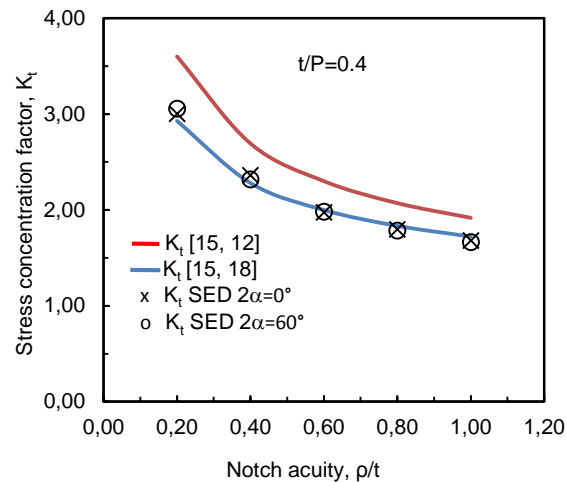

Figure 5. The comparison of SED approach with the data given in [13] and implementing proposed depth reduction factors in [12] and [18] in the case of a symmetric plate under tension with t/P=0.2.
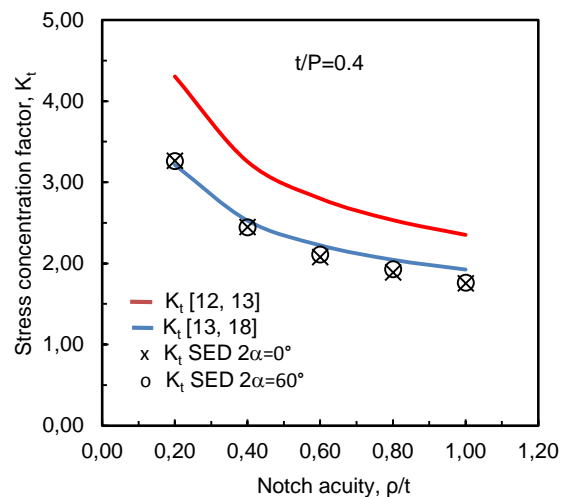
Figure 6. The comparison of SED approach with the data given in [13] and implementing proposed depth reduction factors in [12] and [18] in the case of a symmetric plate under tension with t/P=0.4.

7.2 Axis-symmetric model under tension

The results from FE models of axis-symmetric bars under tension and the comparison with the values predicted by the different available equations are shown in Table 4.

Table 4. Comparison of K_t by SED approach with FE results, the predicted model and SCFs by using equations in [12] and [18] in a wide range of notch acuity, frequency of periodic notch and two opening angles: the case of axis-symmetric model under tension.

t/P	ρ/t	K_t (SED-0)	K_t (SED-60)	K_t (NO-NE) [46,12]	K_t (NO-DR) [46,18]	K_t (KA-NE) ($2\alpha = 60^o$) [15,12]	K_t (KA-DR) ($2\alpha = 60^o$) [15,18]	K_t (PM)	Δ% (KA-DR&SED)	Δ% (PM&SED)
0.01	0.20	4.48	4.53	4.35	4.35	4.51	4.51	4.50	-0.44	-0.66
	0.40	3.32	3.17	3.24	3.23	3.35	3.35	3.34	5.68	5.36
	1.00	2.41	2.32	2.26	2.26	2.33	2.33	2.32	0.43	0.00
	2.00		1.86	1.79	1.79	1.83	1.83	1.82	-1.61	-2.15
0.2	0.20	4.08	4.12	4.26	3.76	4.39	3.80	3.88	-7.77	-5.83
	0.40	3.03	3.04	3.17	2.86	3.27	2.89	2.94	-4.93	-3.29
	1.00	2.11	2.12	2.23	2.08	2.29	2.09	2.12	-1.42	0.00
	2.00		1.68	1.77	1.69	1.81	1.70	1.71	1.19	1.79
0.4	0.20	3.15	3.21	4.02	3.14	4.11	3.14	3.06	-2.18	-4.67
	0.80	1.88	1.86	2.34	1.99	2.38	1.97	1.94	5.91	4.30
	1.00	1.75	1.73	2.16	1.87	2.20	1.85	1.82	6.94	5.20
0.6	0.20	2.62	2.79	3.76	2.80	3.80	2.78	2.64	-0.36	-5.38
	0.40	2.12	2.12	2.86	2.23	2.89	2.21	2.12	4.25	0.00
	0.80	1.67		2.24	1.83	2.25	1.82	1.75	8.98	4.79
0.8	0.20	2.43		3.51	2.57	3.53	2.55	2.39	4.94	-1.65
	0.40	1.90		2.70	2.07	2.71	2.06	1.95	8.42	2.63
	0.60	1.68		2.35	1.86	2.35	1.84	1.76	9.52	4.76
1.0	0.20	2.29		3.31	2.41	3.32	2.39	2.24	4.37	-2.18
	0.40	1.77		2.58	1.96	2.57	1.95	1.85	10.17	4.52
1.2	0.20	2.09		3.14	2.28	3.14	2.27	2.14	8.61	2.39
	0.40	1.65		2.47	1.88	2.45	1.87	1.78	13.33	7.88
1.4	0.2	1.99		3.01	2.19	3.00	2.18	2.07	9.55	4.02
1.6	0.2	1.93		2.89	2.11	2.88	2.10	2.01	8.81	4.15
1.8	0.2	1.94		2.80	2.04	2.78	2.04	1.97	5.15	1.55
2.0	0.2	1.95		2.71	1.99	2.69	1.98	1.94	1.54	-0.51

The results obtained by implementing equations provided in Refs [15] and [13] used in combination with the reduction factor according to Eqs (7) and (9) are listed in the table.

Similar to the symmetric models under tension loading, it can be noted that in the case of small frequency of periodic notches (t/P=0.01), there is a close agreement between SED results and those obtained by using equations in Refs [15] and [13], either by applying reduction factor provide in Refs [12] and [18]. By increasing t/P, overestimation caused by the application of Eq. (7) [12] is very high. The maximum error between the SED results from FE analyses and the

values of K_t calculated by the reduction factor suggested in [18] is about 10%. By applying Eq. (12) for γ, the relative deviation in terms of K_t between the present predictions and numerical results is within 5%.

Two arbitrary cases characterized by a depth to pitch ratio, t/P=0.2 and 0.4 are shown in Figures 7 and 8 to compare the results from SED approach with the values provided by equations in [15] employing together with the expressions for the notch reduction factor according to Eq. (7) and (9).
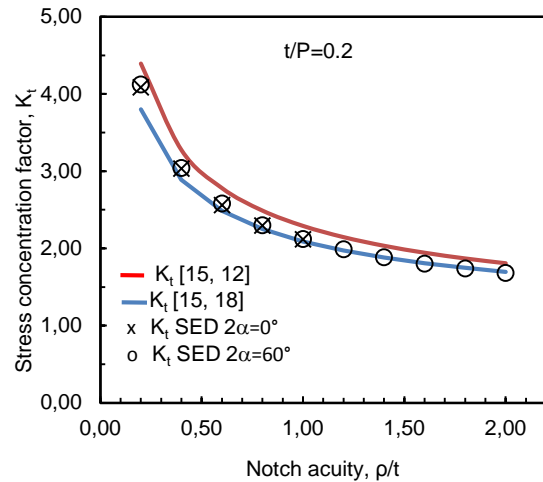
Figure 7. The comparison of SED approach with the data given in [15] and implementing proposed depth reduction factors in [12] and [18] in the case of an axis-symmetric model under tension with t/P=0.2.
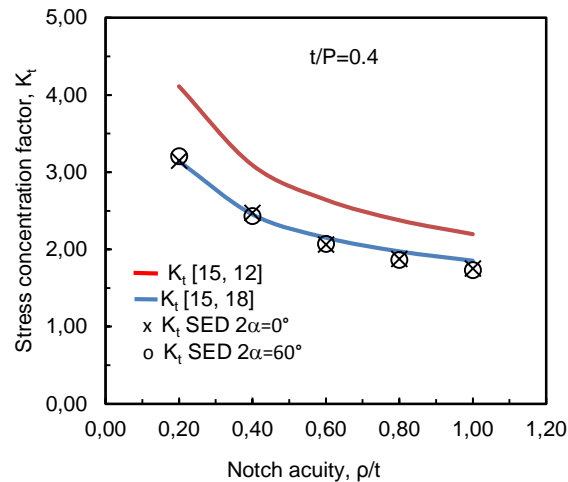
Figure 8. The comparison of SED approach with the data given in [15] and implementing proposed depth reduction factors in [12] and [18] in the case of an axis-symmetric model under tension with t/P=0.4.

7.3 Axis-symmetric model under bending

The results from SED approach and the comparison with available equations are listed in Table 5 for round bars under bending loading. Similar to previous cases, the results for two specific depth to pitch ratios (t/P=0.2 and 0.4) have been explicitly shown in Figures 9 and 10 to compare the numerical values, based on SED, with those provided by the equations reported in [15], employing Eqs (7) and (9) for γ [12, 18].

Figure 9. The comparison of SED approach with the data given in [15] and implementing proposed depth reduction factors in [12] and [18] in the case of an axis-symmetric model under bending with t/P=0.2.
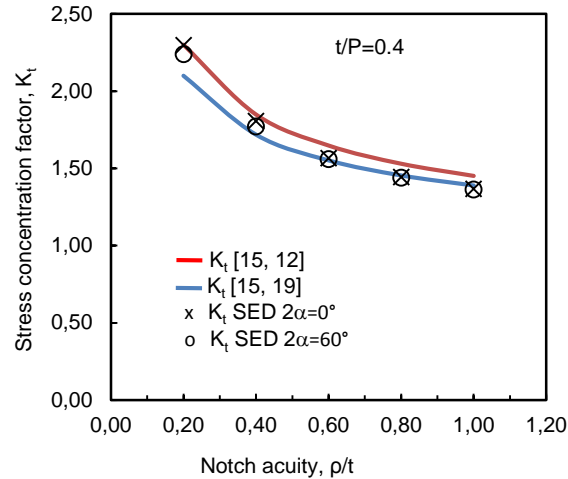

Figure 10. The comparison of SED approach with the data given in [15] and implementing proposed depth reduction factors in [12] and [18] in the case of an axis-symmetric model under bending with t/P=0.4.

In the case of axis-symmetric model under bending, for small frequencies of periodic notches (t/P=0.01), a good agreement between SED approach and the values obtained by the application of equations for single notches according to Ref. [15] and [13] either by applying Eq. (7) and (9) for γ can be observed in Table 5.

Table 5. Comparison of K_t by SED approach with FE results, the predicted model and SCFs by using equations given in [12] and [18] in a wide range of notch acuity, frequency of periodic notch and two opening angles: the case of axis-symmetric model under bending.

t/P	ρ/t	K_t (SED-0)	K_t (SED-60)	K_t (NO-NE) [46,12]	K_t (NO-DR) [46,18]	K_t (KA-NE) ($2\alpha = 60^o$) [15,12]	K_t (KA-DR) ($2\alpha = 60^o$) [15,18]	K_t (PM)	Δ% (KA-DR&SED)	Δ% (PM&SED)
0.01	0.20	3.79	3.83	3.79	3.79	3.83	3.83	3.82	0.00	-0.26
	0.40	2.82	2.81	2.84	2.84	2.83	2.83	2.82	0.71	0.36
	1.00	2.02	1.98	2.01	2.01	1.98	1.98	1.97	0.00	-0.51
	2.00		1.61	1.61	1.61	1.58	1.58	1.58	-1.86	-1.86
0.2	0.20	3.67	3.70	3.73	3.39	3.76	3.40	3.46	-8.11	-6.49
	0.40	2.73	2.74	2.80	2.58	2.79	2.57	2.61	-6.20	-4.74
	1.00	1.92	1.93	1.99	1.87	1.96	1.86	1.88	-3.63	-2.59
	2.00		1.55	1.60	1.54	1.57	1.52	1.53	-1.94	-1.29
0.4	0.20	3.00	3.06	3.58	2.95	3.60	2.93	2.87	-4.25	-6.21
	0.80	1.80	1.78	2.09	1.84	2.07	1.83	1.81	2.81	1.69
	1.00	1.68	1.66	1.94	1.73	1.92	1.72	1.70	3.61	2.41
0.6	0.20	2.54	2.70	3.39	2.67	3.40	2.64	2.52	-2.22	-6.67
	0.40	2.06	2.06	2.58	2.12	2.57	2.10	2.02	1.94	-1.94
	0.80	1.68		2.02	1.73	3.40	1.70	1.67	3.61	2.41
0.8	0.20	2.37		3.22	2.48	3.22	2.45	2.31	3.38	-2.53
	0.40	1.86		2.47	1.99	2.46	1.97	1.88	5.91	1.08
	0.60	1.65		2.14	1.78	2.13	1.77	1.70	7.27	3.03
1.0	0.20	2.26		3.07	2.34	3.06	2.31	2.18	2.21	-3.54
	0.40	1.75		2.38	1.90	2.36	1.88	1.80	7.43	2.86
1.2	0.20	2.06		2.95	2.23	2.93	2.21	2.09	7.28	1.46
	0.40	1.63		2.30	1.83	2.28	1.82	1.74	11.66	6.75
1.4	0.2	1.94		2.84	2.14	2.72	2.12	2.02	9.28	4.12
1.6	0.2	1.85		2.75	2.07	2.72	2.05	1.97	10.81	6.49
1.8	0.2	1.81		2.67	2.01	2.64	2.00	1.94	10.50	7.18
2.0	0.2	1.78		2.60	1.96	2.57	1.95	1.91	9.55	7.30

Increasing the frequency of periodic notch (t/P) leads to higher values of the SCFs due to the overestimation caused by the reduction factor proposed in [12] (see Figure 10). The maximum deviation between the SCFs obtained by the SED method and the values obtained by applying the reduction factor [18] is about 12%, confirming the soundness of the recent proposal [18], while the new expression for γ assures a maximum relative deviation less than 6% and in many

cases less than 3% if compared with results from SED approach. This holds true for a wide range of notch acuities.

7.4 Axis-symmetric model under torsion

Dealing with torsion loading of single notches, the main contribution to the analytical study of smooth notched shafts under torsion was given in Ref. [12] where the SCF of shafts weakened by deep and shallow circumferential notches was determined. In [47] an accurate analysis demonstrated that the solution in [12] leads to low values of the SCF when applied to deep grooves of small-base radii. In Ref. [48] the results provided in [47] were fully confirmed while in [49] a general numerical technique by using Neuber-Papkovich's displacement functions was presented.

Much more recently, the SCFs of a round bar with rounded V-notches under torsion by means of the body force method is analysed providing a set of formulas useful to determine the theoretical SCF for any notch dimension [46]; these formulas yield error of K_t less than 1% with respect to the numerical results. A new analytical frame has been recently developed creating a link between the generalized notch stress intensity factor and the maximum shear stress at the notch tip [50]. As a result of taking advantage of that frame simple expressions for the SCFs, valid for a large bulk of different configurations have been provided.

The expressions proposed in Ref. [46] have been used here for the case of single notches under torsion, being these classical equations well consolidated and used from the scientific community. It is worth noting that the same results can be obtained by using new equations reported in [50] with a maximum deviation within 1% with respect to the equations given in [46].

The results from axis-symmetric bars weakened by periodic notches under torsion are listed in Table 6. The comparison between the results from SED models and those obtained by the combined application of different equations taken from the literature is reported in the table.

An arbitrary case corresponding to a depth to pitch ratio equal to 0.4 is chosen to compare the FE results with the results from solution given in [15], employed together with the equivalent notch reduction factor provided in [19] (see Figure 11). In the case of smaller depth to pitch ratio

(t/P=0.2), the data determined by SED almost coincide with the equation presented in [15], used in combination with the expressions for γ reported in [12] and in [19].

Table 6. Comparison of K_t by SED approach with FE results, the predicted model and SCFs by using equations given in [12] and [19] in a wide range of notch acuity, frequency of periodic notch and two opening angles: the case of axis-symmetric model under torsion.

t/P	ρ/t	K_t (SED-0)	K_t (SED-60)	K_t (NO-NE) [46,12]	K_t (NO-DR) [46,19]	K_t (KA-DR) ($2\alpha = 0^o$) [15,19]	K_t (KA-NE) ($2\alpha = 60^o$) [15,12]	K_t (KA-DR) ($2\alpha = 60^o$) [15,19]	K_t (PM)	Δ% (KA-DR,SED)	Δ% (PM,SED)
0.01	0.20	2.48	2.42	2.39	2.39	2.48	2.42	2.42	2.42	0.00	0.00
	0.40	1.93	1.92	1.91	1.91	1.94	1.93	1.93	1.93	0.52	0.52
	1.00	1.51	1.49	1.49	1.49	1.49	1.49	1.49	1.49	0.00	0.00
	2.00		1.30	1.29	1.29	1.28	1.28	1.28	1.28	-1.54	-1.54
0.2	0.20	2.46	2.40	2.35	2.27	2.33	2.39	2.30	2.36	-4.17	-1.67
	0.40	1.92	1.91	1.88	1.83	1.85	1.91	1.85	1.89	-3.14	-1.05
	1.00	1.48	1.48	1.48	1.45	1.45	1.48	1.45	1.47	-2.03	-0.68
	2.00		1.28	1.28	1.27	1.26	1.28	1.26	1.27	-1.56	-0.78
0.4	0.20	2.30	2.24	2.27	2.09	2.11	2.30	2.10	2.16	-6.25	-3.57
	0.80	1.44	1.44	1.53	1.46	1.45	1.53	1.45	1.48	0.69	2.78
	1.00	1.37	1.36	1.45	1.40	1.39	1.45	1.39	1.41	2.21	3.68
0.6	0.20	2.06	2.05	2.17	1.95	1.95	2.20	1.95	1.99	-4.88	-2.93
	0.40	1.63	1.62	1.77	1.63	1.62	1.78	1.62	1.65	0.00	1.85
	0.80	1.34		1.49	1.42	1.40	1.49	1.40	1.41	4.48	5.22
0.8	0.20	1.92		2.09	1.86	1.84	2.10	1.84	1.86	-4.17	-3.12
	0.40	1.51		1.72	1.57	1.55	1.72	1.55	1.56	2.65	3.31
	0.60	1.35		1.56	1.45	1.43	1.55	1.43	1.44	5.93	6.67
1.0	0.20	1.81		2.02	1.78	1.76	2.02	1.76	1.76	-2.76	-2.76
	0.40	1.43		1.67	1.52	1.50	1.66	1.50	1.50	4.90	4.90
1.2	0.20	1.69		1.95	1.72	1.70	1.95	1.70	1.68	0.59	-0.59
	0.40	1.36		1.63	1.49	1.46	1.62	1.46	1.45	7.35	6.62
1.4	0.2	1.61		1.90	1.67	1.65	1.89	1.65	1.62	2.48	0.62
1.6	0.2	1.54		1.86	1.63	1.61	1.84	1.61	1.58	4.55	2.60
1.8	0.2	1.49		1.82	1.60	1.58	1.80	1.58	1.54	6.04	3.36
2.0	0.2	1.46		1.78	1.57	1.55	1.76	1.55	1.51	6.16	3.42

Figure 11. The comparison of SED approach with the data given in [15] and implementing proposed depth reduction factors in [12] and [19] in the case of an axis-symmetric model under torsion with t/P=0.4.

The effect of torsion loading on SCFs has been found different than tension and bending loadings. In contrast to previous cases, the data in Table 6 clearly show that the use of the reduction factor proposed in [12] is close to the use of the recent equation for γ [19]. Although, by increasing t/P the deviation between the equation provided in [12] and the equation given in [19] increases, it is very limited under torsion.

As stated above, dealing with torsion loading, there is a lower sensitivity of the SCFs on the equivalent notch depth with respect to the tension case, where a small variation of t induces very large variations of K_t.

In agreement with tension and bending loadings, the effect of the considered notch opening angles by using equations given in [15] was found to be negligible.

The reduction factor according to Eq. (12) provides a maximum error less than 5% by comparing the assessed values and the results directly obtained from FE modeling.

8. Conclusions

By using the averaged SED in several FE models, the SCF of flat plates and round bars weakened by periodic V- and U-notches subjected to axial tension, bending and torsion has been calculated.

According to Neuber's formula, the SCF of the periodic notches can be evaluated by considering a single notch characterized by the same shape but a reduced depth. Depth reduction factors proposed in the past by Neuber and recently revised by other Authors have been compared and the relative deviations have been documented showing the soundness of the recent proposals both for normal stress and torsion. On the other hand, Neuber's equation is characterized by a tendency of large overestimations particularly evident by increasing t/P ratio.

The unique advantage of SED method due to using a coarse mesh in FE model is the most prominent application of such a technique in the current study. It is shown that SED-based calculations in the middle notch of the component are accurate enough to estimate the relevant SCFs in the case of periodic notches in flat plates and round bars under normal (tension and bending) and torsion loadings. Consequently, a new depth reduction factor based on SED is proposed, which is quite accurate for any value of the notch acuity. The method based on SED and coarse meshes can be easily extended to real three-dimensional components weakened by periodic notches.

Acknowledgements

References

[1]   Ayatollahi MR, Nejati M. Experimental evaluation of stress field around the sharp notches using photoelasticity. Materials & Design 2011;32(2):561-9.

[2]   Ayatollahi MR, Torabi AR. Brittle fracture in rounded V-shaped notches. Mater Des 2010;31(1):607.

[3]   Carpinteri A, Brighenti R, Vantadori S. Notched double-curvature shells with cracks under pulsating internal pressure. International Journal of Pressure Vessels and Piping 2009;86(7):443-53.

[4]   Paris PC, Sih GC. Stress analysis of cracks, in Fracture Toughness Testing and its applications. American society for testing and materials, Philadelphia 1965:30-81.

[5]   Sih GC. Strength of stress singularities at crack tips for flexural and torsional problems. Journal of Applied Mechanics, Trans ASME 1963;30:419-25

[6]   Sih GC. Stress distribution near internal crack tips for longitudinal shear problems. Journal of Applied Mechanics, Trans ASME 1965;32:51-8

[7]   Sih GC. Heat conduction in the infinite medium with lines of discontinuity Journal of Applied Mechanics, Trans ASME 1965;32:293-8

[8]   Kassir MK, Sih GC. Three dimensional crack problems The Netherlands Noordhoff Int. Publ.; 1975.

[9]   Sih GC. Methods of analysis and solutions of crack problems. The Netherlands: Noordhoff Int. Publ 1973.

[10]   Sih GC. Handbook of stress intensity factors. Benthlehem, Pennsylvania: Institute of Fracture and Solid Mechanics, Leigh University; 1973.

[11]   Pilkey WD, Pilkey DF. Peterson's stress concentration factors. New Jersey: John wiley and sons; 2008.

[12]   Neuber H. Theory of Notch Stresses. Springer Verlag; 1958.

[13]   Noda NA, Takase Y. Stress Concentration Factor Formulas Useful for All Notch Shapes in a Flat Test Specimen Under Tension and Bending. Journal of Testing and Evaluation (JTE) 2002;30(5):13.

[14]   Kato A. Two dimensional stress analysis on a personal computer. Mem Coll Engng, Chubu University 1990;26:1-9.

[15]   Kato A. Design equation for stress concentration factors of notched strips and grooved shafts. The Journal of Strain Analysis for Engineering Design 1992;27(1):21-8.

[16]   Kato A, Mizuno T. Stress concentration factors of grooved shafts in torsion. J Strain Analysis 1985;20:173-7.

[17]   Noda NA, Sera M, Takase Y. Stress concentration factors for round and flat test specimens with notches. International Journal of Fatigue 1995;17(3):163-78.

[18]   Dragoni E, Castagnetti D. Concentration of normal stresses in flat plates and round bars with periodic notches. Journal of Strain Analysis for Engineering Design 2010;45(7):495-503.

[19]   Dragoni E, Castagnetti D. Concentration of shear stresses in shallow periodic notches. Journal of Strain Analysis for Engineering Design 2011;46:397-404.

[20]   Croccolo D, Vincenzi N. Stress concentration factors in compression–fit couplings Proc IMechE Vol 224 Part C: J Mechanical Engineering Science 2010;224(6):1143-52.

[21]   Scire`Mammano G, Dragoni E. Stress concentrations around a pressurized hole close to a uniformly loaded boundary. Journal of Strain Analysis for Engineering Design 2009;44:569-82.

[22]   Chen YZ, Wang ZX. Multiple and periodic notch problems of elastic half-plane by using BIE based on Green's function method. International Journal of Computational Methods 2010;7(4):539-57.

[23]   Endersby SN, Parker AP, Bond TJ, Underwood JH. Stress concentration, stress intensity and fatigue lifetime calculations for shrink-fit compound tubes containing axial holes within the wall. ASTM Special Technical Publication 1997;1321:385-96.

[24]   Wang SW, Sun SJ, Wen AL, Wang WD, Nishida SI. Research of fatigue limit and stress concentration on structural steel with double-notches. Key Engineering Materials; 2010. p. 849-52.

[25]   Fujimoto Y, Iwata M, Nagai K. Fatigue test using multi-notched specimen and its reliability analysis. 1989; 1989. p. 1603-10.

[26]   Sih GC. Energy-density concept in fracture mechanics. Engineering Fracture Mechanics 1973;5(4):1037-40.

[27]   Sih GC. Some basic problems in fracture mechanics and new concepts. Engineering Fracture Mechanics 1973;5(2):365-77.

[28]   Sih GC. Strain-energy-density factor applied to mixed-mode crack problems International Journal of Fracture 1974;10:1974.

[29]   Sih GC. Surface and volume energy density applied as failure criterion. Dordrecht: Kluwer Academic Publisher; 1991.

[30]   Sih GC, Ho JW. Sharp notch fracture strength characterized by critical energy density. Theoretical and Applied Fracture Mechanics 1991;16(3):179-214.

[31]   Sih GC. Multiscaling in molecular and continuum mechanics: interaction of time and size from macro to nano. Springer; 2007.

[32] Sih GC, Tang XS. Scaling of volume energy density function reflecting damage by singularities at macro-, meso- And microscopic level. Theoretical and Applied Fracture Mechanics 2005;43(2):211-31.

[33] Tang XS, Sih GC. Weak and strong singularities reflecting multiscale damage: Micro-boundary conditions for free-free, fixed-fixed and free-fixed constraints. Theoretical and Applied Fracture Mechanics 2005;43(1):5-62.

[34] Lazzarin P, Zambardi R. A finite-volume-energy based approach to predict the static and fatigue behavior of components with sharp V-shaped notches. International Journal of Fracture 2001;112(3):275-98.

[35] Berto F, Lazzarin P. A review of the volume-based strain energy density approach applied to V-notches and welded structures. Theoretical and Applied Fracture Mechanics 2009;52(3):183-94.

[36] Lazzarin P, Berto F. Some expressions for the strain energy in a finite volume surrounding the root of blunt V-notches. International Journal of Fracture 2005;135(1-4):161-85.

[37] Berto F, Barati E. Fracture assessment of U-notches under three point bending by means of local energy density. Materials & Design 2010;32(2):822-30.

[38] Gómez F, Elices M, Berto F, Lazzarin P. Local strain energy density to assess the static failure of U-shaped notches in plates under mixed mode loading. 2007;International Journal of Fracture:29-45.

[39] Gómez F, Elices M, Berto F, Lazzarin P. Fracture of V-notched specimens under mixed mode (I + II) loading in brittle materials. International Journal of Fracture 2009;159(2):121-35.

[40] Gomez FJ, Elices M. A fracture criterion for blunted V-notched samples. International Journal of Fracture 2004;127(3):239-64.

[41] Gómez FJ, Elices M, Berto F, Lazzarin P. A generalised notch stress intensity factor for U-notched components loaded under mixed mode. Engineering Fracture Mechanics 2008;75(16):4819-33.

[42] Gómez FJ, Elices M, Berto F, Lazzarin P. Fracture of U-notched specimens under mixed mode: Experimental results and numerical predictions. Engineering Fracture Mechanics 2009;76(2):236-49.

[43] Lazzarin P, Berto F, Elices M, GÓMez J. Brittle failures from U- and V-notches in mode I and mixed, I + II, mode: a synthesis based on the strain energy density averaged on finite-size volumes. Fatigue & Fracture of Engineering Materials & Structures 2009;32(8):671-84.

[44] Lazzarin P, Berto F, Gomez FJ, Zappalorto M. Some advantages derived from the use of the strain energy density over a control volume in fatigue strength assessments of welded joints. International Journal of Fatigue 2008;30(8):1345-57.

[45] Lazzarin P, Berto F, Zappalorto M. Rapid calculations of notch stress intensity factors based on averaged strain energy density from coarse meshes: Theoretical bases and applications. International Journal of Fatigue 2010;32(10):1559-67.

[46] Noda N-A, Takase Y. Stress concentration formula useful for all notch shape in a round bar (comparison between torsion, tension and bending). International Journal of Fatigue 2006;28(2):151-63.

[47] Rushton KR. Stress concentrations arising in the torsion of grooved shafts. Int J Mech Sci 1967;9:697-705.

[48] Hamada M, Kitagawa H. Numerical solutions of two-dimensional elastic plastic problems by conformal mapping and finite difference method (elastic torsion of circumferentially grooved shafts). Bull Japan Soc Mech Eng 1968;11:605-11.

[49] Matthews GJ, Hooke CJ. Solution of axis-symmetric torsion problems by point matching. Journal of Strain Analysis for Engineering Design 1971;6:124-33.

[50] Zappalorto M, Berto F, Lazzarin P. Practical expressions for the notch stress concentration factors of round bars under torsion. International Journal of Fatigue 2010;33(3):382-95.

Appendix A

Equations for flat plates and round bars under tension, bending and torsion [15]

$$K_t = k_0 - \frac{2}{\pi}(k_0 - 1)tan^{-1}\{A(\rho/d)^B\}$$
$$A = P(t/\rho)^Q$$
$$B = R(t/\rho)^{-S}$$

Loading condition	Notch shape	k_0			
Tension bending	Shallow circular and U-shaped	$k_0 = 1 + 2.065(t/\rho)^{0.535}$			
	V-shaped	$k_0 = 1 + (k_u - 1)\left\{1 - \left(1 - cos\frac{\alpha}{2}\right)^E\right\};$ $E = 5.41(t/\rho)^{-0.34}$ $(k_u: k_0 \text{ of shallow circular or } U - notch)$			
Torsion	U-shaped	$k_0 = 1 + (t/\rho)^{0.556}$			
	V-shaped	$k_0 = 1 + (k_u - 1)\left\{1 - \left(tan\frac{\alpha}{4}\right)^E\right\};$ $E = 0.8 + 4.2(t/\rho)^{-0.6}$ $(k_u: k_0 \text{ of shallow circular or } U - notch)$			
Component	Loading	P	Q	R	S
Strip	Tension	3.63	0.54	0.94	0.072
	Bending	6.55	0.49	0.87	0.059
Shaft	Tension	5.47	0.53	0.94	0.066
	Bending	8.27	0.50	0.88	0.051
	Torsion	7.63	0.45	0.87	0.059

For geometrical parameters see Figure A1.
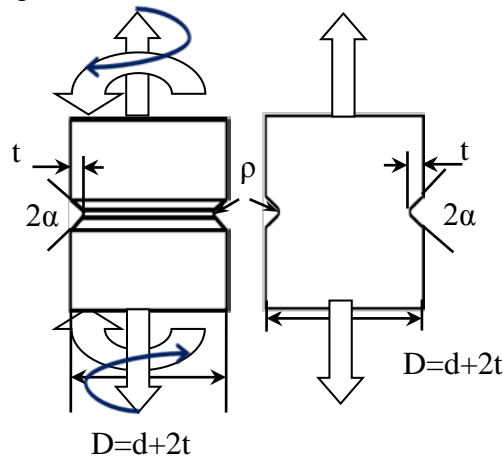
A1. Geometrical parameters in Ref. [15].

Equations for flat plates and round bars under tension [13]

$$\xi = \sqrt{t/\rho}, \quad \eta = \sqrt{\rho/t}, \quad \lambda = 2t/D$$

If $\frac{\rho}{a} \leq 1.0$

$$x = 2 - \rho/a$$

$$K_{tE} = 1 + 2\sqrt{t/\rho}$$

If $0 \leq \eta < 1.0$

$$K_{ts} = (1.148 - 0.160\eta - 0.0345\eta^2 + 0.0693\eta^3)K_{tE}$$

If $0 \leq \xi < 1.0$

$$K_{ts} = (1.000 - 0.127\xi + 0.2908\xi^2 - 0.1420\xi^3)K_{tE}$$

$$K_{tH} = \frac{2(a/\rho + 1)\sqrt{a/\rho}}{(a/\rho + 1)\tan^{-1}\sqrt{a/\rho} + \sqrt{a/\rho}}$$

$$K_{td} = (1.0015 - 0.054409x + 0.092227x^2 - 0.071641x^3)K_{tH}$$

$$K_{tN} = \frac{(K_{ts} - 1)(K_{td} - 1)}{((K_{ts} - 1)^m + (K_{td} - 1)^m)^{1/m}} + 1$$

$(1.4 \leq m < 2.8)$
If $0.0 \leq x \leq 2.0, \ 0.0 \leq \lambda \leq 1.0$

$$\begin{aligned}
K_t/K_{tN} &= (1.0009 - 0.0035609x + 0.0018408x^2) + (0.24237 + 0.722x - 0.4555x^2)\lambda \\
&+ (-1.7412 - 1.6597x + 1.7671x^2)\lambda^2 + (4.113 + 1.1214x - 2.9433x^2)\lambda^3 \\
&+ (-4.0762 + 0.076204x + 2.3538x^2)\lambda^4 \\
&+ (1.4622 - 0.26027x - 0.72205x^2)\lambda^5
\end{aligned}$$

Equations for round bars under tension [46]

If $0.0 \leq x \leq 2.0, \ 0.0 \leq 2t/D \leq 1.0$

$$K_t \Big/ K_{tN}^{m=2.8} = (1.0001 + 0.0036x - 0.0065x^2 + 0.0021x^3)$$
$$+(0.0116 + 1.404x - 1.285x^2 + 0.1799x^3)\lambda$$
$$+ (-0.1311 - 8.165x + 9.687x^2 - 2.124x^3)\lambda^2$$
$$+ (0.4240 + 16.94x - 22.77x^2 + 5.618x^3)\lambda^3$$
$$+ (-0.5156 - 15.07x + 21.71x^2 - 5.571x^3)\lambda^4$$
$$+ (0.2112 + 4.890x - 7.332x^2 + 1.896x^3)\lambda^5$$

$$K_{tN}^{m=2.8} = \frac{(K_{ts} - 1)(K_{td} - 1)}{((K_{ts} - 1)^{2.8} + (K_{td} - 1)^{2.8})^{1/2.8}} + 1$$

Where

$$K_{ts}/K_{tE} = (1.000 - 0.127\xi + 0.2908\xi^2 - 0.1420\xi^3)$$

(If $0 \leq \xi < 1.0$)

$$K_{ts}/K_{tE} = (1.148 - 0.160\eta - 0.0345\eta^2 + 0.0693\eta^3)$$

(If $0 \leq \eta < 1.0$)

$$\xi = \sqrt{t/\rho}, \quad \eta = \sqrt{\rho/t}, \quad \lambda = 2t/D$$

$$x = 2 - \rho/a$$

$$K_{tE} = 1 + 2\sqrt{t/\rho}$$

$$K_{td}/K_{tH} = (1.0011 - 0.025485x + 0.006131x^2 + 0.006131x^3)K_{tH}$$

$$K_{tH} = (1/N)\{(a/\rho)\sqrt{a/\rho + 1} + (0.5 + v)(a/\rho) + (1 + v)(\sqrt{a/\rho + 1} + 1)\}$$

$$N = a/\rho + 2v\sqrt{a/\rho + 1} + 2$$

Equations for round bars under bending [46]

(If $1.0 \leq x \leq 1.9$):

$$A = x - 1.0$$
$$K_t \Big/ K_{tN}^{m=2.8} = (0.99533 - 0.0035974A + 0.0051222A^2)$$

$+(-0.32401 - 1.2760A - 0.83101A^2)\lambda + (9.9470 + 22.740A + 4.1519A^2)\lambda^2$
$+ (-78.13 - 145.14A - 0.32590A^2)\lambda^3 + (288.43 + 463.53A - 36.046A^2)\lambda^4$
$+ (-578.45 - 825.96A + 91.919A^2)\lambda^5 + (647.76 + 836.06A - 100.76A^2)\lambda^6$
$+ (-380.88 - 450.51A + 52.837A^2)\lambda^7 + (91.652 + 100.57A - 10.954A^2)\lambda^8$

(If $1.9 \leq x \leq 1.99$):

$$B = x - 1.9$$

$$K_t \big/ K_{tN}^{m=2.8} = (0.99540 - 0.0054492B + 0.0060139B^2)$$

$+(-1.95570.65302B - 0.34860B^2)\lambda + (29.326 - 10.901B + 3.2846B^2)\lambda^2$
$+ (-175.64 + 78.343B - 31.852B^2)\lambda^3 + (555.91 - 254.28B + 107.53B^2)\lambda^4$
$+ (-1010.7 + 413.27B - 143.87B^2)\lambda^5 + (1059.8 - 340.54B + 51.147B^2)\lambda^6$
$+ (-595.49 + 127.03B + 41.581B^2)\lambda^7 + (138.76 - 13.576B - 27.476B^2)\lambda^8$

where

$$K_{ts}/K_{tE} = (1.000 - 0.127\xi + 0.2908\xi^2 - 0.1420\xi^3)$$

(If $0 \leq \xi < 1.0$)

$$K_{ts}/K_{tE} = (1.148 - 0.160\eta - 0.0345\eta^2 + 0.0693\eta^3)$$

(If $0 \leq \eta < 1.0$)

$$\xi = \sqrt{t/\rho}, \quad \eta = \sqrt{\rho/t}, \quad \lambda = 2t/D$$

$$x = 2 - \rho/a$$

$$K_{tE} = 1 + 2\sqrt{t/\rho}$$

$$K_{td}/K_{tH} = (0.99744 + 0.014732x - 0.024870x^2 + 0.014924x^3)K_{tH}$$

$$K_{tH} = (1/N)(3/4)(\sqrt{a/\rho + 1} + 1)\{3(a/\rho) - (1 - 2v)\sqrt{a/\rho + 1} + 4 + v\}$$

$$N = 3(a/\rho + 1) + (1 + 4v)\sqrt{a/\rho + 1} + (1 + v)/(\sqrt{a/\rho + 1} + 1)$$

Equations for round bars under torsion [46]

If $0.0 \leq x \leq 2.0$, $0.0 \leq 2t/D \leq 0.9$

(If $0.0 < x \leq 1.95$):

$$K_t \Big/ K_{tN}^{m=2.6} = (0.99999 - 0.0026822x + 0.0053295x^2 - 0.0016953x^3)$$
$$+ (0.0026579 - 0.32756x + 0.031522x^2 - 0.081859x^3)\lambda$$
$$+ (-0.0076275 + 6.129x - 4.8157x^2 + 2.3235x^3)\lambda^2$$
$$+ (-0.23987 - 30.899x + 30.141x^2 - 12.484x^3)\lambda^3$$
$$+ (1.0501 + 63.622x - 66.952x^2 + 26.072x^3)\lambda^4$$
$$+ (-1.4274 - 57.780x + 63.046x^2 - 23.742x^3)\lambda^5$$
$$+ (0.62212 + 19.268x - 21.460x^2 + 7.9153x^3)\lambda^6$$

(If $1.95 < x \leq 1.99$):

$$A = x - 1.0$$
$$K_t \Big/ K_{tN}^{m=2.6} = (1.0025 - 0.0093115A - 0.0058186A^2 + 0.025526A^3)$$
$$+ (-1.1232 + 0.77408A + 0.76457A^2 - 1.5432A^3)\lambda$$
$$+ (10.849 - 5.3371A - 6.5696A^2 + 12.729A^3)\lambda^2$$
$$+ (-38.451 + 23.186A + 9.7978A^2 - 98.794A^3)\lambda^3$$
$$+ (63.849 - 53.490A + 9.3650A^2 + 285.633A^3)\lambda^4$$
$$+ (-50.412 + 56.678A - 27.335A^2 - 328.903A^3)\lambda^5$$
$$+ (15.286 - 21.788A13.972A^2 + 130.778A^3)\lambda^6$$

$$K_{tN}^{m=2.6} = \frac{(K_{ts} - 1)(K_{td} - 1)}{((K_{ts} - 1)^{2.6} + (K_{td} - 1)^{2.6})^{1/2.6}} + 1$$

where
$$K_{ts}/K_{tE} = (1.000 - 0.089464\xi + 0.13872\xi^2 - 0.050088\xi^3)$$
(If $0 \leq \xi < 1.0$)

$$K_{ts}/K_{tE} = (0.81595 + 2.0675\eta - 7.2824\eta^2 + 12.045\eta^3 - 9.6241\eta^4 + 2.9783\eta^5 + 12.045\eta^3)$$
(If $0.05 \leq \eta < 1.0$)

$$\xi = \sqrt{t/\rho}, \quad \eta = \sqrt{\rho/t}, \quad \lambda = 2t/D$$

$$x = 2 - \rho/a$$

$$K_{tE} = 1 + \sqrt{t/\rho}$$

$$K_{td}/K_{tH} = (1.0004 - 0.0054166x + 0.031712x^2 - 0.034608x^3 + 0.013315x^4)K_{tH}$$
$$K_{tH} = 3(1 + \sqrt{a/\rho + 1})^2 / (4(1 + 2\sqrt{a/\rho + 1}))$$

Paper VI

On three-dimensional stress analysis of periodic notched plates under tension

Abstract: By using the finite element method, three-dimensional models of a number of periodic blunt and sharp notches subjected to tension loading are investigated. The aim of this research is to investigate the thickness effect on the location of maximum stress and notch stress intensity factor (NSIF) of corresponding blunt and sharp periodic notches respectively. With this aim, different number of periodic notches as well as different notch opening angles are examined. While for two-dimensional plates weakened by periodic notches some results are available in the literature, this paper first faces the problem of three-dimensional cases. A total of about 100 geometrical configurations are investigated.
It is found that, the effect of plate thickness of periodic notched components can be characterized by the relative value with respect to the depth of the notch (H/t). For the blunt periodic notches with relatively higher values of H/t ratio, the value of the maximum tensile stress is located near the free surface. On the contrary for lower values of H/t, it is placed at the middle plane. The same behaviour is observed for sharp periodic notches in terms of notch stress intensity factors.

Keywords: Periodic notches, three-dimensional problems, notch stress intensity factor, stress concentration factor

1. Introduction

The solutions of plane theory of elasticity, are still popular and serve as a basis for many engineering design procedures, standards and failure assessment codes due to their convenience and relative simplicity. In terms of numerical costs, two-dimensional models, based on plane stress or plane strain assumption, are much more computationally efficient, much easier to build and verify in comparison with the corresponding three-dimensional counterparts. Furthermore, three-dimensional equations of elasticity are not very amenable to analytical techniques.

In order to evaluate the dominant state of stress for dealing with crack problems, a simple empirical rule as being thin and thick enough is proposed for plane stress and plane strain condition respectively. On the other hand, until now there is no generally accepted criterion for identifying what thicknesses correspond to plane-stress or to plane-strain conditions.

A large number of publications in the recent literature [1-8] address the above mentioned issue. By considering some realistic crack shapes in three-dimensional (3D) finite element (FE) models

and using automatic crack growth techniques, the extent of surface regions in cracked bodies under tension loading condition was investigated in [9]. Based on their findings, the extent of both regions (extent of surface and near surface) was related to the elastic stress concentration factor (SCF) of the corresponding uncracked geometries and a linear relationship was found. In [10] by using a user defined material model based on the analytical approach, a simulation of brittle fracture in isotropic materials in 3D space was performed. In another work, some detailed 3D FE models of spot welds for different ration values of sheet metal thickness and spot-weld diameter are investigated [11]. The aim was to study the mechanical behavior of spot welds under tensile-shear and symmetric coach-peel loading conditions. In [12] by using 3D FE models, a modified equation for the SCF of an isotropic plate with a centered countersunk hole is proposed. Factorial and multi parameter fit analyses were conducted on the FE results to formulate a general parametric equation for the maximum SCF in terms of the four dimensionless geometric parameters. The advantage of proposed equations is demonstrated by comparing them with other method in the literature.

An extensive review [3] of some recent analytical, numerical and experimental results is presented to investigate the effect of plate thickness on elastic deformation as well as quasi-brittle fracture of plate components. For a plate under the in-plane loading condition, two basic assumption for the state of stress in the frame of plane theories of elasticity, namely plane stress (zero transverse stress) and plane strain (zero transverse strain), are commonly used [13].

In dealing with periodic blunt notches and by using the strain energy density (SED) approach, plane strain condition is assumed to evaluate the SCFs of a number of flat plates and round bars with periodic U- and V-notches. Tension, bending and torsion loading conditions have been considered [14].

Bolts, screws and rotary shouldered connections, as examples of periodic notched components, play an important role in the performance of the machinery. There are numerous studies in the literature addressing the fatigue life of the bolts. Among the others, the effect of thread pitch on the fatigue life of bolts is studied experimentally in [15]. In another study, the effect of nut geometry, curved spring washer and a sealing material on the fatigue life of M12 and M16 ISO

bolts was investigated in [16]. An innovative technique is proposed in [17, 18] with the aim of increasing the fatigue strength of rotary shouldered connections used in oil drilling industry.

In the presence of sharp periodic notches and by means of SED, the plane theory of elasticity is assumed to study the variability of the notch stress intensity factors (NSIFs) of periodic sharp notches in Ref. [19]. A new model of depth reduction factor for different ratios of relative depth of the notch is proposed to match the results from the SED approach. In the case of shallow notches, the results are compared with some semi-analytical solutions provided in [20]. In addition, based on the best fit of numerical data from the SED approach, some polynomials for non-dimensional NSIFs in the case of intermediate and deep notches are presented. In another work by the authors [21], some very simple expressions were derived for the direct evaluation of the SED and the NSIF of plates with infinite width as a function of the notch spacing in the case of narrow sharp notches.

In this study, for the first time, an attempt is made to investigate the thickness effect on the location of maximum stress and notch stress intensity factor (NSIF) of corresponding blunt and sharp periodic notches in three-dimensional plates weakened by periodic blunt and sharp notches. A number of sophisticated three-dimensional finite element models are built with this aim.
In addition, different number of periodic notches as well as different notch opening angles are examined.

2. Finite element model and SED calculation

In the present paper, both types of 3D blunt and sharp periodic notches are analyzed by means of the FE method within ANSYS software. Six models with different geometrical configurations (summarized in Table 1) have been considered. A total of about 100 geometrical configurations are investigated.
The geometrical parameters, namely, notch depth (t), notch radius (ρ), pitch of the notch (p), notch opening angle (2α), plate thickness (H), width of the plate (W) and plate length (L) and boundary conditions are shown in Fig. 1, in which E is Young's modulus of elasticity, υ is

Poisson's ratio, Ux is the applied displacement and σ_n is the equivalent of applied remote stress. For all the FE models the elastic isotropic material with E=206 GPa, ν=0.3 is used. The value of σ_n=100 MPa for all the models is assumed. Of course, the value of applied Ux is varied, depending on the length of the plate (L), as it is shown in Fig.1.
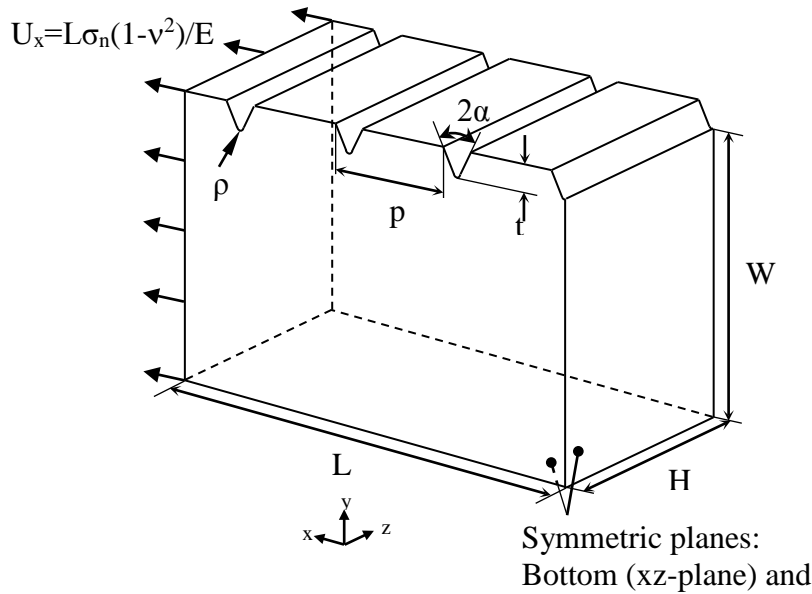
Fig. 1: The geometrical parameters of 3D periodic notched plate and boundary conditions.

Table 1: Different models with geometrical parameters (2α: notch opening angle; ρ: notch radius; p: pitch of the notch; t: notch depth; h: thickness of the plate; N: number of notches).

Model Number	2α (^{o})	ρ (mm)	p (mm)	t (mm)	H (mm)	N
1	60	0.1	2.5	0.5	10, 5.0, 2.0, 1.0	3-9
2	60	1.0	25	5.0	10, 5.0, 2.0, 1.0	3-5
3	120	0.1	2.5	0.5	10, 5.0, 2.0, 1.0	3-9
4	120	1.0	25	5.0	10, 5.0, 2.0, 1.0	3-5
5	60	0.0	2.5	0.5	10, 5.0, 2.0, 1.0	3-9
6	120	0.0	2.5	0.5	10, 5.0, 2.0, 1.0	3-9

As it can be seen from Table 1, the first four models correspond to blunt notches, whereas the last two represent the sharp notch configurations. Furthermore, the models 2 and 4 are the scaled-up geometries (only in xy-plane) of the corresponding models 1 and 3 respectively. The

sample mesh pattern of both types (blunt and sharp periodic notches) has been depicted in Fig. 2.
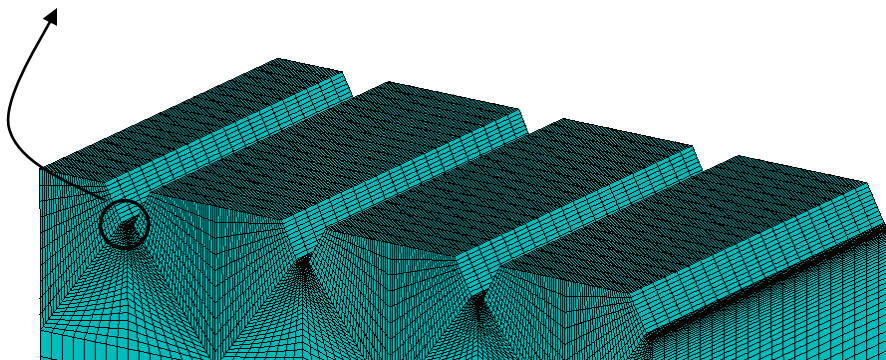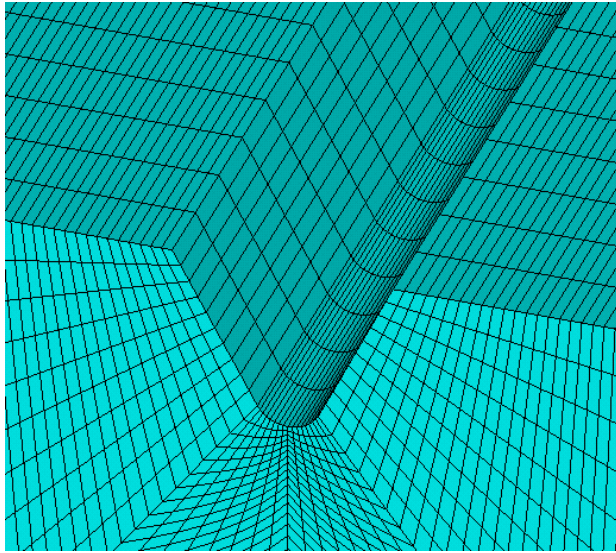
(a)
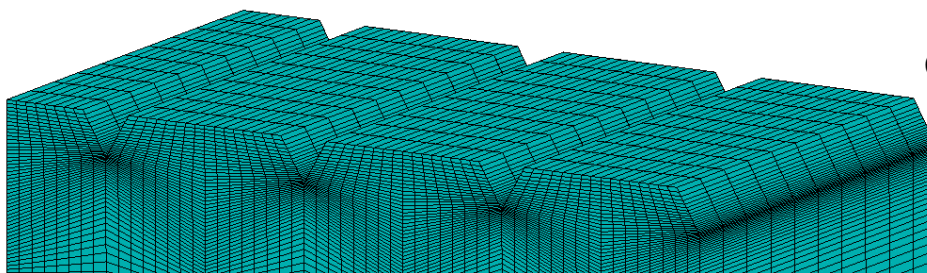
(b)

Fig. 2: Sample mesh pattern used for: (a) blunt periodic notches ($\rho \neq 0.0$); (b) sharp periodic notches ($\rho = 0.0$).

3. Results and discussions

In order to present the results in a more systematic manner, the selected results for each FE model (tabulated in Table 1) are presented and discussed in that order.

3.1 Model 1: 2α=60°; ρ=0.1mm; p=2.5mm; t=0.5mm (H=10, 5.0, 2.0 and 1.0 mm; N=3-9)

Fig. 3 shows the variation of tensile stress at the middle notch of periodic notched plates along the thickness of the plate (H=10 mm) for different number of notches.
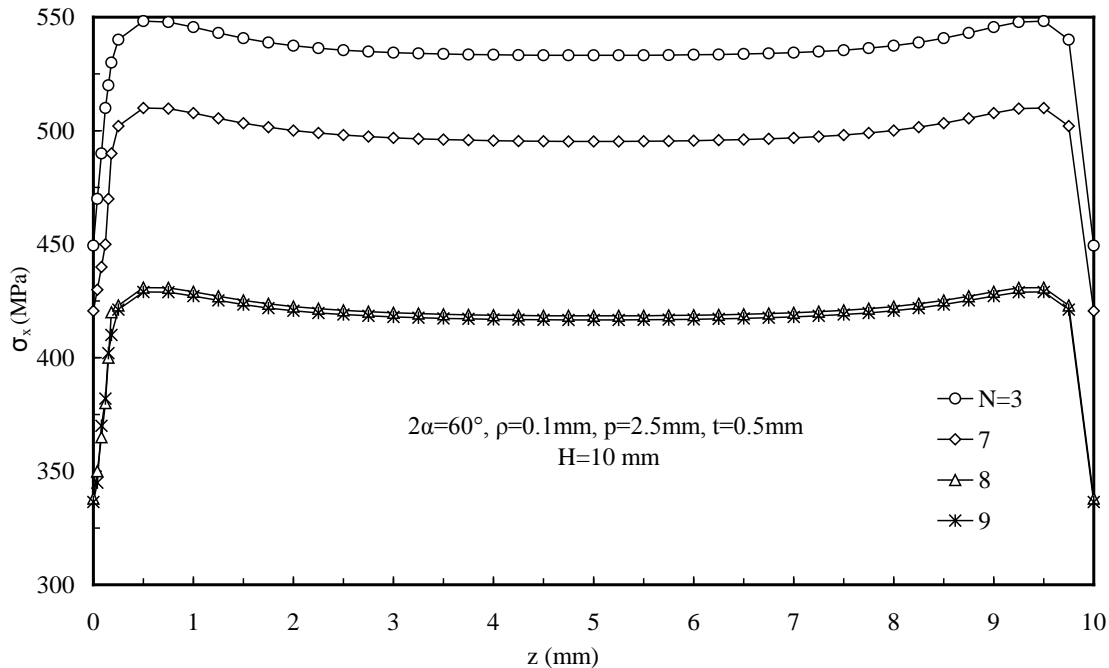
Fig. 3: The variation of tensile stress at the middle notch of periodic notched plates along the thickness of the plate (H=10 mm) for different number of notches (Model 1).

From Fig. 3, two essential trends can be observed. The first feature belongs to periodic notches, which shows the effect of number of notches on the variation of tensile stress. In fact, as it is expected, increasing the number of notches leads to decrease in the value of tensile stress at the

middle notch of periodic notched plate. The second characteristic is that the maximum tensile stress is not placed on the surface (2D assumption) nor at the middle of the plate, but very close to the surface (at a distance $z \approx 0.5$ mm).
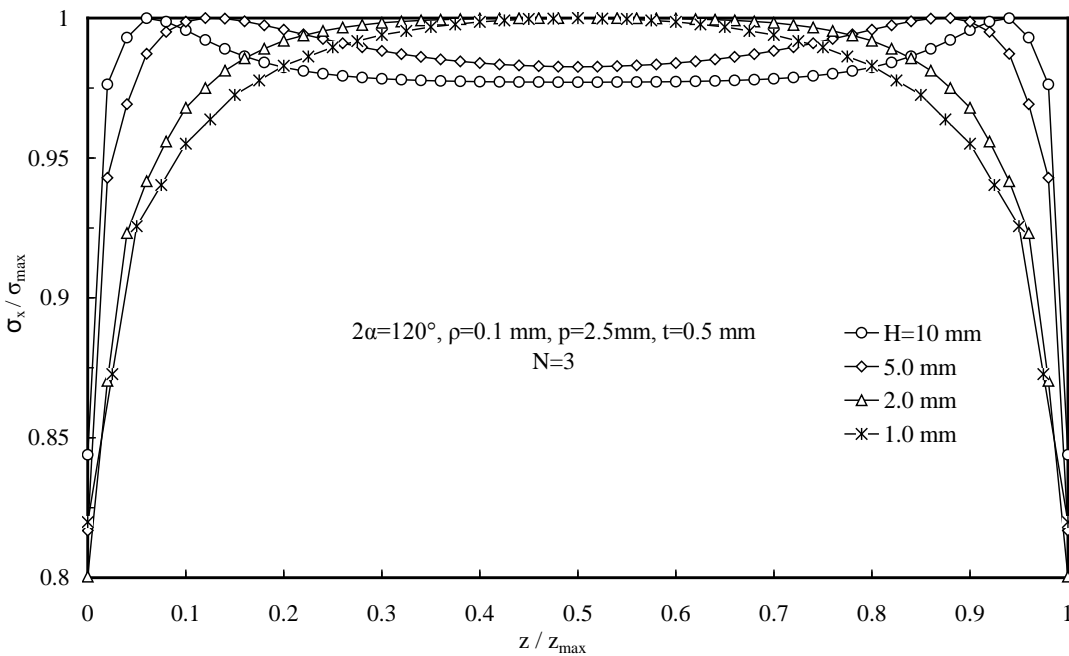
The variation of normalized tensile stress (σ_x/σ_{max}) at the middle notch of periodic notched plate (N=3) as a function of normalized thickness (z/z_{max}) of the plate for different values of plate thickness (H) is depicted in Fig. 4.
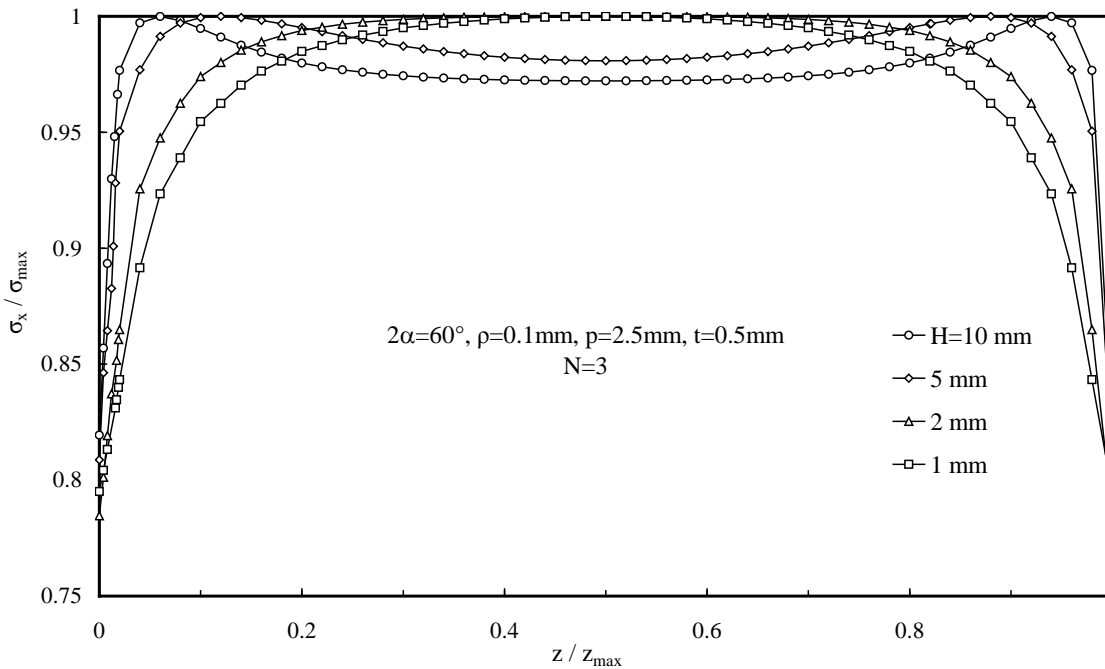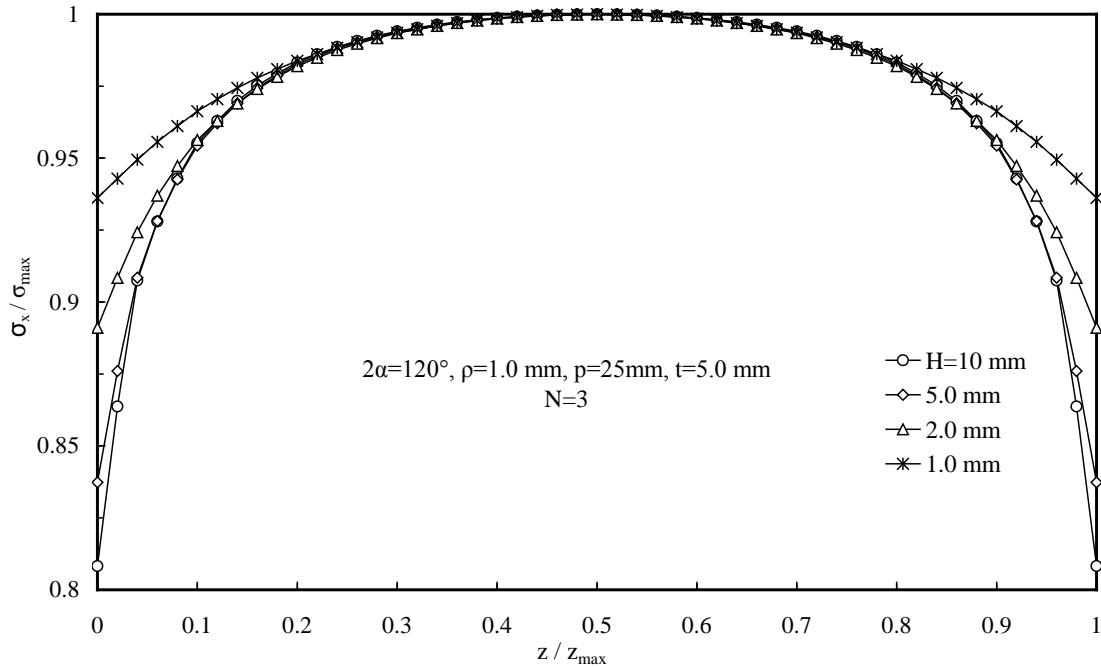

Fig. 4: The variation of normalized tensile stress (σ_x/σ_{max}) at the middle notch of periodic notched plate as a function of normalized thickness (z/z_{max}) of the plate for different values of plate thickness (H)

According to Fig. 4, the effect of thickness of plate on the tensile stress is clearly evident. For the relatively thinner plates, the maximum stress appears to be at the middle of the plate and that confirms the plane stress assumption of 2D FE models. However, increasing the thickness of the plate leads to generating the maximum tensile stress at the near surface location. In particular, for the case of thicker plates (H=5 and 10 mm), the shift of maximum stress from the mid plane to the closer location of the free surfaces is clearly evident.

3.2 Model 2: 2α=60°; ρ=1.0 mm; p=25mm; t=5.0 mm (H=10, 5.0, 2.0 and 1.0 mm; N=3-5)

As it is mentioned earlier (Section 2), Model 2 is the scaled-up geometry (only in xy-plane) of Model 1.

Fig. 5 shows the variation of tensile stress at the middle notch of periodic notched plates along the thickness of the plate (H=10 mm) for different number of notches (N=3-5). (Model 1).
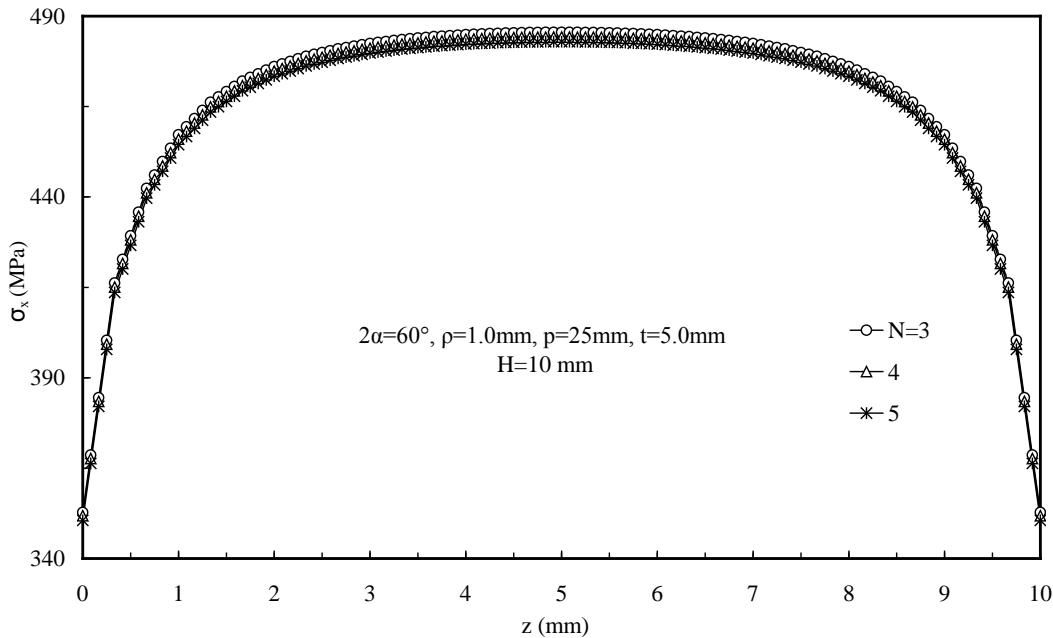
Fig. 5: The variation of tensile stress at the middle notch of periodic notched plates along the thickness of the plate (H=10 mm) for different number of notches (Model 2).

As it can be seen from Fig. 5, although the plate seems thick (H=10 mm), no effect of number of notches on the tensile stress is observed. In addition, in contrast to Model 1, the maximum tensile stress is located at the mid-plane. This behavior will be discussed in Fig. 6 by comparing the different thicknesses of the plates with periodic notches.

The variation of normalized tensile stress (σ_x/σ_{max}) at the middle notch of periodic notched plate (N=3) as a function of normalized thickness (z/z_{max}) of the plate for different values of plate thickness (H) is depicted in Fig. 6.
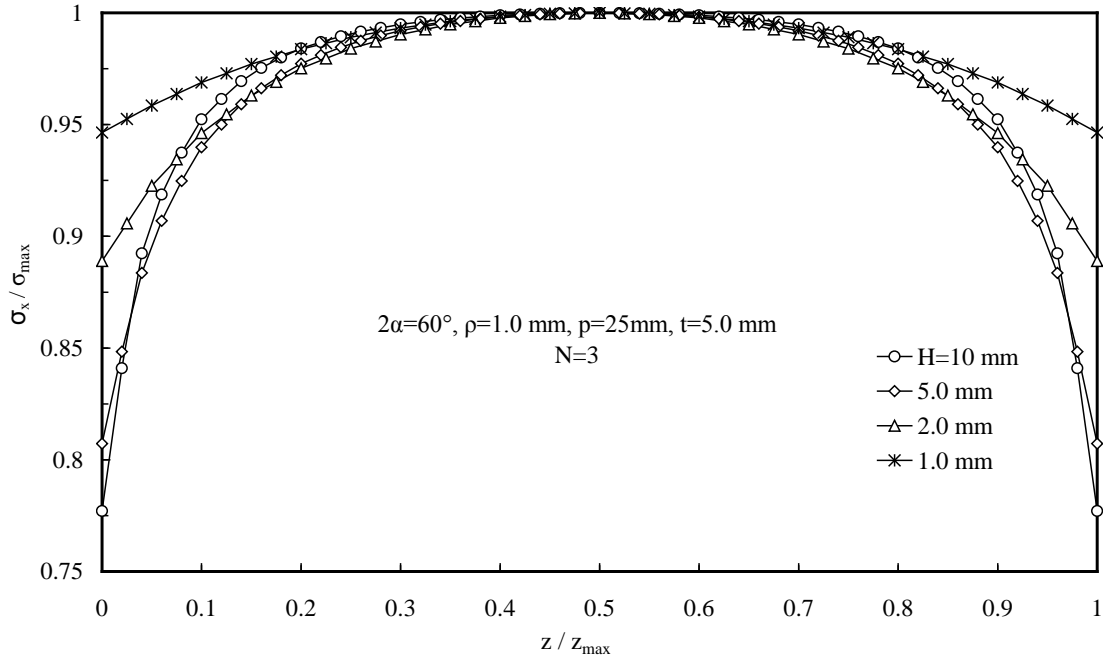
Fig. 6: The variation of normalized tensile stress (σ_x/σ_{max}) at the middle notch of periodic notched plate as a function of normalized thickness (z/z_{max}) of the plate for different values of plate thickness (H) (Model 2).

By comparing the different plate thicknesses of periodic notches in Fig. 6, the location of maximum tensile stress evidently is placed at the middle of the plate. This can be explained by the value of plate thickness to the notch depth ratio (H/t). For instance, considering Model 1 (Fig.3), when the ratio H/t=1.0/0.5=2.0, the maximum stress appears to be at the middle of the plate. Similarly, for Model 2, with the same ratio of H/t=10/5.0=2.0, the same behaviour can be observed. In other words, the effect of plate thickness of notched components can be characterized by the relative value with respect to the depth of the notch (H/t).

This is specially important in the investigation of one-plane scaled geometries (e.g. Model 2, in which the geometry of Model 1 is scaled-up 10 times in only the xy-plane).

3.3 Model 3: 2α=120°; ρ=0.1mm; p=2.5mm; t=0.5mm (H=10, 5.0, 2.0 and1.0 mm; N=3- 9)

Model 3 is similar to Model 1, with the only difference of the notch opening angle. In Model 3 a larger notch opening angle (2α=120°) is considered in comparison wi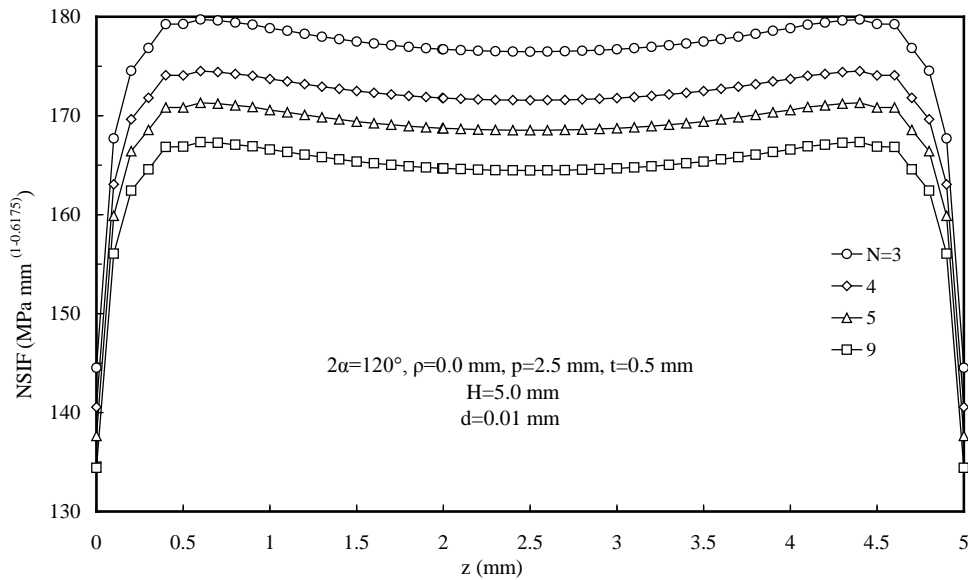th 2α=60° used in Model 1. Fig. 7 shows the variation of tensile stress at the middle notch of periodic notched plates along the thickness of the plate (H=10 mm) for different number of notches.
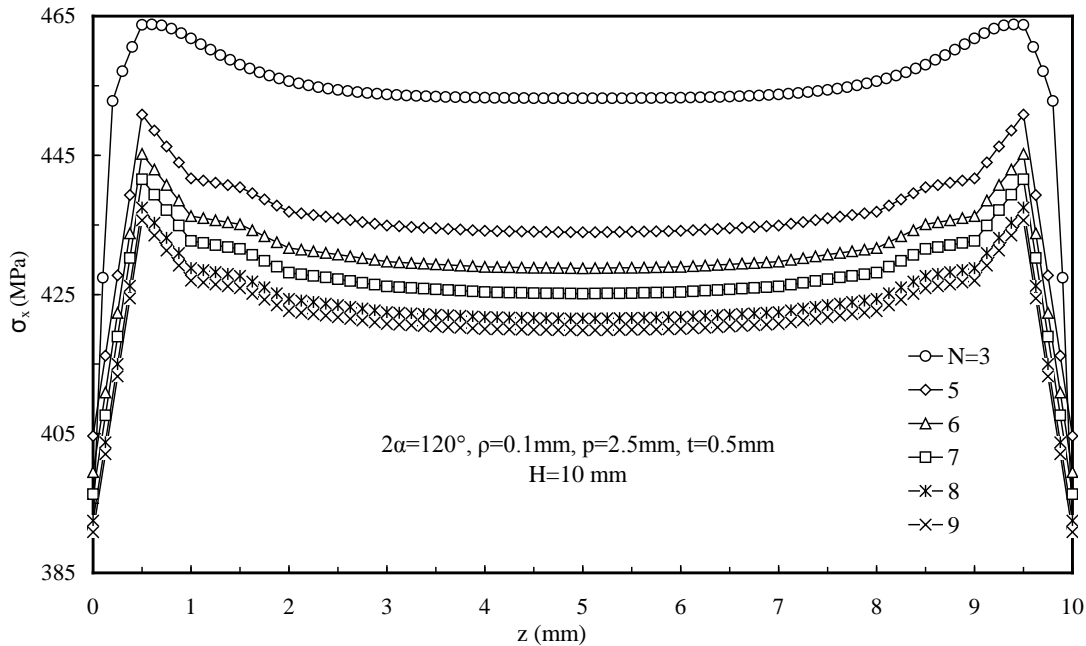

Fig. 7: The variation of tensile stress at the middle notch of periodic notched plates along the thickness of the plate (H=10 mm) for different number of notches (Model 3).

Fig. 7 evidently shows a similar trend to Fig. 3. The variation of the tensile stress at the middle notch of the plate along the thickness as well as the effect of the number of notches on the tensile stress can be observed from the Figure.

The variation of the normalized tensile stress (σ_x/σ_{max}) at the middle notch of the periodic notched plate (N=3) as a function of the normalized thickness (z/z_{max}) of the plate for different values of plate thicknesses (H) is depicted in Fig. 8.

3.4 Model 4: 2α=120°; ρ=1.0 mm; p=25mm; t=5.0 mm (H=10, 5.0, 2.0 and 1.0 mm; N=3-5)

Model 4 is also similar to Model 2, with the difference of the notch opening angle. In Model 4 a notch opening angle equal to 120° is considered in comparison with 2α=60° investigated in Model 2. In addition, Model 4 is the scaled-up geometry (only in xy-plane) of Model 3.

The variation of normalized tensile stress (σ_x/σ_{max}) at the middle notch of periodic notched plate (N=3) as a function of normalized thickness (z/z_{max}) of the plate for different values of plate thickness (H) is depicted in Fig. 9. As it can be seen from Fig. 9 and similarly to Fig. 6, the location of the maximum tensile stress clearly is placed at the middle of the plate for different plate thicknesses. The reason for this behaviour is explained in the discussion of Fig. 6.

Fig. 8: The variation of normalized tensile stress (σ_x/σ_{max}) at the middle notch of periodic notched plate (N=3) as a function of normalized thickness (z/z_{max}) of the plate for different values of plate thickness (H) (Model 3).

Fig. 9: The variation of normalized tensile stress (σ_x/σ_{max}) at the middle notch of periodic notched plate (N=3) as a function of normalized thickness (z/z_{max}) of the plate for different values of plate thickness (H) (Model 4).

3.5 Model 5: $2\alpha=60°$; $\rho=0.0$ mm; $p=2.5$mm; $t=0.5$mm (H=10, 5.0, 2.0 and1.0 mm; N=3-5)

Models 5 and 6 represent the sharp periodic notch configurations. The only difference between the two models is the notch opening angle. In Model 5 a relatively medium notch opening angle $2\alpha=60°$ is considered in comparison with a larger notch opening angle $2\alpha=120°$ in Model 6.

Due to the existence of singularity point at the tip of sharp notches and in order to evaluate the results in different locations of the 3D FE models, as it is shown in Fig. 9, in addition to the along-thickness path for studying the variation of tensile stress along the plate thickness (path-2), a path for different distance from the tip of the notch (path-1) is considered.

By examining the different distances from the notch tip (path-1 in Fig. 10), the distance d=0.01 mm from notch tip is considered to present the results in terms of NSIF along the thickness for both Models 5 and 6.

According to Fig. 11, the maximum NSIF appears to be at the location very close to the surface of the plate with periodic notches (z≈0.5 mm). This behaviour is similar to the one found in Fig.

2 (Model 1) in terms of tensile stress for the blunt notches. Furthermore, the NSIF decreases as the number of notches increases.

3.6 Model 6: 2α=120°; ρ=0.0 mm; p=2.5mm; t=0.5mm (H=10, 5.0, 2.0 and 1.0 mm; N=3-5)

As it is mentioned in section 3.5, Model 6 is the same as Model 5 with the only difference of the notch opening angle which is $2\alpha=120°$ in the latter case.

Fig. 12 shows the variation of the NSIF at the middle notch of periodic notched plates along the thickness of the plate (H=5 mm) for different number of notches.
A similar trend to Fig. 11 both in terms of NSIF variation and the effect of number of notches is observed in Fig. 12.

In addition, in order to validate the choice of d=0.01 mm from the notch tip for NSIF evaluation, the variation of NSIF along the notch bisector line of the plate for different values of along-thickness path (path-2 in Fig. 10) is shown in Fig. 13.
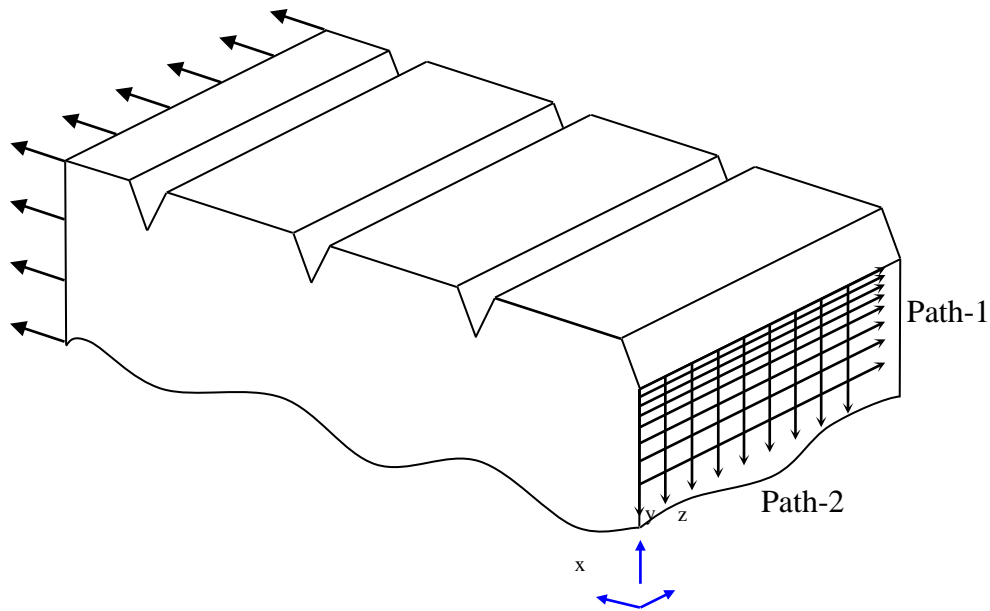
Fig. 10: Schematic diagram of different paths used for NSIF evaluation along the thickness of the plate.

Fig. 11 shows the variation of NSIF at the middle notch of periodic notched plates along the thickness of the plate (H=5 mm) for different number of notches.
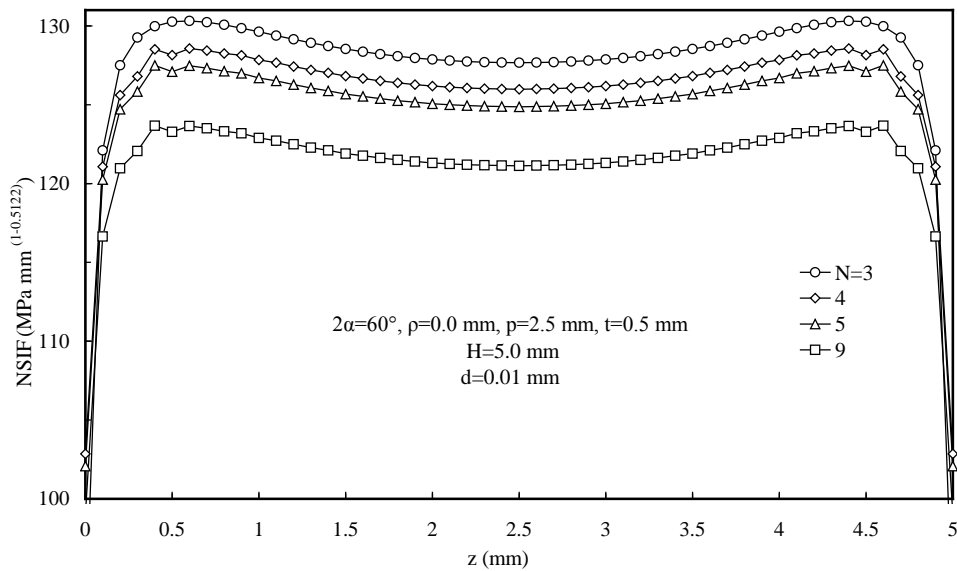
Fig. 11: The variation of NSIF at the middle notch of periodic notched plates along the thickness of the plate (H=5 mm) for different number of notches (Model 5).

Fig. 12: The variation of NSIF at the middle notch of periodic notched plates along the thickness of the plate (H=5 mm) for different numbers of notches (Model 6).
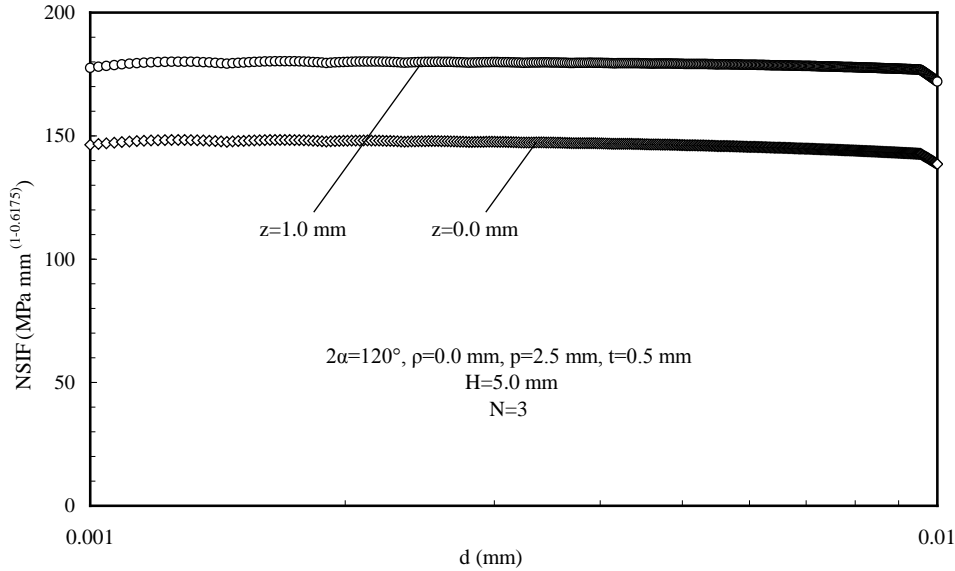
Fig. 13: the variation of NSIF along the notch bisector line of the plate for different values of along-thickness path (path-2 in Fig. 10).

4. Comparison with 2D plane solution

In order to validate the 3D FE analyses, Model 2 (see Table 1) with the following geometrical dimensions is selected: $2\alpha=60°$; $\rho=1.0$ mm; $p=25$mm; $t=5.0$ mm; $H=10$ mm; $W=290$ mm; $N=3$. The results in terms of σ_{max} at the middle notch of plate with periodic notches have been compared with those from 2D plane element models, as it is shown in Fig. 14.

As it can be seen from Fig. 14, the $\sigma_{max}=461.8$ MPa of plane model (a) is about 5% lower than $\sigma_{max}=484.8$ MPa of 3D model (b). The location of σ_{max} in 3D model is placed in this case at the middle of the plate (see also Fig. 5), in contrast to other cases where the maximum of the principal stress is placed close to the surfaces (see Fig. 3).

Due to multi-factors dependence (such as thickness and type of applied loading) of 3D component, it is not possible to provide a general assessment of the range of possible errors associated with 2D simplifications. However, for the considered class of problem, i.e. under mode I loading, the range of error related to 2D simplifications varies between 5-10%. Some previous works dealing with single notches subjected to mode I loading confirms this trend (see for example Refs [22-25]). In dealing with mode II and mode III loadings the differences between a 3D model and the corresponding 2D counterpart can be larger due to the presence of

coupled, induced modes [26-33], which will be investigated also for periodic notches in future contributions.

5. Conclusions

This study is aimed to face for the first time three-dimensional effects in plates weakened by periodic notches. While some recent papers provide useful information for plane plates with periodic notches (blunt and sharp), no results have been presented up to now to discuss the 3D effects due to finite values of the plate thickness. This paper is mainly focused on closing this gap and presenting some results from 3D plates
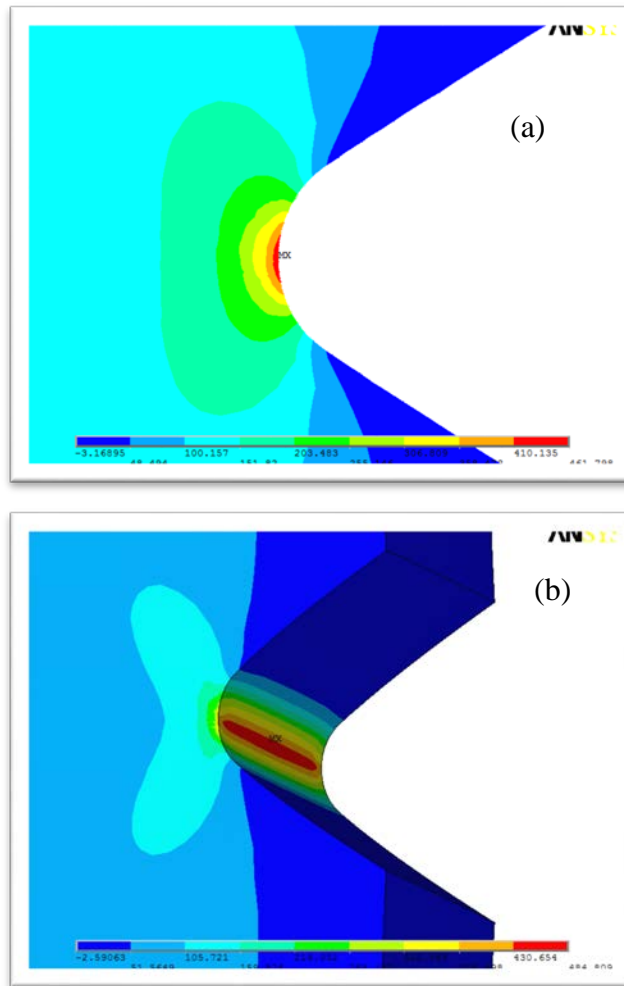
Fig. 14: Comparison of 3D and 2D models in term of σ_{max}.

weakened by periodic notches of both sharp and blunt types. Different geometrical parameters have been varied in the models to have results from about one hundred new accurate 3D models. In particular the thickness of the plate, the notch opening angle, the pitch of the notch and the notch depth have been varied to investigate a wide number of geometrical configurations.

The main result of this study is that the effect of the plate thickness in periodic notched components can be characterized by the relative value between the plate thickness and the notch depth (H/t). For blunt periodic notches under tension with relatively higher values of H/t ratio (H/t>2.0), the value of maximum tensile stress is located near the free surfaces while, on the contrary, for lower values (H/t<2.0) it is placed at the mid-plane. The same behaviour is observed for sharp periodic notches subjected to tension loading, in terms of notch stress intensity factors. The number of notches has been also investigated showing that a saturation effect is always found for N=9.

References

1. Kotousov A. On stress singularities at angular corners of plates of arbitrary thickness under tension. International Journal of Fracture, 2005, 132: 29-36.

2. Kotousov A. Fracture in plates of finite thickness. International Journal of Solids and Structures, 2007, 44: 8259-8273.

3. Kotousov A, Lazzarin P, Berto F, Harding S. Effect of the thickness on elastic deformation and quasi-brittle fracture of plate components. Engineering Fracture Mechanics, 2010, 77: 1665-1681.

4. Lazzarin P, Zappalorto M. A three-dimensional stress field solution for pointed and sharply radiused V-notches in plates of finite thickness. Fatigue & Fracture of Engineering Materials & Structures, 2012, 35: 1105-1119.

5. Pook LP. Stress intensity factor expressions for regular crack arrays in pressurized cylinders. Fatigue & Fracture of Engineering Materials & Structures, 1990, 13: 135-143.

6. Pook LP. A note on corner point singularities. International Journal of Fatigue, 1992, 53: 3-8.

7. Pook LP. Finite element analysis of corner point displacements and stress intensity factors for narrow notches in square sheets and plates. Fatigue & Fracture of Engineering Materials & Structures, 2000, 23: 979-992.

8. Pook LP. A finite element analysis of cracked square plates and bars under antiplane loading. Fatigue & Fracture of Engineering Materials & Structures, 2003, 26: 533-541.

9. Branco R, Antunes FV, Ricardo LCH, Costa JD. Extent of surface regions near corner points of notched cracked bodies subjected to mode-I loading. Finite Elements in Analysis and Design, 2012, 50: 147-160.

10. May M, Kilchert S, Hiermaier S. 3D modeling of fracture in brittle isotropic materials using a novel algorithm for the determination of the fracture plane orientation and crack surface area. Finite Elements in Analysis and Design, 2012, 56: 32-40.

11. Deng X, Chen W, Shi G. Three-dimensional finite element analysis of the mechanical behavior of spot welds. Finite Elements in Analysis and Design, 2000, 35: 17-39.

12. Darwish F, Gharaibeh M, Tashtoush G. A modified equation for the stress concentration factor in countersunk holes. European Journal of Mechanics - A/Solids, 2012, 36: 94-103.

13. Berto F, Lazzarin P, Kotousov A, Pook LP. Induced out-of-plane mode at the tip of blunt lateral notches and holes under in-plane shear loading. Fatigue & Fracture of Engineering Materials & Structures, 2012, 35: 538-555.

14. Afshar R, Berto F. Stress concentration factors of periodic notches determined from the strain energy density. Theoretical and Applied Fracture Mechanics, 2011, 56: 127-139.

15. Majzoobi GH, Farrahi GH, Habibi N. Experimental evaluation of the effect of thread pitch on fatigue life of bolts. International Journal of Fatigue, 2005, 27: 189-196.

16. Majzoobi GH, Farrahi GH, Hardy SJ, Pipelzadeh MK, Habibi N. Experimental results and finite-element predictions of the effect of nut geometry, washer and Teflon tape on the fatigue life of bolts. Fatigue and Fracture of Engineering Materials and Structures, 2005, 28: 557-564.

17. Korin I, Perez Ipiña J. Controlled residual stresses introduction to improve fatigue resistance of rotary shouldered connections used in oil drilling industry. International Journal of Pressure Vessels and Piping, 2010, 87: 696-703.

18. Korin I, Perez Ipiña J. Experimental evaluation of fatigue life and fatigue crack growth in a tension bolt-nut threaded connection. International Journal of Fatigue, 2011, 33: 166-175.

19. Lazzarin P, Afshar R, Berto F. Notch stress intensity factors of flat plates with periodic sharp notches by using the strain energy density. Theoretical and Applied Fracture Mechanics, 2012, 60: 38-50.

20. Savruk M, Kazberuk A. A plane periodic boundary-value problem of elasticity theory for a half-plane with curvilinear edge. Materials Science, 2008, 44: 461-470.

21. Berto F, Lazzarin P, Afshar R. Simple new expressions for the notch stress intensity factors in an array of narrow V-notches under tension. International Journal of Fracture, 2012, 176: 237-244.

22. Berto F, Lazzarin P, Wang C. Three-dimensional linear elastic distributions of stress and strain energy density ahead of V-shaped notches in plates of arbitrary thickness. International Journal of Fracture, 2004, 127: 265-282.

23. Kotousov A, Wang CH. A generalized plane-strain theory for transversely isotropic plates. Acta Mechanica, 2003, 161: 53-64.

24. Li Z, Guo W. Three-dimensional elastic stress fields ahead of blunt V-notches in finite thickness plates. International Journal of Fracture, 2001, 107: 53-71.

25. Li Z, Guo W, Kuang Z. Three-dimensional elastic stress fields near notches in finite thickness plates. International Journal of Solids and Structures, 2000, 37: 7617-7632.

26. Berto F, Kotousov A, Lazzarin P, Pegorin F. On a coupled mode at sharp notches subjected to anti-plane loading. European Journal of Mechanics, A/Solids, 2013, 38: 70-78.

27. Berto F, Kotousov A, Lazzarin P, Pook LP. On scale effect in plates weakened by Rounded V-Notches and subjected to in-plane shear loading. International Journal of Fracture, 2013, 180: 111-118.

28. Berto F, Lazzarin P, Kotousov A. On the presence of the out-of-plane singular mode induced by plane loading with KII = KI = 0. International Journal of Fracture, 2011, 167: 119-126.

29. Berto F, Lazzarin P, Kotousov A. On higher order terms and out-of-plane singular mode. Mechanics of Materials, 2011, 43: 332-341.

30. Berto F, Lazzarin P, Kotousov A, Harding S. Out-of-plane singular stress fields in V-notched plates and welded lap joints induced by in-plane shear load conditions. Fatigue and Fracture of Engineering Materials and Structures, 2011, 34: 291-304.

31. Berto F, Lazzarin P, Marangon C. The effect of the boundary conditions on in-plane and out-of-plane stress field in three dimensional plates weakened by free-clamped V-notches. Physical Mesomechanics, 2012, 15: 26-36.

32. Harding S, Kotousov A, Lazzarin P, Berto F. Transverse singular effects in V-shaped notches stressed in mode II. International Journal of Fracture, 2010, 164: 1-14.

33. Kotousov A, Berto F, Lazzarin P, Pegorin F. Three dimensional finite element mixed fracture mode under anti-plane loading of a crack. Theoretical and Applied Fracture Mechanics, 2012, 62: 26-33.

Paper VII

Three-dimensional Stress Analysis of a Plate Weakened by an Inclined Diamond Hole Under Various Loading Conditions

Abstract: Three-dimensional (3D) elastic stress distributions in the vicinity of the sharp corners of an inclined diamond hole in a plate are investigated. A detailed 3D finite element model under different loading conditions is analyzed to study the intensity of different fracture modes due to the thickness effect. The stress results are compared with those provided by a recent theory which reduces the 3D governing equations of elasticity to a differential equation system, which includes a bi-harmonic equation and a harmonic equation. They provide the solution of the corresponding in-plane and out-of-plane notch problem, respectively, and have to be concurrently satisfied. Comparing numerical results and theoretical stress distributions, a good agreement is found.

Keywords: Analytical expressions, finite element analysis, diamond hole, three-dimensional.

I. INTRODUCTION

Due to convenience and relative simplicity, solutions of plane theory of elasticity are popular and serve as a basis for many engineering design procedures, standards and failure assessment codes. In terms of numerical costs, two-dimensional models, based on plane stress or plane strain assumptions, are much more computationally efficient, easier to build and verify in comparison with the corresponding three-dimensional counterparts. However, to approach the through-the-thickness effect of real components, requires alternative methods such as three-dimensional theory of elasticity or finite element (FE) method.

The coupling effect was investigated for through-the-thickness cracks in finite thickness plates using analytical and numerical methods [1-3]. In particular, the three-dimensional stress field at sharp notches with arbitrary notch opening angles based on the first order plate theory by [4] is studied in [5, 6]. The coupled mode in shear loading was called 'the out-of-plane mode, or Mode O', to distinguish it from the conventional Mode 3. It was also demonstrated that the out-of-plane mode is provoked by the three-dimensional effects linked to Poisson's ratio of the material and described by the same characteristic equation as the conventional Mode III.

The local interaction between the loading modes for the case of pointed and sharply radiused notches in plates with finite thickness was re-analysed in [7]. It was demonstrated that the governing equations of three-dimensional elasticity can be reduced to a bi-harmonic equation and a harmonic equation. The former provides the solution of the corresponding plane notch problem, while the latter gives the anti-plane elasticity problem. Having the two equations simultaneously satisfied in a 3D problem, justifies the theoretical and mutual interaction between different modes. The main aim of this study is to examine the proposed theory in [7] by investigating the stress fields in the vicinity of the sharp corners of a diamond hole in a plate with finite thickness under tension and twisting loading conditions.

II. METHODOLOGY

Analysis of three-dimensional stress fields

Recently, a new approach to the analysis of three-dimensional problems has been developed by Lazzarin and Zappalorto [7] who assume the Kane and Mindlin [4] hypothesis for displacement components as given by:

$$u_x = u(x,y) \quad u_y = v(x,y) \quad u_z = bz \times w(x,y) \tag{1}$$

where b is a constant value. As a result, the normal strains ε_{xx}, ε_{yy}, ε_{zz} as well as γ_{xy} are independent of z, whereas, the other two shear components, i.e, γ_{yz} and γ_{xz}, depend on z. We have:

$$
\begin{aligned}
&\varepsilon_{xx} = \frac{\partial u}{\partial x}; \ \varepsilon_{yy} = \frac{\partial v}{\partial y}; \ \varepsilon_{zz} = bw \\
&\gamma_{xy} = \frac{\partial u}{\partial y} + \frac{\partial v}{\partial x}; \ \gamma_{yz} = bz\frac{\partial w}{\partial y}; \ \gamma_{xz} = bz\frac{\partial w}{\partial x}
\end{aligned}
\tag{2}
$$

By invoking the stress-strain relationship, also the stress components σ_{xx}, σ_{yy}, τ_{xy} and σ_{zz} are independent of z, whereas the out-of-plane shear stress components depend on z, according to the following equations:

$$\sigma_{zz} = \frac{E}{(1-2v)(1+v)}[(1-v)\varepsilon_{zz} + v(\varepsilon_{xx} + \varepsilon_{yy})]$$
$$= \frac{E}{(1-2v)(1+v)}[(1-v)bw + v(\frac{\partial u}{\partial x} + \frac{\partial v}{\partial y})] \qquad (3)$$
$$\tau_{yz} = G\gamma_{yz} = Gbz\frac{\partial w}{\partial y}; \quad \tau_{xz} = G\gamma_{xz} = Gbz\frac{\partial w}{\partial x}$$

By imposing the equilibrium in z direction, one obtains:

$$\nabla^2 w = 0 \qquad (4)$$

where ∇^2 denotes the two-dimensional Laplacian operator.

Similarly, considering the equilibrium in x and y directions, applying differentiation and by using the Schwarz theorem for partial derivatives, the following equation can be obtained:

$$\frac{\partial^2 \sigma_{xx}}{\partial x^2} + \frac{\partial^2 \sigma_{yy}}{\partial y^2} + 2\frac{\partial^2 \tau_{xy}}{\partial y \partial x} = 0 \qquad (5)$$

Due to the fact that the stress components σ_{xx}, σ_{yy}, τ_{xy} and σ_{zz} do not depend on z, Eq. (5) is automatically satisfied by the classic Airy stress function ϕ (x,y):

$$\sigma_{xx} = \frac{\partial^2 \phi}{\partial y^2}; \quad \sigma_{yy} = \frac{\partial^2 \phi}{\partial x^2}; \quad \tau_{xy} = -\frac{\partial^2 \phi}{\partial x \partial y} \qquad (6)$$

Now, by using the generalized Hooke's law for stresses and strains and satisfying the in-plane compatibility equations, one obtains [7]:

$$\nabla^4 \phi = v\nabla^2 \sigma_{zz} = 0 \qquad (7)$$

Here the equality to zero is guaranteed by the third of Beltrami-Mitchell's equations, considering the fact that the stress components σ_{xx}, σ_{yy}, τ_{xy} and σ_{zz} do not depend on z.

Subsequently, any three-dimensional notch problem can be converted into a bi-harmonic problem (typical of plane stress or plane strain conditions) and a harmonic problem (typical of out-of-plane shear case), provided that the displacement law according to Kane and Mindlin's Eq. (1) is satisfied. The final equation system is:

$$\begin{cases} \nabla^4 \phi = 0 \\ \nabla^2 w = 0 \end{cases}$$

(8a-b)

where ϕ and w are defined implicitly according to Eqs (3) and (6), respectively. Note that, both equations (8a-b) must be satisfied simultaneously.

It is worth mentioning that the solution given in [7] is not valid on the free surfaces of the plate, due to the presence of some edge effects, such as corner point singularities [8-11] that might play an important role on stress intensities.

III. EXAMPLES AND APPLICATIONS

In this section, a three dimensional model with an inclined diamond hole in a finite thickness plate under different loading conditions is considered. In order to demonstrate the degree of accuracy of the theory developed in [7], the analytical frame of the theory is explained first and then verified by the 3D finite element (FE) models under tension and torsion loading conditions respectively.

The spatial diamond hole problem

An inclined diamond hole in a plate with finite thickness under tension and torsion is considered. The inclination angle is 22.5º, as shown in Fig. 1. Such an inclination induces local in-plane mixed mode stresses (mode I + mode II), which can be solved by using Williams' plane solution for re-entrant corners, according to Eq. (8a), where the function ϕ is as follows [7, 12]:

$$\phi = r^{\lambda_1+1}[A_s \cos((\lambda_1+1)\theta) + B_s \cos((1-\lambda_1)\theta)] +$$
$$r^{\lambda_2+1}[A_a \sin((\lambda_2+1)\theta) + B_a \sin((1-\lambda_2)\theta)]$$

(9)
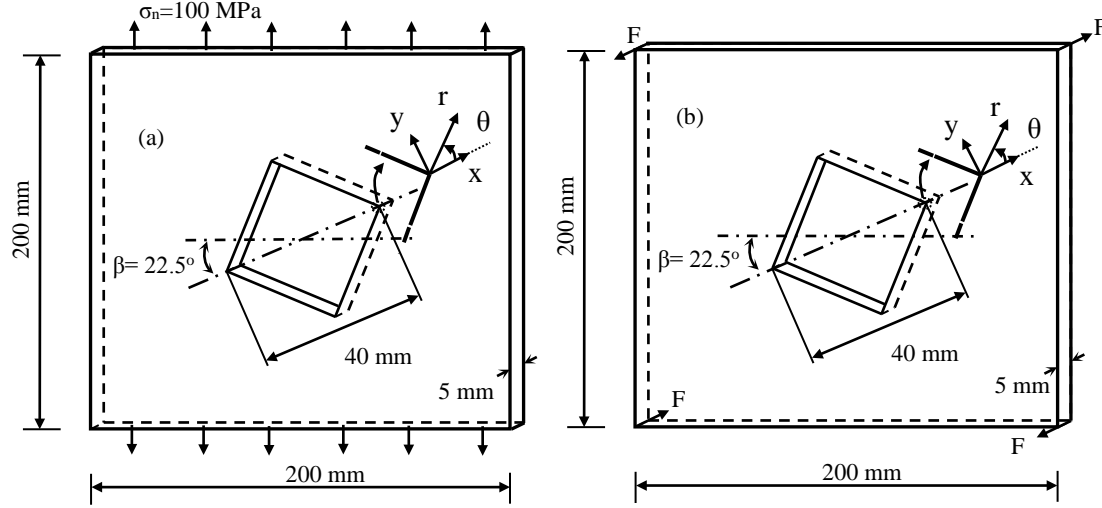
Fig. 1: Finite thickness plate weakened by inclined diamond hole under tension (a) and torsion (b).

Having a fixed value of the through the thickness coordinate, z, and using the polar coordinate system at the notch tip, the in-plane stresses vary according to Williams' singularity degrees $1-\lambda_1$ and $1-\lambda_2$ for mode I and II, respectively.

In the presence of a sharp V-shaped notch, the stress distributions of symmetric type with respect to the angle bisector (mode I) are [12-14]:

$$\begin{Bmatrix} \sigma_{\theta\theta} \\ \sigma_{rr} \\ \tau_{r\theta} \end{Bmatrix} = \frac{1}{\sqrt{2\pi}} \frac{r^{\lambda_1-1} \cdot K_1}{(1+\lambda_1) + \chi_1(1-\lambda_1)} \times$$
$$\left[\begin{Bmatrix} (1+\lambda_1)\cos(1-\lambda_1)\theta \\ (3-\lambda_1)\cos(1-\lambda_1)\theta \\ (1-\lambda_1)\sin(1-\lambda_1)\theta \end{Bmatrix} + \chi_1(1-\lambda_1) \begin{Bmatrix} \cos(1+\lambda_1)\theta \\ -\cos(1+\lambda_1)\theta \\ \sin(1+\lambda_1)\theta \end{Bmatrix} \right]$$

(10)

The skew-symmetric stress distributions (Mode II) are:

$$
\left\{ \begin{array}{c} \sigma_{\theta\theta} \\ \sigma_{rr} \\ \tau_{r\theta} \end{array} \right\} = \frac{1}{\sqrt{2\pi}} \frac{r^{\lambda_2-1} \cdot K_2}{(1-\lambda_2)+\chi_2(1+\lambda_2)} \times
$$

$$
\left[\left\{ \begin{array}{c} -(1+\lambda_2)\sin(1-\lambda_2)\theta \\ -(3-\lambda_2)\sin(1-\lambda_2)\theta \\ (1-\lambda_2)\cos(1-\lambda_2)\theta \end{array} \right\} + \chi_2(1+\lambda_2) \left\{ \begin{array}{c} -\sin(1+\lambda_2)\theta \\ \sin(1+\lambda_2)\theta \\ \cos(1+\lambda_2)\theta \end{array} \right\} \right]
$$

(11)

Parameters K_1 and K_2 are the notch stress intensity factors (NSIFs) related to Mode I and Mode II stress distributions, respectively, λ_1 and λ_2 are Williams' eigenvalues [12] and, finally, χ_1 and χ_2 are parameters which depend on the opening angle [12-14].

Subsequently, the stress field intensities can be quantified by the corresponding NSIFs [15]:

$$
\left\{ \begin{array}{l} K_1(z) = \lim_{r\to 0} \sqrt{2\pi} r^{1-\lambda_1} \sigma_{\theta\theta}(\theta=0) \\ K_2(z) = \lim_{r\to 0} \sqrt{2\pi} r^{1-\lambda_2} \tau_{r\theta}(\theta=0) \end{array} \right.
$$

(12a-b)

However, due to the nature of three-dimensional problems, in addition to the in-plane stresses, the out-of-plane shear stress components τ_{zr} and $\tau_{z\theta}$ can be obtained by using the following w function [16]:

$$
w = D_s r^{\lambda_{3,s}} \cos(\lambda_{3,s}\theta) + D_a r^{\lambda_{3,a}} \sin(\lambda_{3,a}\theta)
$$

(13)

where $\lambda_{3,s}=2\lambda_{3,a}=\pi/\gamma$, so that only the skew-symmetric part of w contributes to the singular behavior of stress fields [7]. Accordingly, anti-plane mode III shear stresses near the notch tip can be determined as:

$$
\left\{ \begin{array}{l} \tau_{zr} = \dfrac{K_3(z) r^{\lambda_{3,a}-1}}{\sqrt{2\pi}} \sin(\lambda_{3,a}\theta) \\ \tau_{z\theta} = \dfrac{K_3(z) r^{\lambda_{3,a}-1}}{\sqrt{2\pi}} \cos(\lambda_{3,a}\theta) \end{array} \right.
$$

(14a-b)

and

$$K_3(z) = \lim_{r \to 0} \sqrt{2\pi} r^{1-\lambda_{3,a}} \tau_{z\theta}(\theta = 0) \tag{15}$$

where $K_3(z)$ is the mode III NSIF. Eq. (15) can be considered as the extension to the out-of-plane mode of Gross and Mandelson's definitions [15] provided for the in-plane modes, see Eqs (12a-b).

Tension loading

In order to validate the theoretical frame developed in [7], a detailed FE analysis on the model shown in Fig. 2 under tension loading is performed. The normal stress σ_n=100 MPa is applied on the far end of the plate. The ANSYS package is used to perform the finite element analyses (FEA). Material is assumed as isotropic and linear elastic with the Young's modulus E = 206000 MPa and the Poisson's ratio ν = 0.3. The 20-nodes brick element is used. With the aim of obtaining the desired degree of accuracy, a very fine and regular mesh pattern, specially close to the diamond corners is constructed as shown in Fig. 2.
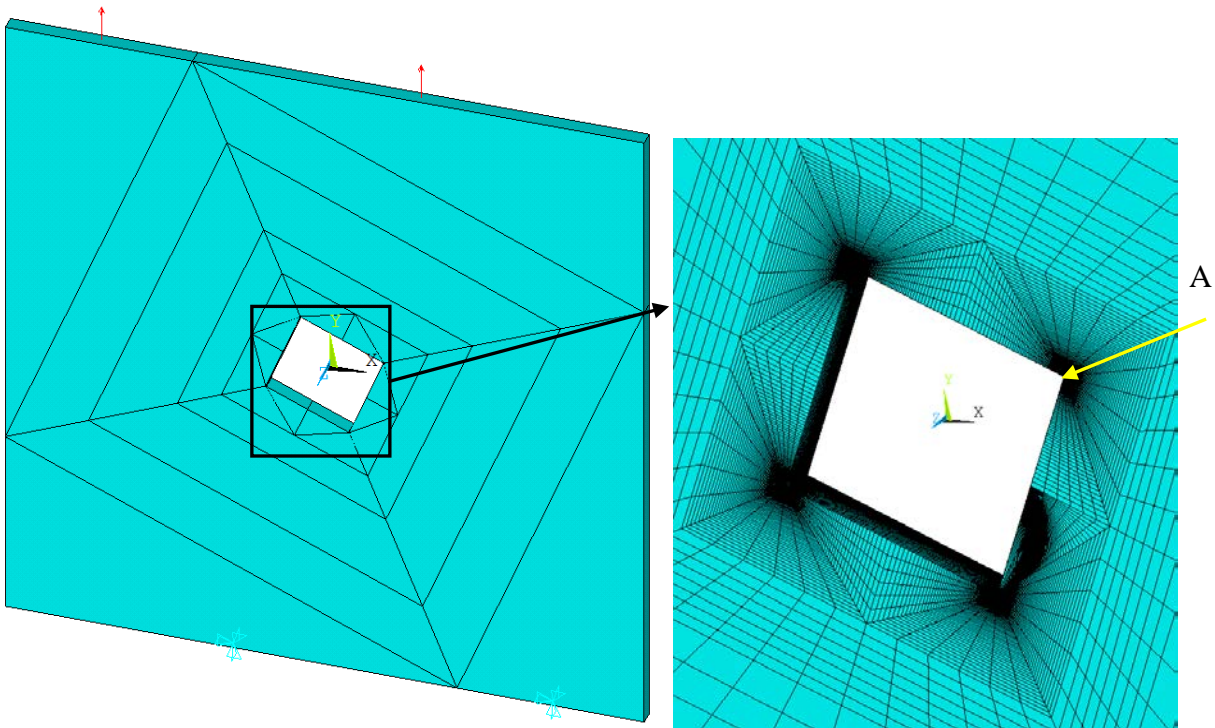
Fig. 2: Mesh pattern used for stress analysis of finite thickness plate weakened by inclined diamond hole under tension.
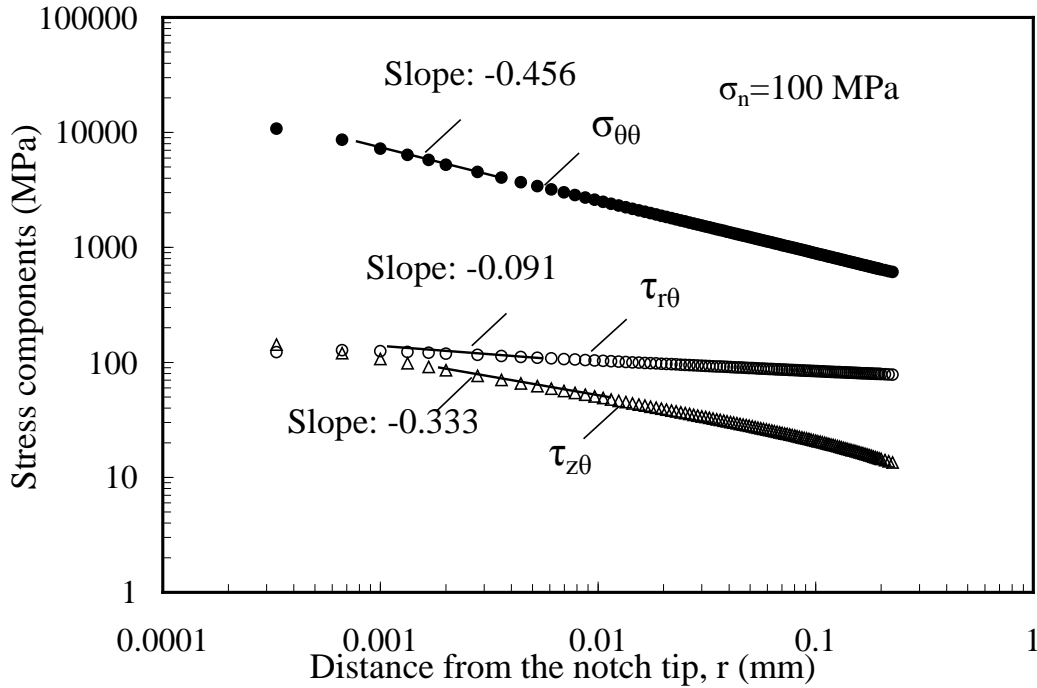
Fig. 3: Stress components $\sigma_{\theta\theta}$, $\tau_{r\theta}$ and $\tau_{z\theta}$ along the notch bisector line of an inclined diamond hole in a thick plate under tension. Distance from the free surface z=0.5 mm.

The variation of three stress components $\sigma_{\theta\theta}$, $\tau_{r\theta}$ and $\tau_{z\theta}$ along the notch bisector line and close to the notch tip (corner A in Fig. 2) are shown in Fig. 3. All the stresses are calculated on the plane 0.5 mm far from the free surface of the plate.   It can be seen from Fig. 3 that, as expected, the value of $\sigma_{\theta\theta}$ is much higher than the other two stresses, showing the dominance of mode I fracture for the plate under tension.

Fig. 4 shows the through the thickness variation of the NSIFs K_1, K_2 and K_3 in a distance from mid-plane to the free surface of the plate. The notch tip at corner A is selected again for the NSIFs evaluations.
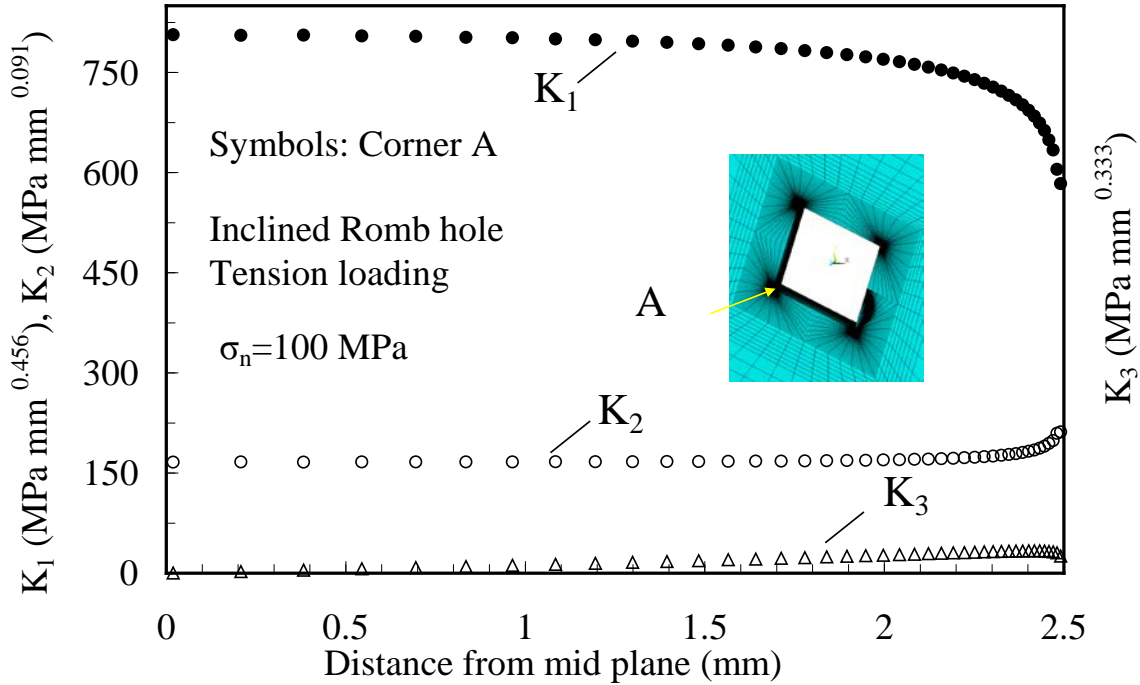
Fig. 4: Plots of NSIFs along the thickness of the plate with inclined diamond hole under tension.

From Fig. 4, it can be observed that the value of K_3 is relatively lower than the other two NSIFs. The intensity of K_3 varies from case to case. Here, the main aim was to document the existence of the out-of-plane mode, which can be detected only by means of 3D models. This specific mode is expected to increase as the plate thickness increases [11]. It is evident, the linear change of K_3 through the thickness of the plate up to the maximum value, which is located in the vicinity of the free surface. In parallel, the variability of in-plane NSIFs (K_1 and K_2) is shown: K_2 is constant on the major part of the plate thickness, whereas the variation of K_1 is more distributed through the thickness of the plate.

Torsion loading

The plate with inclined diamond hole with the same material properties and element type as of the tension loading is also investigated under torsion loading conditions.
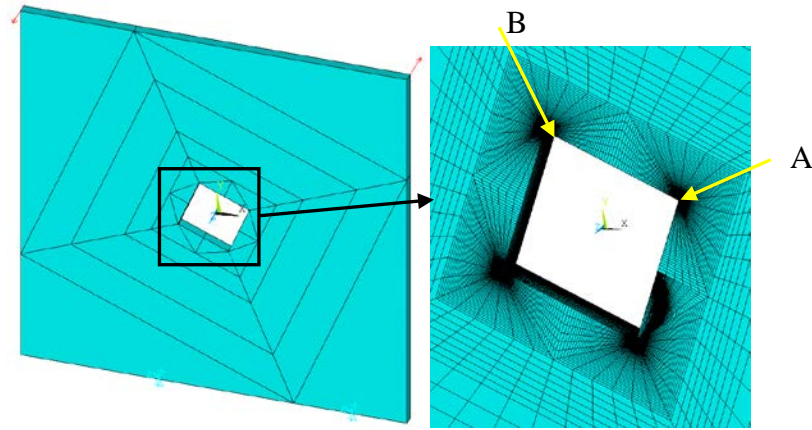
Fig. 5: The mesh pattern used for analysis of finite thickness plate weakened by inclined diamond hole under torsion.

The applied shear stress is set according to the expression $\tau_n=3F/t^2$, valid for the narrow rectangular section, which induces a nominal shear stress $\tau_n=100$ MPa on the gross section of the plate (Fig. 5).

Similar to the tension loading condition, the variation of three stress components $\sigma_{\theta\theta}$, $\tau_{r\theta}$ and $\tau_{z\theta}$ along the notch bisector line and close to the notch tip (corner A) are shown in Fig. 6. All the stresses are calculated on the plane 0.5 mm far from the free surface of the plate.
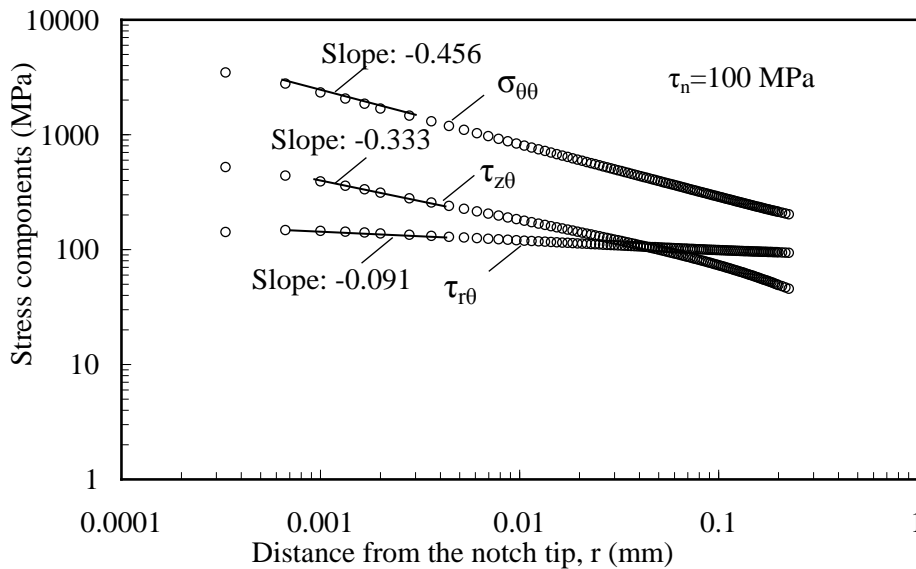
Fig. 6: Stress components $\sigma_{\theta\theta}$, $\tau_{r\theta}$ and $\tau_{z\theta}$ along the notch bisector line of an inclined diamond hole in a plate under torsion. Distance from the free surface z=0.5 mm.

It is worth noting from Fig. 6 that $\sigma_{\theta\theta}$ (corresponding to induced mode I) is again much higher than the $\tau_{z\theta}$ corresponding to the applied mode III.

Due to the twisting loading, the stresses at the two corners A and B (Fig. 5) are different. Hence, both corners are considered for NSIFs evaluation through the thickness of the plate, as it is shown in Fig. 7.
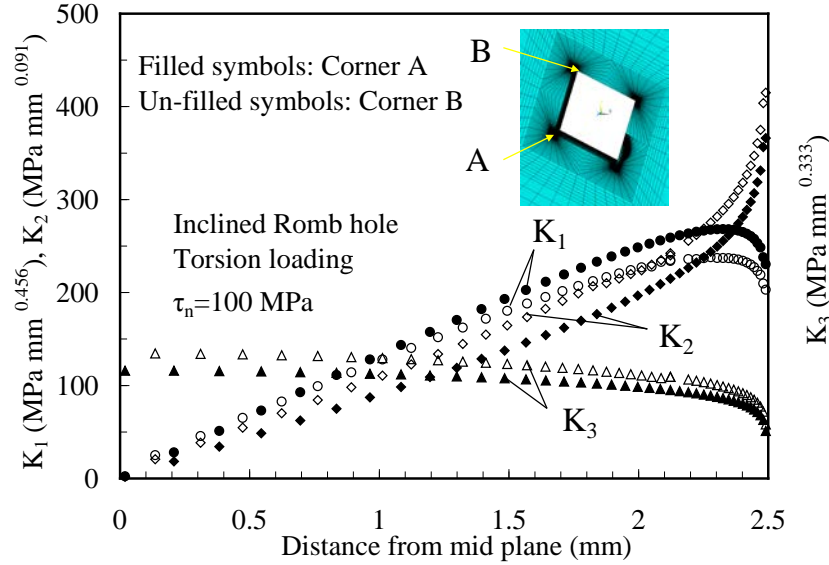
Fig. 7: Plots of NSIFs along the thickness of the plate with inclined diamond hole under torsion.

Fig. 7 shows the linear variation of K_1 and K_2 through the thickness of the plate and a parabolic trend of K_3. It was shown in [17] that the equation system (8a-b) is valid even when the displacement field is no longer according to the Kane-Mindlin hypothesis, i.e. Eq. (1), but is also when given in the following more general form:

$$u_x = f'(z) \times u(x,y) \quad u_y = f'(z) \times v(x,y)$$
$$u_z = f(z) \times w(x,y) \tag{16}$$

where $f(z)$ can be regarded as a generic polynomial function of order n:

$$f(z) = a_0 + a_1 z + a_2 z^2 + ... + a_n z^n \tag{17}$$

185

It is noteworthy that Eq. (17), similar to the equation proposed in [18] for the crack case, automatically satisfies all the six compatibility equations [17].

In addition, apart from very near surface location (i.e. z>2.25 from mid-plane), where some edge effects such as corner point singularity may exist [8-11], on a plane at z=0.5 mm from the free surface some differences between the NSIFs values at the two corners A and B can be observed. Considering the corner A, the mode I seems to be the dominant mode of fracture and K_2 has a relatively lower value (about 25% lower than K_1) at z=0.5 mm from the free surface. On the other hand, for corner B, both K_1 and K_2 are dominant and have an equal value at the same distance from the free surface. For both corners, mode III has a negligible effect with a relatively higher value at corner B.

Finally, in-plane stress components ($\sigma_{\theta\theta}$, σ_{rr} and $\tau_{r\theta}$) as well as anti-plane shear stresses (τ_{zr} and $\tau_{z\theta}$) obtained from FEA on a circular path with radius r=0.002 mm centered at the notch tip (corner A), compared with the theoretical prediction according to Eqs (10-11) and (14), are shown in Figs 8 and 9, respectively.
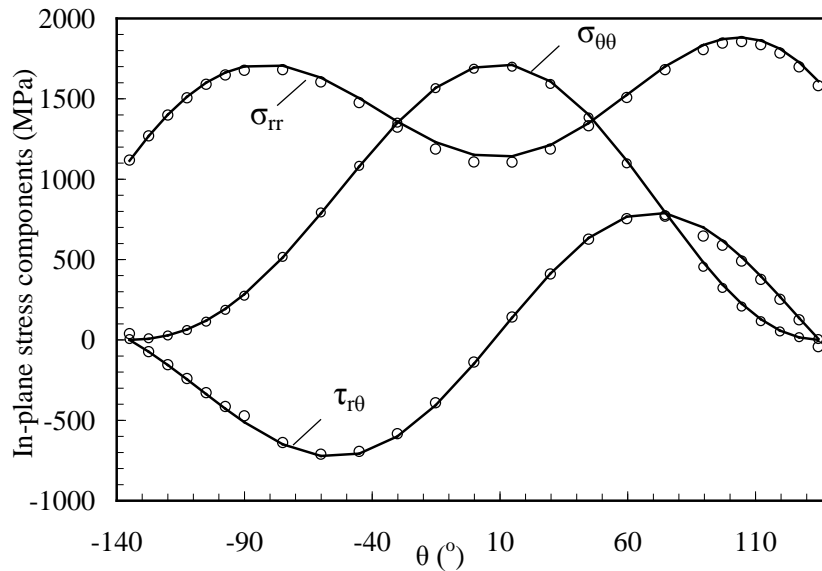
Fig. 8: In-plane stress components ($\sigma_{\theta\theta}$, σ_{rr} and $\tau_{r\theta}$) obtained on a circular path with radius r=0.002 mm centered at the notch tip (corner A) and comparison with the theoretical predictions [7]. Inclined diamond hole in a plate under torsion (τ_n=100 MPa). Distance from the free surface z=0.5 mm.
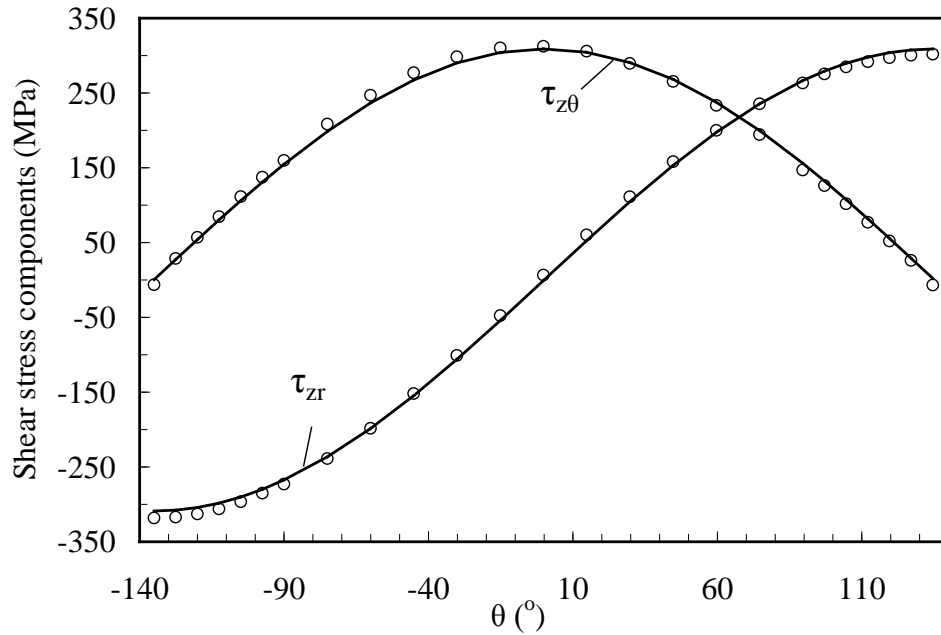
Fig. 9: Anti-plane shear stresses (τ_{zr} and $\tau_{z\theta}$) obtained on a circular path with radius r=0.002 mm centered at the notch tip (corner A) and comparison with the theoretical predictions [7]. Inclined diamond hole in a plate under torsion (τ_n=100 MPa). Distance from the free surface z=0.5 mm.

As it can be seen from Figs 8 and 9 a very sound agreement is observed between the numerical results and analytical predictions proposed in [7]. A good agreement with the theoretical results was also found for the tension loading conditions.

IV. CONCLUSIONS

In this study an attempt is made to examine the proposed theory in [7] by investigating the stress fields in the vicinity of the sharp corners of a diamond hole in a plate with finite thickness under tension and twisting loading conditions. The FE results have confirmed the presence of coupled modes at the V-notch tip, showing a good agreement with the in-plane and out-of-plane theoretical stress distributions.

REFERENCES

[1] T. Nakamura and D. M. Parks, "Antisymmetrical 3-D stress field near the crack front of a thin elastic plate". *International Journal of Solids and Structures*, Vol. 25, pp. 1411-1426, 1989.

[2] Z. H. Jin and R. C. Batra, "A crack at the interface between a Kane-Mindlin plate and a rigid substrate". Eng. Fract. Mech. , Vol. 57, pp. 343-354, 1997.

[3] M. Heyder, K. Kolk, and G. Kuhn, "Numerical and experimental investigations of the influence of corner singularities on 3D fatigue crack propagation". Engineering Fracture Mechanics, Vol. 72, pp. 2095-2105, 2005.

[4] T. R. Kane and R. D. Mindlin, "High-frequency extensional vibrations of plates". Journal of Applied Mechanics, Trans. ASME, pp. 277-283, 1956.

[5] A. Kotousov, "On stress singularities at angular corners of plates of arbitrary thickness under tension". International Journal of Fracture, Vol. 132, pp. L29-L36, 2005.

[6] A. Kotousov, "Fracture in plates of finite thickness". International Journal of Solids and Structures, Vol. 44, pp. 8259-8273, 2007.

[7] P. Lazzarin and M. Zappalorto, "A three-dimensional stress field solution for pointed and sharply radiused V-notches in plates of finite thickness". Fatigue and Fracture of Engineering Materials and Structures, Vol. 35, pp. 1105-1119, 2012.

[8] L. P. Pook, "A finite element analysis of cracked square plates and bars under antiplane loading". Fatigue & Fracture of Engineering Materials & Structures, Vol. 26, pp. 533-541, 2003.

[9] L. P. Pook, "Finite element analysis of corner point displacements and stress intensity factors for narrow notches in square sheets and plates". Fatigue & Fracture of Engineering Materials & Structures, Vol. 23, pp. 979-992, 2000.

[10] L. P. Pook, "A note on corner point singularities". International Journal of Fatigue, Vol. 53, pp. 3-8, 1992.

[11] F. Berto, P. Lazzarin, A. Kotousov, and S. Harding, "Out-of-plane singular stress fields in V-notched plates and welded lap joints induced by in-plane shear load conditions". Fatigue and Fracture of Engineering Materials and Structures, Vol. 34, pp. 291-304, 2011.

[12] M. L. Williams, "Stress singularities resulting from various boundary conditions in angular corners of plates in extension". J. Appl. Mech., Vol. 19, pp. 526-528, 1952.

[13] P. Lazzarin and R. Tovo, "A unified approach to the evaluation of linear elastic stress fields in the neighborhood of cracks and notches". International Journal of Fracture, Vol. 78, pp. 3-19, 1996.

[14] P. Lazzarin and R. Tovo, "A notch intensity factor approach to the stress analysis of welds". Fatigue and Fracture of Engineering Materials and Structures, Vol. 21, pp. 1089-1103, 1998.

[15] R. Gross and A. Mendelson, "Plane elastostatic analysis of V-notched plates". Int J Fract Mech, Vol. 8, pp. 267-276, 1972.

[16] A. Seweryn and K. Molski, "Elastic stress singularities and corresponding generalized stress intensity factors for angular corners under various boundary conditions". Engineering Fracture Mechanics, Vol. 55, pp. 529-556, 1996.

[17] M. Zappalorto and P. Lazzarin, "Three-dimensional elastic stress fields ahead of notches in thick plates under various loading conditions". Eng. Frac. Mechanics, In Press., 2013.

[18] R. J. Hartranft and G. C. Sih, "An approximate three-dimensional theory of plates with application to crack problems". International Journal of Engineering Science, Vol. 8, pp. 711-729, 1970.

Paper VIII

Three-dimensional finite element analysis of single-lap joints: effect of adhesive thickness and Poisson's ratio

Abstract. Three-dimensional (3D) elastic stress distributions in the vicinity of overlap corners of single-lap joints are investigated. A detailed 3D finite element (FE) model is carried out to study the intensity of the in-plane and out-of-plane stress distributions along the plate width direction. The effects of adhesive thickness and Poisson's ratio are also studied. The FE results show the presence of coupled modes at the overlap corners of the joint. In particular, sharp increment of out-of-plane fracture mode very near the lateral free surface of the joint is worth noting.

Introduction

Adhesive joints have been intensively studied over the last years and there are numerous studies about this topic in the literature. A review of major analytical models for adhesively bonded joints is presented in [1, 2]. The literature review shows that almost all analytical models for adhesively bonded lap joints are two-dimensional.

As is well known, due to the different elastic properties of the connected materials, adhesively bonded joints present zones of high stress concentration at the overlap corners. For bi-material problems, stress singularity arise, even in the absence of any geometrical discontinuity [3]. Based on the stress function approach, the evaluation of the in-plane singular stress fields in bonded joints of different materials was presented, among others, in [4]. The proposed analytical formulation allowed an accurate characterization of the two-dimensional (2D) local stress field even in the case of joints with comparable elastic properties.

In this study, three-dimensional (3D) elastic stress distributions in the vicinity of overlap corners of single-lap joints are investigated. A detailed 3D finite element (FE) model is carried out mainly with the aim to show an out-of-plane shear stress distribution in the highly stressed region. The effects of the adhesive thickness and the Poisson's ratio variations are studied in detail.

Finite element modeling

A 3D model of the single-lap joint is developed using ANSYS package. The dimensions and material properties of the single-lap joint are given in Fig. 1. Due to the symmetry of the joint along the width, only half of the model is modeled. Different values of the adhesive thickness (h_{adh}=0.1, 0.25 and 0.5 mm) and the Poisson's ratio (ν_{adh}=0.1, 0.35 and 0.499) are examined. The materials considered for the analysis are represented by a steel for the adherend (E=206 GPa and ν=0.30) and by an epoxy resin for the adhesive (E_{adh}=3500 MPa and ν_{adh}=0.1, 0.35 and 0.499). A perfect adhesion is assumed at the interfaces between adhesive layer and adherents. The model is meshed with 4-node hexahedral elements (SOLID185) and a very fine mesh (with minimum mesh size of 4×10^{-4} mm) is used to precisely capture the stress field at the very close distance from the overlap corners, corners A and B in Fig. 1 (c). The comparison between the stress fields at the two interfaces, as well as at the middle of the adhesive, shows higher stresses (both shear stresses and peel stresses) at the lower interface, *i.e.* at the corner A. Hence, the reported results here are only for that corner, which is the most critical interface corner. Finally, due to the very small size of the zone governed by the leading order linear elastic singularities, a very small distance (0.005 mm far from the singular point) will be used here to plot the relevant stress intensity factors.

(a) (b) (c)
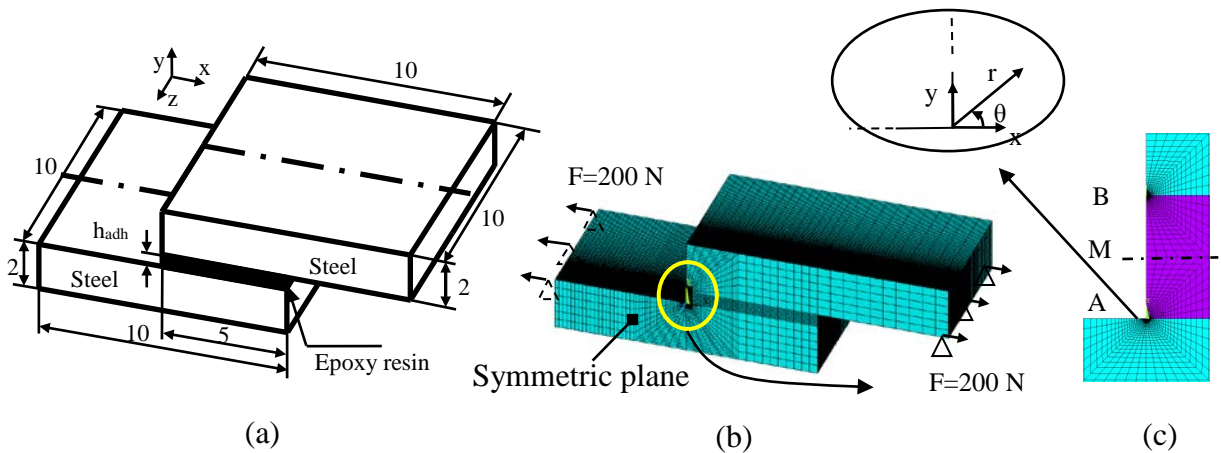
Fig. 1 Geometrical dimensions (in mm) and materials of a single-lap joint (a); finite element model and boundary conditions (b); overlap corners and mid-plane path used for stress evaluation.

Results and discussions

Stress analysis in the adhesive

In the case of an isotropic elastic material weakened by a sharp V-notch, the notch stress intensity factors (NSIFs) are usually evaluated along the notch bisector line using Gross and Mendelson's definitions [5]. In this study, with the main aim of studying the coupled mode fracture due to the 3D effect, the *apparent* NSIFs are evaluated at the interface between the adhesive and adherent. In addition, the stress singularity exponents ξ_i are different from the traditional ones, $1-\lambda_i$, proposed by Williams for isotropic materials [6], due to the combined effect of geometric discontinuity and the elastic properties of the faces materials. The differences in terms of the in-plane stress singularity degrees are widely discussed in the literature, see Ref. [4] and references reported therein.

The stress variations in terms of $\sigma_{\theta\theta}$, $\tau_{r\theta}$ and $\tau_{z\theta}$ at lower interface of a single-lap joint with the adhesive thickness $h_{adh}=0.1$ mm and the Poisson's ratio $\nu_{adh}=0.35$ are shown in Fig. 2 (a). Subsequently, the stress intensities can be quantified by the relevant in-plane *apparent* notch stress intensity factors, A-NSIFs, where K_1^{app}, K_2^{app} in Eq. (1a-b), and K_3^{app} in Eq.(2), can be seen as simple extensions of Gross and Mendelson's definitions.

With reference to isotropic materials, an analytical frame dealing with the combined presence of in-plane and out-of-plane stress singularities is reported in [7] clarifying why Mode II and Mode III cannot exist in isolation. The main aim of the present contribution is to document the presence of an out-of-plane mode also for the geometry shown in Fig.1.

The three A-NSIFs are plotted in Fig. 2(b). Furthermore, in order to better document the variations of the A-NSIFs in the vicinity of the lateral free surface of the lap-joint, a distance of 0.5 mm from the free surface is selected and the results are depicted in Fig. 2(c).

$$\begin{cases} K_1^{app}(z) = \lim_{r \to 0} \sqrt{2\pi} r^{\xi_1} \sigma_{\theta\theta} & \text{(at the interface, } \theta=0 \text{ in Fig. 1.c)} \\ K_2^{app}(z) = \lim_{r \to 0} \sqrt{2\pi} r^{\xi_2} \tau_{r\theta} \end{cases} \tag{1a-b}$$

$$K_3^{app}(z) = \lim_{r \to 0} \sqrt{2\pi} r^{\xi_3} \tau_{z\theta} \qquad \text{(at the interface, } \theta=0) \tag{2}$$

(a)

(b)

(c)
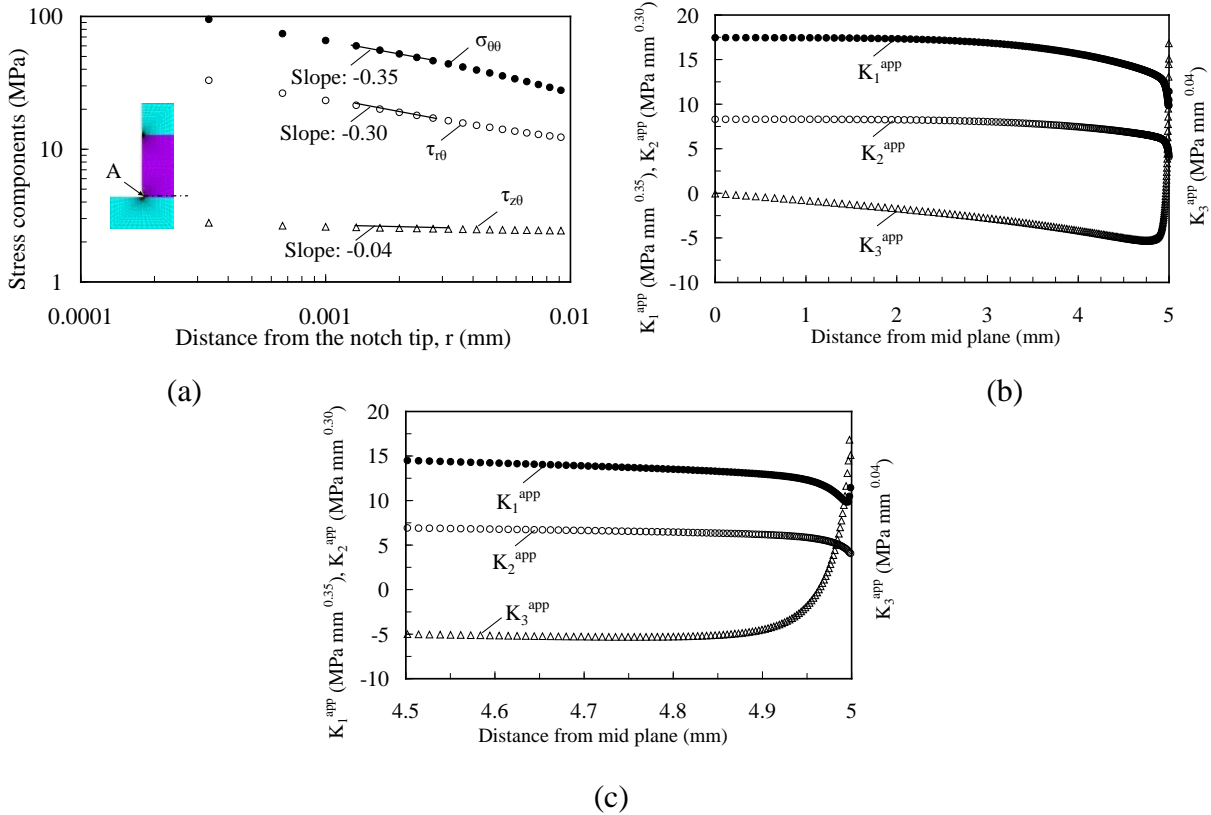
Fig. 2 Stress components along the adhesion line, as a function of the distance from point A, at the distance z=0.5 mm from the lateral free surface of the joint (a); plots of the apparent NSIFs along the width of the joint (b) and in the vicinity of the lateral surface, $4.5 \le z \le 5.0$ mm, (c).

As it can be seen from Fig.2 (a), despite a very low value of singularity index of $\tau_{z\theta}$ (ξ_3=0.04), all the three stress components $\sigma_{\theta\theta}$, $\tau_{r\theta}$ and $\tau_{z\theta}$ are singular, being the peel stress the maximum one. The singularity indexes of shear and peel stresses are almost the same ($\xi_1 \approx \xi_2$ =0.30). The corresponding stress distributions at corner A, plotted along the width of the joint in Fig. 2(a), demonstrate that the hoop stress component $\sigma_{\theta\theta}$ is dominant in a large part of the joint width. However, in a very limited zone close to the surface (about 0.05 mm from it), an increase of mode III shear stress components is evident. On the surface, some edge effects such as corner point singularities may exist [8-10]. A very fine 3D mesh has been used in the vicinity of overlap corners; nevertheless, the equilibrium requirement for K_3^{app}, which should be zero at the lateral free surface, is only partially satisfied. However, the out-of-plane mode K_3^{app} is found to be strongly reduced after reaching to its maximum value.

Effect of adhesive thickness

The effect of adhesive thickness (h_{adh}) on the apparent mode I and mode III NSIFs is shown in Fig. 3(a), that for mode II in Fig. 3(b).

(a) (b)
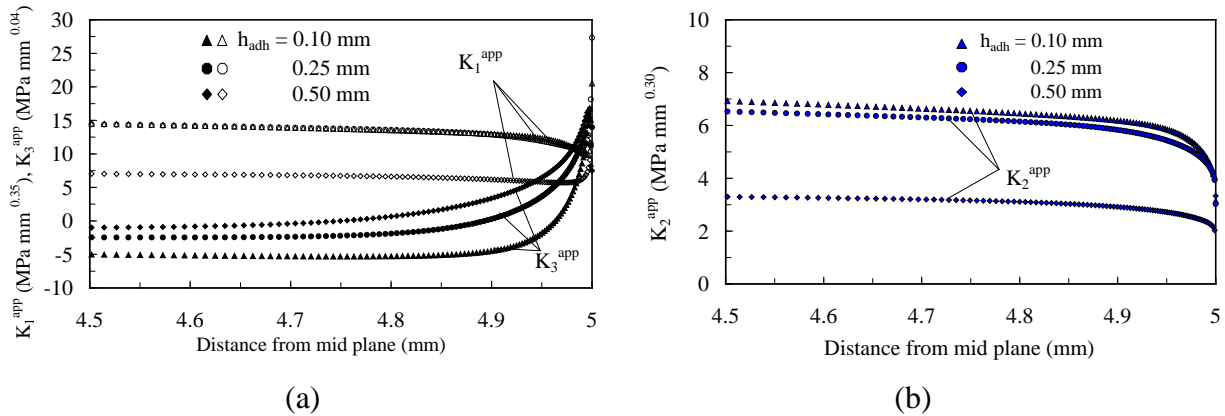
Fig. 3 Plots of the A-NSIFs along the width of the joint, at the lower interface, for different adhesive thicknesses; mode I and mode III (a); mode II (b).

According to Fig. 3(a-b), as the thickness of adhesive increases, K_1^{app} and K_2^{app} decrease whereas K_3^{app} increases, in particular, in the close vicinity of the surface. Furthermore, a large variation of K_2^{app} is worth noting as a function of the adhesive thickness, whereas limited is the variation along the major part of adhesive width. However, the in-plane stress intensities increase with increasing the thickness of the adhesive. This is why the joints with thicker adhesive are relatively weaker.

Effect of adhesive Poisson's ratio

The effect due to the Poisson's ratio of the adhesive (ν_{adh}) on the apparent NSIFs is shown Fig. 4(a) and (b) considering separately modes I-III and mode II. All plots are valid in the zone close to the lateral free surface of the joint, 4.5 mm $\leq$ z $\leq$ 5.0 mm.

(a)   (b)
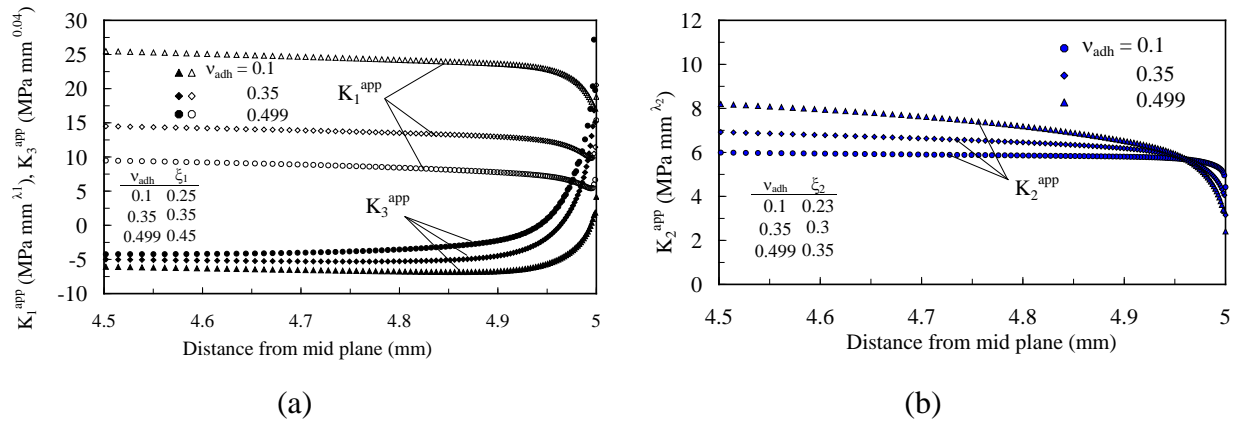
Fig. 4 Plots of the A-NSIFs along the width of the joint, at the lower interface, for different Poisson's ratio of the adhesive; mode I and mode III (a); mode II(b).

From Fig. 4(a-b) it is evident that K_2^{app} and K_3^{app} increase as the Poisson's ratio of the adhesive increases (for K_2^{app} this holds true for a very large zone of the adhesive width, $0 \leq z \leq 4.95$ mm). In the vicinity of the lateral free surface, the variation of K_2^{app} becomes strong and depends on the Poisson's ratio of the adhesive, see Fig. 4(b). Opposite is the trend of K_1^{app}, which decreases as ν_{adh} decreases. Variations of this parameter are, once again, mainly confined close to the lateral free surface of the bonded joints ($z > 4.95$ mm). Finally, one should note that the increase of the singularity degree varies under mode I and mode II, being greater in the former case, where it ranges from 0.25 to 0.45 by changing ν_{adh} from 0.1 to about 0.5. Surprising, the degree of singularity corresponding to mode III is found to be almost constant ($\xi_3 \approx 0.04$) with increasing the adhesive Poisson's ratio.

Conclusions

The 3D FE analysis of single lap-joint with elastic material properties shows the presence of coupled modes at the overlap corners. In particular sharp increment of out-of-plane fracture mode near the lateral free surface of the joint is worth noting.

References

[1] L. F. M. da Silva, P. J. C. das Neves, R. D. Adams, and J. K. Spelt: *International Journal of Adhesion and Adhesives*, Vol. 29 (2009), pp. 319-330.

[2]   L. F. M. da Silva, P. J. C. das Neves, R. D. Adams, and J. K. Spelt: *International Journal of Adhesion and Adhesives*, Vol. 29 (2009), pp. 331-341.

[3]   D. B. Bogy: *International Journal of Solids and Structures*, Vol. 6 (1970), pp. 1287-1313.

[4]   P. Lazzarin, M. Quaresimin, and P. Ferro: *Journal of Strain Analysis for Engineering Design*, Vol. 37 (2002), pp. 385-398.

[5]   R. Gross and A. Mendelson: *International Journal of Fracture Mechanics*, Vol. 8 (1972), pp. 267-276.

[6]   M. L. Williams: *Journal of Applied Mechanics*, Vol. 19 (1952), pp. 526-528.

[7]   P. Lazzarin and M. Zappalorto: *Fatigue and Fracture of Engineering Materials and Structures*, Vol. 35 (2012), pp. 1105-1119.

[8]   F. Berto, P. Lazzarin, A. Kotousov, and S. Harding: *Fatigue and Fracture of Engineering Materials and Structures*, Vol. 34 (2011), pp. 291-304.

[9]   L. P. Pook: *International Journal of Fatigue*, Vol. 53 (1992), pp. 3-8.

[10] L. P. Pook: *Fatigue & Fracture of Engineering Materials & Structures*, Vol. 23 (2000), pp. 979-992.

5. Supplementary investigations: collaboration with industries

Besides the investigations presented in the published articles, two collaborative industry projects with: Omera s.r.l. and Officine Meccaniche Zanetti s.r.l. are successfully implemented. In this chapter, the most promising results are briefly outlined.

Collaboration with OMERA s.r.l: Optimization of bolt-nut connection to reduce the stress concentration

1. Introduction:

1.1 Fatigue failure in a bolt-nut connection

Some important characteristics of fatigue failure can be summarized as follows:

- Fatigue failures account for about 90% of all service failures due to mechanical loads.

- The material subjected to fatigue failures will fail at a stress much lower than its tensile strength.

- Fatigue failures occur without a considerable plastic deformation, that is why they occur without any warning.

- Fatigue surface appears as a smooth region, showing beach marks or origin of fatigue crack.

An example of fatigue failure in a bolt-nut connection is shown in Fig. 1. It should be noted that in all the cases shown in Fig. 1, failure occurs in the first engaging thread between bolt and nut [1].
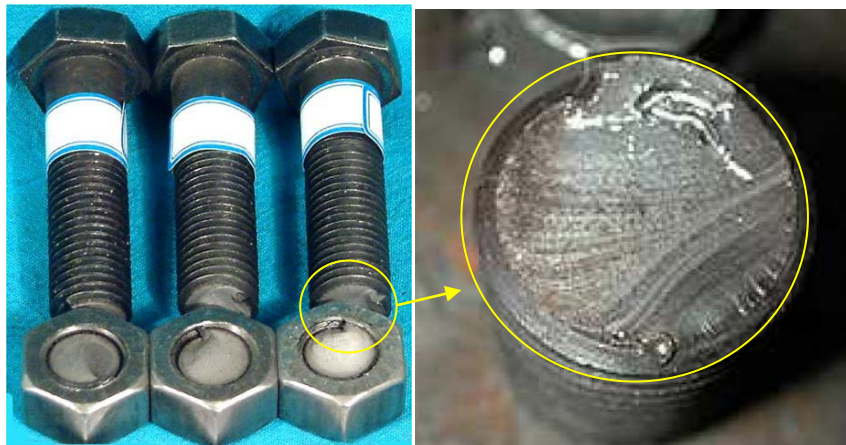
Fig. 1 Fatigue failure in a bolt-nut connection [1].

The factors influencing fatigue properties can be listed as follows:

- *Stress concentration*
- Size effect
- Surface effects
- Combined stresses
- Cumulative fatigue damage and sequence effects
- Metallurgical variables
- Corrosion
- Temperature

Among the above-mentioned factors, stress concentration is one of the crucial factors. Effect of stress concentration on fatigue can be stated according to the following proportionality:

Stress raiser ⇧ ⟶ *Fatigue strength* ⇩ ⇩
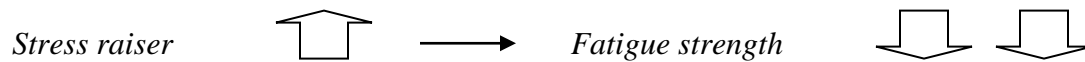
Therefore, the following points for design and fabrication of mechanical components, in particular for bolt-nut connections, need to be considered:

- The stress raiser should be avoided as much as possible from design to fabrication process.
- In the case of inevitable notches in a component (such as *bolts and nuts*), the stress concentration needs to be reduced.
- The effect of stress raiser (or notch) on *fatigue strength* is determined by comparing the *S-N curve* of *notched* and *un-notched* specimens.

2. Modeling of bolt-nut connections

Three bolt-nut geometries as M30, M33 and M245 are considered in this study. The assembly, as well as the boundary conditions of M30-M33 and M245 are shown in Fig. 2 and 3, respectively. Due to the enhanced convergence of numerical calculations, the equivalent displacement of applied load is used. The corresponding applied load values for the three connections are given in Table 1.
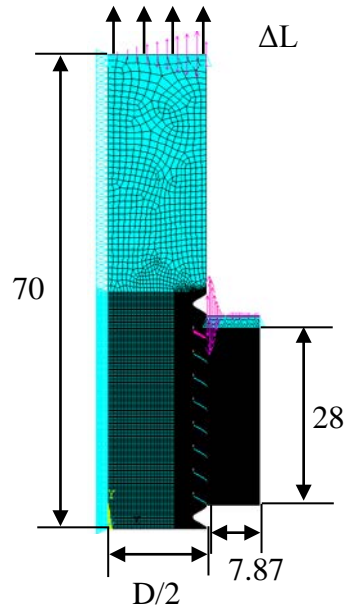
Fig. 2 Bolt-nut connection: geometry and boundary conditions (M30 and M33); dimensions are in mm.
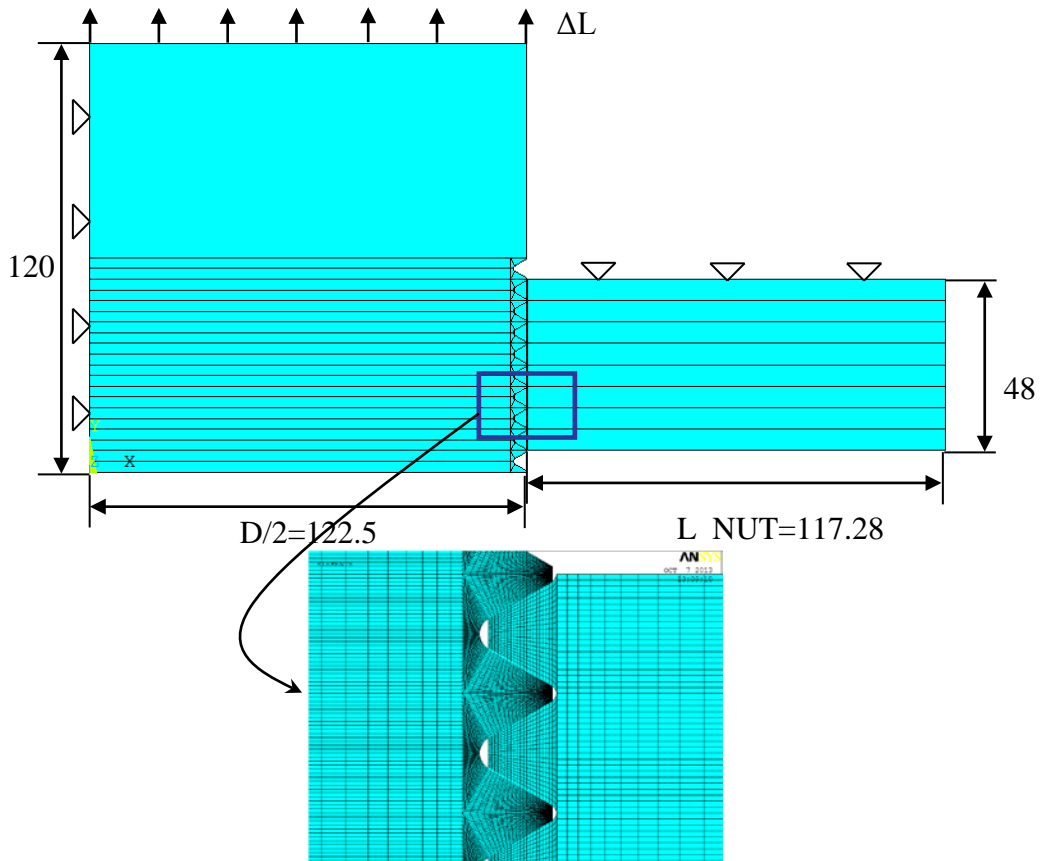
Fig. 3 Bolt-nut connection: geometry, mesh and boundary conditions (M245); dimensions are in mm.

Table 1 The corresponding applied load values for the three bolt-nut connections.

	σ_g (MPa)	ε	L (mm): BOLT	ΔL (mm)
M30	356	0.0018	70	0.126
M33	364	0.0019	70	0.133
M245	120	0.0006198	120	0.074

The geometrical parameters for different connections and the corresponding dimensions are given in Fig. 4 and Table 2 respectively.
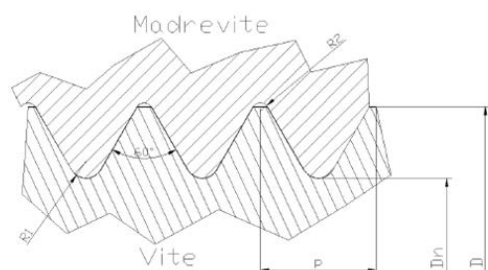
Fig 4.1: rappresentazione schematica della filettatura ISO con riferimenti simbolici
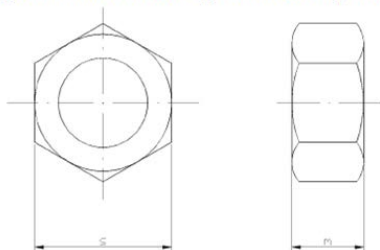
Fig 4.2: rappresentazione schematica di un dado con riferimenti simbolici

Fig. 4: The geometrical parameters for different connections.

Table 2 The geometrical dimensions for the different connections.

		M30	M33	M245	
D	[mm]	30	33	245	Nominal diameter
p	[mm]	3.5	3.5	6	Pitch
D_n	[mm]	25.706	28.706	237.639	Main diameter
R1	[mm]	0.505	0.505	0.866	Fillet radius of bolt
R2	[mm]	0.2528	0.2528	0.433	Fillet radius of nut
s	[mm]	46	50	480	Nut diameter
m	[mm]	24	26	275	Nut width
A_r	[mm^2]	561	694	45000	Net area

2.1Material models

Two material models are used in this study: For the case of M30 and M33, the Ramberg-Osgood elastoplastic model (Fig. 5) and for the case of M245, the experimental test data of C45 Normalized carbon steel (Fig. 6) is employed as an input in the Ansys material model. Ramberg-Osgood elastoplatic model is according to Eq. (1):

$$\varepsilon = \frac{\sigma}{E} + \left(\frac{\sigma}{K'} \right)^{1/n'}$$ (1)

Where: E=190000 MPa, K'=1338 and n'=0.089.
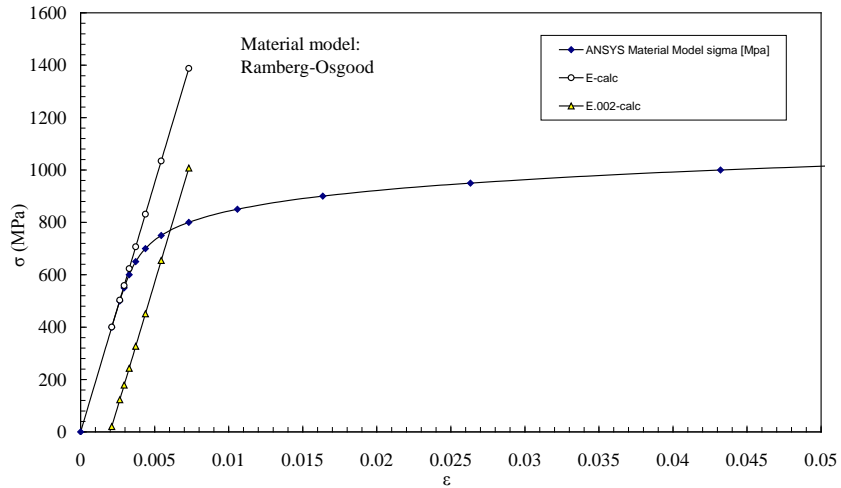
Fig. 5 Ramberg-Osgood elastoplatic model used for M30 and M33
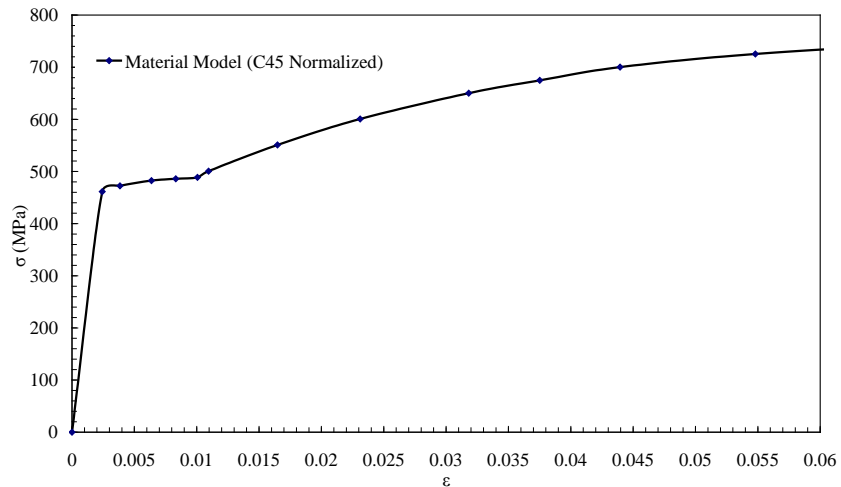
Fig. 6 Material model (C45 Normalized) used for M245

3. Results and discussions

In this section, the Neuber's rule for nonlinear material behavior as an analytical tool for comparison with the numerical results is explained. Afterwards, the numerical results for each case of bolt-nut connection are discussed.

3.1 Neuber's rule

For nonlinear material behavior, where local plastic deformation can occur near the notch root, the elastic stress concentration factors can not be applied. Neuber established a Rule that is useful beyond the elastic limit relating the effective stress and strain concentration factors to the theoretical stress concentration factor. Neuber's rule can be written as follows:

$$K_\sigma K_\varepsilon = K_t^2 \qquad (2)$$

where $K_\sigma = \sigma_{max} / \sigma_{nom}$, $K_\varepsilon = \varepsilon_{max} / \varepsilon_{nom}$ and K_t is theoretical stress concentration factor.

Eq. (2) implies that K_t is the geometric mean of K_σ and K_ε (i.e., $K_t = (K_\sigma K_\varepsilon)^{1/2}$).

By replacing the K_σ and K_ε into Eq. (1) yields:

$$\sigma_{max} \varepsilon_{max} = K_t^2 \sigma_{nom} \varepsilon_{nom} \qquad (3)$$

Usually, K_t and σ_{nom} are known, and ε_{nom} can be calculated from the stress-strain curve for the material, therefore Eq. (3) becomes:

$$\sigma_{max} \varepsilon_{max} = C \qquad (4)$$

In particular, if σ_{nom} is in elastic range, ε_{nom} can be obtained from Hook's law ($\varepsilon_{nom} = \sigma_{nom} / E$):

$$\sigma_{max} \varepsilon_{max} = (K_t \sigma_{nom})^2 / E = C \qquad (5)$$

Where C is a known constant. By solving Eq. (3) simultaneously with the stress-strain relation, the values of σ_{max} and ε_{max} are found, and the effective stress concentration factor (K_t) can then be determined. One should note that, in this procedure the material stress-strain curve must be known.

Neuber's rule was derived specifically for sharp notches in prismatic bars subjected to two-dimensional shear, but the rule has been applied as a useful approximation in other cases, especially those in which plane stress conditions exist. The rule has been shown to give poor results for circumferential grooves in shafts under axial tension [2].

3.2 Stress calculations for the case of M30

Three different friction coefficients (μ=0.0, 0.15 and 0.30) are considered. Due to the ductile material properties of the connection, the von-Mises stress is considered as the maximum stress at the first engaged thread of the bolt. The schematic results for each friction coefficient are shown in Figs. 7-9. The comparison of numerical and analytical results is summarized in Table 3. A very sound agreement can be observed between the numerical and analytical (Neuber's rule) results.
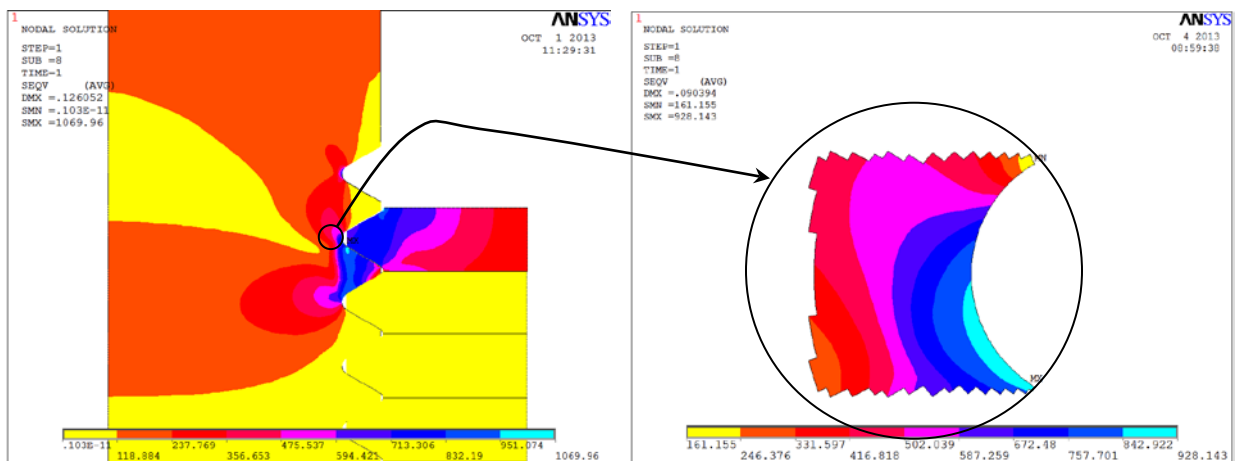
Fig. 7 The von-Mises stress at the first engaged thread of the bolt for the case of μ=0.0.
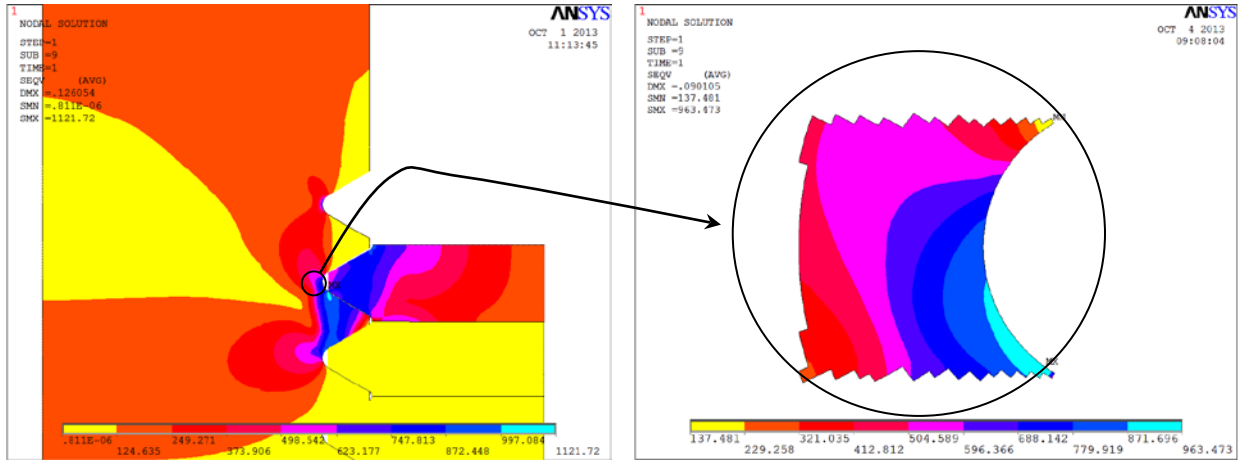
Fig. 8 The von-Mises stress at the first engaged thread of the bolt for the case of μ=0.15.
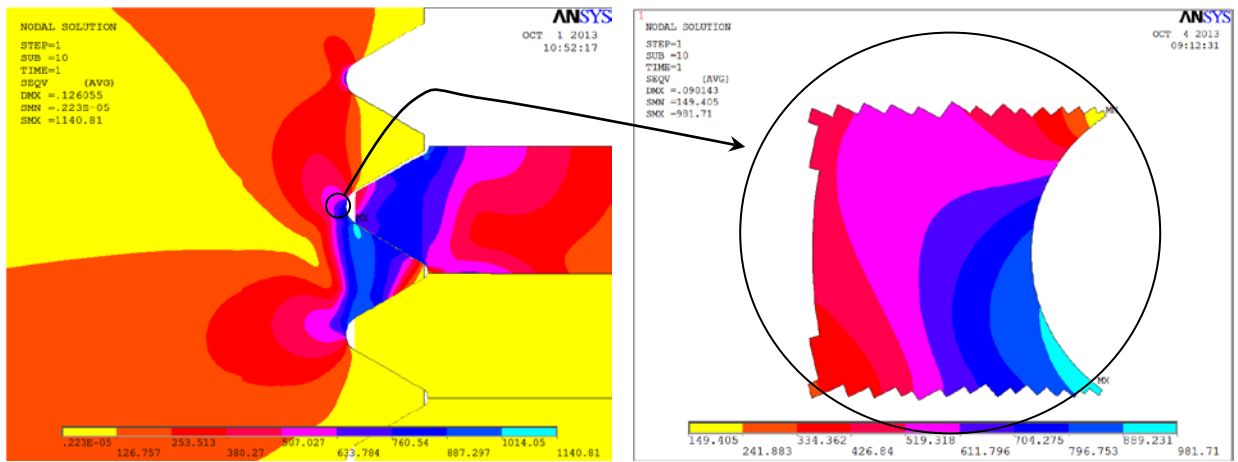
Fig. 9 The von-Mises stress at the first engaged thread of the bolt for the case of μ=0.30.

Table 3 Comparison between numerical and analytical results for different friction coefficients for the case of M30.

M30	μ	$\sigma_{VM\text{-}contact}$ (MPa)	$\sigma_{VM\text{-}Bolt}$ (MPa): FEM	$\sigma_{max\text{-}Bolt}$ (MPa): NEUBER	Δ%
	0.0	1069	928	964	3.84
	0.15	1121	963	964	0.10
	0.30	1140	981	964	-1.73

3.3 Stress calculations for the case of M33

Two different friction coefficients (μ=0.0 and 0.15) are considered. Similar to the case of M30, because of the ductile material properties of the connection, the von-Mises stress is considered as the maximum stress at the first engaged thread of the bolt. The schematic results for each friction coefficient are shown in Figs. 10 and 11. The comparison of numerical and analytical results is summarized in Table 4. The results show a very good agreement.
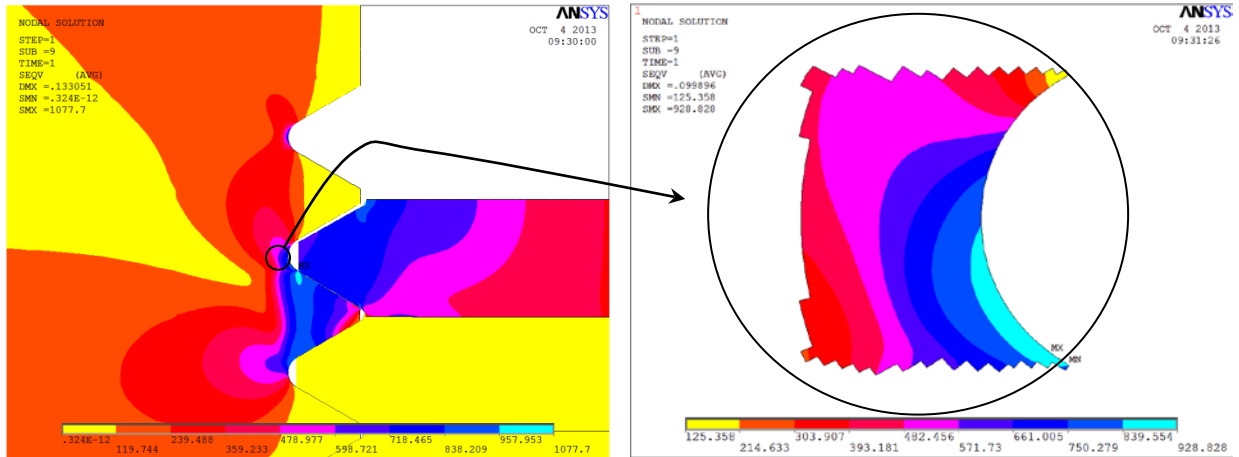
Fig. 10 The von-Mises stress at the first engaged thread of the bolt for the case of μ=0.0.
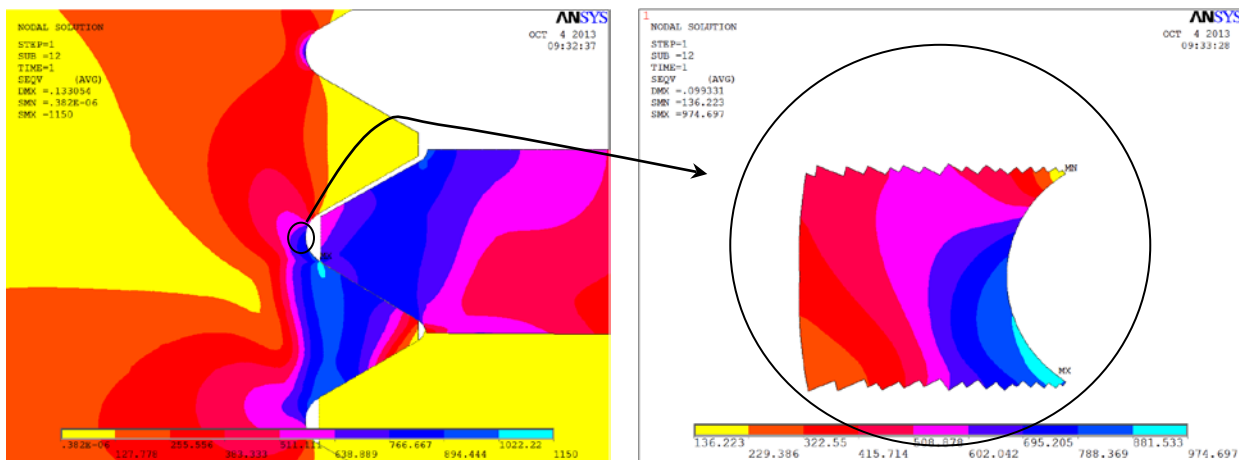
Fig. 11 The von-Mises stress at the first engaged thread of the bolt for the case of μ=0.15.

Table 4 Comparison between numerical and analytical results for different friction coefficients for the case of M33.

M33	μ	$\sigma_{VM\text{-}contact}$ (MPa)	$\sigma_{VM\text{-}Bolt}$ (MPa): FEM	$\sigma_{max\text{-}Bolt}$ (MPa): NEUBER	Δ%
	0.0	1077	928	975	5.1
	0.15	1150	974	975	0.1

The graphical method of obtaining the maximum stress according to the Neuber's rule for both M30 and M33 is depicted in Fig. 12.
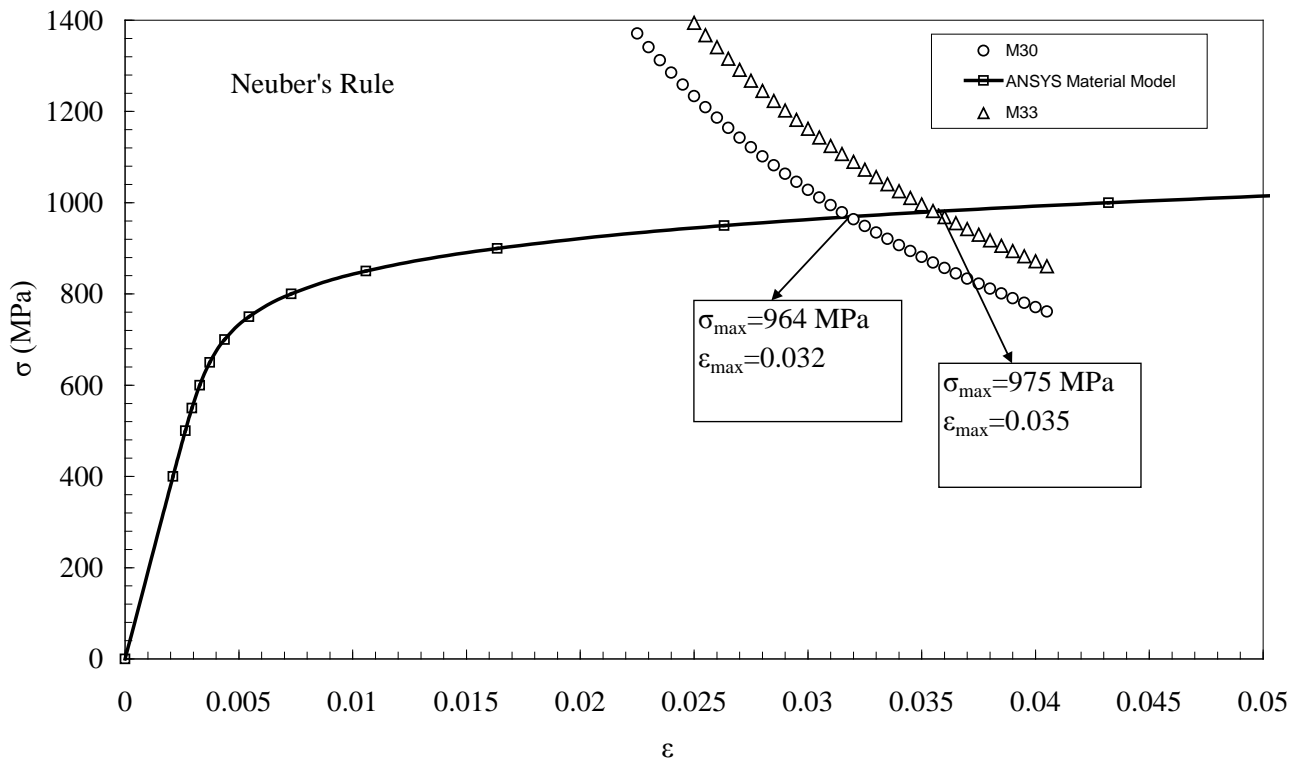
Fig. 12 The graphical method of obtaining the maximum stress according to the Neuber's rule for both M30 and M33.

3.4 Stress calculations for the case of M245

For the case of M245, only one friction coefficient (μ=0.15) is considered. Due to the ductile material properties of the connection, the von-Mises stress is considered as the maximum stress

at the first engaged thread of the bolt. The schematic results in terms of von-Mises stress, total, plastic and elastic strain are demonstrated in Fig. 13.
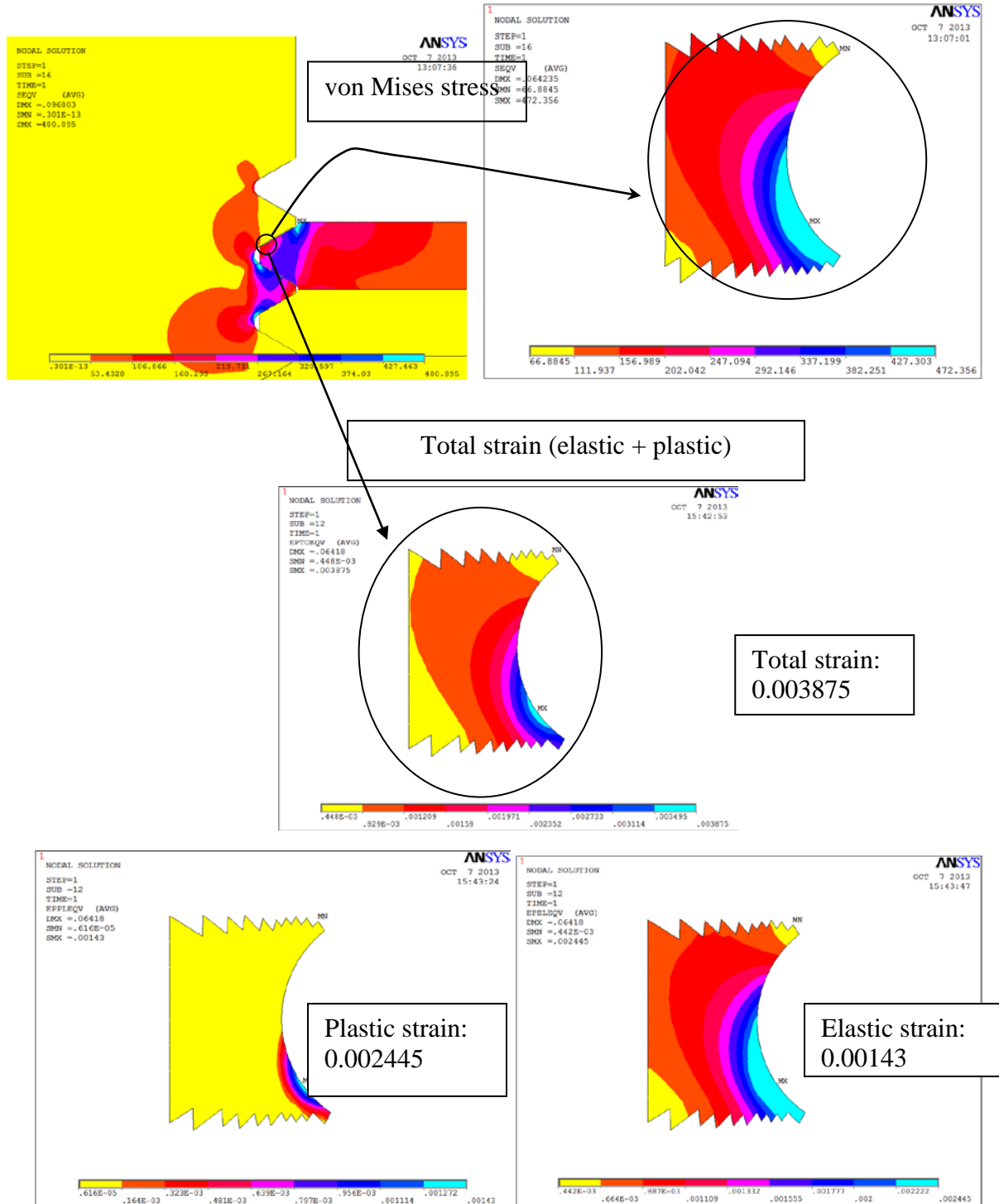
Fig. 13 The von-Mises stress, total, plastic and elastic strain at the first engaged thread of the bolt for the case of $\mu=0.15$.

In order to calculate the theoretical stress concentration (K_{tn}) of the connection, an elastic material property is assumed. The two stresses as von-Mises and maximum principal stress are obtained at the first engaged thread of the bolt (Fig. 14). The higher stress (peak stress) is selected for calculation of K_{tn}. The results are given in Table 5.
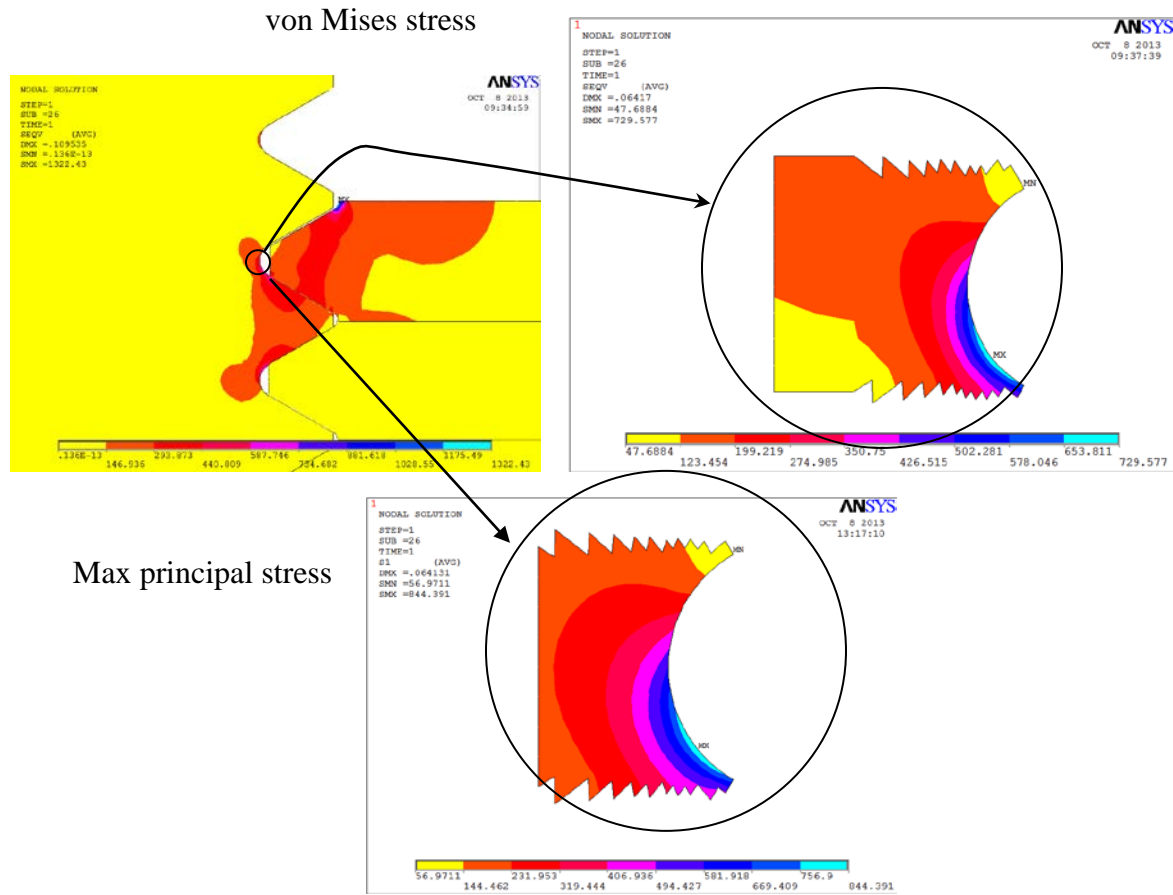
Fig. 14 The von-Mises stress and maximum principal stress at the first engaged thread of the bolt for the case of μ=0.15.

Table 5 the calculation of K_{tn} for the case of M245.

M245	$\sigma_{\text{max-Bolt}}$ (MPa): LINEAR ELASTIC (peak stress)	σ_n (MPa)	K_{tn}
	844	120	844/120=7

The comparisons of numerical and analytical results are shown in Fig. 15 (graphically) and Table 6. The relative error seems increasing for the larger bolt-nut connections (2.7 % for M245 in comparison with 0.1 % for M30 and M33).
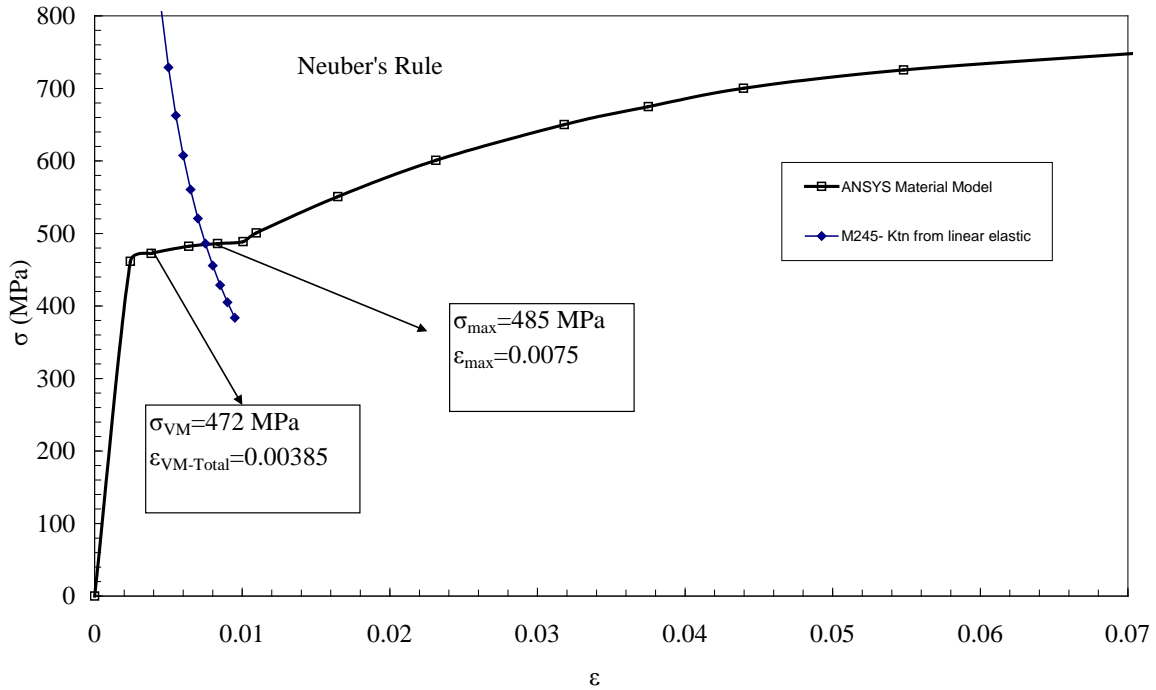
Fig. 15 The graphical method of obtaining the maximum stress according to the Neuber's rule for both M245.

Table 6 Comparison between numerical and analytical results for the case of M245.

M245	μ	$\sigma_{VM\text{-}Bolt}$ (MPa): FEM	$\sigma_{max\text{-}Bolt}$ (MPa): NEUBER	$\Delta\%$
	0.15	472	485	2.7

4. Optimization of bolt-nut connection to reduce the stress concentration

The following 3-step approach is used in this study with that aim of reduction of stress concentration in bolt-nut connection:

Step 1: To analyze the original model, both for the case of linear (to find the stress concentration factor K_{tn}), as well as nonlinear material modeling and finding the peak stress in term of von-Mises stress at the first engaged thread on the bolt. Selecting the von-Mises criteria is based on the suitability of the criteria for elastoplastic materials, which is the case in this study.

Step 2: To use the optimization module in ANSYS, in order to reduce the stress concentration by modifying the bolt-nut geometry. First, the initial optimized design is modeled. The two parameters as shank diameter of the bolt (d_shank) and the length of the notch by adding a step (W_e) are selected for the optimization purpose. Linear material is assumed, as the aim was to reduce the peak stress and subsequently the stress concentration factor. Results are compared with the original case.

Step 3: To analyze the geometrical optimized model from step 2 by applying the elastoplastic material properties. The results then are compared with original model.

As following, the later steps (step 2 and 3) are explained in more details:

Step 2: optimization

The fellow chart of the optimization procedure (step 2) is explained in Fig. 16.
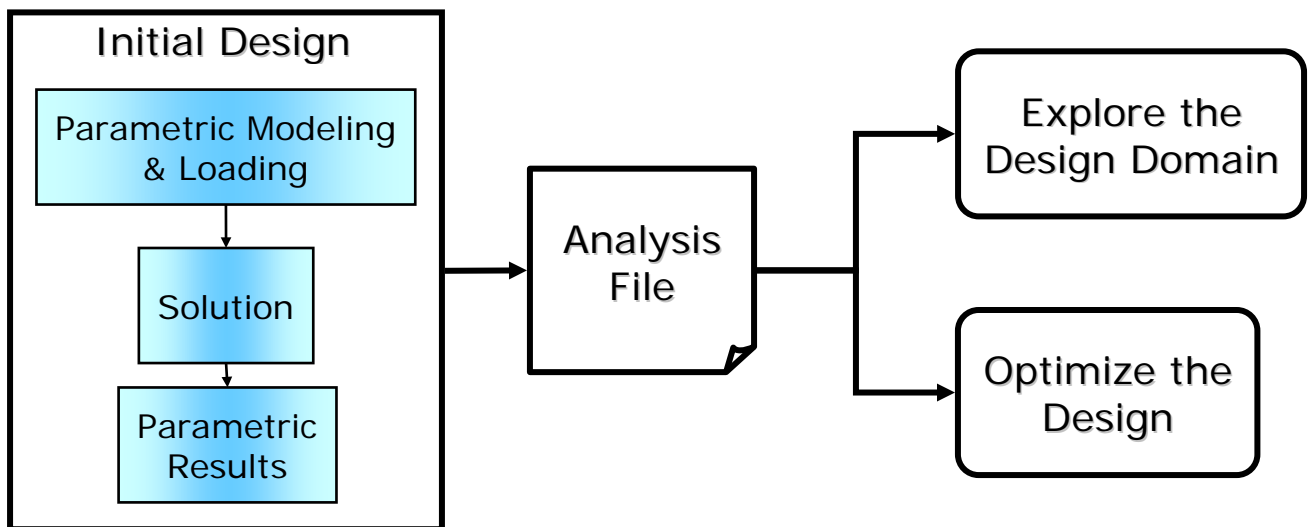
Fig. 16 The fellow chart of the optimization procedure.

The two models used for optimization (a): original model, (b): initial optimization model are shown in Fig. 17.

ΔL

(a): Original model

120

D_o/2=122.5

48

L_NUT=117.28

d_shank

ΔL

(b): Initial
optimization model

120

W_e

D_o/2=122.5

24

L_NUT=117.28
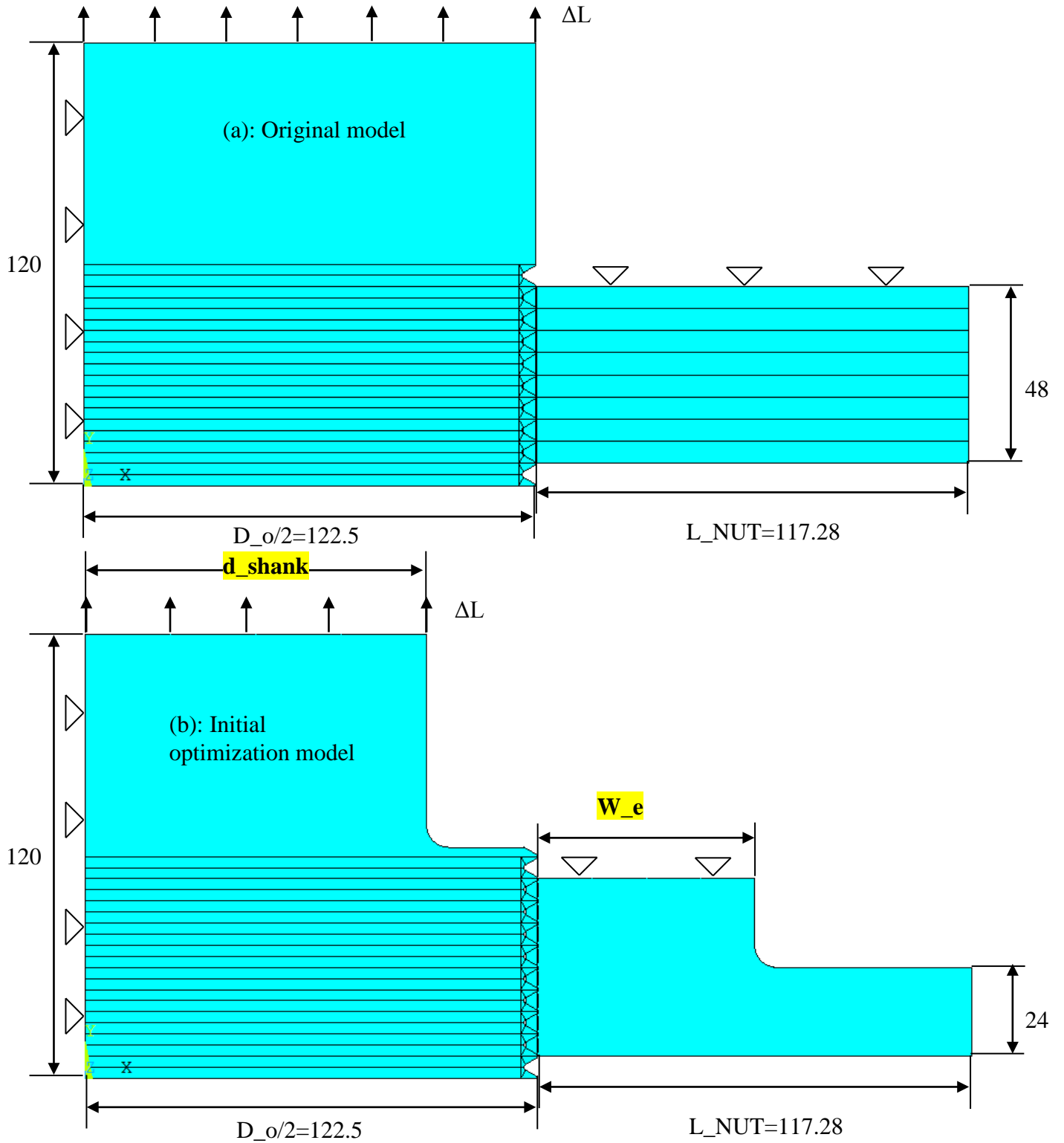
Fig. 17 The two models used for optimization (a): original model, (b): initial optimization model

As it can be seen from Fig. 17 (b), the two parameters as shank diameter of the bolt (d_shank) and the length of the notch by adding a step (W_e) are selected for the optimization purpose. This method is selected based on the study in [3], which is DIRECT optimization technique to reduce the stress concentration in bolt-nut connections. The method is based on modifying the bolt by adding a groove to the lower end of the bolt, or reducing the shank diameter of the bolt. In addition modification on the nut is performed by adding a step or taper to the nut. These modifications lead to reduction of SCF up to 75%.

The optimization procedure is explained in detail as follows:

!-------------------Assign analysis file----------------------------

The APDL file is assigned by the following command. The file needs to be located in the same directory as of the "working directory" of ANSYS.

/OPT

OPANL,'M245-OPT-SEQV','txt',' '

  !----------------Independent variables-----------------

The independent variables (d_shank and W_e) and their range and tolerances are defined by the following commands:

OPVAR,d_shank,DV,0.75*D_o/2,0.95*D_o/2,0.01,

OPVAR,W_e,DV,0.2*L_NUT,0.6*L_NUT,0.01,

!----------------Objective variables--------------------

The objective is set as minimization of nodal stress in term of von-Mises stress.

 OPVAR,SEQV,OBJ, , ,10,

!----------------Optimization method------------------

The first-order method is used in this analysis. The number of iteration are set to 10 with maximum of iterations=100.

OPTYPE,FIRS

OPFRST,10,100,.2,

OPEXE

!----------Plot results-----------------------------------

After solution, the results can be plotted by using the following commands:

PLVAROPT,d_shank, W_e

PLVAROPT,d_shank, SEQV

PLVAROPT,W_e, SEQV

!---

The comparison of K_{tn} for three case of original model, initial optimized model and optimized model is summarized in Table 7.

Table 7: K_{tn} comparison of: original model, initial optimized model and optimized model

M245	d_shank (mm)	W_e (mm)	σ_n (MPa)	$\sigma_{VM\text{-}Bolt}$ (MPa): LINEAR ELASTIC (Von Mises)	K_{tn}
Original	122.5	117.28	120	729	6.075
Initial optimization model	98	58.5602227	120	390	3.25
Best model	92.3965151	58.5602227	120	351	2.925

Step 3: using nonlinear material properties for the optimized model

Finally, The von-Mises stress at the first engaged thread of the bolt of original and optimized model is compared in Table 8. The enhancement of the stress state through the optimization procedure can be observed.

Table 8: the von-Mises stress of original and optimized model at the first engaged thread of the bolt.

M245	d_shank (mm)	W_e (mm)	σ_n (MPa)	$\sigma_{VM\text{-}Bolt}$ (MPa)
Original	122.5	117.28	120	472
Best model	92.3965151	58.5602227	120	321

References

1. G. H. Majzoobi, et al., "Experimental results and finite-element predictions of the effect of nut geometry, washer and Teflon tape on the fatigue life of bolts". Fatigue and Fracture of Engineering Materials and Structures, 28, No. 6, 557-564 (2005).

2. H. O. Fuchs, *Discussion: Nominal Stress or Local Strain Approaches to Cumulative Damage in Fatigue under Complex Loading*, 1977, Society of Automotive Engineers: Warrendale, PA. p. 203–207.

3. S. Venkatesan and G. L. Kinzel, "Reduction of Stress Concentration in Bolt-Nut Connectors". Journal of Mechanical Design, 128, No. 6, 6 (2005).

Collaboration with OMZ S.r.l: Stress analysis of different lamination roll designs by using finite element method: comparison case study

Calculating the lamination pressure applied on the working roll

Scheme of lamination process of a strip between the working rolls and deformed shape of the rolls due to the lamination are shown in Fig. 1.
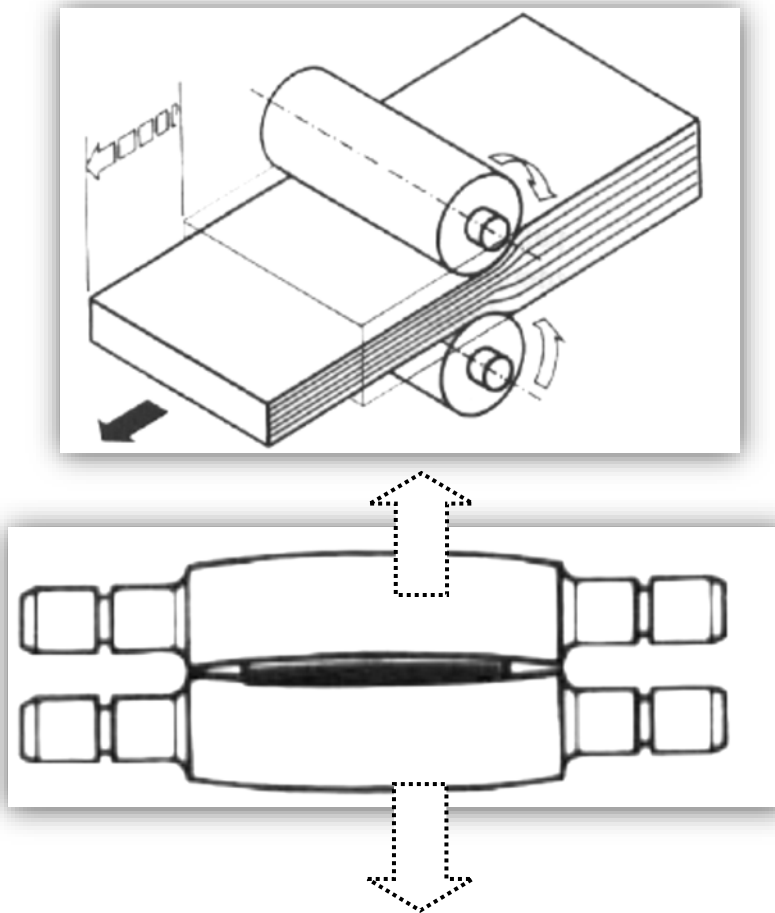
Fig. 1. Scheme of lamination process of a strip between the working rolls

In order to perform the finite element analysis, the value of applied pressure on the working roll during the lamination is required. The schematic of applied loads on the roll is depicted in Fig. 2. The applied pressure can be calculated from Eq. (1).
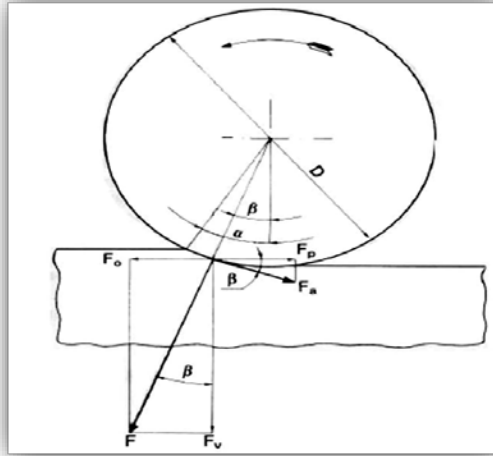
Fig. 2. Schematic of the applied loads on the working roll

$$P = \frac{F}{l * \dfrac{\alpha * \pi}{180} * \dfrac{D}{2}}$$

(1)

l = length of the roll (in contact with Zinc: 1440 mm)

α = Angle of applied load ($\cong 10°$)

D = Diameter of the roll (487.5 mm)

F = Applied lamination load (850,000 kg=8500,000 N)

$\Longrightarrow$
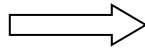
P=138 MPa

The above pressure is applied on the finite element models, as shown in Fig. 6.

Three-dimensional stress analysis: strength of the material in the case of brittle fracture

For brittle materials, such as cast iron, failure tends to occur more catastrophically with the sudden material cracking. In fact, this happens when the tensile stress reaches a critical value. Therefore, given any set of stresses, one determines the maximum normal stress from among all possible planes and compares this stress with the critical stress for failure. This maximum normal stress is the maximum principal stress, which also is donated by σ_1. As following, the theory

related to calculation of the principal stresses in the case of spatial stress problem is explained briefly.

The 3-D stresses, so called spatial stress problem, are usually given by the six stress components σ_x, σ_y, σ_z, τ_{xy}, τ_{yz}, and τ_{xz}, (see Fig. 3) which consist in a three-by-three symmetric matrix (stress tensor):

$$T_3 = \begin{bmatrix} \sigma_x & \tau_{xy} & \tau_{xz} \\ \tau_{xy} & \sigma_y & \tau_{yz} \\ \tau_{xz} & \tau_{yz} & \sigma_z \end{bmatrix} \tag{2}$$

The three principal stresses σ_1, σ_2, and σ_3, which are eigenvalues of the three-by-three symmetric matrix of Eq. (2) and the three maximum shear stresses τ_{max1}, τ_{max2}, and τ_{max3}, which can be calculated from σ_1, σ_2, and σ_3.
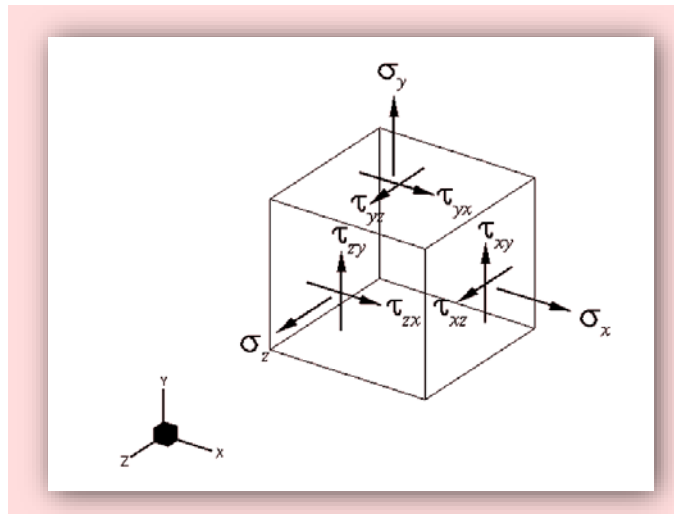
Fig.3. 3-D stress state represented by axes parallel to X-Y-Z

Imagine that there is a plane cut through the cube in Fig. 4 and the unit normal vector λ of the cut plane has the direction cosines λ_x, λ_y and λ_z:

$$\lambda = (\lambda_x , \lambda_y , \lambda_z) \tag{3}$$
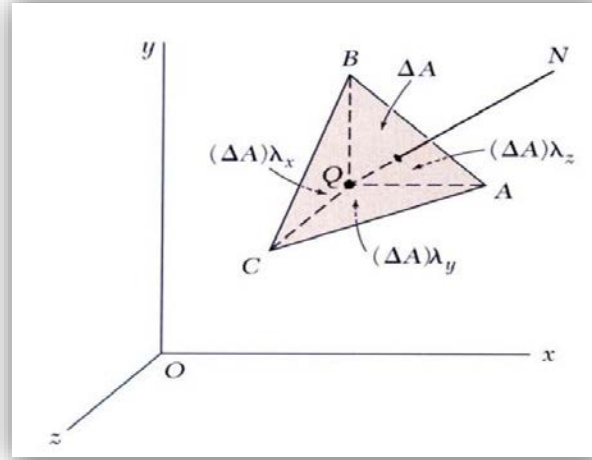
Fig.4. a plane cut through the cube.

Then satisfying the equilibrium, the normal stress on this plane can be represented by

$$\sigma_n = \sigma_x \lambda^2_x + \sigma_y \lambda^2_y + \sigma_z \lambda^2_z + 2\tau_{xy}\lambda_x\lambda_y + 2\tau_{yz}\lambda_y\lambda_z + 2\tau_{xz}\lambda_x\lambda_z \tag{4}$$

There exist three sets of direction cosines, λ_1, λ_2, and λ_3 - the three principal axes, which make σ_n achieve extreme values σ_1, σ_2, and σ_3 - the three principal stresses, and on the corresponding cut planes, the shear stresses vanish! The problem of finding the principal stresses and their associated axes is equivalent to finding the eigenvalues and eigenvectors of the following problem:

$$(\sigma I_3 - T_3)\, \lambda = 0 \tag{5}$$

The three eigenvalues of Eq. (5) are the roots of the following characteristic polynomial equation:

$$\det (\sigma I_3 - T_3) = \sigma^3 - A\sigma^2 + B\sigma - C = 0 \tag{6}$$

where

$$A = \sigma_x + \sigma_y + \sigma_z \tag{7}$$

$$B = \sigma_x \sigma_y + \sigma_y \sigma_z + \sigma_x \sigma_z - \tau^2_{xy} - \tau^2_{yz} - \tau^2_{xz} \tag{8}$$

$$C = \sigma_x \sigma_y \sigma_z + 2\,\tau_{xy}\tau_{yz}\tau_{xz} - \sigma_x \tau^2_{yz} - \sigma_y \tau^2_{xz} - \sigma_z \tau^2_{xy} \tag{9}$$

Numerically, one can always find one of the three roots of Eq. (6), i.e. σ_1, using line search algorithm. Then combining Eqs (5) and (6), one obtains simple quadratic equations and therefore

218

obtains two other roots of Eq. (6), i.e. σ_2 and σ_3. To this end, one can re-order the three roots and obtains the three principal stresses, e.g.

$$\sigma_1 = \max(\sigma_1, \sigma_2, \sigma_3) \tag{10}$$

$$\sigma_3 = \min(\sigma_1, \sigma_2, \sigma_3) \tag{11}$$

$$\sigma_2 = (A - \sigma_1 - \sigma_3) \tag{12}$$

Now, substituting σ_1, σ_2, or σ_3 into Eq. (5), one can obtains the unit vectors λ_1, λ_2, and λ_3, respectively, of the corresponding principal axes.

Similar to Fig. 3, one can imagine a cube with their faces normal to λ_1, λ_2, or λ_3. For example, one can do so in Fig. 3 by replacing the axes X,Y, and Z with λ_1, λ_2, and λ_3, respectively, replacing the normal stresses σ_x, σ_y and σ_z with the principal stresses σ_1, σ_2, and σ_3, respectively, and removing the shear stresses τ_{xy}, τ_{yz}, and τ_{xz}. The corresponding 3-D Mohr's circle is shown in Fig. 5.
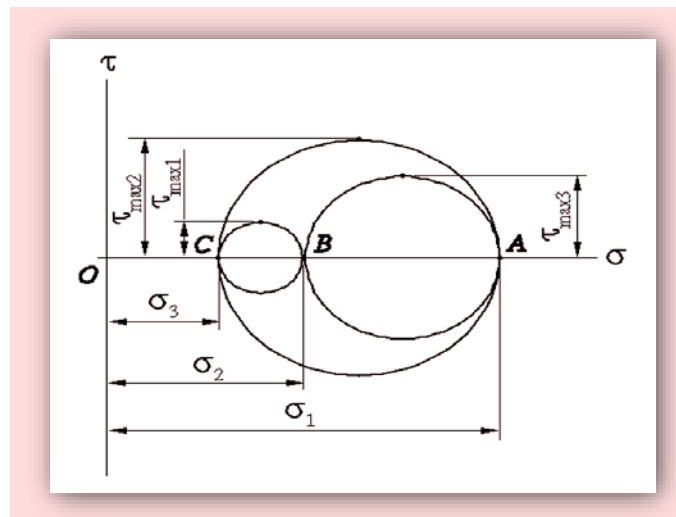
Fig.5. Mohr's circles for spatial (3-D) stresses

Three models used in the structural analysis

The aim of this project is to compare three different designs of rolls in term of strength of the component (mainly longitudinal deformation, as well as contact pressure due to interference fit for the case of Model-2) under working conditions by using finite element modeling (FEM). Due to symmetry of the models in all three planes, i.e. yz, xz and xy planes, only 1/8 of the model is considered in the analysis, as it is shown in Fig. 6.
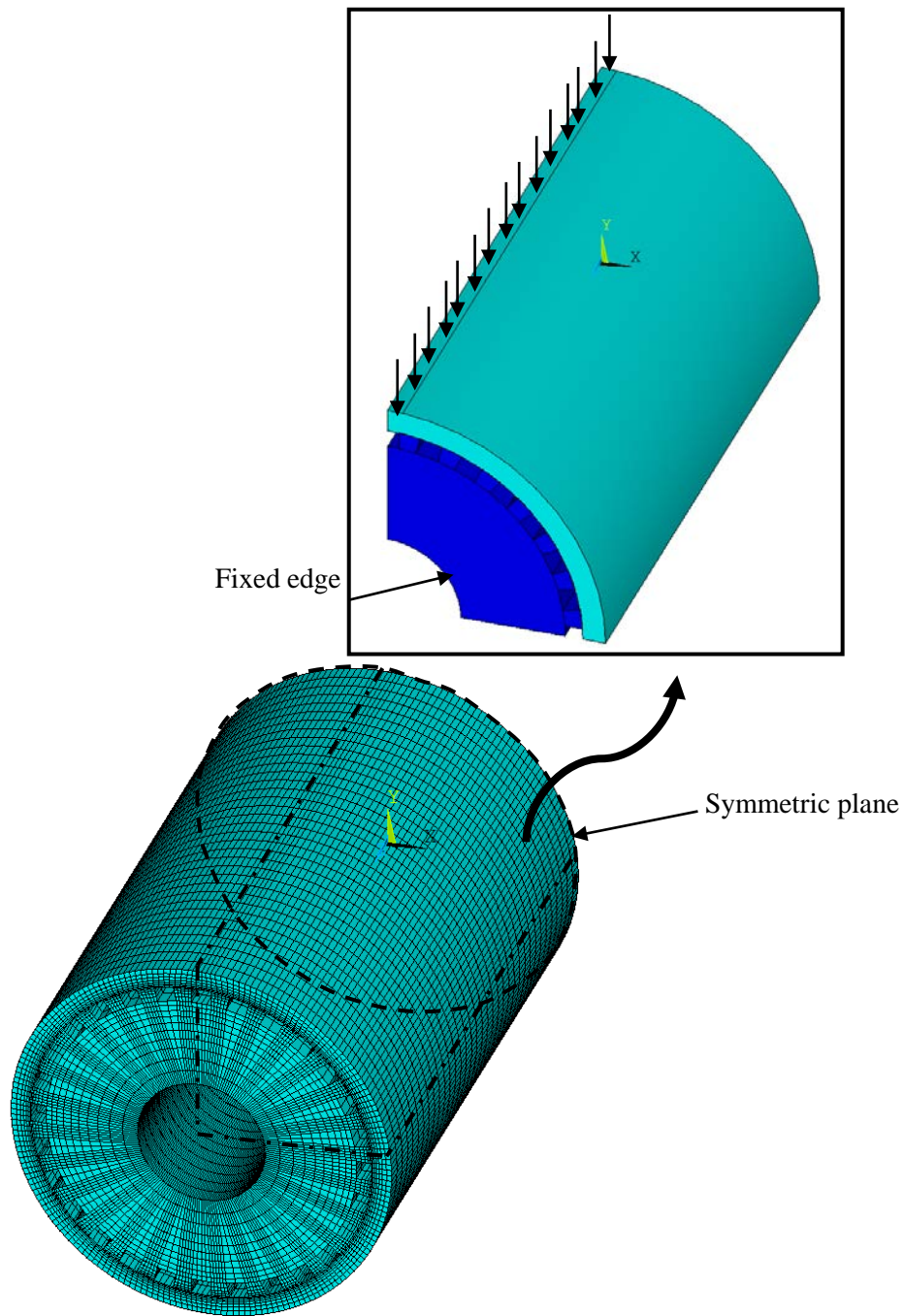
Fig. 6. Finite element model and boundary conditions.

The three models are shown in Fig. 7. One should note that Model-3 is the same as Model-2 with only two differences: first, the contact between the shaft and sleeve in Model-3 is not defined. Second, some of the sharp corners of Model-2 are filleted in Model-3.
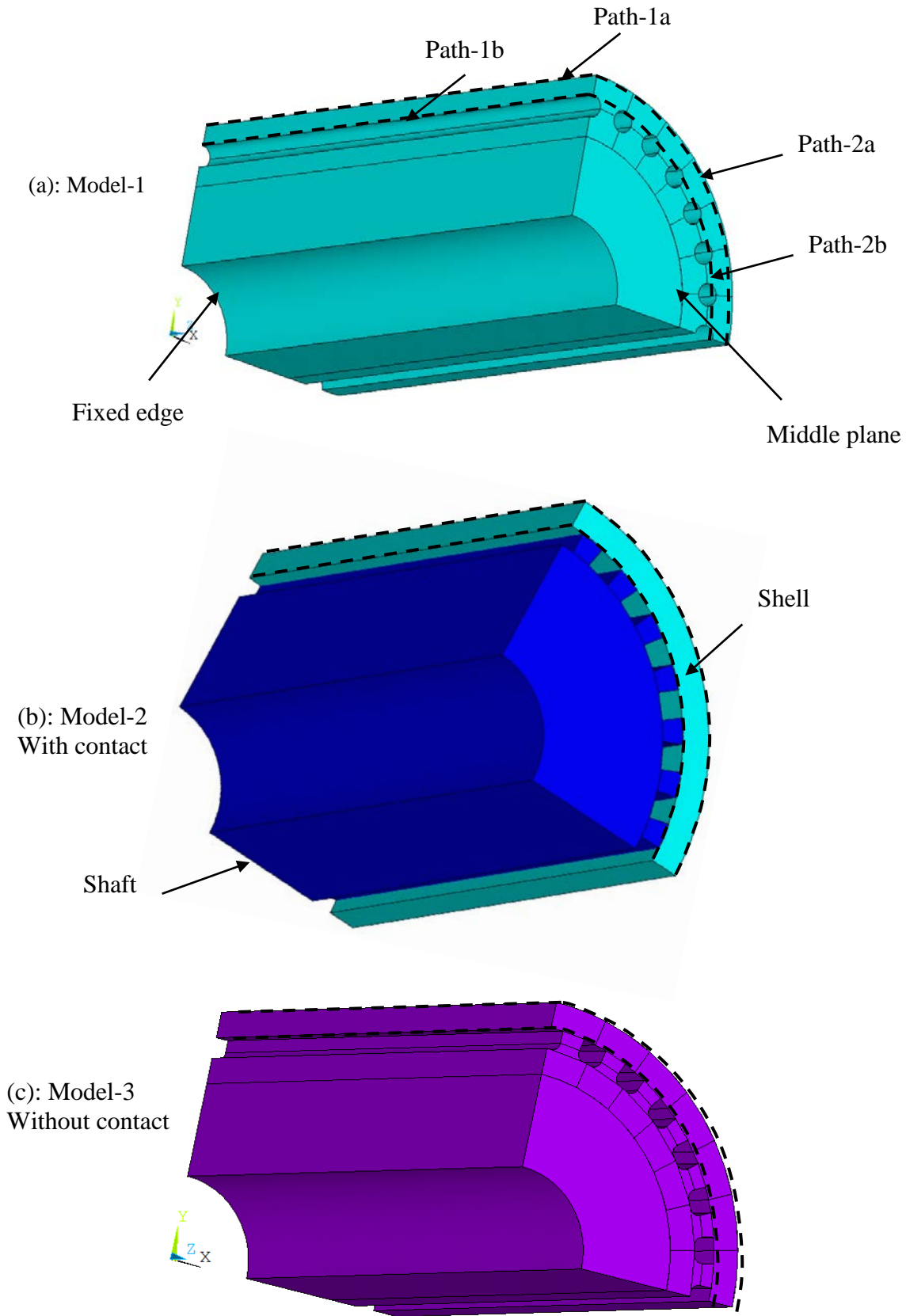
Fig. 7. Three models used in the analysis.

As following, Model-2 is selected to present the corresponding FEM results. Afterwards, the three models in terms of maximum principal stress and vertical deformation along the longitudinal directions (Path 1a and 1b Fig. 7) have been compared. In addition, the principal stresses in the circumferential directions (Path 2a and 2b Fig. 7) for each model are calculated and compared.

Load step 1 (LS-1): Interference stress as a result of press-fitting
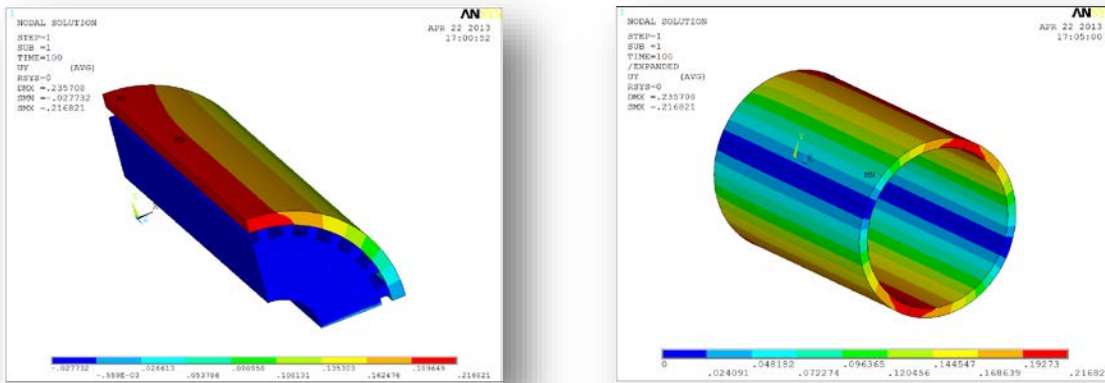
Fig. 8. Deformation of the shell at the end of LS-1.
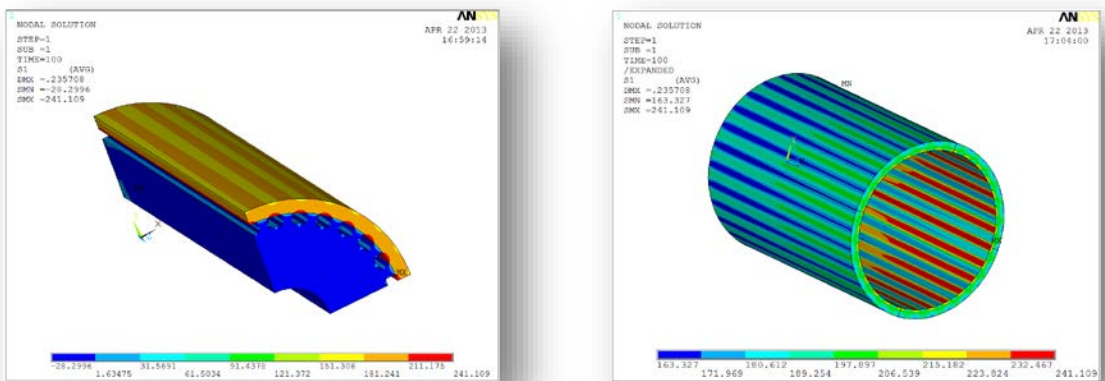
Fig. 9. Maximum stress of the shell at the end of LS-1.

Load step 2 (LS-2): Applying load on the external surface of the roll
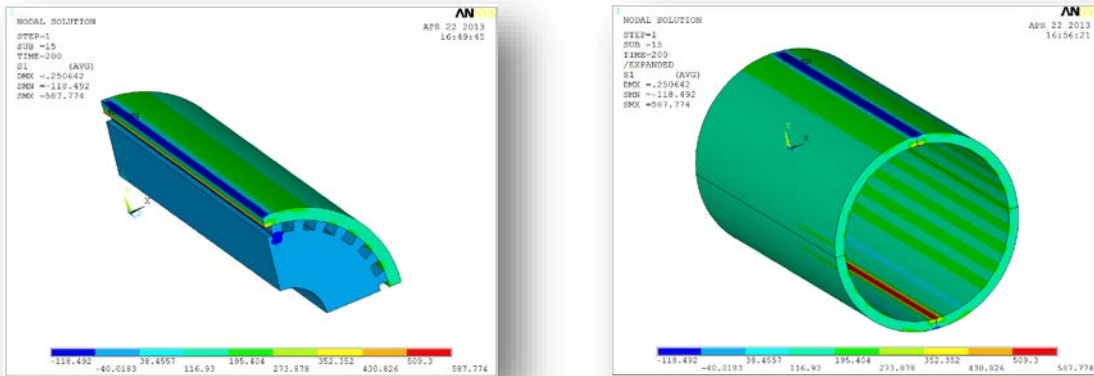
Fig. 10. Deformation of the shell at the end of LS-2.
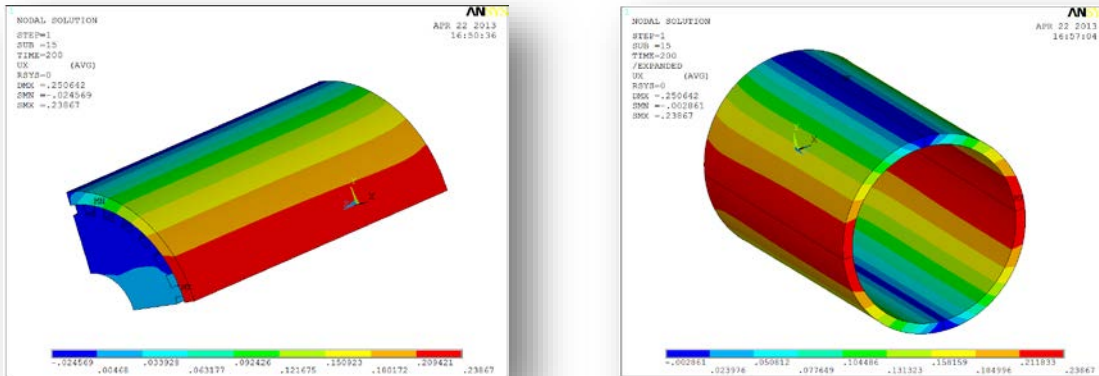
Fig. 11. Maximum stress of the shell at the end of LS-2.

Comparison of the three models

In this section the three models have been compared in terms of maximum principal stress and vertical deformation along the longitudinal directions (Path 1a and 1b Fig. 7) in Figs. 12-15. In addition, the principal stresses in the circumferential directions (Path 2a and 2b Fig. 7) for each model are calculated and compared in Figs. 16 and 17.
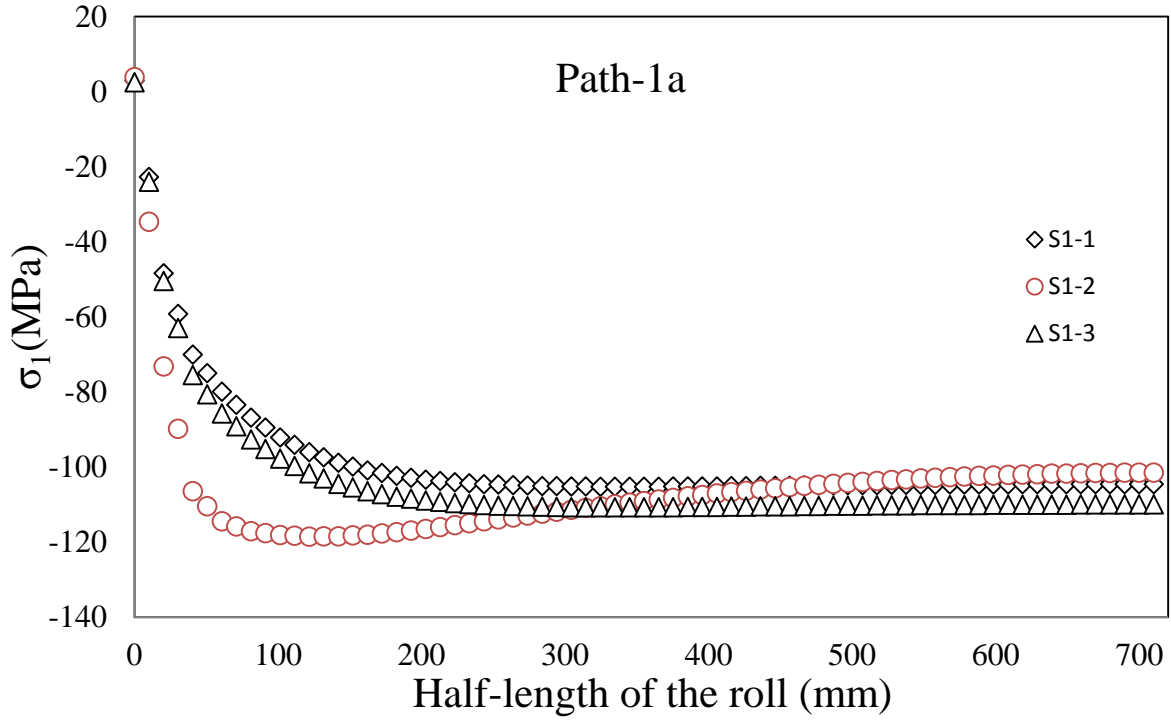
Fig. 12. Maximum stress comparison for the three models on longitudinal Path –1a.
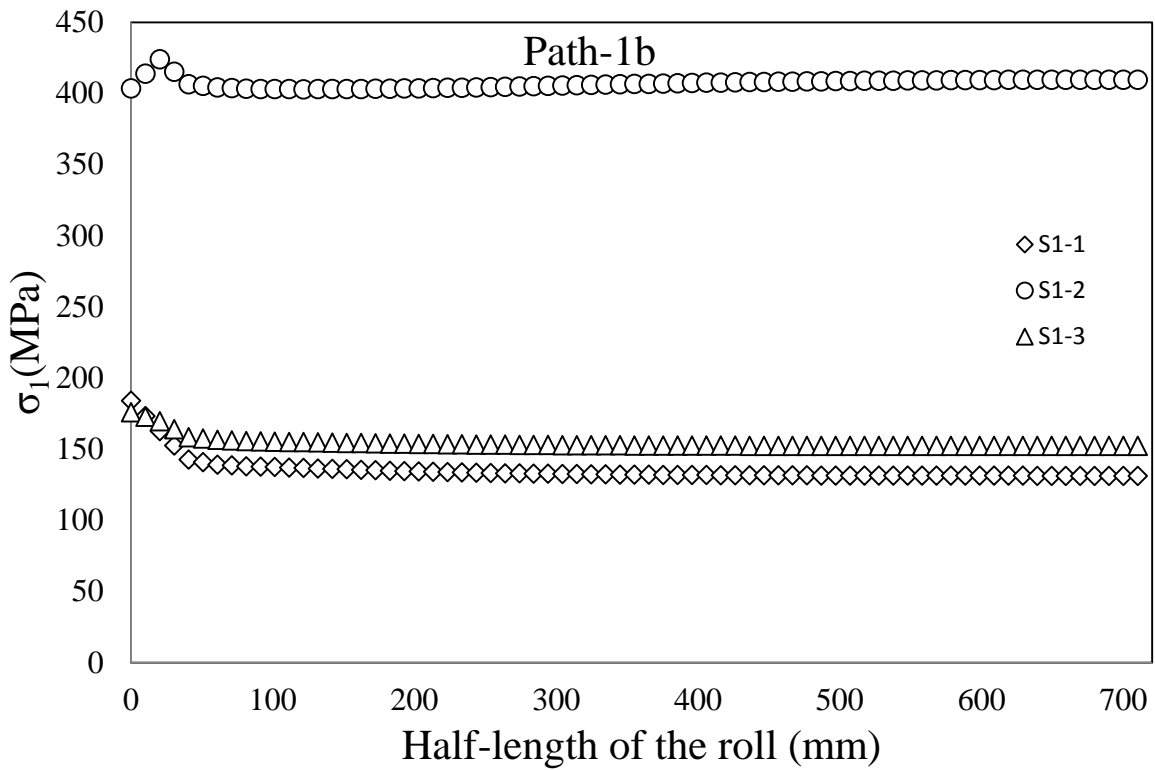
Fig. 13. Maximum stress comparison for the three models on longitudinal Path –1b.

It can be seen from Figs. 12 and 13 that despite a relative higher principal stress (σ_1=425 MPa) for model-2 at path-1b, due to the interference fit between shell and shaft, still it is well below the critical yield stress of the shell (σ_y=1100 MPa).
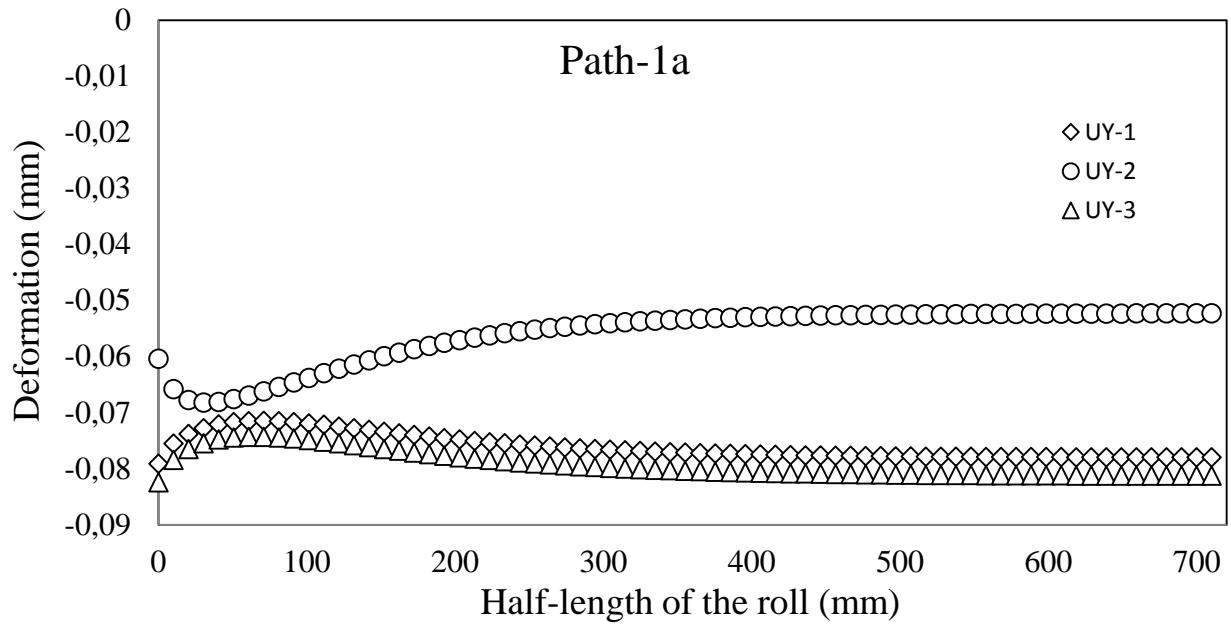
Fig. 14. Deformation comparison in Y direction for the three models on longitudinal Path –1a.
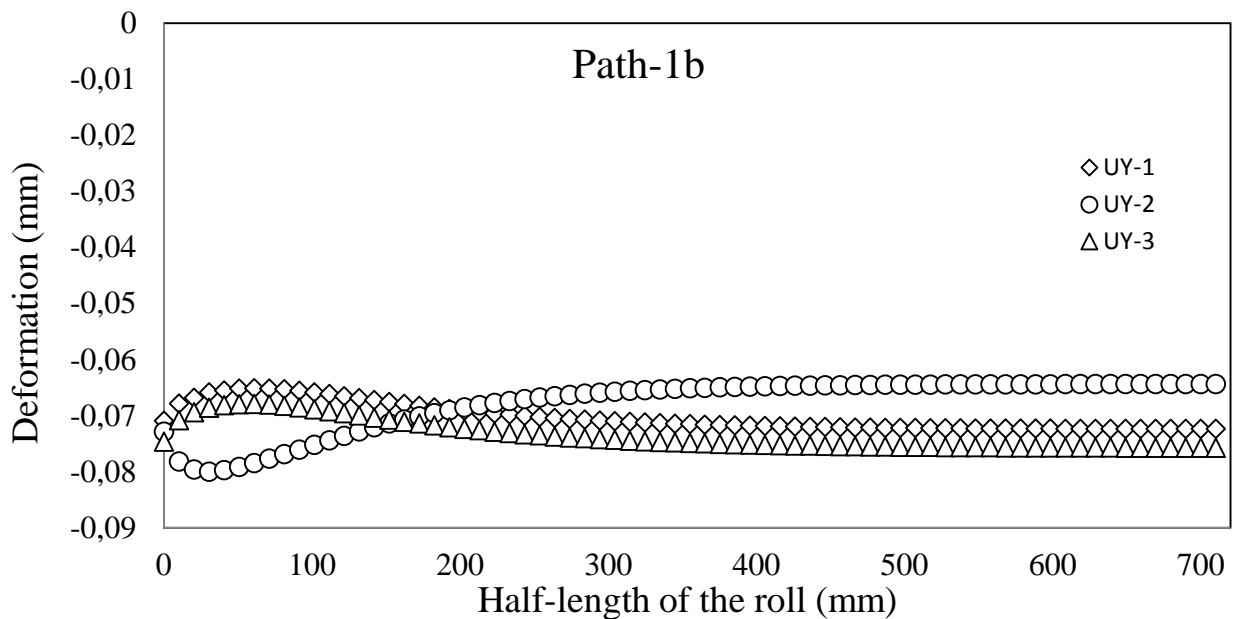
Fig. 15. Deformation comparison in Y direction for the three models on longitudinal Path –1b.

In term of longitudinal deformation (along the shell), it can be seen From Figs 14 and 15 that, surprisingly, the smaller dispalcent occure for model-2, which gives an advantage of adopting the model-2 for the lamination application in this study.
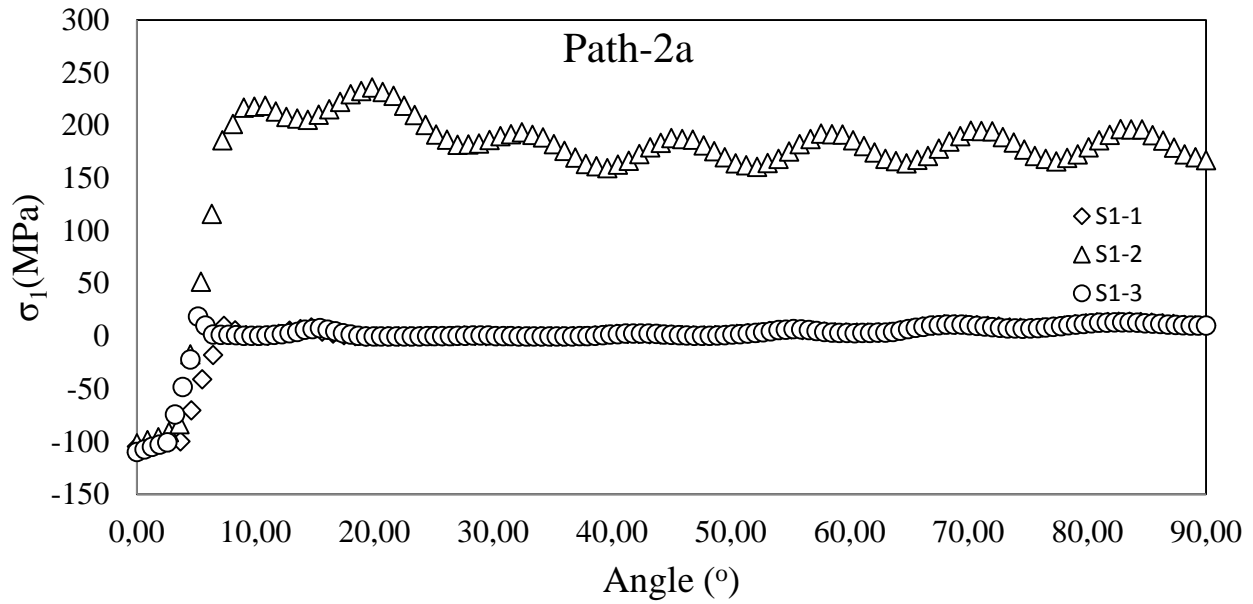
Fig. 16. Maximum stress comparison for the three models on circumferencial Path –2a.
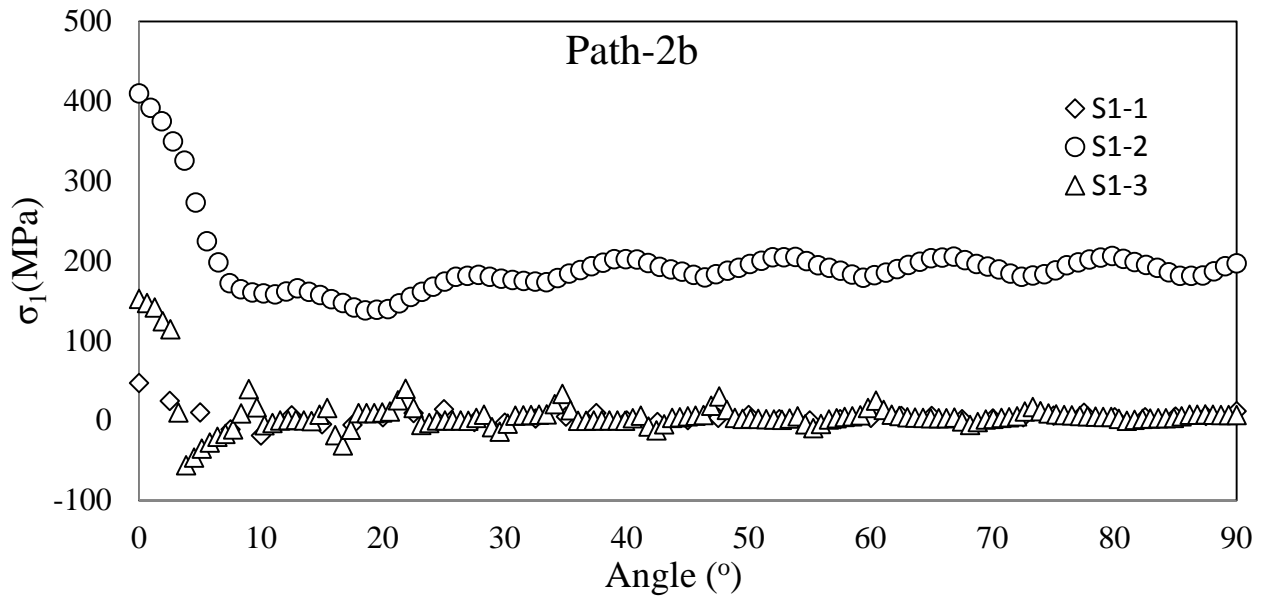
Fig. 17. Maximum stress comparison for the three models on circumferencial Path –2b.

Finally, comaprisons of circumferetial stresses for the three models in Figs 16 and 17 show that, similar to the longitudinal stresses, the maximum principal stress for model-2 due to the interference fit is well below the critical yield stress of the shell.

Comparison of different thicknesses of the shell for Model-3
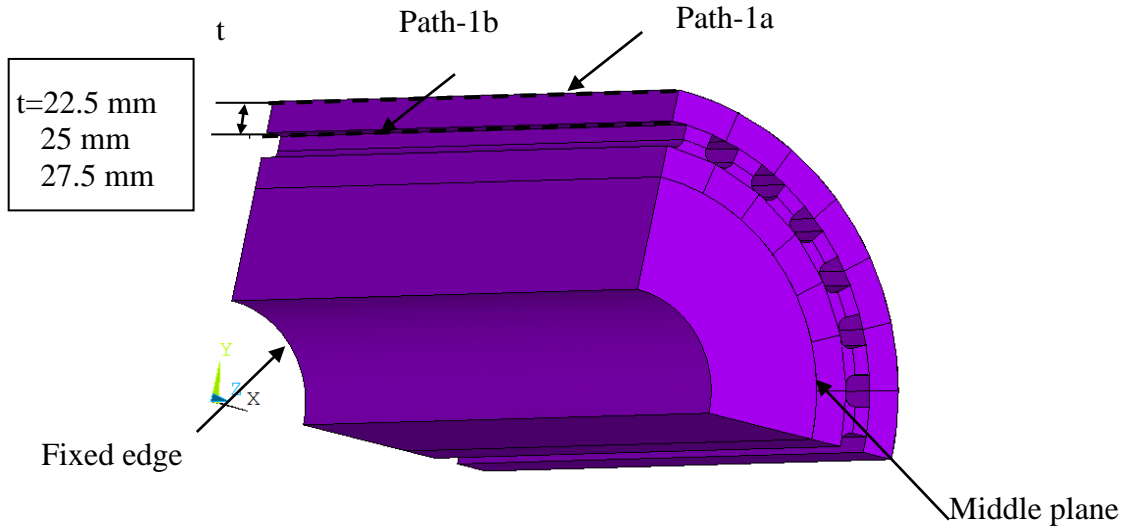
Fig. 14. Comparison of different thicknesses of the shell for Model-3.

Deformation comparison on Path-1a and b
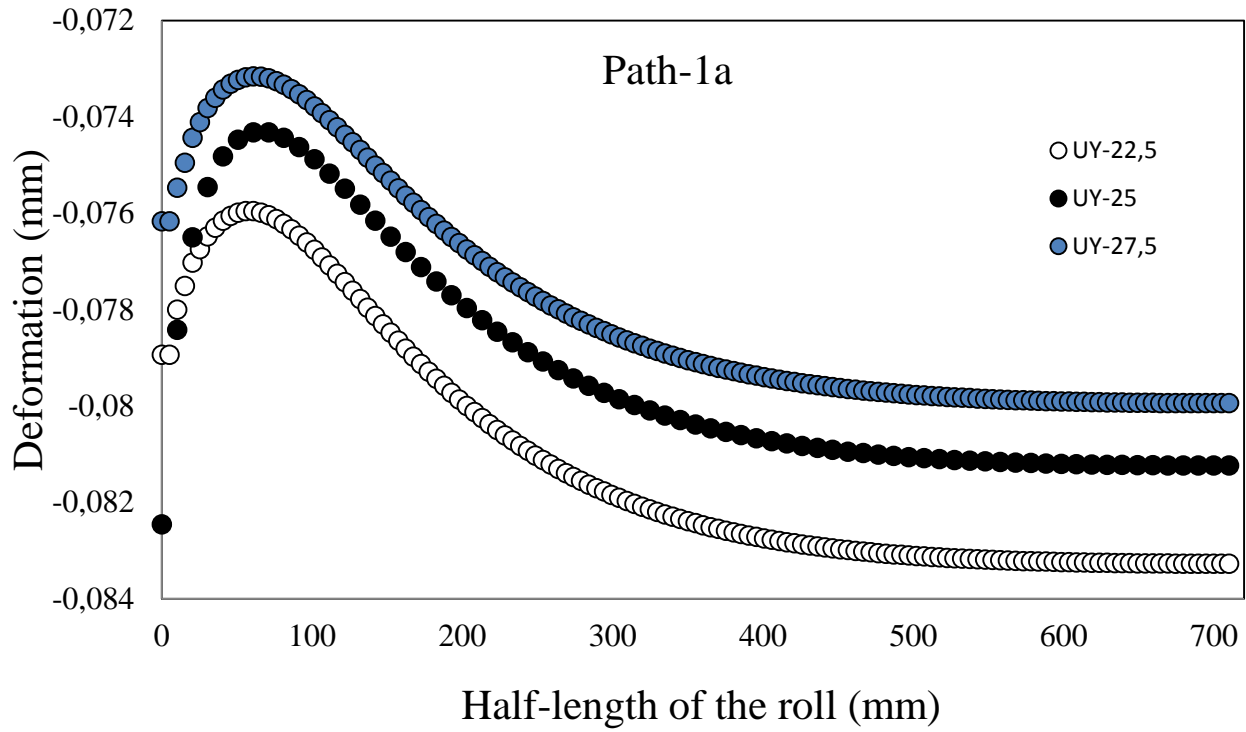
Fig. 18. Deformation comparison in Y direction for the three different thicknesses of the shell on longitudinal Path –1a.
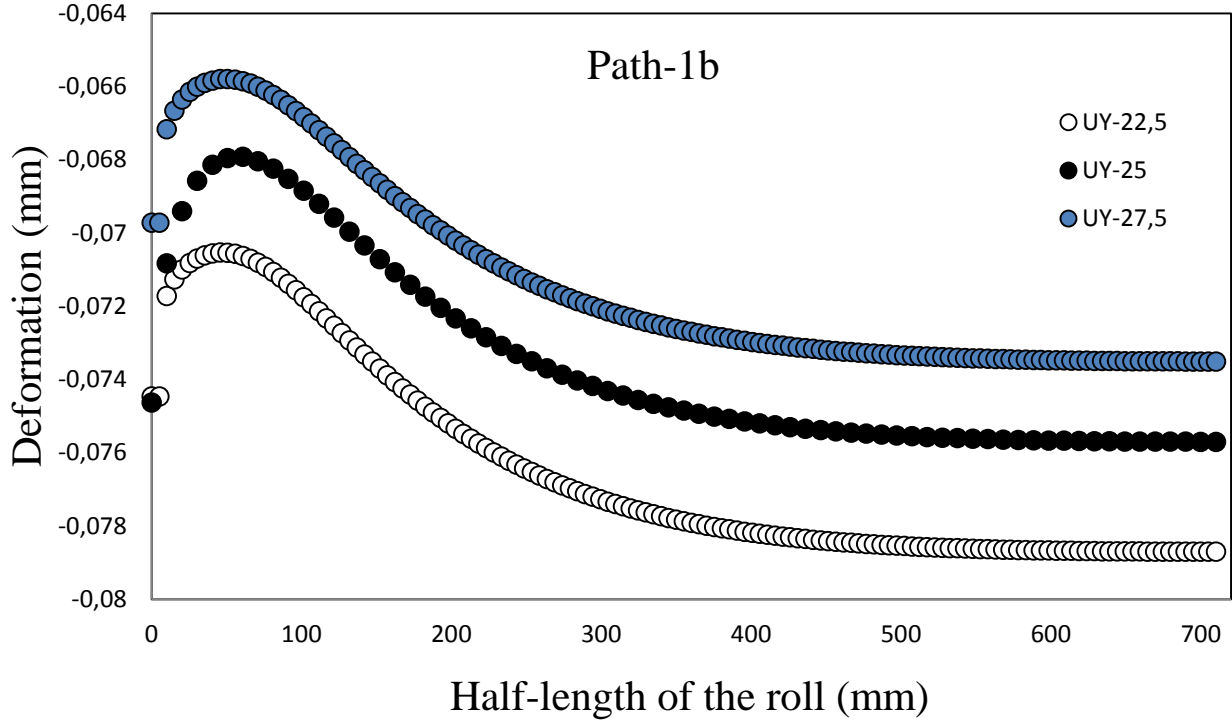
Fig. 19. Deformation comparison in Y direction for the three different thicknesses of the shell on longitudinal Path –1b.

Max. stress comparison on Path-1a and b
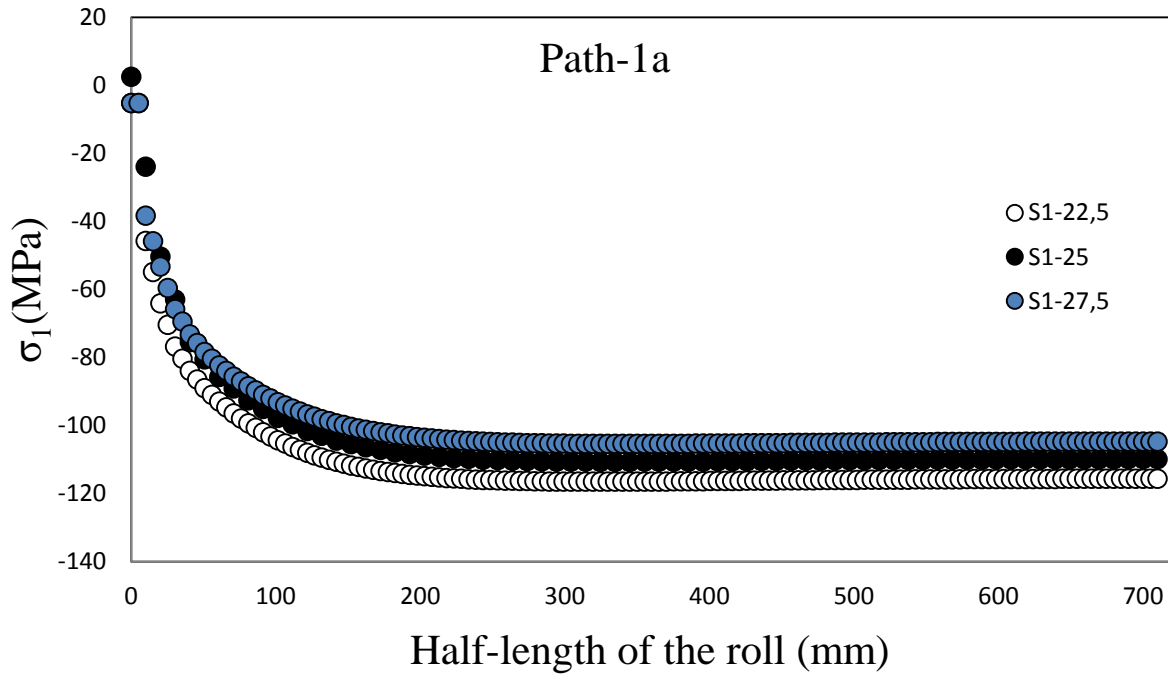
Fig. 20. Maximum stress comparison in Y direction for the three different thicknesses of the shell on longitudinal Path –1a.
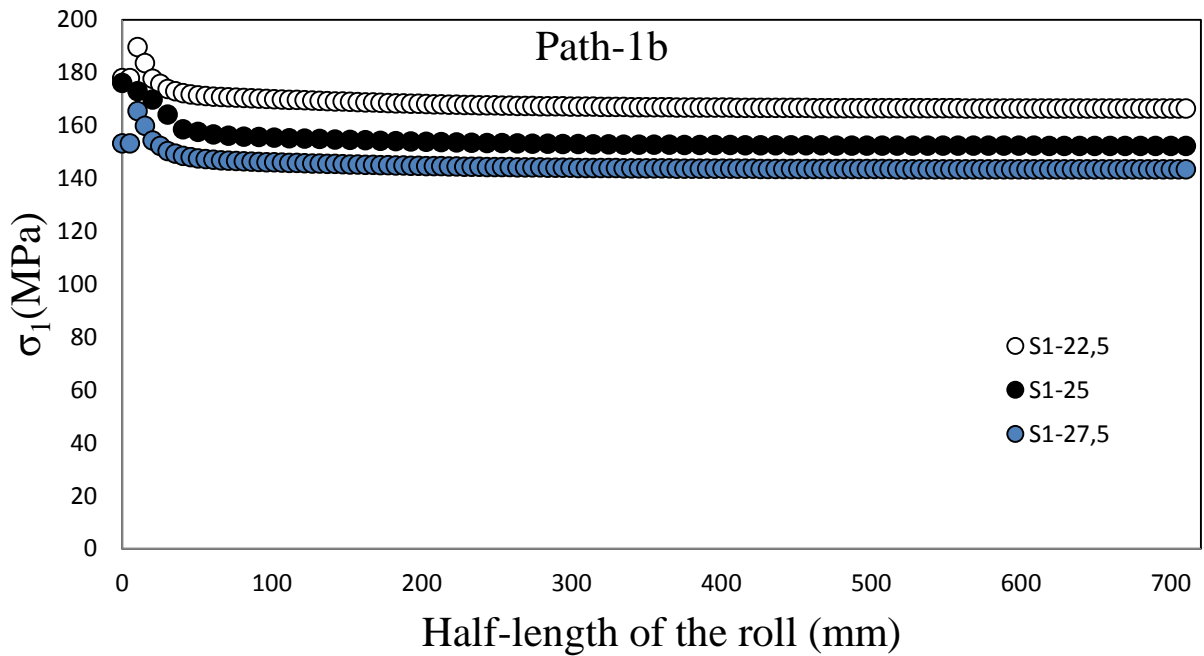
Fig. 21. Maximum stress comparison in Y direction for the three different thicknesses of the shell on longitudinal Path –1b.

As expected, the deformation, as well as stress comaprison confirms the higher stress and deformation of thinner shells, compared to the shells with higher thickness.

Thermal analysis

The thermodynamics parameters obtained from the literature [1-3] are given as follows:

- Temperature of molten Zinc in contact with external surface of the roll: 650 °C
- Temperature of inlet water: 35°C
- Temperature of outlet water: 45°C
- Specific heat of steel: 430 $\frac{J}{Kg°C}$
- Convective heat transfer coefficient of water-steel: 200 $\frac{W}{m^2 K}$
- Heat conduction coefficient of steel: 20 $\frac{W}{mK}$

Thermal analysis

Th simplified section of the roll with the temperatures in working condition is shown in Fig. 22.
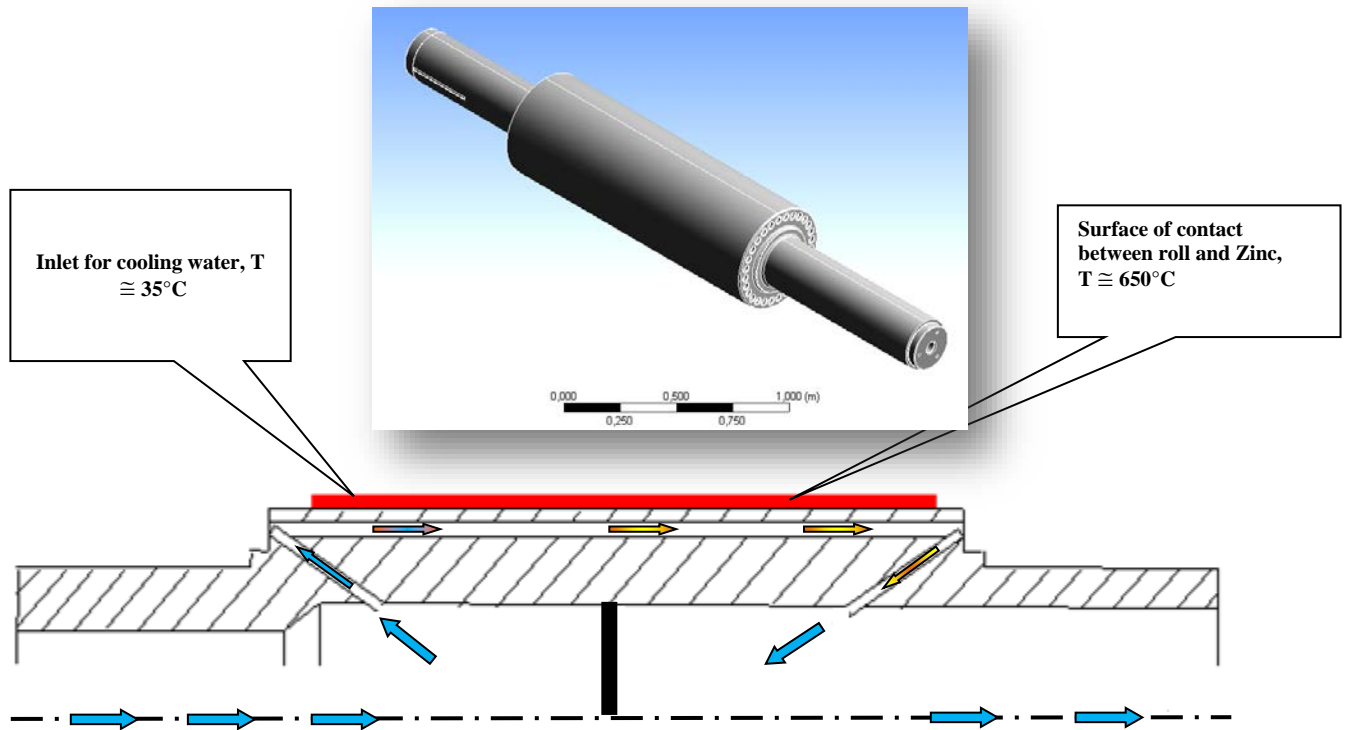
Fig. 22: Simplified section of the roll with the temperatures in working condition.

The two models used in the thermal analysis are shown in Fig. 23. Due to symmetry of the model, only 1/16 of the model is considered for thermal analysis.

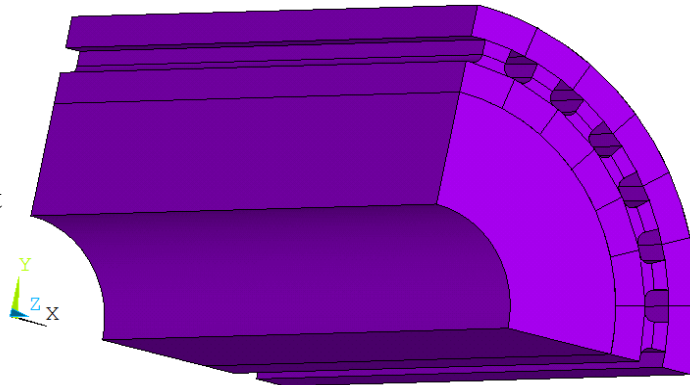(a): Model-1
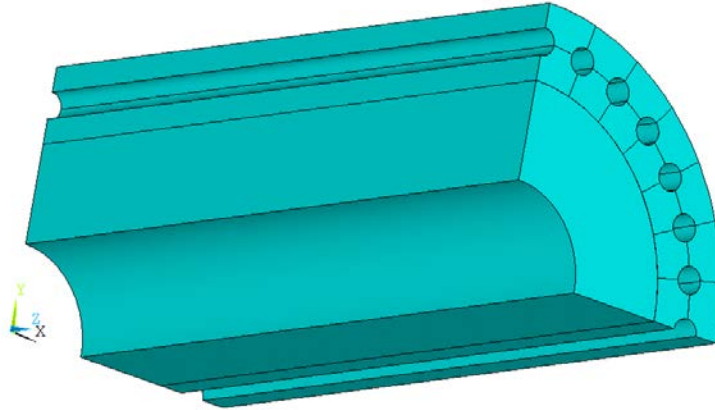
(b): Model-2
Without contact

Fig. 23. Two models used in the thermal analysis.

Different paths by considering various distances from the roll surface (y=10, 15, 20 mm), as well as a path on the minimum distance from the internal surface of the hole to the roll surface are considered. The corresponding results are shown in Fig. 24.
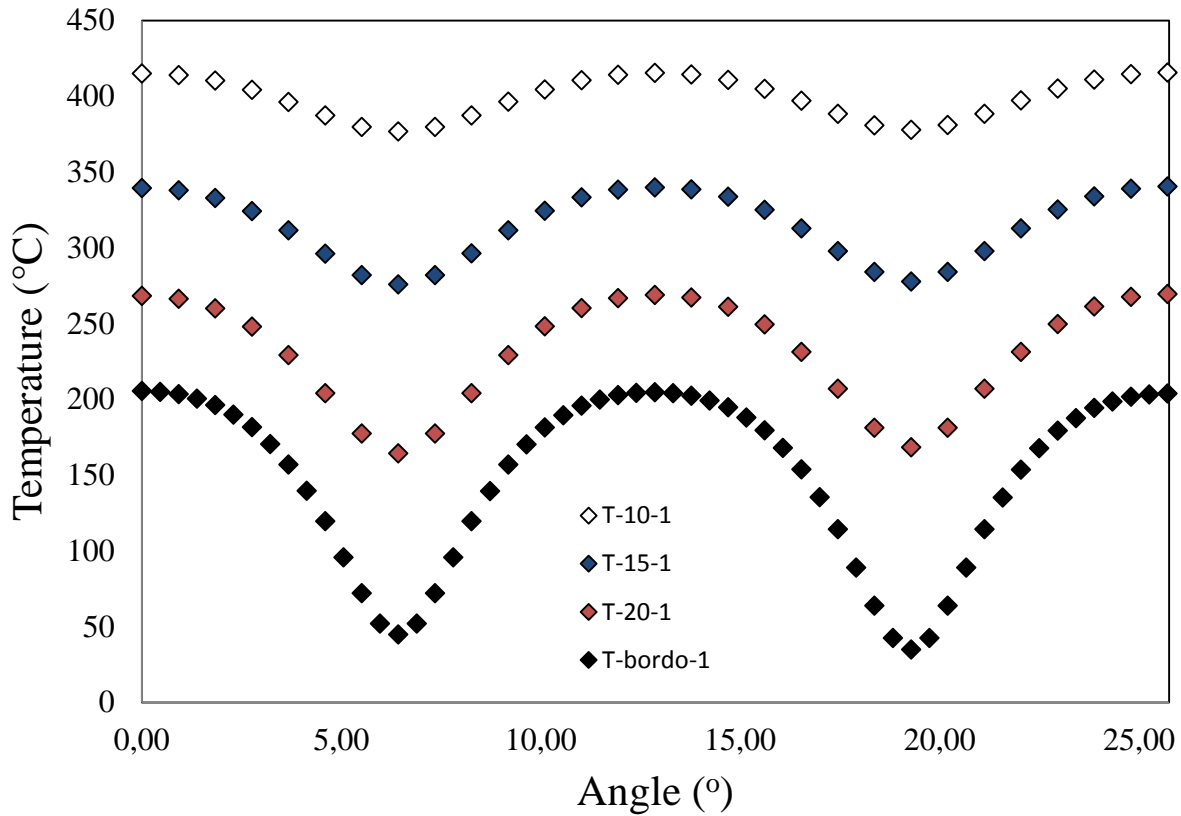
Fig. 24: temperature distribution for different paths of Model-1.

Obviously, as it is expected, the closer to the roll surface, the higher the temperature with more uniform variation.

Similarly for Model 2, different paths by considering various distances from the roll surface (y=10, 15, 20 mm), as well as a path on the minimum distance from the internal surface of the hole to the roll surface are considered. The corresponding results are shown in Fig. 25.
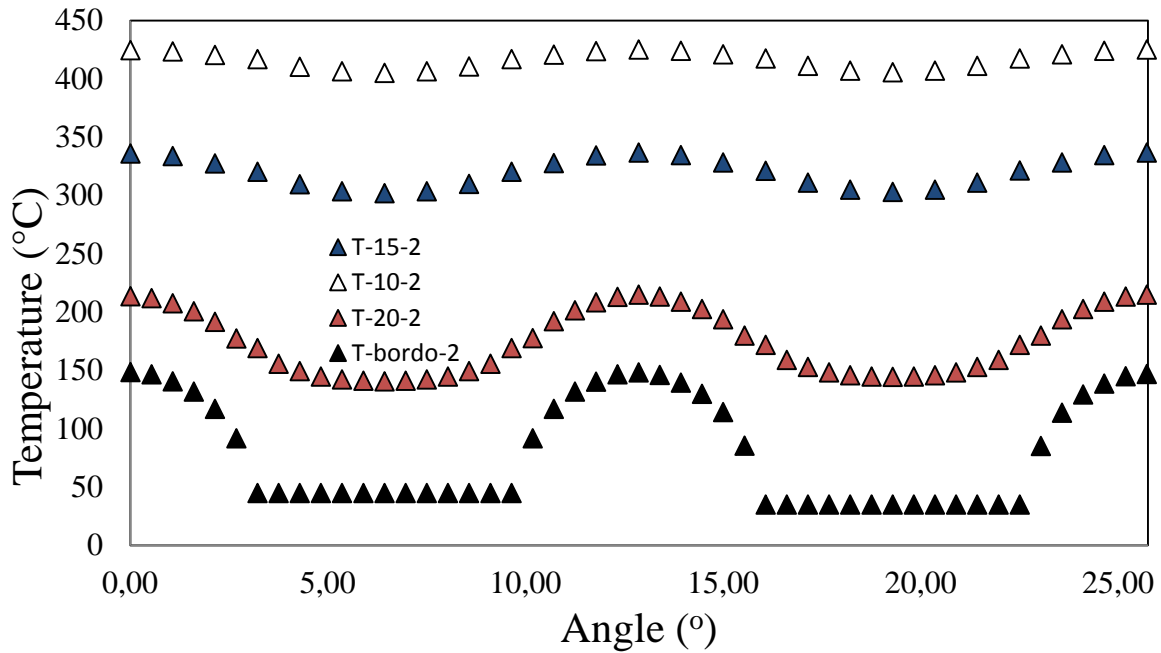
Fig. 25: temperature distribution for different paths of Model-2.

In the same manner, as it is expected, the closer to the roll surface, the higher the temperature with more uniform variation trend.

In the following Figures (Figs. 26 and 27), the both trend of temperature distribution are compared.
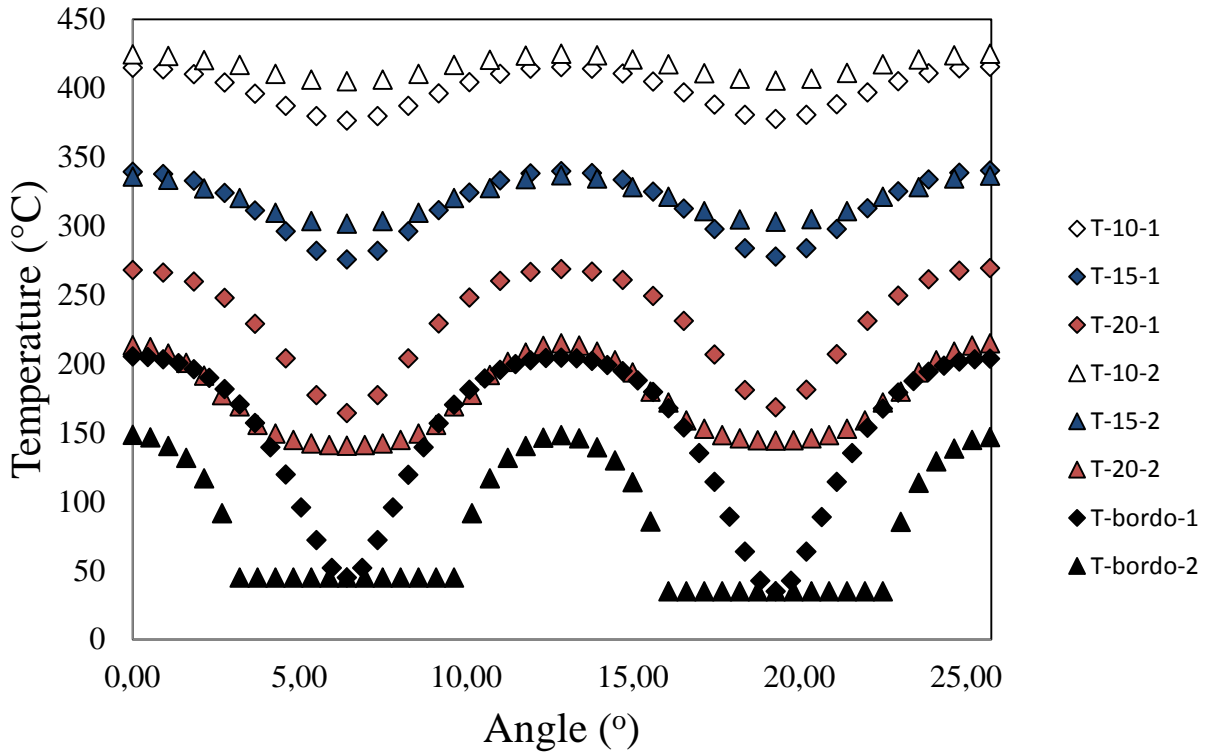
Fig. 26: Temperature distribution comparisons for different models.

The comparison of temperature distributions for both models shows that the temperature distribution at the near surface of the roll for both models seems the same. However, the relative advantage of Model-2, by having the lower temperature (about 25 % less), at a distance y=20 mm from the surface of the roll and beyond is evident.
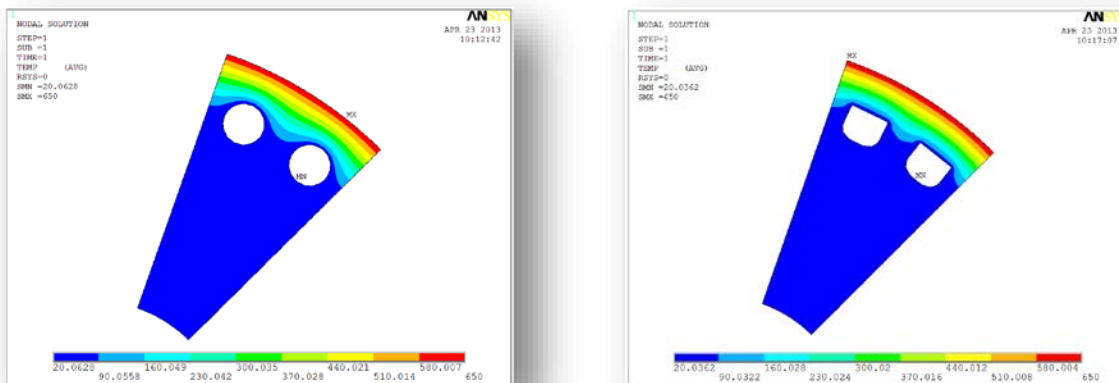

Fig. 27.Temperature distribution for two different designs.

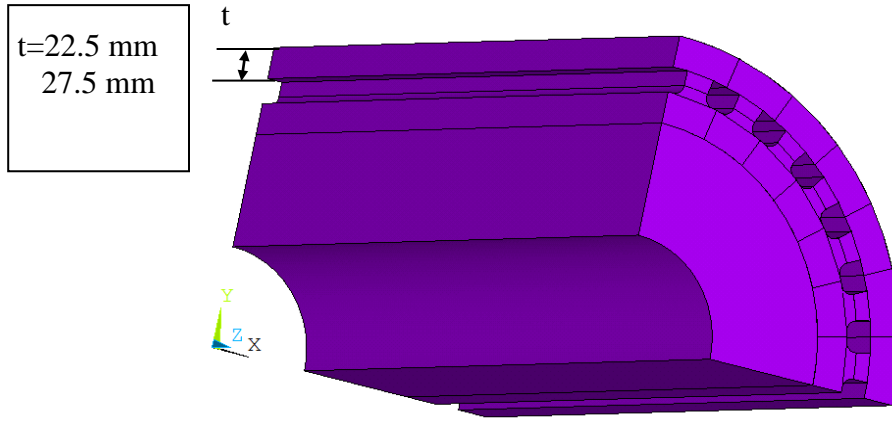*Comparison of different thicknesses of the shell for Model-3*

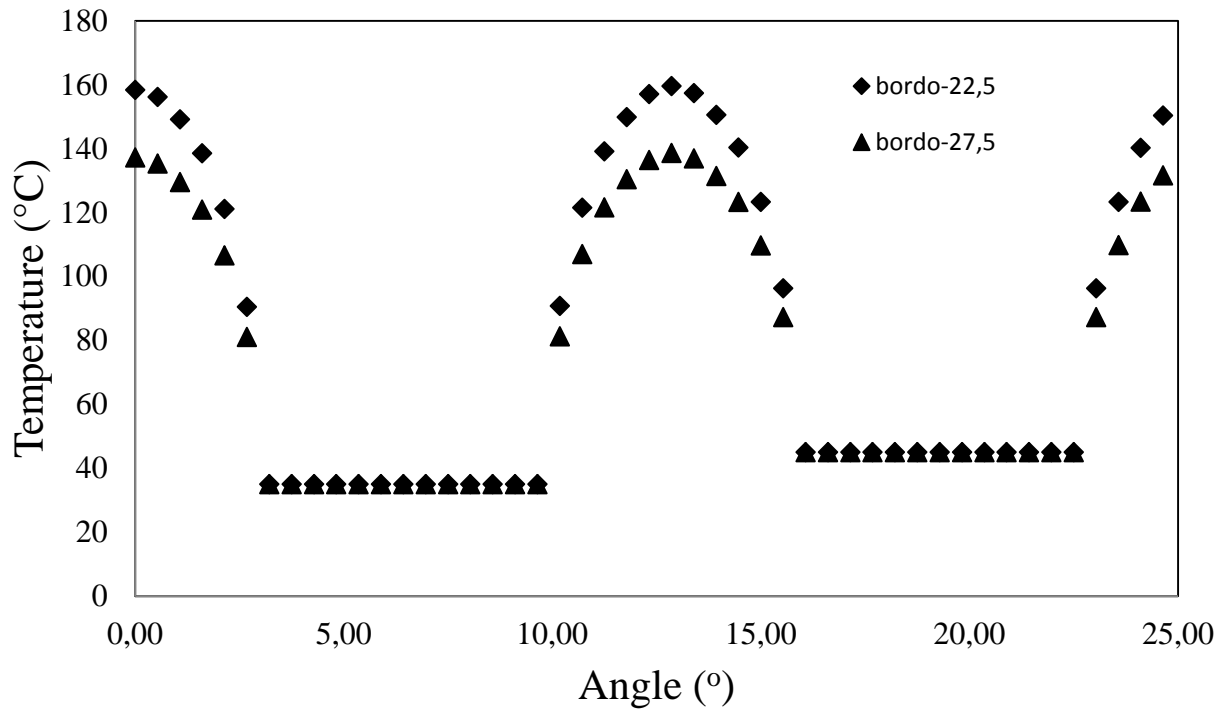Fig. 28. Comparison of different thicknesses of the shell for Model-3.

Fig. 29: Temperature distribution comparisons for different thicknesses of the shell.

References:

[1] D.Q.Kern: Process Heat transfer, McGraw Hill 1950.

[2] Bonanni, Cavallini, Mattarolo: Trasmissione del calore, Cleup 1985.

[3] www.matweb.com ; database online di materiali ingegneristici.

6. Synthesis

Main findings

As following the main findings of each investigation are briefly outlined:

Paper I

A new model of depth reduction factor for different ratios of relative depth of the notch of periodic sharp-notched component is proposed to match the results from SED approach. In the case of shallow periodic sharp notches, the results of this study are compared with those provided by other researchers in the recent literature. In addition, based on the best fit of numerical data from the SED approach, some polynomials for non-dimensional NSIF in the case of intermediate and deep notches are presented.

Paper II

Taking advantage of some recent closed form expressions for the strain energy density in a control volume embracing the notch tip, some simple expressions are derived for the Notch Stress Intensity Factors of an infinite array of double symmetric lateral notches and edge notches under tension loading. The new expressions are applicable to narrow notches when the ratio between the notch depth and the plate width, a/W, is lower than 0.025, providing very accurate results.

Paper III

Due to the desirability of analytical expressions for NSIFs evaluation, the numerical results, obtained from the strain energy density (SED) approach, are used to find some simple analytical expressions for the prediction of NSIFs of periodic sharp notches in a very wide range of notch configurations.

Paper IV

The main advantages of the strain energy density (SED) approach and some recent applications of the SED to the fatigue analysis of welded joints are reviewed. The NSIF ratio of two scaled geometries of periodic sharp notches is a function of averaged SED in the control volume embracing the middle notch tip. The new results are very useful for the assessment under fatigue *loading*.

Paper V

Two new expressions of the notch depth reduction factor for the case of periodic blunt notches under normal stresses (tension and bending) and torsion are proposed to match the results from SED approach. The results of this study are compared with those provided by other researchers in the past and recent literature.

Paper VI

It is found that, the effect of plate thickness of periodic notched components can be characterized by the relative value with respect to the depth of the notch (H/t). For the blunt periodic notches with relatively higher values of H/t ratio, the value of the maximum tensile stress is located near the free surface. On the contrary, for lower values of H/t, it is placed at the middle plane. The same behavior is observed for sharp periodic notches in terms of notch stress intensity factors.

Paper VII

The stress results are compared with those provided by a recent theory which reduces the 3D governing equations of elasticity to a differential equation system, which includes a bi-harmonic equation and a harmonic equation. Comparing numerical results and theoretical stress distributions, a good agreement is found.

Paper VIII

The FE results show the presence of coupled modes at the overlap corners of the joint. In particular, sharp increment of out-of-plane fracture mode very near the lateral free surface of the joint is worth noting.

Outlook: Potential for future research

Using the SED approach, the NSIFs and SCFs of periodic sharp and blunt notches are calculated. A very wide range of notch configurations for both type of periodic notched components under static loading are considered. The SED approach is also very convenient and gives accurate results for the fatigue failure prediction of notched components. The extension of results of this study for the case of fatigue loading would be useful. In particular, experimental testing of bolt-nut connections and comparing with theoretical findings would be promising.

7. Publications and conference presentations

Peer-reviewed publications:

1. R. Afshar, F. Berto, P. Lazzarin, L.P. Pook, Analytical expressions for the notch stress intensity factors of periodic V-notches under tension by using the strain energy density approach, Journal of Strain Analysis for Engineering Design, 2013, 48 (5), 291-305.
2. R. Afshar, F. Berto and P. Lazzarin, Three-dimensional Stress Analysis of a Plate Weakened by an Inclined Diamond Hole Under Various Loading Conditions, 2013, Lecture Notes in Engineering and Computer Science 3 LNECS , pp. 1953-1958.
3. R. Afshar, F. Berto,and P. Lazzarin, Three-dimensional finite element analysis of single-lap joints: effect of adhesive thickness and Poisson's ratio, Key Engineering Materials, 2014, Vols. 577-578, pp 393-396.
4. R. Afshar, F. Berto, On three-dimensional stress analysis of periodic notched plates under tension, Science China Physics, Mechanics & Astronomy, 2013 (DOI: 10.1007/s11433-013-5277-0).
5. R. Afshar, F. Berto, Strain energy density applied to shallow threaded plates with sharp notches under fatigue, Structural Durability & Health Monitoring, 2013, 9:2, 167-180.
6. P. Lazzarin, R. Afshar, F. Berto, Notch stress intensity factors of flat plates with periodic sharp notches by using the strain energy density, Theoretical and Applied Fracture Mechanics, 2012, 60, 38-50.
7. F. Berto, P. Lazzarin , R. Afshar, Simple New Expressions for the Notch Stress Intensity Factors in an Array of Narrow V–Notches Under Tension, Int. J. of Fracture, 2012, 176:237-244.
8. R. Afshar, F. Berto, Stress concentration factors of periodic notches determined from the strain energy density, Theoretical and Applied Fracture Mechanics, 2011, 56:127–139.
9. A. A. Oshkour, N. A. Abu Osman, Y. H. Yau, F. Berto and R. Afshar, Three-dimensional finite element analysis of the functionally graded femoral prostheses, Materials and Design, 2013, 56:998-1008.
10. A. Amini, R. Afshar, F. Berto Effects of geometrical parameters on the stress field of three-dimensional plates weekend by periodic notches, Strength of Materials (Submitted).

Conference Proceedings:

11. R. Afshar, F. Berto,and P. Lazzarin, Three-dimensional finite element analysis of single-lap joints: effect of adhesive thickness and Poisson's ratio, International Conference on Fracture and Damage Mechanics, 2013, 17-19 September, Alghero, Sardinia, **Italy**.
12. R. Afshar, F. Berto and P. Lazzarin, Three-dimensional Stress Analysis of a Plate Weakened by an Inclined Diamond Hole Under Various Loading Conditions, World Engineering Conference, 2013, 2-5 July, London, **UK**.
13. R. Afshar, I. Palomba, D. Richiedei, A. Trevisani, Mode selection in reduced-order models for ultrasonic horns under longitudinal vibration, International Operational Modal Analysis Conference, 2013, 13-15 May, Guimaraes, **Portugal**.
14. F. Berto and P. Lazzarin, R. Afshar. On the array of narrow shallow sharp notches under tension, Mesomechanics, 2012, 24-28 Sept. Budapest, **Hungary**.

15. R. Afshar, F. Berto and P. Lazzarin, Strain energy density approach for stress analysis of periodic sharp-notched flat plates under tension , 41° convegno nazionale AIAS, **Vicenza**, 5-8 Settembre 2012.

16. R. Afshar, F. Berto and P. Lazzarin, Stress concentration factors of flat plates with periodic notches by using strain energy density, 40° convegno nazionale AIAS, **Palermo**, 7-10 Settembre, 2011.

Poster:

17. A. A. Oshkour, N. A. Abu Osman, Y. H. Yau, R. Afshar and F. Berto, Three-dimensional finite element analysis of the functionally graded femoral prostheses, International Conference on Mechanics of Biomaterials and Tissues 2013, 8-12 December, Sitges, **Spain**.

8. Curriculum vitae

Reza Afshar has done his PhD studies in material mechanics in doctoral school of mechatronics and product innovation at Univerity of Padova from 2011-2013. He received his first degree in Mechanical Engineering from Iran in 2000, then after working in industry for about 8 years continued his studies at University Putra Malaysia in Mechanical Engineering, leading to Master degree in 2009. He was awarded a PhD scholarship by University of Padova in 2011.

His research expertise is related to mechanical fracture of metallic materials, finite element modeling, design of devices and biomechanical fixtures, failure assessment, biomechanical testing and modal analysis. His industrial experience has developed through his work as a mechanical design engineer (2 years) and repair and maintenance supervisor (4 years) after his graduation in 2000 in Iran. He has worked in several areas in mechanical engineering field. He speaks English, Italian and Persian.